DOKUZ EYLÜL UNIVERSITY
GRADUATE SCHOOL OF NATURAL AND APPLIED SCIENCES

A PARAMETRIC INVESTIGATION STUDY BY NUMERICAL ANALYSIS ON THE CONTRIBUTION OF JET GROUT COLUMNS FOR LIQUEFACTION MITIGATION

by
Uğur Can ERGİNAĞ

July, 2015
İZMİR

A PARAMETRIC INVESTIGATION STUDY BY NUMERICAL ANALYSIS ON THE CONTRIBUTION OF JET GROUT COLUMNS FOR LIQUEFACTION MITIGATION

A Thesis Submitted to the
Graduate School of Natural and Applied Sciences of Dokuz Eylül University
In Partial Fullfilment of the Requirements for the Degree of Master of Science
in Civil Engineering, Geotechnical Engineering Program

by
Uğur Can ERGİNAĞ

July, 2015
İZMİR

M.Sc THESIS EXAMINATION RESULT FORM

We have read the thesis entitled **"A PARAMETRIC INVESTIGATION STUDY BY NUMERICAL ANALYSIS ON THE CONTRIBUTION OF JET GROUT COLUMNS FOR LIQUEFACTION MITIGATION"** completed by **UĞUR CAN ERGİNAĞ** under supervision of **PROF. DR. ARİF ŞENGÜN KAYALAR** and we certify that in our opinion it is fully adequate, in scope and in quality, as a thesis for the degree of Master of Science.

Prof. Dr. Arif Şengün KAYALAR

Supervisor

Prof. Dr. Gürkan Özden

(Jury Member)

Prof. Dr. M. Yalçın Koca

(Jury Member)

Prof.Dr. Ayşe OKUR

Director

Graduate School of Natural and Applied Sciences

ACKNOWLEDGEMENTS

I owe many thanks to Prof. Dr. Arif Şengün Kayalar for his unconditional guidance in every step of this study. I wish to declare my appreciation for his continuously unlimited assistance, support and patience that brings that study to this stage and therefore, it cannot be forgotten. Without his knowledge on geotechnical engineering, it is not possible to not only overcome technical issues but also comprehend concepts that are vital for both as being engineer and MSc candidate. Hence, it is a joy to work under such valuable mentor.

I also want to thank Prof. Dr. Gürkan Özden for this technical guidance that broadens my horizon in certain aspects of geotechnical engineering. It is a fact that it would be even more difficult to finish this graduate study without his significant help.

I am grateful to Dr. Fabian Dedecker for his help on numerical analysis based on finite difference, without whom I would not be able to finish this study.

I want to acknowledge the support of Prof. Dr. Kemal Önder Çetin about technical issues in this study.

Last, but not least, I sincerely grateful to Ozan Alver for his immeasurable support throughout this study.

Uğur Can ERGİNAĞ

A PARAMETRIC INVESTIGATION STUDY BY NUMERICAL ANALYSIS ON THE CONTRIBUTION OF JET GROUT COLUMNS FOR LIQUEFACTION MITIGATION

ABSTRACT

As dynamic motion source earthquakes release energy propagating outward and result in many hazards including soil liquefaction phenomenon. Actually, liquefaction is primary concern for fully saturated, cohesionless soil. Therefore, various ground treatment methods are used in order to improve soil against liquefaction. As a soil improvement method, jet grout columns which are also known as high modulus columns are commonly preferred as a liquefaction mitigator. However, jet grout columns have become general engineering practice in terms of liquefaction mitigation although their effectiveness has not been validated thoroughly by both case and numerical analyses. Besides, only total stress analysis that does not take excess pore water pressure into account widely form numerical studies. Thus, in this study, role of jet grout columns as a precaution are investigated parametrically with intensive numerical analyses scheme.

Numerical analyses performed using FLAC3D software in this study stand on three-dimensional, non-linear Finn Model and finite difference-based effective stress analyses. With the help of numerical analyses, two cases, namely, liquefiable soil and this type of soil involving jet grout columns are assessed for liquefaction. In that analyses, different dynamic motion inputs involving different peak acceleration values are used to evaluate contribution of jet grout columns against liquefaction. Also, effects of jet grout column spacing, stiffness of jet grout column and depth of consideration are investigated. Effectiveness of jet grout columns is mainly assessed with respect to pore pressure ratio. In addition, free field results obtained from this type of evaluation is compared with total stress approach.

As the concluding remark, jet grout columns can prevent liquefaction by decreasing pore pressure ratio. Their effectiveness increases with decrease of stiffness and spacing while peak acceleration value of dynamic motion input does not have significant role on their contribution.

Keywords: Liquefaction, finite difference method, non-linear analysis, Finn Model, jet grout columns, effective stress approach, pore pressure ratio

JET-GROUT KOLONLAR İLE SIVILAŞMAYI ÖNLEME ÜZERİNE NÜMERİK ANALİZE DAYALI BİR PARAMETRİK ÇALIŞMA

ÖZ

Dinamik etki kaynağı olan depremlerde açığa çıkan enerji, sıvılaşma da olmak üzere birçok afete neden olabilir. Tamamen suya doygun kohezyonsuz zeminlerde aslında esas sorunu sıvılaşma oluşturur. Bu nedenle sıvılaşmaya karşı zemini güçlendirmek için birçok zemin iyileştirme teknikleri kullanılır. Zemin iyileştirme yöntemi olarak yüksek modüllü kolonlar olarak da bilinen jet grout kolonlar, yaygın bir biçimde sıvılaşma önleyici olarak tercih edilmektedir. Verimliliği vaka analizi veya nümerik çalışmalarla yeterince incelenmiş olmamasına karşın jet grout kolonlar, sıvılaşmayı önleyici olarak genel mühendislik uygulaması haline gelmiştir. Hatta nümerik çalışmaların çoğunu, aşırı boşluk suyu basıncını bile göz önüne almayan toplam gerilme analizleri oluşturur. Bu nedenle jet grout kolonlarının sıvılaşmaya karşı önlem olarak katkısı, parametrik olarak nümerik analizlerle irdelenmiştir.

Nümerik analizler, FLAC3D programında yapılmış olup, üç boyutlu, doğrusal olmayan Finn modeline ve efektif gerilme analiz odaklı sonlu farklar yöntemine dayanır. Nümerik analizlerle vasıtasıyla sadece sıvılaşan zemin ve jet grout kolonları içeren sıvılaşma özelliği gösteren zemin durumları değerlendirilmiştir. Bu analizlerde, farklı maksimum ivmeye sahip olan dinamik etkiler, jet grout kolonların sıvılaşmaya karşı katkısını değerlendirmede kullanılmıştır. Kolonlar arası mesafe, jet grout kolon rijitliği ve farklı derinlik etksi de ayrıca incelenmiştir. Jet grout kolonların sıvılaşma önlemede katkısı boşluk suyu basınç oranıyla değerlendirilmiştir. Ayrıca zemin tepki analizlerinden elde edilen sonuçlar toplam gerilme analiziyle karşılaştırılmıştır.

Sonuç olarak, jet grout kolonların aşırı boşluk suyu basıncını düşürerek sıvılaşmayı önleyebileceği gösterilmiştir. Sıvılaşmayı önlemedeki katkıları, rijitliklerinin azalmasıyla veya kolon aralıklarının artması gözlemlenmiştir. Dinamik etki maksimum ivmesinin, jet grout kolonların verimliliğine etki eden önemli bir etken olmadığı saptanmıştır.

Anahtar kelimeler: Sıvılaşma, sonlu farklar yöntemi, doğrusal olmayan analiz, Finn Modeli, jet grout kolonları, efektif gerilme yaklaşımı, boşluk basıncı oranı

CONTENTS

LIST OF FIGURES

Page

LIST OF TABLES

CHAPTER ONE

INTRODUCTION

No matter how severe earthquake strikes, certain amount of energy is rapidly released from the Earth's crust during this irregular cyclic motion. Therefore, released energy starts to propagate outward from the Earth's crust by means of seismic waves (Chen & Scawthorn, 2003). As a result of that shaking, there exists possibility of occurrence of many seismically induced hazards including liquefaction. Thus, it is vital to both identify and mitigate seismic hazards in order to prevent loss of life and to reduce economical loss (Kramer, 1996).

Liquefaction is one of the extraordinary phenomena that could indicate the damage or effect which could be caused by an earthquake. The reason why liquefaction is an important issue is its strength oriented relationship with soil deposit. During liquefaction, especially in saturated loose granular soils, shear strength and stiffness are significantly reduced resulting in loss of self-stability and therefore, soil acts like fluid (Terzaghi & Peck, 1948). In other words, excess pore water pressure induced by an earthquake diminish shear strength of soil. Thus, liquefaction could commonly occurs near bodies of water in case of an earthquake strikes. Liquefaction can cause collapse of dams or slopes, bearing capacity failure of foundation and lateral spreading. In the past, mentioned liquefaction-based damages were observed several times in the 1964 Alaska, 1964 Niigata, 1983 Nihonkai-Chubu, 1987 Superstition Hills, 1989 Loma Prieta, 1993 Kushiro-Oki, 1994 Northridge, 1995 Kobe, 1999 Kocaeli and 1999 Chi-Chi earthquakes. As a result of that, many researchers have tried to find out safety margin of a soil deposit against liquefaction. Among those studies, "simplified procedure" of Seed and Idriss (1971) has become a consensus for evaluation of liquefaction initiation risk of a soil deposit. In this method, liquefaction initiation is assessed by means of load and capacity terms that are represented by cyclic stress ratio (CSR) and Standard Penetration Test (SPT) blow counts. Although 'simplified method' is accepted as conventional method in the assessment of liquefaction initiation, it does not take excess pore water pressure into account. Therefore, apart from "simplified method", pore pressure ratio (r_u) which is the ratio of excess pore water pressure to static vertical effective stress should be obtained (Martin, Finn & Bolton, 1975; Seed, 1986). That is, it is accepted as onset of liquefaction if r_u approaches to 100% (Seed & Lee, 1966).

In order to prevent liquefaction hazard, there exists certain amount of mitigation strategies. Indeed, with the help of comprehension of liquefaction hazard and its corresponding consequences for predetermined objectives including safety of a structure, an effective mitigation strategy can be attained (Idriss & Boulanger, 2008). In other words, selection of any mitigation method is directly related with how to manage risk or probabilistic evaluation of risk. Mitchell (2008) classified ground improvement methods according to their applicability to different particle sizes. That is, effectiveness of a ground improvement method depends on particle size distribution of a soil deposit. Depending on particle size, vibro methods, deep dynamic compaction, compaction grouting, soil mixing, drainage, exploration compaction and jet grouting are common examples of ground treatment methods. According to Moseley and Kirch (2004), jet grouting which is both mixing and partial replacement of soil with cement is a multi-purpose ground improvement method. In terms of liquefaction mitigation, effectiveness of jet grouting were indicated by various researches based on case analyses (Hausler & Sitar; 2001; Martin, Olgun, Mitchell & Durgunoglu, 2004; Spagnoli, 2008). Apart from case analyses, as an experimental study, Adalier (2003) was able to indicate that stone columns are beneficial as a mitigation strategy in non-plastic silty sands according to his findings by means of centrifuge tests. That is, stone columns are an effective countermeasure against liquefaction if geostatic vertical effective stresses are larger than 45 kPa. Similar to stone column approach, Ozsoy & Durgunoglu (2003) was able to relate effectiveness of jet grout mitigation with ratio of shear modulus of jet grout columns to soil deposit, theoretically. Actually, this method called “unit cell approach” utilizes the study performed to evaluate effectiveness of stone columns (Hayden & Baez, 1994). In this approach, composite shear behaviour is adopted in the distribution of seismically induced shear stress between stone columns and soil. Apart from this theoretical point of view, contribution of jet grout columns as a remediation against liquefaction were also verified by few numerical analyses. While some of analyses were performed by using “simplified approach” called as “total stress approach” (Martin & Olgun, 2007; Olgun & Martin, 2008; Unutmaz, 2012; Callisto, Rampello & Viggiani, 2013; Cristivao et al., 2014), few of them were based on “effective stress approach” related with pore pressure ratio (Almani, A. A. Memon & N. A. Memon, 2012; Almani, Memon, Habib, Lal & Shah, 2013; Keepa, Saul, Murashev & McMillan, 2014). According to mentioned studies, jet grout columns have been shown to be beneficial in terms of mitigation in accordance with shear stiffness difference between jet grout column and soil.

Contrary to static loading, dynamic loading which is defined as repetitively applied load with frequency is much complicated in terms of soil behaviour (Ishihara, 2003). Also, how soil responses to cyclic load including earthquake and vibrations created by machines is not known well in geotechnical engineering point of view. Moreover, if the problem encountered during dynamic loading is related with liquefaction, it becomes more complex. Although uncertainties related with liquefaction and its mitigation have not been eliminated definitely, many advances have been attained thanks to several studies (Hausler & Sitar; 2001). Nonetheless, much research is still needed to identify soil behaviour, liquefaction mechanisms and the way how jet grout columns make contribution to liquefaction mitigation. Indeed, apart from case studies, most of the mentioned studies on jet grout columns stand on numerical analyses and therefore, so as to overcome such kind of problem, numerical analyses based on finite element/difference become mostly preferred method to overcome the problem (Unutmaz, 2012). However, even if numerical analyses are done to identify liquefaction problems like which type of soil liquefies, there exists time-consuming schedule due to long calculation overburden. Besides, this problem gets even worse if dynamic problem consists of liquefaction mitigation. Moreover, another challenge is to determine which type of approach should be adopted so as to attain more accurate and reliable solutions. That is, conventional “total stress approach” may not be reliable or robust for any case. Therefore, solely sticking to the approach that do not control excess pore water pressure during dynamic loading may not be a logical one. Hence, results gathered by means of total stress analysis should be compared with effective stress approach. However, no matter which type of approach is selected, jet grout columns are an effective solution against liquefaction which is the case in 1999 Kocaeli Earthquake although much research is still needed including both case analysis and numerical analysis (Martin, Olgun, Mitchell & Durgunoglu, 2004; Martin & Olgun, 2007).

In this study, it is aimed to indicate by means of 3-D numerical analyses based on finite difference method that jet grout columns can contribute on liquefaction mitigation. Firstly, a soil deposit properties of which are obtained from Wildlife Liquefaction Array (Bennett, McLaughlin, Sarmiento & Youd, 1984) which will be indicated that it can liquefy based on r_u values under dynamic load is obtained. Also, results obtained from effective stress approach will be compared to values computed from total stress approach. Secondly, by using pre-determined jet grout column pattern, contribution of jet grout columns as a countermeasure of liquefaction phenomenon will be investigated parametrically, namely; varying stiffness of jet grout columns, spacing between them, type of dynamic load and depth of consideration. Spacing parameters are 3B, 4B, 5B and 6B while stiffness parameters are low, mean and high levels. These stiffness levels are determined based on ratio of shear moduli of soilcrete column to soil. Corresponding values are 27.4, 35.4 and 44.8 for low stiffness level, mean stiffness level and high stiffness level, respectively. Also, used peak acceleration values are 0.05g, 0.06g, 0.07g and 0.08g. Furthermore, r_u values are obtained for predetermined 16 locations at 2 m, 4 m, 6 m, 8 m, 10 m and 12 m depths in order to find out depth effect. Jet grout columns having diameter of 1 m and length of 12 m will be used throughout this study while depth of numerical model is 15m. Based on given parameters, differences in r_u values between free field case and improved site case will be compared so as to evaluate effectiveness of soilcrete columns. Hence, entire process followed in this study are divided into four main chapters.

In Chapter 2, liquefaction definitions, corresponding elementary mechanism and determination of liquefaction initiation based on conventional total stress approach will be given. Besides, several liquefaction mitigation methods adopted in the past and their efficiencies as liquefaction mitigator will be discussed.

Brief historical background and evolution of modern jet grouting, jet grouting methods, corresponding operating parameters and mechanical properties will be explained in Chapter 3. Furthermore, past studies covering case studies and numerical analyses including both total and effective stress approaches on effectiveness of jet grout columns against liquefaction will be studied in this chapter. Also, two approaches on the prediction of effectiveness of soilcrete columns for liquefaction mitigation will be given.

In Chapter 4, in the light of mentioned information, contribution of jet grout columns on liquefaction mitigation will be intensively investigated by 3-D numerical analyses with respect to r_u values. After indicating that soil liquefies in accordance with r_u values under dynamic loading, improved site r_u values will be obtained and effectiveness of jet grout columns will be assessed with respect to r_u value differences between before and after jet grout columns. Besides, during this evaluation, various parameters such as different spacing, various stiffness levels, dynamic motion of various peak accelerations and depth of consideration will be taken into account.

Finally, Chapter 5 will present the summary and major conclusions of this study. Besides, there will be certain recommendations on future studies.

CHAPTER TWO
PAST STUDIES ON LIQUEFACTION PHENOMENON AND CORRESPONDING MITIGATION METHODS

2.1 Introduction

In this chapter, past studies related with seismic soil liquefaction up to so far is covered. Firstly, liquefaction definitions are given and then, its mechanisms are presented. Thirdly, identification of liquefiable soil is introduced. Fourthly, determination of liquefaction initiation is indicated. Lastly, as a final topic, liquefaction mitigation methods are discussed.

2.2 Liquefaction Definitions

Casagrande (1936a) was able to indicate the unusual behavior of fully saturated contractive sand under undrained conditions. However, the liquefaction term had been used as a first time by Terzaghi and Peck (1948) so as to describe a phenomenon causing suddenly strength loss of fully saturated loose sand deposits leading to flow like viscous fluid under even slight disturbance. In that time, it was found that there exist a possibility of liquefaction triggering slope instability of deposits comprising saturated sand or silty sand under static load. Besides, liquefaction phenomenon had been described as a similar manner that is loss of strength by Mogami and Kubo (1953) by embedding dynamic effect caused by earthquake as cyclic loading into the definition after evaluating effects and hazards of 1948 Tokyo earthquake. Also, they improved the definition by considering deformations of saturated granular soils under undrained conditions source of which are not only monotonic but also transient including repeated disturbance. The hallmark of liquefaction is the excessively generated pore water pressure caused by undrained loading according to them. Nonetheless, up to 1964 Alaska and 1964 Niigata earthquakes, both importance and effects of liquefaction had not been clearly comprehended. During these earthquakes, certain structural collapses containing sinking (Figure 2.1 (a)) and tilting (Figure 2.1 (b)) beneath of which is on saturated sandy soils and damages occurred due to seismically induced liquefaction. It was observed that liquefaction can cause decrease in bearing capacity of structures due to significant loss of shear strength during earthquake. Moreover, Marcuson, Ballard & Ledbetter (1978) described liquefaction as a change of state of a granular soil deposit from solid to viscous fluid caused by reduction of effective stress triggered by increasing of pore water pressure. With the help of tendency of becoming compressed and densified, excess pore water pressure is initiated in case of dynamic loading. The mentioned state transformation behaviour is likely to occur for loose to medium dense granular soil. Besides, soil becomes soften as a result of liquefaction with shear strength loss. Due to modulus degradation, excess amount of shear deformations can occur. As a concluding remark for the definition of liquefaction is that "The sudden drop of shear strength under undrained conditions from yield strength to the substantially smaller critical state strength is known as liquefaction" (Terzaghi, Peck & Mesri, 2006, p. 193).

Figure 2.1 (a) A sinked tank in liquefied soil during Niigata Earthquake (b) a tilted building caused by Niigata Earthquake

2.3 Liquefaction Mechanisms

Seed, Arango & Chan (1976) was able to explain elementary liquefaction mechanism by investigating a soil element A that shear stress caused by cyclic load tries to contract the element (Figure 2.2). At point A, reduction in volume occurs under initial stresses as if it is under drained condition. However, the mentioned behavior is limited due to incompressibility of water that leads to occurrence of positive pore water pressure under undrained condition. Therefore, load transfer from soil grain skeleton to pore water occurs which is named as "recovery" in Figure 2.2 period of which keeps volume change equal to zero that is a necessity for undrained behaviour. Moreover, effective stress decreases by an amount of increase in positive excess pore water pressure. Thus, there exists no volume change along the path A-C. In fact, infinite deformation of soil having residual strength occurs during liquefaction if the specimen is both saturated and cohesionless loose granular. In case of dense cohesionless granular soils, successive cycles cause two-staged deformations. Initially, the soil element has a tendency of becoming contracted and then, it tries to dilate. Also, in deformation point of view, equilibrium is attained when the soil element has ability of resisting against successive cycles without undergoing additional deformations.

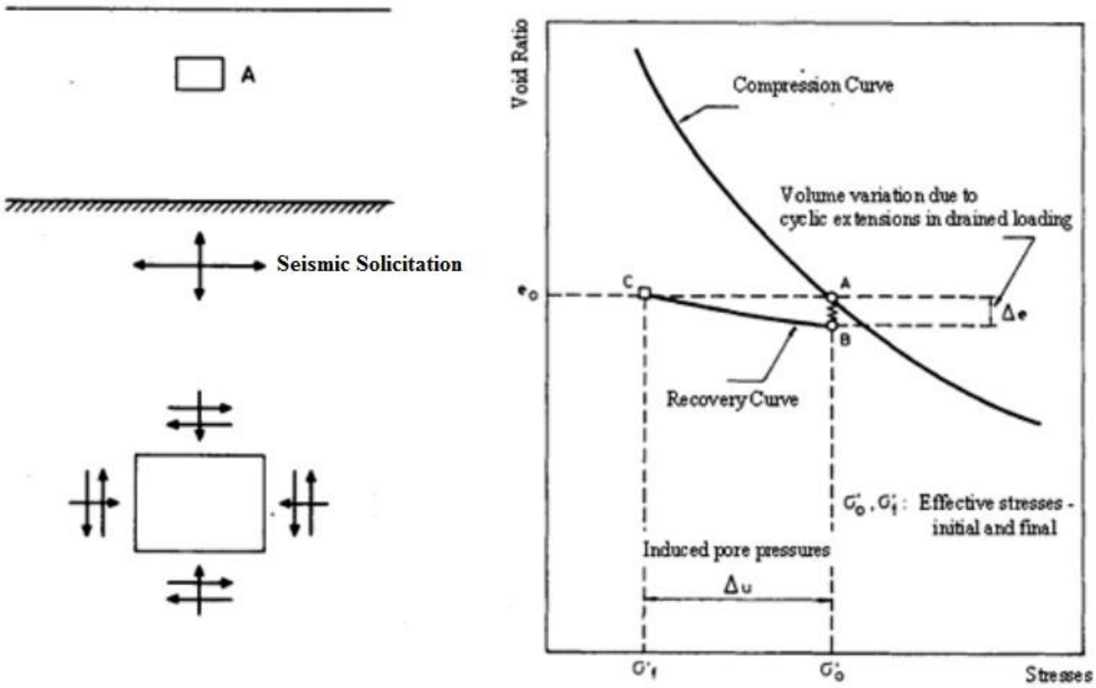

Figure 2.2 Elementary liquefaction mechanism

Although Seed, Arango & Chan (1976) made a definition of liquefaction as mentioned, the behaviour is not observed explicitly unless shear strains does not govern volumetric strain at the start of cyclic loading. If shear strain dominates volumetric strain, dilation of the soil element does not allow occurrence of liquefaction.

Robertson and Wride (1997) explained liquefaction mechanism with two interrelated different responses of soil during earthquake shaking, namely; flow liquefaction and cyclic softening. In terms of evaluation of liquefaction related hazards, these two terms are crucial due to difference between levels of the hazard they can cause (Kramer, 1996). That is, flow liquefaction can result in much severe hazard as compared to cyclic mobility. Whereas, rate of occurrence of cyclic mobility is high. Although cyclic mobility could occur in wide range of site conditions comprising broad range of soil type, insignificant damage can occur as well as severe damage. Due to this variability of effects, it is difficult to separate from each other. However, characteristics of these two terms should be known in order to understand mechanism behind liquefaction.

2.3.1 Flow Liquefaction

Flow liquefaction was defined as the state of soil having very low residual shear strength where equilibrium is lost due to being exposed to either monotonic loading such as construction of new a structure and filling of dam with water or dynamic loading including pile driving process and earthquake. A soil sample attains its own residual strength after undergoing very large strains (Figure 2.3).

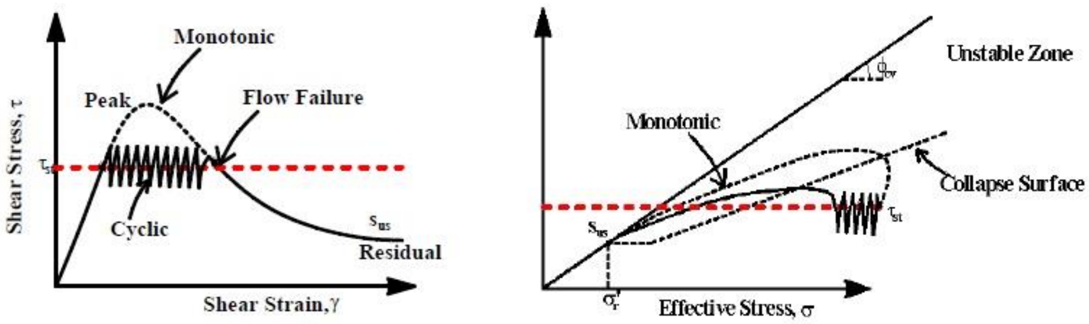

Figure 2.3 Flow liquefaction

Whether loading type is monotonic or dynamic, both of them exert additional forces by affecting internal force equilibrium. Also, if soil does not resist those additional forces, flow liquefaction occurs because of the fact that loss of shear strength takes place. In case of flow liquefaction, rapid and large amount of displacements known as “flow failure” may occur. In past, there exist several examples of flow liquefaction, namely; Zealand flowslide (Koppejan et al., 1948), Fort Peck Dam (Casagrande, 1965), Aberfan flowslide (Bishop, 1973) and Stava tailings dam. Also, in flow liquefaction, the fact that early signings do not usually emerge increase severity of the hazard.

Both Robertson & Catherine (1997) and 1997 Northwestern Center of Engineering Education Center (NCEER) Workshop mentioned required characteristics or properties that there exists possibility of occurrence of flow liquefaction:

- Strain softening response of soil against undrained loading is needed. Furthermore, unchanged shear and effective stress should occur under such kind of loading (Figure 2.4).
- Ultimate undrained shear strength should be lower than the in-situ shear stresses.
- Flow liquefaction may occur under either monotonic loading or cyclic loading.
- In order to attain failure, large amount of volume should be strain soften. Flow type failure could occur while failure type could be slide, as well. The main cause of failure is because of internal stresses.
- Sensitive clays, very loose deposits and silt deposits are more prone to expose flow liquefaction under undrained loading.

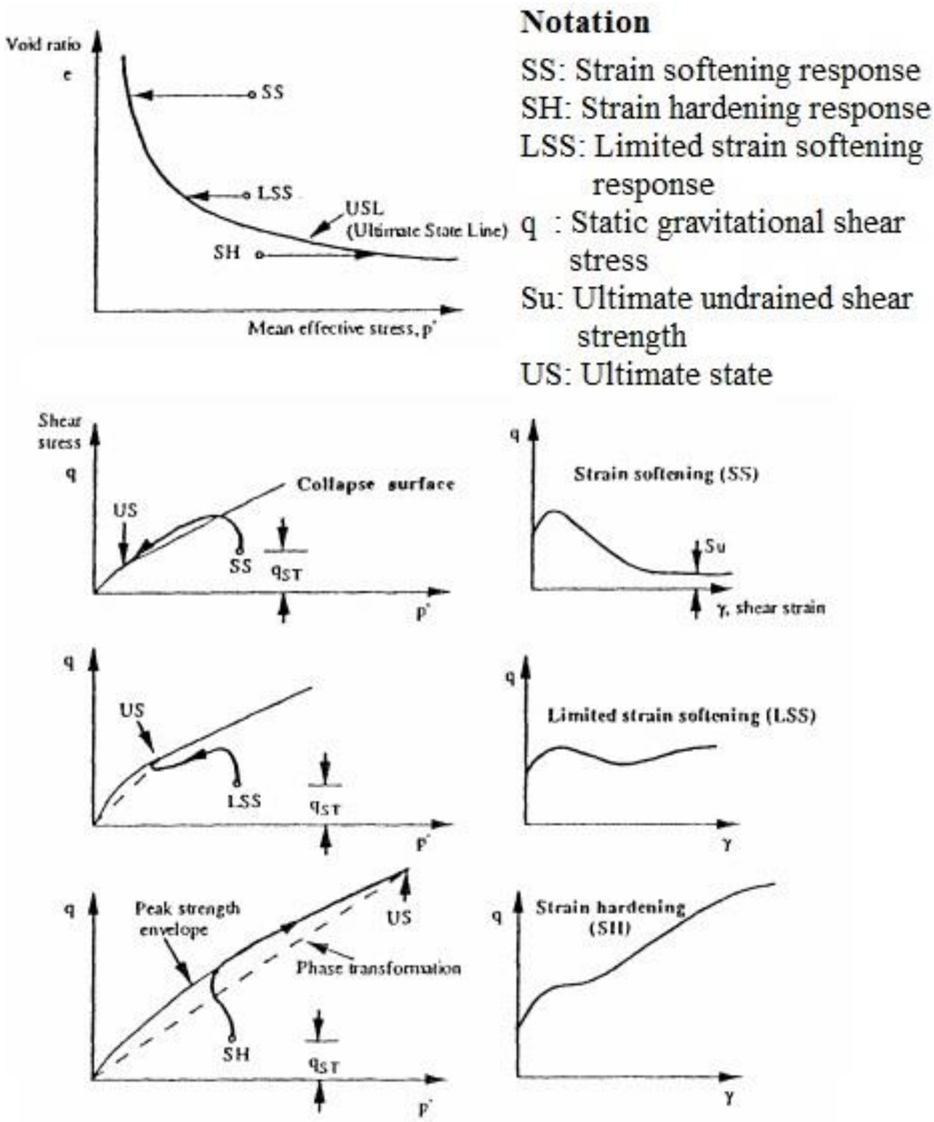

Figure 2.4 Behavior of granular soil under undrained loading

2.3.2 Cyclic Softening

Robertson and Catherine (1997) and 1997 NCEER Workshop described cyclic softening as a phenomenon comprising two sub-phenomenon, namely; cyclic mobility and cyclic liquefaction where it occurs that soil deposits are exposed to relatively low shear stresses as compared to its own ultimate shear strength. In this type liquefaction, incrementally increasing deformations take place triggered by either static or dynamic stresses. Unlike flow liquefaction, cyclic softening may occur for both strain softening and strain hardening.

2.3.2.1 Cyclic Mobility

Cyclic mobility can result in undesired very large deformations known as “lateral spreading” under dynamic load (Kramer, 1996). Unlike flow liquefaction, combination of static and cyclic shear stresses are driving forces and they cause such kind of liquefaction. In order to attain cyclic mobility, the conditions to be introduced should be fulfilled:

- There exist no shear stress reversals. That is, shear stresses should be different than zero.
- Effective stresses should be different than zero. In other words, zero effective stress is not necessarily required.
- External causes result in final deformations of soil except that very loose soils and flow liquefaction take place.

2.3.2.2 Cyclic Liquefaction

Cyclic liquefaction occurs if certain conditions occur;

- It occurs under in-situ shear stresses lower than shear stresses caused by cyclic loading. That is, due to occurrence of shear stress reversal, zero shear stresses could develop provided that cyclic loading can leads to mentioned phenomena (Figure 2.5).
- Effective stress should decrease to zero under cyclic loading.
- Whenever effective stress converges to zero, shear stresses also decreases to zero. If additional shear stresses are applied, soil has a tendency of becoming dilated as pore water pressure decreases. However, even if soft initial strain occurs under initial stresses, it may cause large deformations.
- In generally, deformations become levelled as cyclic loading stops. Unlike flow liquefaction, external factors are the cause of final deformations rather than internal forces.

- For a given cyclic loading having sufficient magnitude and duration, regardless of type sand, almost all types of sand undergo cyclic liquefaction.
- Apart from sandy soil, cyclic liquefaction can occur in clayey soils although resulting deformations are small as compared to sandy soils due to presence of cohesion. Besides, time effect is governing case for deformations of clayey soils.

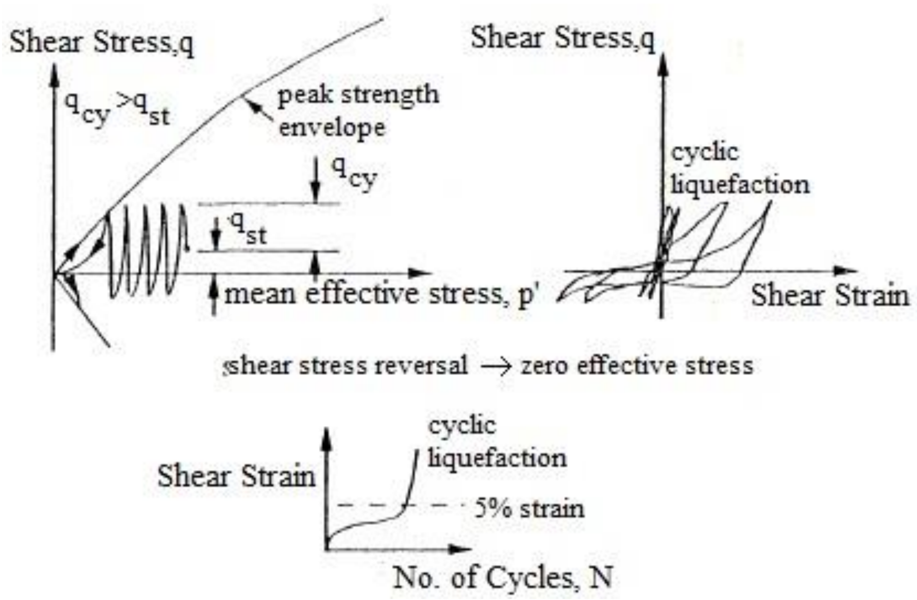

Figure 2.5 Cyclic liquefaction

2.4 Identification of Liquefiable Soil

Generally, fully saturated cohesionless soil deposits are the most important soil type which are highly prone to liquefaction. Also, risk of liquefaction of a soil deposit boosts if it is loose enough to contract under dynamic loading provided that sufficient drainage cannot occur resulting in induced pore water pressure is not likely to dissipate (Terzaghi, Peck & Mesri, 1996). With respect to geological aspect, most common liquefiable sediments are alluvial, beach, terrace deposits including uncontrolled man-made fill (Kramer, 1996). Whether a soil deposit can liquefy or not is determined with respect to compositional, state and historical record criteria.

2.4.1 Compositional Criteria

Being liquefaction-prone is a function of compositional characteristic which directly affects volume change tendency that causes development of dynamically induced excess pore water pressure. Indeed, the volume change tendency is proportional with occurrence of excess pore water pressure (Kramer, 1996). Therefore, size, shape and gradation are important parameters in determination of liquefaction susceptibility.

In the beginning of the evaluation of being susceptible to liquefaction, it was taught that only sand type deposits have such hazardous property. While coarse grained deposits were also considered as highly permeable which drains excess pore water pressure rapidly, finer grained deposits would not allow excess pore water pressure to occur. However, as time passes, gradation boundary for liquefaction has been determined. With this purpose, Tsuchida (1970) was able to evaluate liquefaction potential with respect to grain-size distribution (Figure 2.6 (a)). Based on this figure, it could be said that plastic fines causing decrease in liquefaction potential as it is represented by lower boundary. Along lower boundary, effect of plastic fines decrease and therefore, influence of plastic fines on the contraction ability of sand is restricted which makes possibility of occurrence of liquefaction diminished. The area between upper boundaries refer to coarse grained deposit coefficient of permeability of which is in between 10^{-3} and 10^{-2} m/s. According to Terzaghi, Peck and Mesri (1996), mostly liquefiable sands have coefficient permeability range from 10^{-5} to 10^{-3} m/s. Moreover, Figure 2.6 (a) indicates that liquefaction potential emerges if D_{50} is greater than 0.02 mm and less than 2.0 mm. Also, Ishihara developed the study for tail of dams (Figure 2.6 (b)).

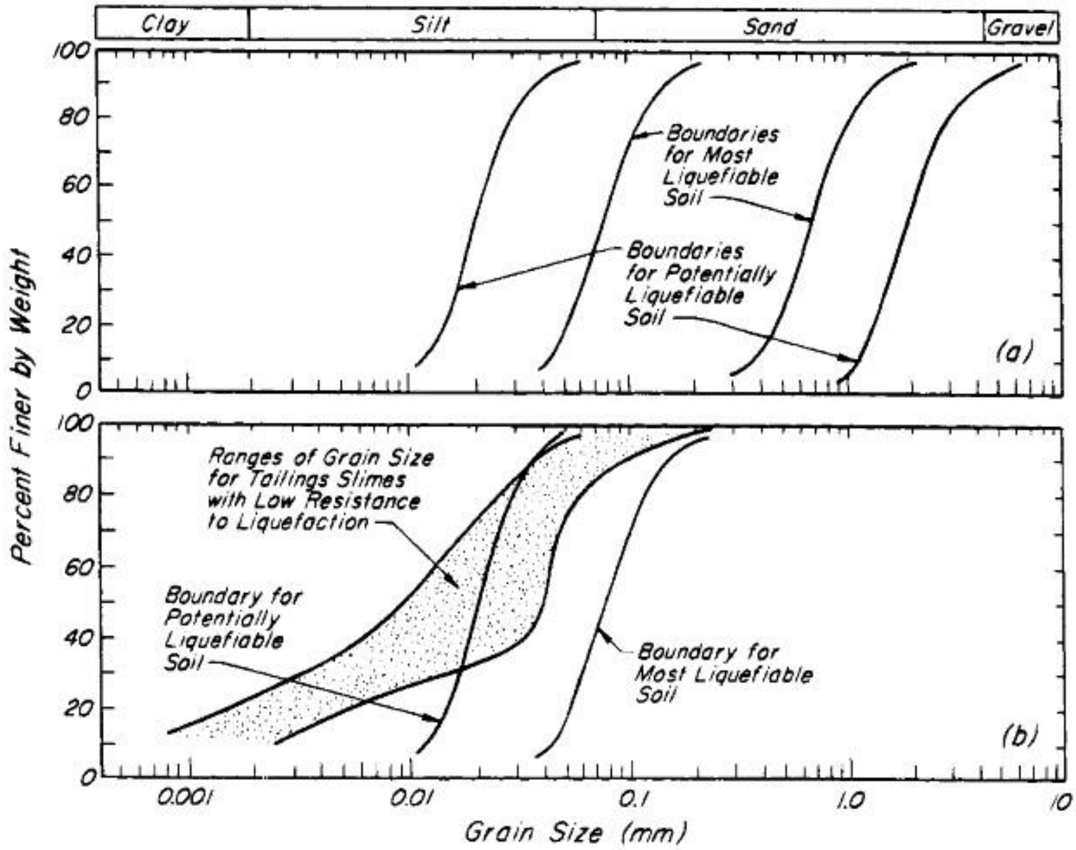

Figure 2.6 (a) Boundaries of liquefaction potential (b) boundaries of liquefaction potential for dam tail

Apart from sandy soil type, non-plastic silts fulfilling certain criteria can also liquefy under undrained conditions (Ishihara, 1985). The mentioned criteria indicated that plasticity characteristics instead of grain size only have impact on liquefaction potential of a fine grained soil. Furthermore, non-plastic cohesionless coarser silts particle shape of whom is bulky are prone to liquefaction (Ishihara, 1993). However, finer silts having platelike or platy shape is not in danger of liquefaction because they have enough cohesion to prevent it. Although consensus on whether all type of clays do not have liquefaction potential, due to strain softening behavior, highly sensitive clays can liquefy. Based on findings gathered from 1964 Niigata and 1964 Alaska Earthquakes, “Chinese Criteria” was established so as to assess liquefaction potential of fine grained soils (Seed & Idriss, 1982). That is, if a fine grained soil satisfy three criteria according to the Chinese Criteria, it is likely to liquefy (Table 2.1)

Table 2.1 Chinese criteria

Fine Grained Soils Having Liquefaction Potential		
Liquid Limit (LL)	**Water Content (w_c)**	**Finest Content (<0.005 mm)**
≤ 35 %	≥ 0.9*LL %	≤ 15 %

Although Chinese Criteria has been robust and it predicted several liquefaction cases, its validity has become under question after 1989 Loma Prieta Earthquake (NCEER, 1997). Due to effect of presence of non-plastic fines and influence of plasticity index on liquefaction potential which were not included in mentioned criteria, it was understood that Chinese Criteria needs to be improved. Therefore, Andrews and Martin (2000) modified the Chinese Criteria (Table 2.2).

Table 2.2 Modified Chinese criteria

	Clay Content (< 10 %) (< 0.002 mm)	**Clay Content (≥ 10 %) (≥ 0.002 mm)**
Liquid Limit < 32 %	High Potential	Laboratory Test Needed
Liquid Limit ≥ 32 %	Laboratory Test Needed	Non-liquefiable

Besides, Bray et al. (2001) emphasized that Chinese Criteria utilizes clay term as only particle size indicator rather than plasticity. Therefore, based on their studies, it is important that effect caused by finer particles should be studied and verified by means of laboratory tests. From this point of view, they were able to show that finer quartz particles smaller than 2 – 5 mm which is also non-plastic behave like cohesionless under dynamic loading and as a result of that, they can liquefy. That is, overall contribution of plasticity as compared to particle size is more governing factor in case of liquefaction They proposed a relationship between plasticity index and ratio of natural water content to liquid limit with respect liquefaction potential (Figure 2.7).

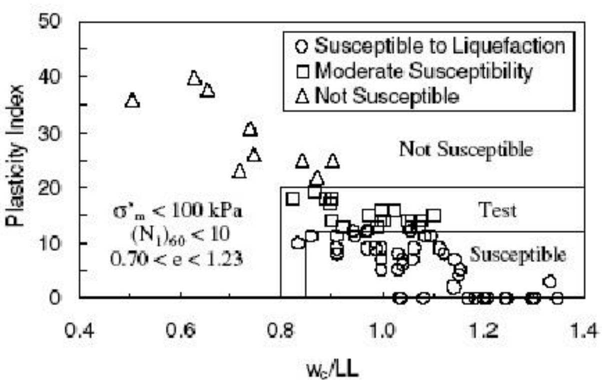

Figure 2.7 Potentially liquefiable fined grains

Apart from mentioned studies on plastic fine grained soils, based on performed tests on samples gathered from Adapazari-Turkey and Chi Chi-Taiwan Earthquakes, Seed et al. (2003) provided similar results on Atterberg limit chart with Bray et al. (2001) that amount of clayey minerals have more importance than the amount of clay-size fraction (Figure 2.8). That is, if liquid limit is less than 37 percent and plasticity index is lower than 12 percent, high potential of liquefaction emerges provided that natural water content is higher than 0.8 times its own liquid limit. The only difference between mentioned one and the preceding approach is the ratio of natural content to liquid limit. The chart corresponding lastly mentioned study divided Atterberg Chart into three parts bounded both plasticity index and liquid limit. Zone A is referred as “classic cyclically induced liquefaction” that closely detects the liquefaction in Adapazari case while Zone B describes the region as potential liquefaction risk. However, it is still not possible to determine what types of silts and clays are susceptible to liquefaction with the help of this chart (Boulanger & Idriss, 2006).

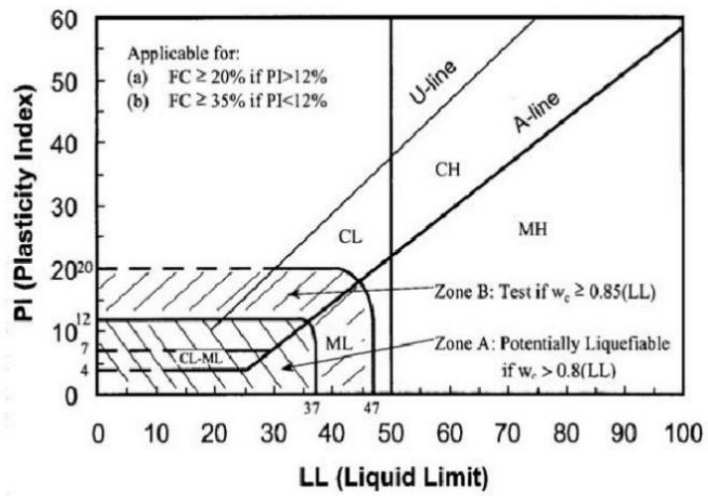

Figure 2.8 Liquefaction potential

Moreover, Idriss and Boulanger (2008) prescribed new evaluation criteria related with cyclic shear strength of fine grained soils. In that criteria, it was assumed that soil behaves as either “Sand-Like” or “Clay-Like” (Figure 2.9). However, they accepted that fine grained soil having plasticity index higher than 7 behaves clay-like soil. If soil behaves sand-like, the soil is susceptible to liquefaction. Also, such kind of soils have relatively low resistance referred as cyclic resistance ratio (CRR) in this figure against shear stresses caused by cyclic loading as compared to soil described as clay-like. Nonetheless, unscaled y-axis in Figure 2.9 is an obstacle in order to assess liquefaction potential of a fine grained soil requiring both laboratory test and judgement.

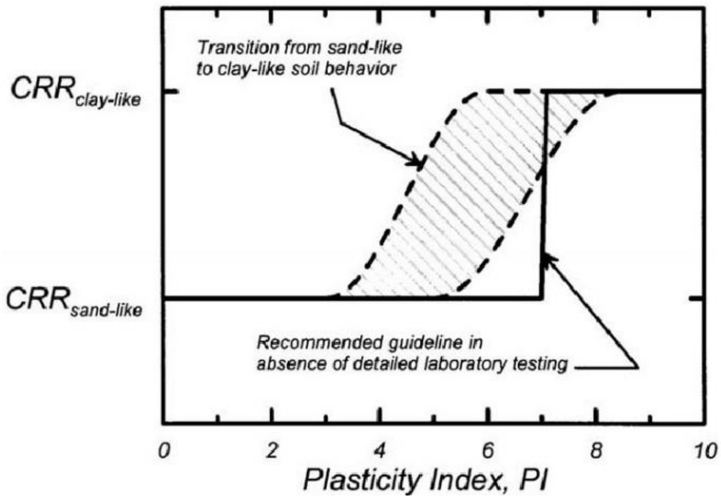

Figure 2.9 The newest criteria for evaluation of liquefaction potential of fine grained

Particle shape is another reason determining liquefaction potential. Rounded shaped rather than angular shaped particles is rapidly densified under dynamic loading. Hence, liquefaction risk of a soil deposit consisting of rounded shaped particles is more prone to liquefaction. Deposits having rounded shape have a tendency of becoming contracted while occurrence of contraction is restricted to some extent by means of grain crushing in angular shaped deposits (Terzaghi, Peck & Mesri, 1996). Situations where importance of particle shape increases are places where it is located in fluvial or alluvial environments. Generally, loose deposits are often encountered at these places (Kramer, 1996).

Gradation is an important factor affecting liquefaction susceptibility. Depending on void ratio, liquefaction potential is less for well graded soil as compared to poorly graded. The reason is that voids between larger particles is partially filled with smaller particles in well graded soil. Also, possible void change in well graded soil is relatively low which prevents occurrence of high excess pore water pressure under undrained conditions. Furthermore, most of past liquefaction involving cases represent that uniform gradation is a factor in these cases (Kramer, 1996).

2.4.2 State Criteria

A soil deposit which only fulfils mentioned compositional criteria may not liquefy under undrained conditions. Therefore, state of soil is crucial criteria with respect to liquefaction. Simply, state describes soil in accordance with its density and stress related characteristics prior to beginning to earthquake.

Casagrande (1936) was able to interpret relationship between stress-strain-void ratio by means of strain-controlled triaxial test under drained conditions. In his work, initially loose and dense state of samples were tested at the same confining pressure so as to find out how void ratio affect. According to series of tests, results of which is accepted as an indicator of what strength of soil is, samples converged to almost same density and void ratio when they were sheared to large deformations (Figure 2.10 (a) & Figure 2.10 (b)). Besides, loose specimens became more densified state as a result of contraction while dense specimens contracted at the beginning of the test and then dilated when their densities decreased at the end of test.

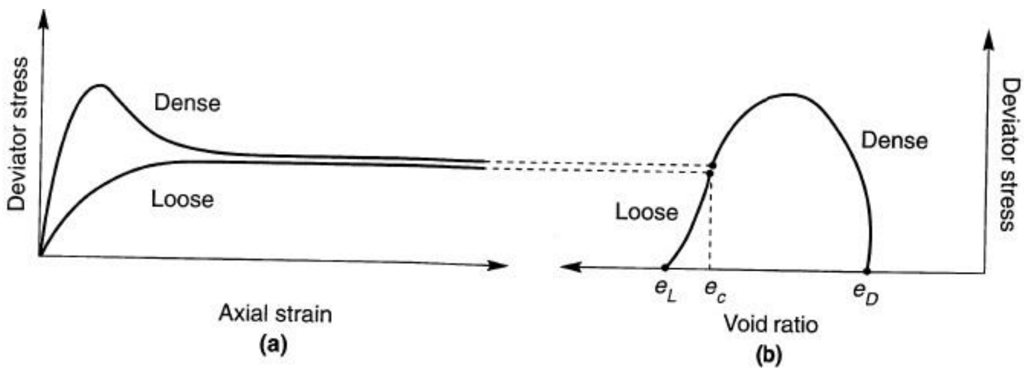

Figure 2.10 (a) Stress-strain relationship (b) corresponding stress-void ratio relationship

The void ratio which converges to a single value regardless of initial density state of specimen at the end of test was termed as "critical void ratio", e_c. That is, no matter how much specimen is sheared cannot affect final density and void ratio at a predetermined confining pressure. This term can be defined as a unique term for predetermined confining pressure (Casagrande, 1936). Therefore, critical void ratio line (CVR) can be obtained by combining locus of each critical void ratios corresponding different effective confining pressure (Figure 2.11). With the help CVR, boundary between loose and dense states can be obtained.

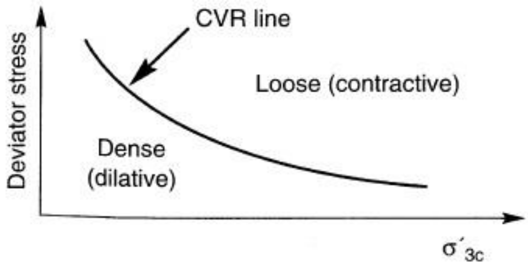

Figure 2.11 Critical void ratio line

Same methodology can be applied for strain controlled test under undrained condition. According to Castro (1969), due to the fact that positive pore water pressure induced by tendency of becoming contracted for loose soil occurs, effective confining pressure starts to decrease while volume cannot alter (Figure 2.12 (a)). Vice versa, negative excess pore water pressure takes place and therefore, effective confining pressure increases during loading. Thanks to corresponding CVR, boundary between liquefiable and non-liquefiable as well as contractive and dilative distinction can be determined (Figure 2.12 (b)).

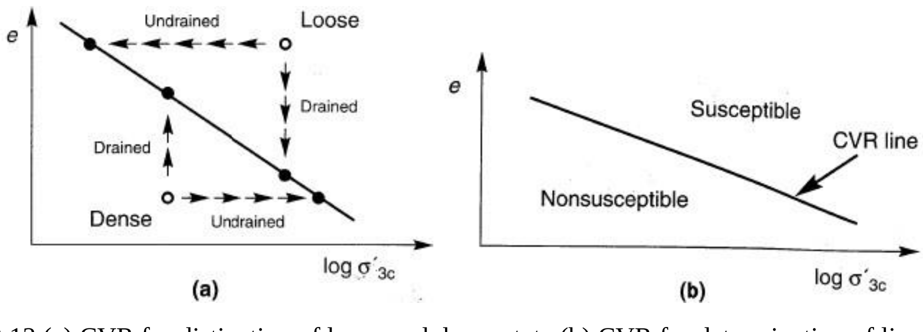

Figure 2.12 (a) CVR for distinction of loose and dense state (b) CVR for determination of liquefaction potential

According to Terzaghi, Peck & Mesri (1996), sand deposit having relative density up to 60 % have liquefaction susceptibility.

2.4.3 Historical Record Criteria

If a soil deposit liquefies under seismic loading and pre-earthquake conditions are preserved after it occurs, there exists high probability of reoccurrence of liquefaction again (Youd, 1984). Therefore, based on post liquefaction evidences, liquefaction map have been continuously updated (Youd, 1991). According to the way mentioned map is created, Ambraseys (1988) represented that an earthquake can trigger liquefaction at a limited epicentral distances. Moreover, he was able to find out that influence area where liquefaction can occur increases as magnitude of earthquake rises up (Figure 2.13).

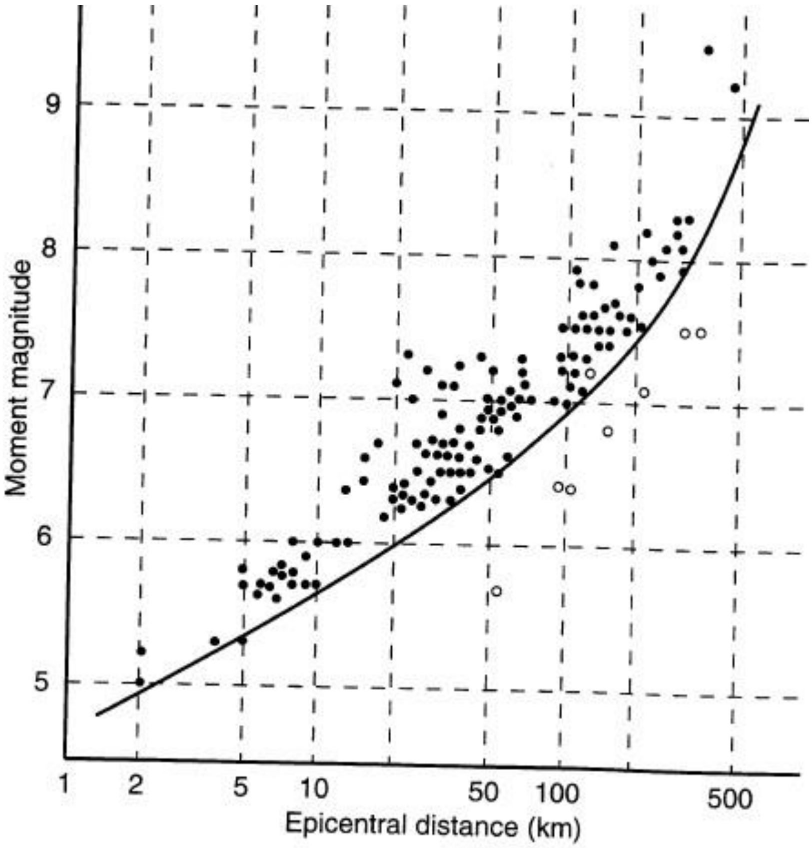

Figure 2.13 Influence area of earthquake with respect to liquefaction

Liquefiable depth of soil is measured up to 15 m based on past cases (Idriss & Boulanger, 2008). There are two main reasons behind it. First one is related with relatively low confining pressure at shallow depths. Therefore, places close to ground surface is under high liquefaction risk as compared deeper depths. Secondly, at shallow depths, younger deposits take place and therefore, they are likely to be less dense than old ones because probability of being shaken by severe earthquake in past is low. Besides, for older deposits, having been exposed to pre-consolidation pressure under drained condition contributes their own internal structure and gives more stability (Terzaghi, Peck & Mesri, 1996). Moreover, the fact that finer particles that represent contractive tendency under undrained condition between larger particles are removed by means of groundwater flow which takes significant time is another reason making older deposits safer against liquefaction (Finn, 1981).

2.5 Determination of Liquefaction Initiation

Dynamic loading can be described by means of released energy during it occurs. Therefore, magnitude of an earthquake are characterized based on Richter scale according to this point of view. Spatial geometry, hypocentral distance and the way how wave is transmitted through rock are main factors affecting intensity of ground shaking of rock underlying liquefiable zone of soil. Actually, response of a site including liquefaction phenomenon against dynamically induced waves is function of its own stiffness and damping properties. Therefore, certain different approaches have been developed and used in order to evaluate whether dynamic motion causes liquefaction or not.

A soil element is subjected to seismically induced all types of wave which result in additional shear stresses and pore pressure apart from geostatic stresses present in it (Figure 2.14). Among all wave forms, vertically propagating from rock motion is not taken into consideration due to its negligible contribution on shear stresses. Although vertical shaking can produce volatile changes in total vertical, horizontal stresses and pore pressure, effective stresses is not influenced (Idriss & Boulanger, 2006). In other words, during an earthquake, upward propagation of horizontal shear waves generates significant shear stresses and strain. In order to assess causes of dynamic loading with respect to liquefaction, “cyclic stress approach” known as “simplified method” or “total stress approach” is the most used approach among various approaches (Kramer, 1996).

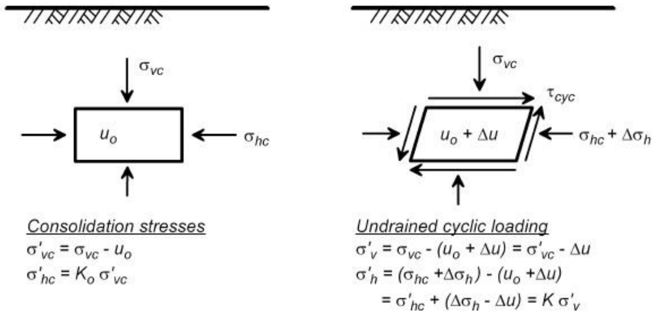

Figure 2.14 Geostatic and cyclically induced stresses

2.5.1 Cyclic Stress Approach

In the evaluation of liquefaction potential, it is crucial to obtain how much load is needed in order to initiate liquefaction. Therefore, mentioned loading term which renders liquefaction potential to just amplitude and number of cycles has started to be used in accordance with cyclic shear stresses. In this approach, there are two main terms, namely; cyclic shear stress caused by seismically generated loading and another cyclic shear stress related with liquefaction resistance (Seed & Idriss, 1971). Slightly modified form of these terms are used in this approach. In other words, "cyclic stress ratio" (CSR) is representative for loading term while "cyclic resistance ratio" (CRR) is an indicator of resistance term. It is accepted as onset of liquefaction if resistance is exceeded by loading.

2.5.1.1 Cyclic Stress Ratio (CSR)

Vertically propagating shear waves in horizontal direction induces shear stresses varying with respect to depth within soil body during earthquake. Actually, such kind of stresses could be calculated in an accurate way based on equation of motion if sufficient amount of data comprising soil profile information and dynamic motion input exist. However, for most cases, information that enables dynamically induced shear stresses to be obtained is not available. Moreover, in generally, depth of borings is not extended to the depth where liquefaction potential is present in site investigation works. Therefore, the approach proposed by Seed and Idriss (1971) has become widely accepted practice to take effect of induced shear stresses into account.

Seismically induced shear stresses which are a function of time for a soil body can be calculated with the assumption of soil being perfectly rigid by using simplified procedure proposed by Seed and Idriss (1971):

$$\tau(t)_{rigid} = \gamma_n h \left(\frac{a(t)}{g}\right) \tag{2.1}$$

where γ_n is natural unit weight of soil body, h is corresponding depth measured from ground surface, a(t) is ground acceleration in horizontal direction at time ‘t’ and g is gravitational acceleration. In fact, using rigid body assumption does not reflect the actual behaviour of soil because of the fact that it behaves as deformable body. Therefore, calculated shear stresses which are assumed as being developed inside soil body are greater than the actual magnitude (Figure 2.15). As a result of that, obtained shear stress magnitude is diminished by using a stress reduction coefficient, r_d.

$$\tau(t)_{deformable} = \gamma_n h \left(\frac{a(t)}{g}\right) r_d \tag{2.2}$$

Furthermore, due to the fact that induced shear stresses vary with respect to depth, an average value rather than changing values is preferred in calculation by multiplying the obtained shear stress where occurs under maximum ground acceleration with a constant which is equal to 0.65 based on past laboratory test data. The constant can be different than 0.65 (Haldar & Tang, 1981). However, it was accepted that 65 percent of peak cyclic shear stress can produce an increase in pore pressure (Kramer, 1996).

$$\tau(t)_{average} = (0.65) \gamma_n h \left(\frac{a(t)}{g}\right) r_d \tag{2.3}$$

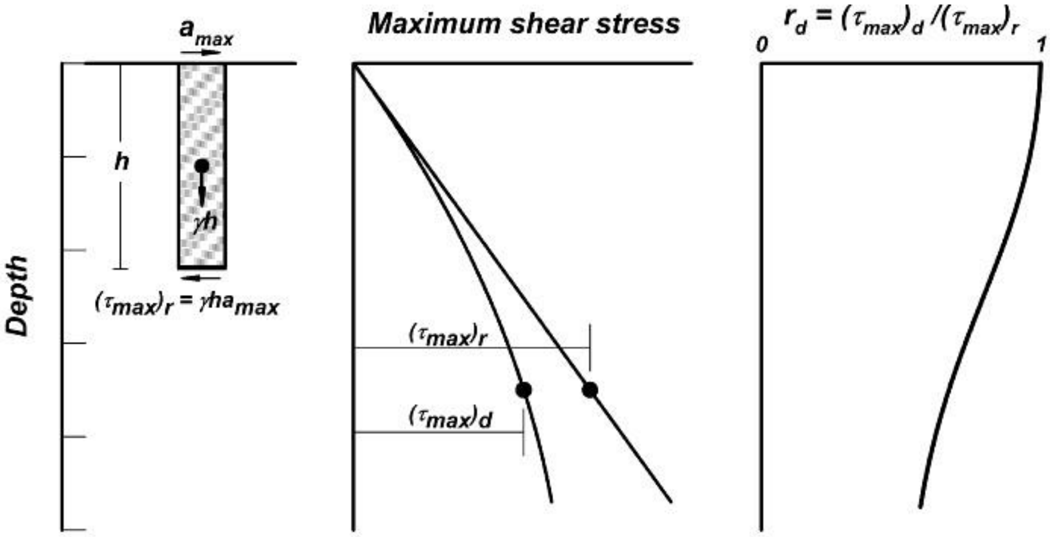

Figure 2.15 Stress reduction factor

In the light of mentioned information, cyclic stress ratio that is defined as normalization of cyclic shear stress by dividing to initial vertical effective stress can be calculated as an average value by assuming that average shear stresses caused by vertically propagating shear waves occur on horizontal plane of layer (Seed & Idriss, 1971). The reason behind normalization of average cyclic shear stress with respect to effective overburden pressure is to obtain more comprehensible dimensionless term rather than confusing term.

$$CSR = \frac{\tau_{ave}}{\sigma'_{vo}} = 0.65\frac{a_{max}}{g}\frac{\sigma_v}{\sigma'_{vo}}r_d \tag{2.4}$$

Where τ_{ave} is cyclic shear stress, σ'_{vo} is initial vertical effective stress, a_{max} is peak ground acceleration in horizontal direction, g is gravitational acceleration, σ_v is total vertical stress and r_d is stress reduction coefficient, also known as non-linear mass participation coefficient.

Hence, with the help of simplified method, irregular stress-time history can be expressed in terms of equivalent stress history having constant amplitude (Seed, Makdisi & Banerje, 1975). The number of equivalent uniform cycles is directly related with magnitude of an earthquake (Figure 2.16). The main reason why equivalent number of cycles is useful is to take advantage of use of single amplitude and uniform cycles instead of irregular cycles. Nonetheless, there is no necessity of making conversion of non-uniform histories. Mentioned simplified method is also used regardless of irregularity of records (Kramer, 1996). Moreover, this method holds true in case of free field condition.

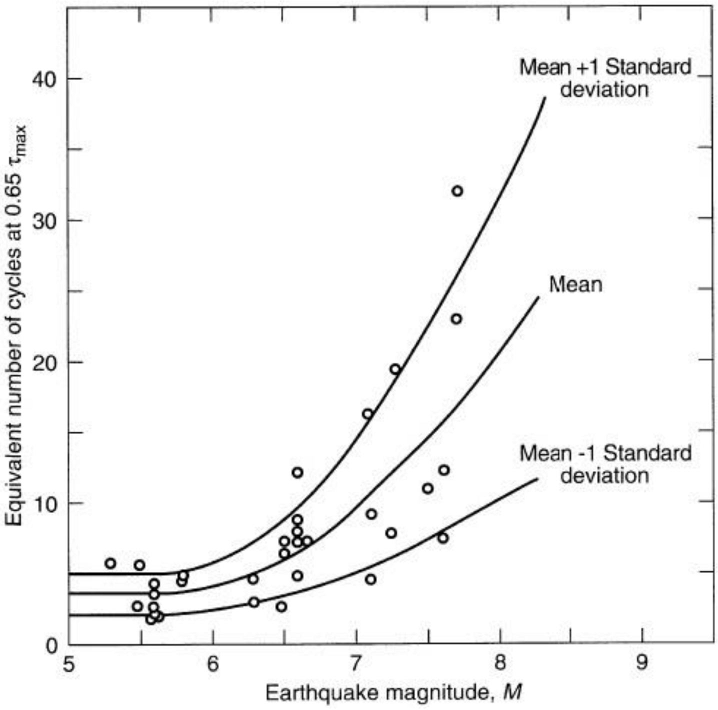

Figure 2.16 Determination of equivalent number of cycles

Seed and Idriss (1971) introduced non-linear mass participation coefficient that represents flexibility of soil body with respect to rigid soil column. That is, if non-linear mass participation coefficient is equal to 1.0, soil column is either fully rigid regardless of depth of interested area or at the ground surface. Also, that coefficient degrades in a quick way as depth of investigation increases. Moreover, with regard to past incidences, general trend of mentioned coefficient was obtained at that study (Figure 2.17). Also, in that study, trendline covering average values of stress reduction factors valid for the upper 12 m which corresponds to 40 ft in Figure 2.17 was also plotted.

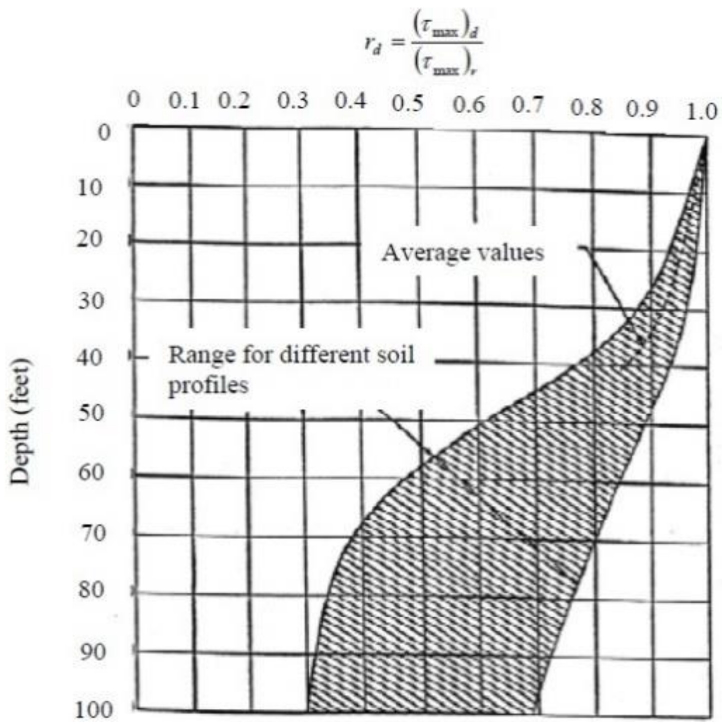

Figure 2.17 General trend of r_d

In 1997 National Center for Earthquake Engineering Center (NCEER) workshop, it was prescribed that the r_d values could be determined by using approach of Liao and Whitman (1986) based on only depth (z) for ordinary works. R_d values can be calculated by using following equations:

$$r_d = 1.00 - 0.00765z \; for \; z \leq 9.15 \; m \tag{2.5}$$

$$r_d = 1.174 - 0.0267z \; for \; 9.15 \leq z \leq 23 \; m \tag{2.6}$$

Also, Cetin et al. (2004) was able to find out that there are certain factors affecting non-linear mass participation coefficient value apart from depth. It was stated that moment magnitude of earthquake, shear wave velocity which is an indicator of soil stiffness and peak ground acceleration are driving factors have impact on r_d values as mentioned in Equation (2.7) and Equation (2.8).

For z < 20 m

$$r_d = \left[\frac{1+\frac{-23.0.13-2.949a_{max}+0.999M_w+0.0525V^*_{s,12\ m}}{16.258+0.201e^{0.341\left(-z+0.0785V^*_{s,12\ m}+7.586\right)}}}{1+\frac{-23.0.13-2.949a_{max}+0.999M_w+0.0525V^*_{s,12\ m}}{16.258+0.201e^{0.341\left(0.0785V^*_{s,12\ m}+7.586\right)}}}\right] \quad (2.7)$$

For z ≥ 20 m

$$r_d = \left[\frac{1+\frac{-23.0.13-2.949a_{max}+0.999M_w+0.0525V^*_{s,12\ m}}{16.258+0.201e^{0.341\left(-z+0.0785V^*_{s,12\ m}+7.586\right)}}}{1+\frac{-23.0.13-2.949a_{max}+0.999M_w+0.0525V^*_{s,12\ m}}{16.258+0.201e^{0.341\left(0.0785V^*_{s,12\ m}+7.586\right)}}}\right] - 0.0046(z-20) \quad (2.8)$$

Where a_{max} is peak ground acceleration at the ground surface in terms of gravitational acceleration, M_w is earthquake moment magnitude, z is depth in meters and $V_{s,\ 12\ m}^*$ is representing shear wave velocity for the upper 12 m. Although proposed equation in determination of r_d values takes into account of several factors related with stiffness of soil and severity of earthquake, Kishida (2008) and Idriss & Boulanger (2008) criticized that r_d values obtained from the relation proposed by Cetin et al. (2004) diminishes quickly with depth although mentioned relation comprises both seismically and stiffness related terms. Hence, they suggested the use of chart prepared by Idriss (1999) for the prediction of r_d values (Figure 2.18).

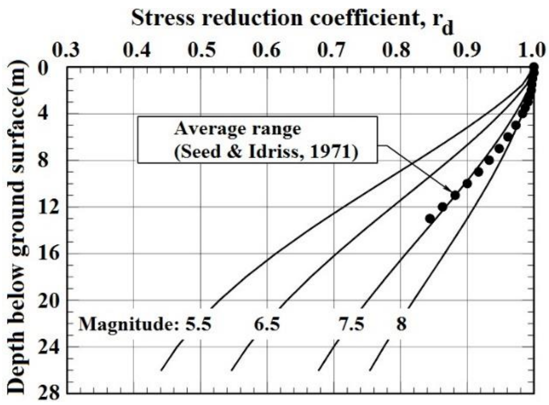

Figure 2.18 Proposed r_d values

2.5.1.2 Correlatively Standard Penetration Test (SPT)-Based CSR Evaluation

After 1964 Alaska and 1964 Niigata Earthquakes, SPT values have been used to assess liquefaction potential or CSR of soil deposit. As a result of that, there have existed several SPT-based correlations on the basis of probabilistic methods (Figure 2.19). In that correlations, potential of liquefaction is expressed in terms of probabilities of 5, 20, 50, 80 and 95%. Liao et al. (1998) were able to make correlations based on case analysis by means of maximum likelihood procedure. However, it can provide over-conservative values at low values of liquefaction potential. Likewise, Youd & Noble (1998) followed similar procedure by using additional field data. However, the problem of overestimation was not handled effectively. However, this correlation can be used for soils comprising variable fine contents. Toprak et al. (1999) processed expanded and recent field data. Nonetheless, overall uncertainty was found at unintended level. Actually, these correlations directly use corrected SPT values. To be able to use such kind of correlations, SPT corrections (Robertson and Wride, 1997) should be made for raw SPT values by using Equation (2.9) with Table (2.3);

$$(N_1)_{60} = N_m * C_N * C_E * C_B * C_R * C_S \tag{2.9}$$

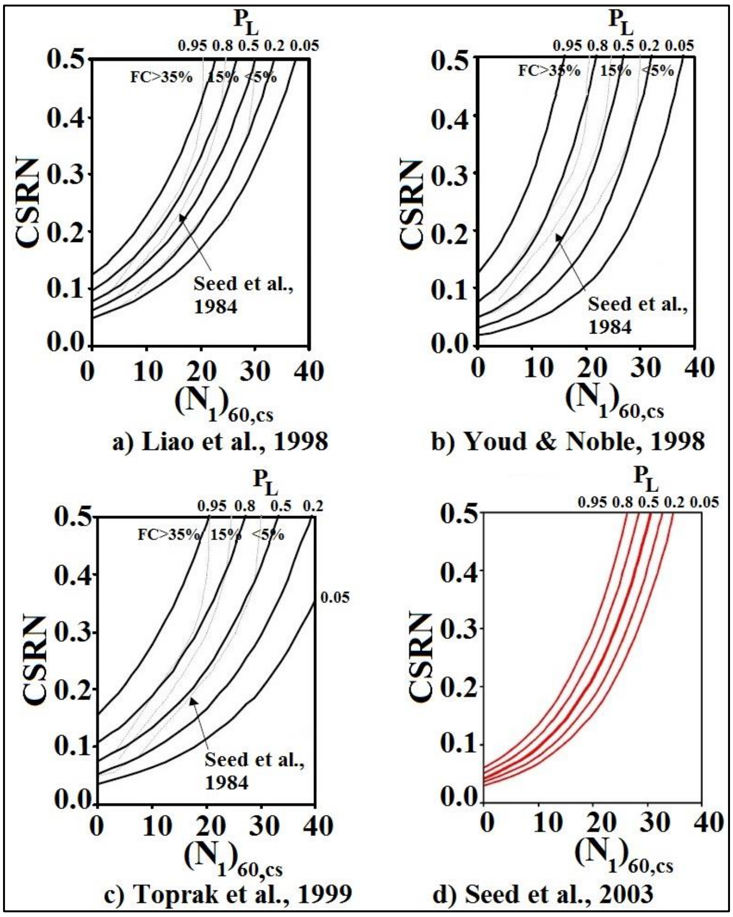

Figure 2.19 Evaluation of liquefaction potential

Table 2.3 SPT correction terms

Factor	Situation	Term	Correction
Overburden Pressure	-	C_N	$(P_a/\sigma_{vo}')^{0.5}$
Overburden Pressure	-	C_N	$C_N \leq 1.7$
Energy Ratio	Donut Hammer	C_E	0.5-1.0
Energy Ratio	Safety Hammer	C_E	0.7-1.2
Energy Ratio	Automatic Hammer	C_E	0.8-1.3
Borehole Diameter	65-115 mm	C_B	1.0
Borehole Diameter	150 mm	C_B	1.05
Borehole Diameter	200 mm	C_B	1.15
Rod Length	<3 m	C_R	0.75
Rod Length	3-4 m	C_R	0.8
Rod Length	4-9 m	C_R	0.85
Rod Length	6-10 m	C_R	0.95
Rod Length	10-30 m	C_R	1.0
Sampling Method	Standard Sampler	C_S	1.0
Sampling Method	Sampler without Liner	C_S	1.0-1.3

2.5.1.3 Cyclic Resistance Ratio (CRR)

In cyclic stress method, apart from loading term as CSR, there exists another term called as CRR standing for shear resistance capacity. According to 1997 NCEER workshop, based on past data, best fit line which is given in Equation (2.10) that is only valid for clean-sands and moment magnitude being equal to 7.5 was proposed so as to assess CRR.

$$CRR_{7.5} = \frac{1}{34-(N_1)_{60}} + \frac{(N_1)_{60}}{135} + \frac{50}{[10(N_1)_{60}+45]^2} - \frac{1}{200} \qquad (2.10)$$

The reason why given equation is valid for only $(N_1)_{60}$ is due to the fact that clean granular soil having $(N_1)_{60}$ value greater than 30 is accepted as non-liquefiable as a result of its own high dense state. Although Equation (2.10) results in raw shear resistance capacity of soil deposit, there are certain factors related with strong motion, gradation, confining pressure and static shear stress affecting CRR. Besides, CRR is directly obtained from correlation which have become consensus among 1997 NCEER participants comprising effect of fines content (Figure 2.20).

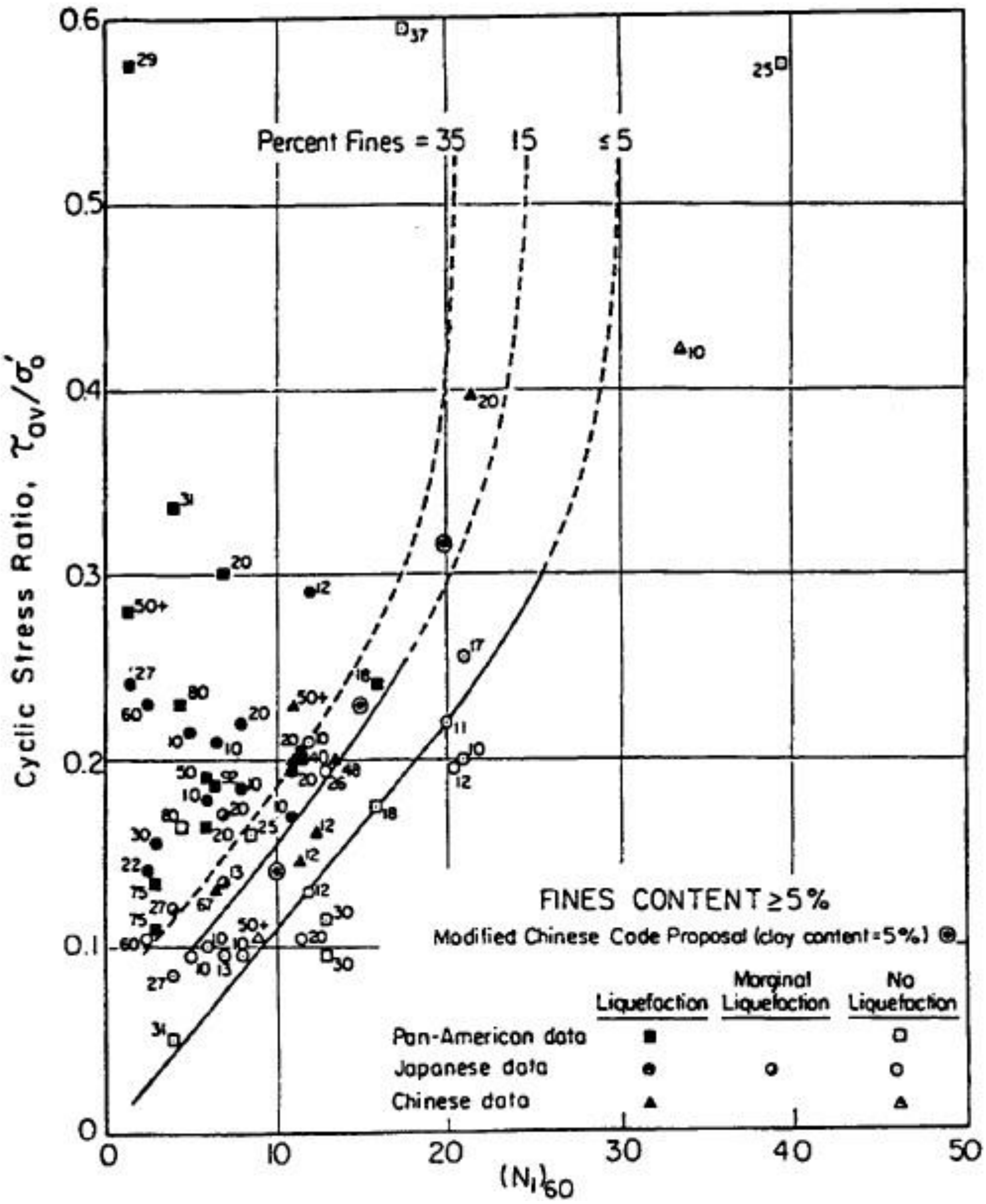

Figure 2.20 CRR-Clean sand SPT value correlation for magnitude 7.5 earthquakes

Cyclic resistance ratio obtained from Equation 2.10 is influenced by several factors; namely, magnitude of earthquake (MSF), fines content, effect of overburden pressure (K_σ) and presence of initial static driving shear stresses (K_α). Therefore, proper modifications should be made (NCEER, 1997). Actual resistance of soil can be obtained by using following equation:

$$CRR = CRR_{7.5}\ MSF\ K_\sigma\ K_\alpha \tag{2.11}$$

Required cyclic stress ratio to initiate liquefaction diminishes with rising of magnitude of earthquake due to the fact that both strong motion duration and its corresponding equivalent number of uniform cycles increases with magnitude, as well. Because of the fact that cyclic resistance ratio is function of both number of cycles (N) and moment magnitudes (M), both two terms are interrelated and they could be adjusted by using Equation (2.12) provided that Equation (2.13) is fulfilled so as to represent an earthquake magnitude of which is different than 7.5 (Idriss, 1999).

$$MSF = \frac{CRR_M}{CRR_{M=7.5}} = \left(\frac{N_{M=7.5}}{N_M}\right)^b = 6.9 \exp\left(\frac{-M}{4}\right) - 0.058 \tag{2.12}$$

$$MSF \leq 1.8 \tag{2.13}$$

Where N is the number equivalent uniform cycle, M is magnitude of earthquake and b is constant depending on type of soil. In the given equation, b average value of which is 0.34 for clean sand is the slope of log(CRR) versus log(N) plot. However, according to Idriss and Boulanger (2008), instead of using the above equations, corresponding chart developed by several researchers can be used (Figure 2.21).

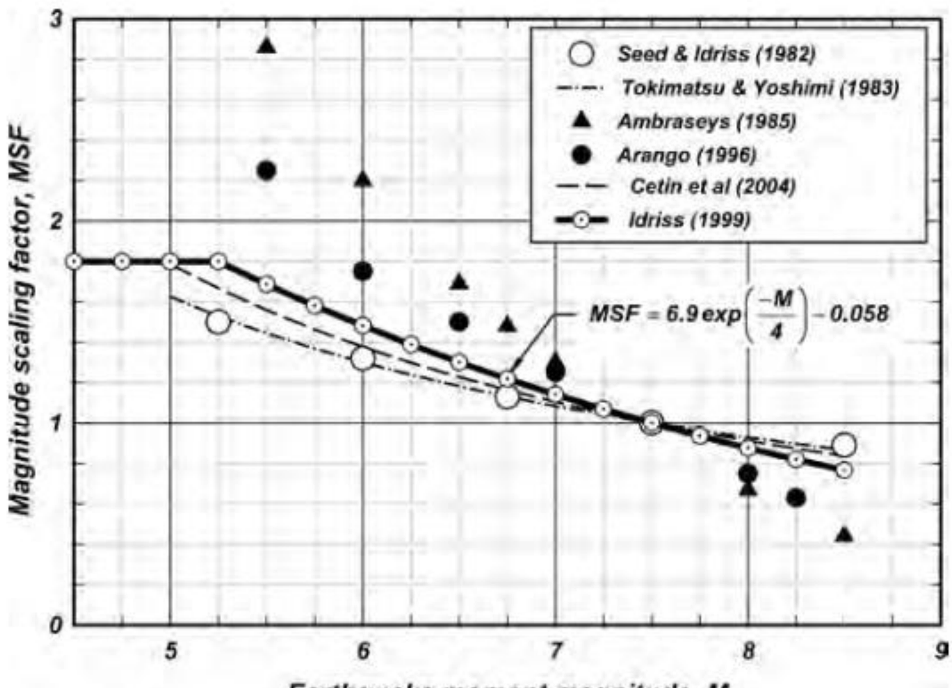

Figure 2.21 MSF factors with respect various earthquake magnitude

In the development of simplified CRR evaluation, increase in fines content with increase in CRR respectively was reported by Seed, Tokimatsu, Harder & Chung (1985). However, the reason whether lowering of penetration resistance as well as CSR or rising of liquefaction resistance causing increased CRR is not certain. However, 1997 NCEER participants made a conclusion on effect of fines content. Therefore, proper correction should be made if fines content is greater than 5%. The correction is to convert SPT values gathered from site to equivalent SPT values as if it is clean sand. Although fines content correction is made with respect to particle size, effect of plasticity should not be neglected. In calculation of CRR, clean sand converted $(N_1)_{60}$ values should be used. Hence, fines content correction can convert $(N_1)_{60}$ values to equivalent clean sand penetration resistance $(N_1)_{60cs}$ with these equations:

$$(N_1)_{60cs} = \alpha + \beta (N_1)_{60} \tag{2.14}$$

$$\alpha = \exp\left[1.76 - \left(\frac{190}{FC^2}\right)\right] \; for \; 5\% < FC < 35\% \tag{2.15}$$

$$\alpha = 5.0 \; for \; FC \geq 35\% \tag{2.16}$$

$$\beta = [0.99 + ((FC^{1.5})/1000)] \; for \; 5\% < FC < 35\% \tag{2.17}$$

$$\beta = 1.2 \; for \; FC \geq 35\% \tag{2.18}$$

Seed (1983) was able to indicate that there exists non-linear relationship between confining stress and liquefaction resistance. That is, increasing effective overburden pressure (K_σ) with increased confining pressure makes strength of soil against liquefaction enhanced. Therefore, in that study, the overburden correction factor was introduced for higher effective overburden stresses exceeding 100 kPa. The reason for that is because of the fact that simplified method was proposed for the depth less than 15 m where low overburden pressure acts and therefore, beyond this limitation, correction factor for high confining pressures caused by high overburden pressure should be taken into account (NCEER, 1997). Also, Vaid & Sivathayalan (1997) represented that this coefficient is strictly dependent on relative density (D_R) and it decreases with increasing D_R when effective overburden pressure is higher than 100 kPa. Hence, mentioned coefficient can be found by applying following equations according to Boulanger and Idriss (2004):

$$K_\sigma = 1 - C_\sigma \ln\left(\frac{\sigma'_{vo}}{P_a}\right) \leq 1.1 \tag{2.19}$$

$$C_\sigma = \frac{1}{18.9 - 17.3D_R} \leq 0.3 \tag{2.20}$$

$$C_\sigma = \frac{1}{18.9 - 2.55\sqrt{(N_1)_{60}}} \leq 0.3 \tag{2.21}$$

Where P_a is atmospheric pressure and D_R is relative density. Later on, they suggested proper graph for the prediction of K_σ with respect various D_R (Figure 2.22).

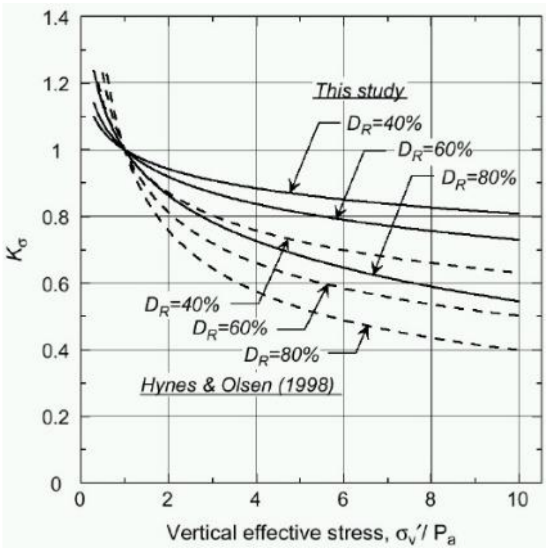

Figure 2.22 K_σ-D_R relationship

Initial static shear stress occurred prior to earthquake strike has influence on liquefaction resistance. Seed (1983) indicated that presence of such kind of shear stress leads to different consequences according to state of soil. That is, liquefaction resistance of loose granular soil which are supposed to contract under dynamic loading tends to decrease while it causes positive contribution for dilative state of which changes from moderately dense to dense. Under geostatic condition, mentioned additional shear stresses do not occur. However, if sloping ground or presence of structure takes place, correction related with the situation should be done. From this point of view, a dimensionless parameter, 'K_α', is intensively used so as to eliminate possible effects of static shear stress in evaluation of CRR. This parameter is obtained by dividing static shear stress to initial effective vertical stress. Hence, Boulanger (2003) proposed following equations comprising state, relative density and confining pressure effects for initial static stress correction:

$$K_\alpha = a + b \exp\left(\frac{-\xi_R}{c}\right) \tag{2.22}$$

$$\alpha = \frac{\tau_{static}}{\sigma'_{vo}} \tag{2.23}$$

$$\xi_R = \frac{1}{Q - \ln(\frac{100(1+2K_0)\sigma'_{vo}}{3P_a})} - D_R \tag{2.24}$$

$$a = 1267 + 636\alpha^2 - 634e^{\alpha} - 632e^{-\alpha} \leq 0.35 \tag{2.25}$$

$$b = \exp(-1.11 + 12.3\alpha^2 + 1.31\ln(\alpha + 0.0001)) \tag{2.26}$$

$$c = 0.138 + 0.126\alpha + 2.52\alpha^3 \tag{2.27}$$

Where Q is an empirical constant depending of state of soil, K_o is coefficient of earth pressure at rest and P_a is atmospheric pressure. Furthermore, K_α can be determined graphically as Seed et al. (2003) suggested (Figure 2.23).

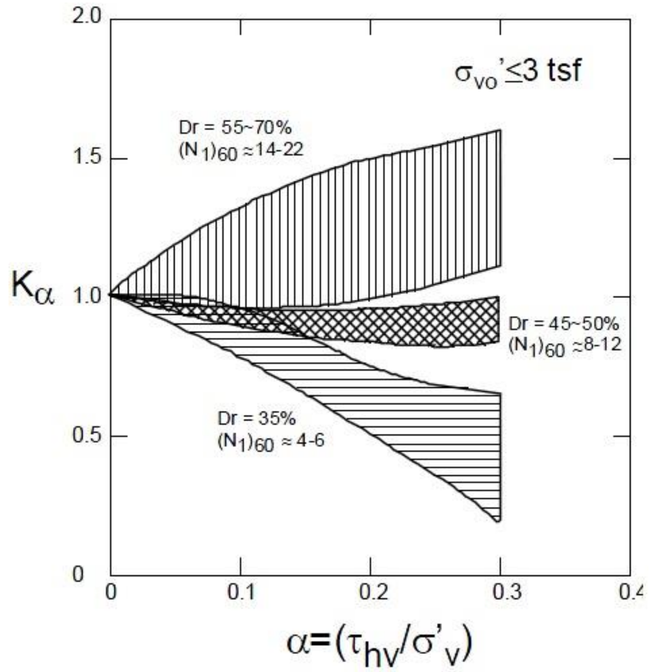

Figure 2.23 K_α values with respect to dimensionless α

2.5.1.5 Evaluation of Initiation of Liquefaction

Liquefaction potential can be evaluated after imposing of dynamic effect and determination of characterization of liquefaction resistance. Actually, in cyclic stress approach, any irregular stress history is expressed in terms of equivalent uniform cyclic stress and liquefaction resistance is also indicated by necessary uniform cyclic stress causing liquefaction having same number of cycles with loading representative cycles. Then, liquefaction potential can be assessed by comparing loading and resistance. Therefore, a factor of safety is defined as the ratio of mentioned two terms (NCEER, 1997):

$$FS = \frac{cyclic\ shear\ stress\ to\ lead\ liquefaction}{equivalent\ cyclic\ shear\ stress\ caused\ by\ earthquake} = \frac{CRR}{CSR} \qquad (2.28)$$

Prior to use Equation (2.28) in the evaluation of liquefaction initiation, it is crucial to apply mentioned corrections for CRR related with fines content, magnitude of earthquake, initial static shear stress and overburden pressure.

Although cyclic stress approach known as simplified method does not take occurrence of excess pore water pressure into account directly, its simplicity makes this method one of the most preferable methods (Ishihara, 1993). However, in most of cases, accuracy of this method is not controlled with results obtained from laboratory test (Kramer, 1996). Furthermore, factor of safety values obtained from Equation (2.28) which are greater than unity cannot guarantee that occurrence of excess pore water pressure is at an acceptable levels. As a result, in this study, results obtained from simplified method is also compared with effective stress approach.

2.6 Liquefaction Mitigation Methods

Strong ground motion can cause various seismically induced hazards. Also, severity of potential hazards may boost if soil indicates poor performance due to its own poor conditions during shaking. Inadequate strength, low stiffness or insufficient drainage may be possible causes for poor performance (Chen & Scawthorn, 2003). Among these hazards, liquefaction is very hazardous phenomenon for saturated cohesionless soils. Liquefaction can lead to excessive settlements caused by bearing capacity failure, lateral spreading and flow failure. Besides, for all types of structures comprising quay walls, bridges, levees and buildings, seismically induced liquefaction foundation deformations continues to be a major reason of damage (Dobry, 1996). Although most of remediation methods have evolved by trial and error approach, the logic behind selection of mitigating method is to improve at least one of the mentioned properties of soil. Also, with the help of mitigating method, possible liquefaction induced deformations have been intended to be eliminated. That is, structural liquefaction hazards such as vertical settlements up to 0.1 m and small lateral displacements lower than 0.3 m during shaking are accepted that liquefaction mitigation method works properly against liquefaction (Youd et al., 1997). However, based on acceptable level of damage and risk corresponding to structure type, performance criteria of liquefaction mitigating method may vary.

Countermeasures against liquefaction induced damage can be categorized into purpose of use, namely; densification, drainage, reinforcement, replacement including mixing (Martin & Lew, 1999). Also, such improvement methods have been used depending on soil type (Hausler & Sitar, 2001). Especially for sandy soil, decomposed granite and deposits used as fill material, many improvement methods were adopted to prevent liquefaction induced ground deformations (Figure 2.24 (a)). For such kind of soils, there have been several attempts to mitigate liquefaction by certain methods (Figure 2.24 (b)).

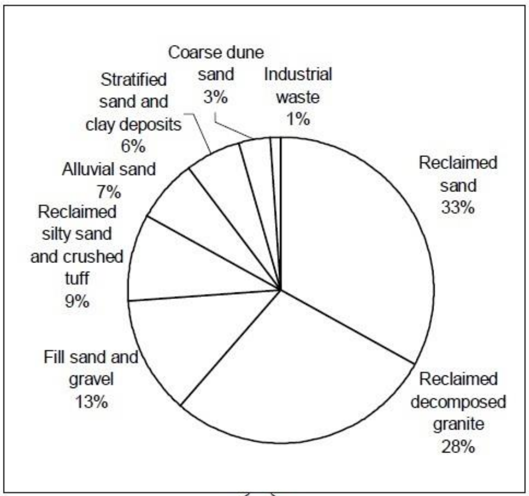

(a)

Method	Performance (Acceptable/ Unacceptable)	Average Increase in $N_{1,60}$
Densification through vibration and compaction		
Sand compaction piles	26 / 5	11
Deep dynamic compaction	15 / 0	5
Vibrorod/vibroflotation	11 / 6	13
Stone columns	7 / 1	8
Preloading	5 / 0	5
Compaction grouting	1 / 1	n/a
Timber displacement piles	1 / 0	n/a
Dissipation of excess pore water pressure		
Gravel drains	5 / 0	7
Sand drains	5 / 0	9
Wick or paper drains	2 / 0	n/a
Restraining effect through inclusions		
Deep soil mixing	4 / 1	n/a
Diaphragm walls	0 / 1	n/a
Stiffening through chemical or cement addition		
Jet grouting	5 / 0	n/a
Chemical grouting	1 / 0	n/a

(b)

Figure 2.24 Past case histories on liquefaction mitigation; (a) liquefied soil types (b) mitigation methods

Vibro-compaction/replacement and deep dynamic compaction methods are common mitigation methods applied in liquefiable soils with respect to densification purpose (Hayden & Baez, 1994). However, these methods resulted in intended outcomes provided that sand contained less than 10 percent fine grained particles passing No. 200 sieve. Also, among drainage methods, permanent dewatering was able to work satisfactorily against liquefaction (Mitchell, Cooke & Schaeffer, 1998). Use of gravel and prefabricated drains were failed to relief total excess pore water pressure and therefore, settlements more than predicted were observed. Jet grouting as a hardening (mixing) method prevented liquefaction-based settlement by treating full range of liquefiable soils (Schaefer, 1997; Martin, Olgun, Mitchell & Durgunoglu, 2004). Although jet grouting is complex method in terms of its own variables, it is more controllable and enables designer to interfere in operating parameters and as a result, treated zone properties. Also, according to Mitchell (2008), jet grouting can be applied to wide range of soil types (Figure 2.25)

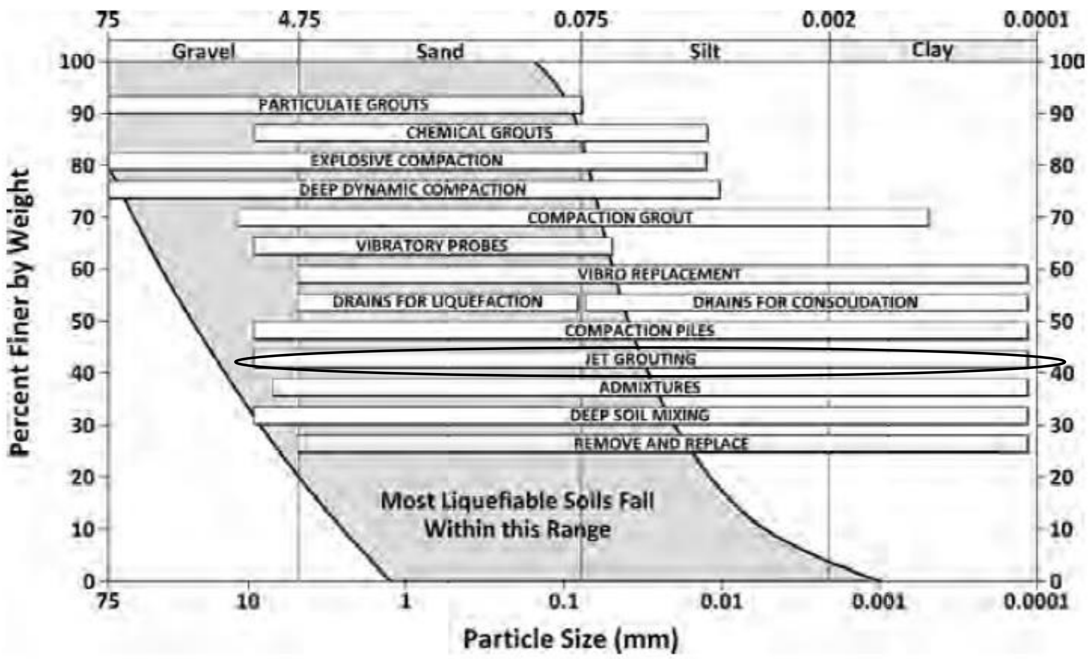

Figure 2.25 Various ground improvement method with respect to particle size

According to Liu & Dobry (1997), regardless of which type of soil improvement method is used, entire thickness of liquefiable zone should be treated in order to prevent effects of liquefaction (Figure 2.26).

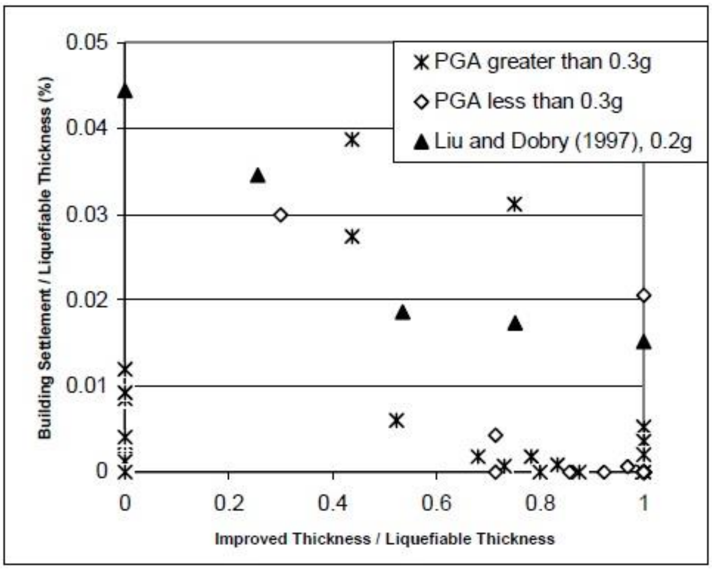

Figure 2.26 Effect of treatment depth as compared to liquefied zone

CHAPTER THREE
PAST STUDIES ON JET GROUT COLUMNS AND THEIR CONTRIBUTION ON LIQUEFACTION MITIGATION

3.1 Introduction

In this chapter, widely accepted studies related with jet grouting as a countermeasure against liquefaction are presented in a detailed manner. First, historical evaluation of jet grouting is briefly summarized. Then, modern jet grouting application methods are presented. Third, several important parameters in jet grouting are given and as a fourth topic, design issues of jet grout columns are provided. Fifth, jet grout column known as 'soilcrete' properties are expressed with respect to common engineering practice application. Finally, contribution of jet grout columns for liquefaction mitigation is stated by means of case studies and numerical analyses.

3.2 Historical Evaluation of Jet Grouting

In mining industry, with the realizing of scouring power of water, soil had been excavated in the Middle Age. Although jet grouting is patented in the 1960s in England (Nicholson, 1963), more sophisticated use of jet grouting was realized in Japan. Until the advent of modern jet grouting (Miki & Nikanishi, 1984), advances up to modern jet grouting method have continued in two distinct technological way emerging in the earliest of 1970s (Figure 3.1).

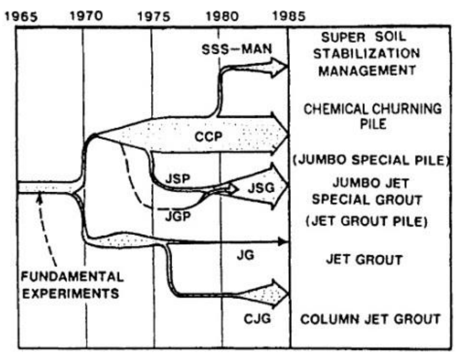

Figure 3.1 Evaluation of jet grouting

Actually, apart from cutting and eroding use, jet grouting was used to improve tightness by ejecting chemical-based slurry as jetting medium beneath of chemical disposal (Miki & Nikanishi, 1984). This technique which involves chemical jetting medium was called as ‘Chemical Churning Pile’ (CCP) (Nakanishi, 1974). In CCP method, injection was provided by nozzles having diameter of 1.2 to 2.0 mm which is located at the bottom of rotating drilling rod. However, cement based slurry took place of chemical mixtures due to environmental aspects. In 1973, CCP method was developed by adopting high pressure injection which is larger than 350 Bar and high flow rate that is in the range of 100 to 250 lt/min (Guatteri, Kauschinger, Dona & Perry, 1988). Besides, nozzle diameter was increased up to 2.4 mm. Likewise previous method, to obtain column diameters larger than 80 cm, compressed air started to be used around grout jet. With advent of that method in 1972 called ‘Jumbo Special Pile’ (JSP), column diameter was extended up to 200 cm.

In 1975, a more sophisticated method called as ‘Jet Grout’ (JG) emerged adopting the idea of using high speed water jet in only horizontal excavation before filling the eroded zone progressively. Also, mentioned idea was also developed in ‘Column Jet Grout’ (CJG) which is accepted as the modern jet grouting method with the use of rotating rods leading to high strength of soilcrete during withdrawal process. Until that day, panel jet grouting had been used causing low strength. In this method, pressurized air is also used as auxiliary fluid in order to increase eroding potential.

Finally, in 1980, ‘Super Soil Stabilization Management Method’ (SSS-MAN) was found which was accepted as the last advance according to Kauschinger and Welsh (1989). In that technique, the first step is drilling of pilot hole in reverse direction and then air pressurized water jet is lowered and soil is excavated by rotating injecting only water at very high pressure during withdrawal. Afterwards, with the help of sonic transducer, diameter of column is surveyed. If diameter does not fulfill the project requirements, extra jetting is performed until attaining required diameter. Finally, water filled hole is replaced with grout by means of tremie pipes. As technological advances have occurred (Bruce, 1988), anticipated column diameters have also increased (Table 3.1).

Table 3.1 Advances in jet grouting methods

Name	Principle of Operation	Jetting Pressure (MPa)	Jetting Nozzle Diameter (mm)	Rotation (rpm)	Anticipated Column Diamter (cm)	Notes
Jet Grout (JG)	Upper water and Lower grout jet	20	-	None	-	Panels Ony
Chemical Churning Pile (CCP)	Single Grout Jet	20-40	1.2-3.0	20	30-60	Chemicals now replaced by cement
Jumbo Special Grout (JSG)	Single jet of grout enveloped in air	20	3-3.2	6	80-200	-
Column Jet Grout (CJG)	Upper water and air jet and lower grout jet	40-50	1.8-3.0 (Upper) 3.0-5.0 (Lower)	5	150-300	Reffered as half replacement
Mini Max (MM)	Like CCP but uses special cement	20	1.2	20	80-160	Specially for very weak soil and organics
Jumbo Mini Max (JMM)	As for MM except for addition of 20-40 cm wing jet	20	1.2	20	200	Specially for very weak soil and organics
Super Soil Stabilization Management (SSS-Man)	Air water jet used to excavate volume completely under water, then, tremied full of desired material	20-60	2-2.8	3-7	200-400	Absolute control over shape, effective to over 70 m, completed replacement

In the late 1980s, dual jets in which eroding fluids collide with each other have started to be used in order to fulfill required quality. Although dual jet limits its own eroding capacity, it promises the exact required diameter regardless of type of soil (Figure 3.2).

Figure 3.2 Dual jets

3.3 Jet Grouting Methods

Simply, jet grouting is a soil improvement method which is the combination of two main stages, namely; eroding of soil and filling it with grout medium. Once drill string proceeds to intended depth, soil is eroded by high pressure fluid and then, water cement mixture known as 'grout' is poured at a high level of pressure from rotating rod during withdrawal of rods. As mentioned earlier, invention of rotating rods were crucial in the advancing process because it provides required strength to soilcrete which is one of the most important parameters with respect to design. Depending on the way how soil is eroded and grout process, there exits three jet ground methods, namely; single fluid, double fluid and triple fluid (Shibazaki, 1996). Although required equipment does not depend on type of method, the way how equipment is used, especially in eroding part of production of a soilcrete, is only the difference between these methods (Figure 3.3). In jet grouting process, cement used for grout is stored in cement bins placed at the site and its freshness should be preserved well. Grout is prepared at batching plant according to intended mixture ratio. After mixing of cement and mixture, grout is conveyed to high pressure pumps and then it is transmitted as high pressure grout to drill rig machine. Finally, this high pressure fluid is poured into soil and jet grout column is obtained (Lunardi, 1997).

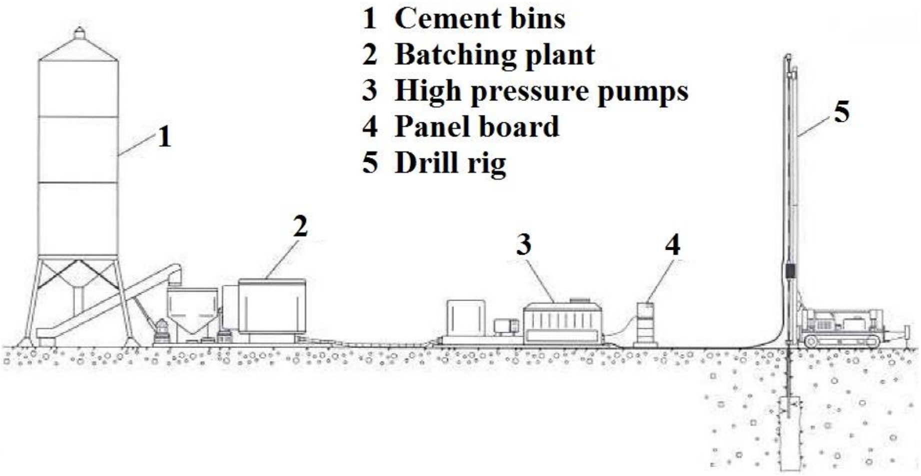

Figure 3.3 Jet grtouting equipment

3.3.1 Single Fluid Method (F1)

Single fluid method is the simplest form among three techniques which utilizes cement based fluid to erode and mix the soil (Lunardi, 1997). In other words, grout is utilized for both eroding and injection. However, especially below ground water level, heaving may occur. Also, due to the absence of auxiliary material such as air and water, required eroding diameter may not be attained under high level stresses (Figure 3.4 and Figure 3.5 (a)).

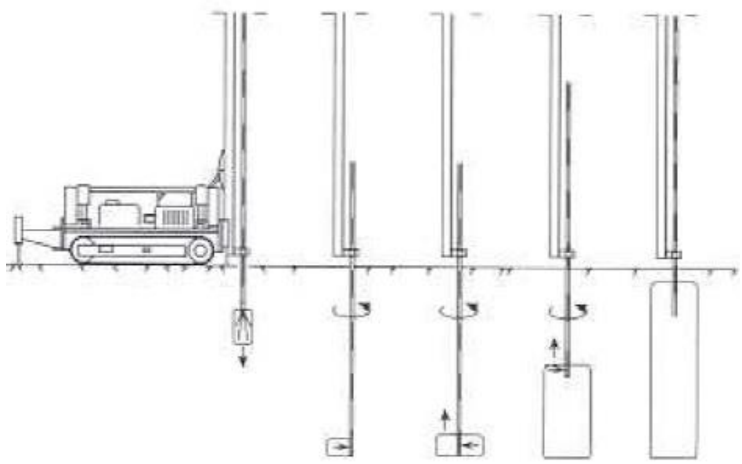

Figure 3.4 Single fluid method

3.3.2 Double Fluid Method (F2)

By adding compressed air into the single fluid method as auxiliary material, range of sphere of erosion can be increased especially for places under groundwater level (Figure 3.5 (b)). Function of air in this method is to create a buffer zone between groundwater and grout resulting in deeper penetration of grout and to prevent falling of eroded soil into grout which controls energy loss. However, there exists a possibility of grout loss to the surface due to rise of air content of grout. In case of encountering such a problem, ground improvement quality may decrease. In comparison to single fluid method, larger column diameter could be obtained (Lunardi, 1997).

3.3.3 Triple Fluid Method (F3)

In the triple fluid method, two nozzle groups at different levels which are employed for distint purposes, one group is responsible for eroding and other group is liable to grouting process. As compared to mentioned two methods, compressed air and jetting water are auxillary fluid in erosion process (Figure 3.5 (c)). Location of grouting nozzles are at approximately half meter below water-air jetting nozzle so as to make excavated soil particles transmitted to the surface which limits grout ejecting (Xanthakos, Abramson & Bruce, 1994). Although more erosion of soil than double fluid method can be achieved, triple fluid method promises both erosion and grout injection independent from each other which enables optimization of jetting parameters by providing more control in quality point of view (Lunardi, 1997).

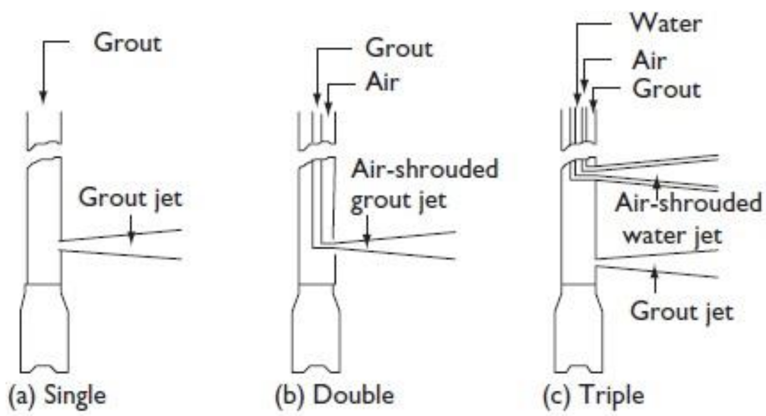

Figure 3.5 Jet grouting methods; (a) single fluid (b) double fluid (c) triple fluid

3.4 Operating Parameters in Jet Grouting

There are certain parameters that are fluid pressure, water/cement ratio, pull-out rate and rotational speed of drill rod in jet grouting process affecting soilcrete properties. Although determination of mentioned parameters have theoretical background, in site application, results obtained from field tests may not coincide with those found from calculations due to variability of soil properties.

3.4.1 Fluid Pressure

In order to erode soil, high pressure is required to obtain soilcrete column for a predetermined diameter. That is, if eroding fluid pressure is greater than the unconfined compressive strength of soil, large diameter jet grout columns are obtained (Spagnoli, 2008). Instead of using high pressure, same soilcrete diameter can be obtained by using low pressure eroding fluid with longer application time. However, such an application results in extension of construction time of jet grout columns which is an undesired situation with respect to loss of time and money. Operational pressure can be as high as up to 600 bar depending on pumping power.

Flow rate can be obtained by using law of energy conservation. Before calculating discharge at the nozzle, fluid velocity at the nozzle (V_n) is found:

$$V_n = m\sqrt{2gp_n} \tag{3.1}$$

Where m is efficiency of nozzle, g is gravitational acceleration and p_n is pressure at the nozzle. Due to physical restrictions, maximum efficiency of any nozzle is on the order of 0.9. Also, with the help of continuum law, discharge at the nozzle can be obtained:

$$Q_n = V_n A_n \tag{3.2}$$

Where A_n is the area of nozzle.

3.4.2 Nozzle Effect

Both number and diameter of nozzles influence jet grouting process with respect to soilcrete diameter. Amount of grout injected to ground, as a result of that, rate of treatment strictly depends on them. However, in order to maintain high pressure, high power pumps are needed to attain high flow rates. Enlarging nozzle diameter provides better efficiency as compared to increasing of number of nozzles while delivered grout volume is kept constant (Lunardi, 1997). As number of nozzles increases, efficiency starts to drop because of high head loss. In case of low power injection pump, limiting number of nozzles by increasing size of nozzle diameter is a common practice in jet grouting. Besides, shape of nozzle is an important factor from efficiency point of view. That is, high pressure can be obtained by using narrower angles according to Shibazaki (2003). Also, additional straight portion after narrowed transition zone increases utilization of benefit of high pressure in wide area (Figure 3.6).

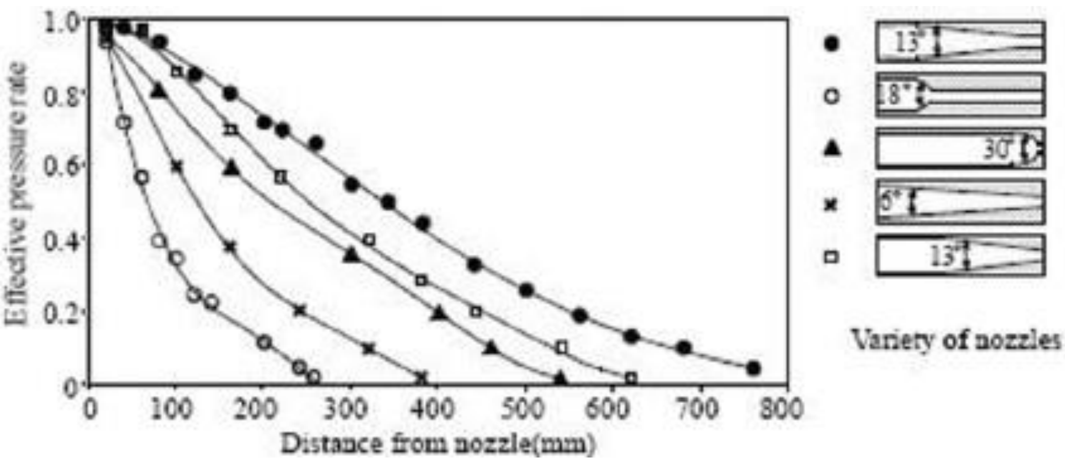

Figure 3.6 Effect of narrowing angle of nozzle

3.4.3 Water/Cement Ratio (w/c)

Water/cement ratio is crucial with respect to mechanical properties of soilcrete. That is, uniaxial compressive strength of soilcrete is a function of soil-grout mixture. Besides, in order to attain proper workability of grout, w/c ratio should not be high. In other words, according to Littlejohn (1982), by using low water/cement ratio, negative effects of bleeding and viscosity decreases (Figure 3.7). In engineering practice, this ratio is less than three (Bruce, 2002). Moreover, the ratio even lower than unity should be adopted if prime concern is strength.

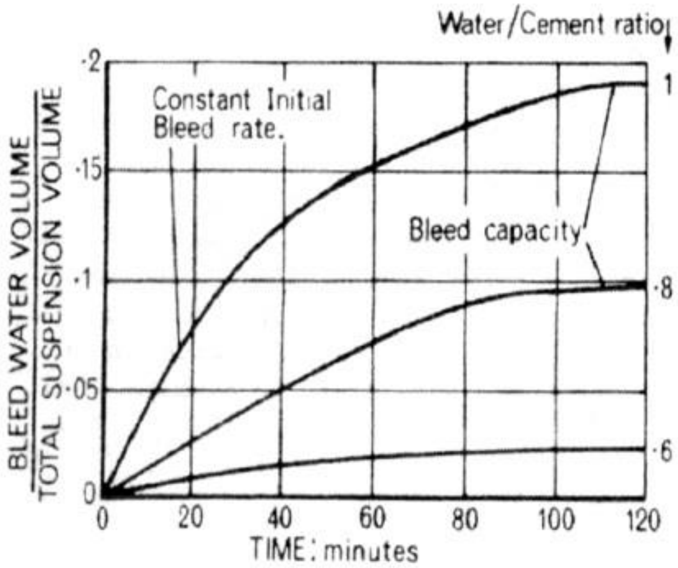

Figure 3.7 Effect of water/cement ratio on bleeding

3.4.4 Pull-out Rate and Angular Velocity of Drill Rod

In jet grouting, there exist two methods for the way the drill rod is lifted (Figure 3.8).

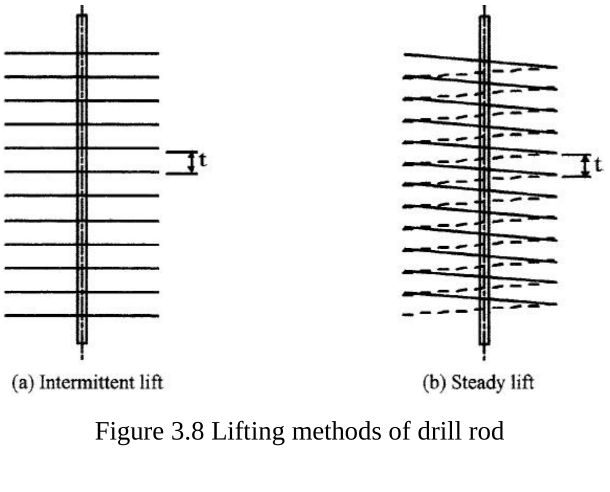

Figure 3.8 Lifting methods of drill rod

Although intermittent lift method in which drill rod is lifted with constant time interval enables how much rotation of drill rod is necessary to compute by means of integration of unit flow rate over the lifting thickness at that time step, required rotation cannot be obtained in an exact way in steady lift method. Therefore, it is possible to obtain required diameter for each step. Although soil properties and as a result of that computed thickness varies, as engineering practice, optimum lifting thickness is obtained by means of many trial and error method. That is, 5 cm lifting interval is accepted as optimum for those columns diameter of whom is less than 2 m. As intended diameter rises up, lifting interval becomes larger. Nonetheless, in case of very low extraction speed, desired diameter may not be obtained due to accumulation of grout along outer surface of drill rod.

Angular velocity of drill rod is another factor affecting soilcrete diameter. Due to the fact that angular velocity and pull-out rate is interrelated parameters, optimization of these parameters (Moseley & Kirsch, 2004) is computed according to Equation (3.3):

$$D = KP^{\alpha}Q^{\beta}N^{\lambda}V_n^{\delta} \tag{3.3}$$

Where D is soilcrete diameter, P is pressure of fluid, Q is flow rate, N is angular speed, V_n is pull-out rate and remaining exponential terms are constants. Likewise pull-out rate, there exists a lower limit for angular velocity in order to prevent reflection of grout from disturbed soil. Also, according to Shibazaki (1996), an increase in angular velocity rises up soilcrete diameter (Figure 3.9).

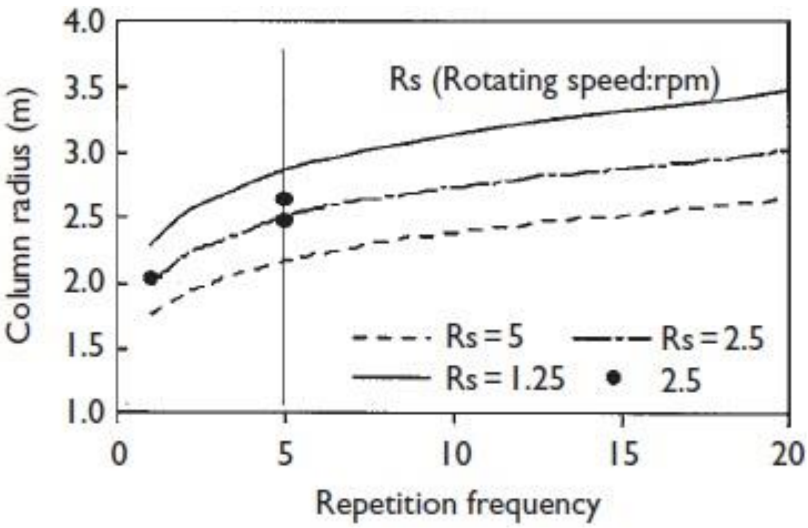

Figure 3.9 Effect of angular velocity on soilcrete diameter

3.4.5 Operating Parameters and Corresponding Properties with respect to Jet Grouting Methods

Depending on jet grouting method, operating parameters varies. Six parameters are enough for single fluid method, namely; fluid pressure, number of nozzles and corresponding diameter, water/cement ratio, pull-out rate and angular velocity of drill rod (Kauschinger & Welsh, 1989). In case of double fluid method, in addition to F1, air pressure and delivery rate parameters are needed. Apart from parameters used in F2, water pressure, number of nozzle and its size are additional parameters in F3 (Table 3.2).

Table 3.2 Operating parameters with respect to jet grouting methods

Jetting Parameter	F1	F2	F3
Injection Pressure			
Water jet (MPa)	-	-	30-55
Grout jet (MPa)	30-55	30-55	1-4
Compressed air (MPa)	-	0.7-1.7	0.7-1.7
Flow Rates			
Water jet (lt/min)	-	-	70-100
Grout jet (lt/min)	60-150	100-150	150-250
Compressed air (m^3/min)	Not used	1-3	1-3
Nozzle Sizes			
Water Jet	-	-	1.8-2.6
Grout Jet	1.8-3.0	2.4-3.4	3.5-6
Number of water jets	-	-	1-2
Number of water jets	2-6	1-2	1
Cement Grout W-C Ratio		0.8-1 to 2-1	
Cement consumption (kg/m^3)	400-1000	150-550	150-650
Rod Rotation Speed (rpm)	10-30	10-30	3-8
Lifting Speed (min/m)	3-8	3-10	10-25
Column Diameter			
Coarse-grained soil (m)	0.5-1.0	1-2	1.5-3
Fine-grained soil (m)	0.4-0.8	1-15	1-2
Soilcrete Strength			
Sandy soil (MPa)	10-30	7.5-15	10-20
Clayey soil (MPa)	1.5-10	1.5-5	1.5-7.5

Among mentioned methods, F1 is considered as both the simplest and straightforward method. The why such an acceptance is made is due to its usage for not only cutting but also mixing the soil. On the other hand, for double and triple fluid methods, air is utilized as auxiliary in cutting process. Although preferring those two methods provide advantage in obtaining larger diameter, air lifting efficiency may drop as jetting direction is rotated from vertical to horizontal with respect to ground level. Therefore, single fluid method is slightly more advantageous than other techniques for horizontal jet grouting. Also, according to Kauschinger et al. (1992), certain degree of compaction of soil which covers a distance equal to half diameter around outside of perimeter of jet grout column could be obtained. Moreover, by means of F1, columns having diameter in the range of 50 to 120 cm for sand and 40 to 60 cm for cohesive soil could be obtained. Besides, the stiffest column could be obtained by F1 as compared to other columns obtained from remaining two methods which have same cement dosage with single fluid method. Power of the pump and permitted flow rate are the factors limiting single fluid method.

In F2, compressed air as an auxiliary cutting power is utilized that enables column diameter to be obtained as twice as the diameter which could be obtained by single fluid method. Actually, the effect of compressed air is mainly due to the fact that air forms buffer zone between groundwater and jetting medium thereby enabling deeper penetration. Moreover, this effect can be extended by prevention of cutting from falling soil particles into jetting medium which diminishes loss of energy. On the contrary to benefits of this method, due to high air content, jet grout columns have relatively lower strength. Furthermore, using annulus that conducts air flow between grout carrying pipes and outer rod make both operation and system more complex. Despite mentioned drawbacks, this technique permits working with lower grouting pressure that reduces wearing effect on grout pump (Guatteri, Kauschinger, Dona & Perry, 1988).

F3 is regarded as the most complicated method. Although rate of constructing a jet grout column is the slowest among all methods, the largest column diameter can be attained by using this method due to its ability to totally replace soil with jetting medium. In order to obtain maximum benefit from this method from diameter point of view (Tornaghi & Perelli, 1985), location of air-water jet nozzle should be at the upper part of the monitor (Figure 3.10). That is, it should be located above point of grout injection. As Parry-Davies, Bruin, Wardle & Nixon (1992) stated that the most efficient use of this technique for sandy-gravelly soil can be attained by orienting air-water nozzle having gap equal to 180^0 between itself and grout nozzle location of which is at 150 mm below from air-water nozzle in vertical direction.

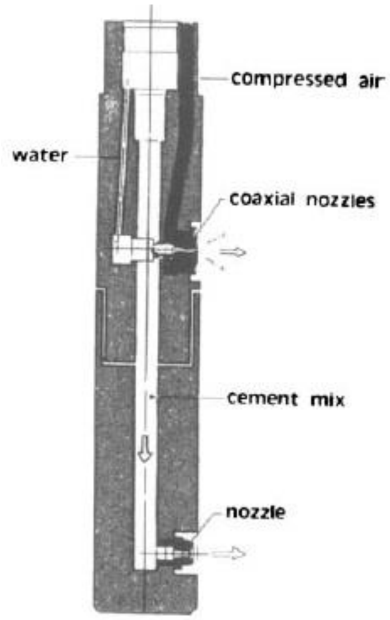

Figure 3.10 Monitor of F3

After advances in mentioned methods, according to Wang, Shen, Ho & Kim (2013), widely accepted parameters were determined (Table 3.3).

Table 3.3 Widely accepted operating parameters after advances in jet grouting

Parameters	**F1**	**F2**	**F3**
Water Pressure (MPa)	-	-	30-40
Flow Rate of Water (lt/min)	-	-	80-200
Number of Nozzles	-	-	1-2
Nozzle Diameter (mm)	-	-	1.5-3
Air Pressure (MPa)	-	0.7-1.5	0.7-1.5
Flow Rate of Air (m^3/min)	-	8-30	4-15
Grout Pressure (MPa)	40-70	30-70	7-10
Flow Rate of Grout (lt/min)	100-300	100-600	120-200
Grout Density (g/m^3)	1.25-1.6	1.28-1.8	1.5-2
Number of Nozzles	1-6	1-2	1-3
Nozzle Diameter (mm)	1-4	2-7	5-10
Withdrawal Rate (cm/min)	15-100	10-30	6-15
Rotation Speed (rpm)	7-20	2-20	7-15

3.4.6 Design Aspects of Operating Parameters

Before starting to obtain operational parameters, preliminary work should be performed. Due to the interdependency of those parameters, soilcrete properties may vary significantly. As a first step for preliminary work, classification tests in order to identify the soil with respect to grain size distribution, bulk density, water content and Atterberg limits (for cohesive soil) should be performed. Also, soil relative density should be estimated from available SPT or CPT data. Then, by taking both theoretical and practical aspects into account, initial parameters can be computed. Moreover, trial jet grout columns should be constructed and tested. After completion of mentioned steps, by making proper corrections, final parameters should be obtained (Xanthakos & Abramson, 1994).

3.4.6.1 Determination of Proper Grout

In order to attain large diameter, viscosity and rigidity are driving factors with respect to rheology. If viscosity of grout is low enough, it is possible to treat large area. However, for strength concerns, water/cement ratio should be in the range of 0.6 and 1.2. In the determination of w/c ratio, permeability, water content of soil and particle size distribution have major role. That is, soilcrete has relatively lower strength if soil is highly permeable due to leakage of grout. However, by adding certain amount of bentonite which is up to 5 percent by weight during drilling, loss of grout is decreased; however, it causes reduction in strength. Nonetheless, very low permeability values cause also undesired outcomes with respect to strength point of view. The reason for that is poor drainage of water from grout leading to high water content and therefore, low stiffness (Shibazaki, 2003).

3.4.6.2 Effect of Soil Types on Estimation of Operating Parameters and Soilcrete Diameter

In radial jet grouting, flow rate, pressure and pull-out rate are important parameters which determine how much energy is required. Also, regardless of soil type, energy dissipation as moving away from the nozzle increases exponentially (Miki & Nakanishi, 1984). Therefore, eroding fluid pressure diminishes along jet axis (Figure 3.11). Also, as it is shown in Figure (3.11), air coupling effect significantly reduces energy loss. Apart from that, in case of large particle size, due to reflection of eroding fluid, additional energy loss takes place affecting directly shape of jet grout column.

Moreover, cohesive soils due to cohesion result in more energy loss via damping (Melegary & Garassino, 1997).

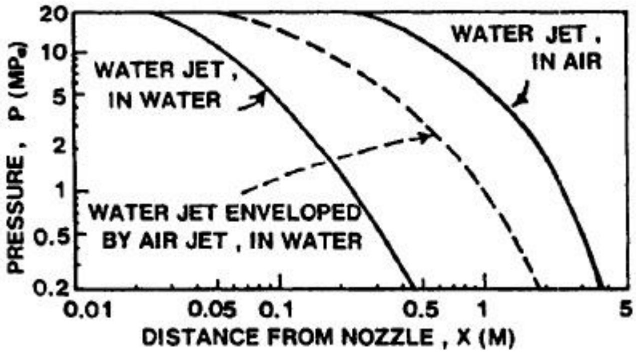

Figure 3.11 Pressure decrease along jet axis

Computed jet grout column diameter may not be obtained due to energy absorbance of soil during construction. That is, due to damping of relatively dense grout/soil mixture, theoretical value of diameter is not entirely compatible in real value of it. Also, mentioned absorbance varies from any type of soil to another Croce & Flora, 2000; Burke, 2004). Furthermore, jet grouting methods end up different diameter even if all parameters are kept constant (Figure 3.12)

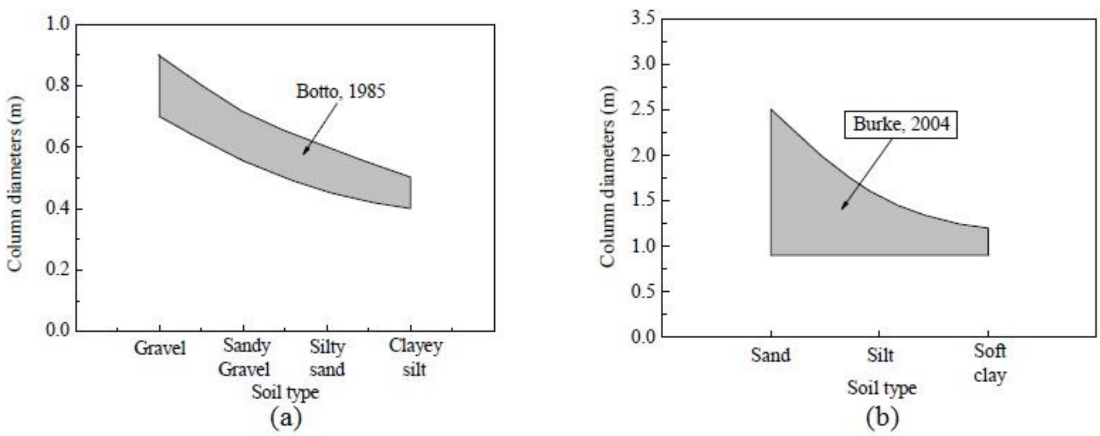

Figure 3.12 Possible column diameters with respect to soil type; (a) F1 (b) F3

Pull-out rate which is also defined as the time being exposed to grouting has also an influence on soilcrete diameter. Column diameter can be increased by extending time of lifting of drill rod with an increasing in grouting pressure (Figure 3.13 (a)).

Also, as density of soil increases, pull-out rate should be decreased according to Yahiro and Yoshida (1973) (Figure 3.13 (b)).

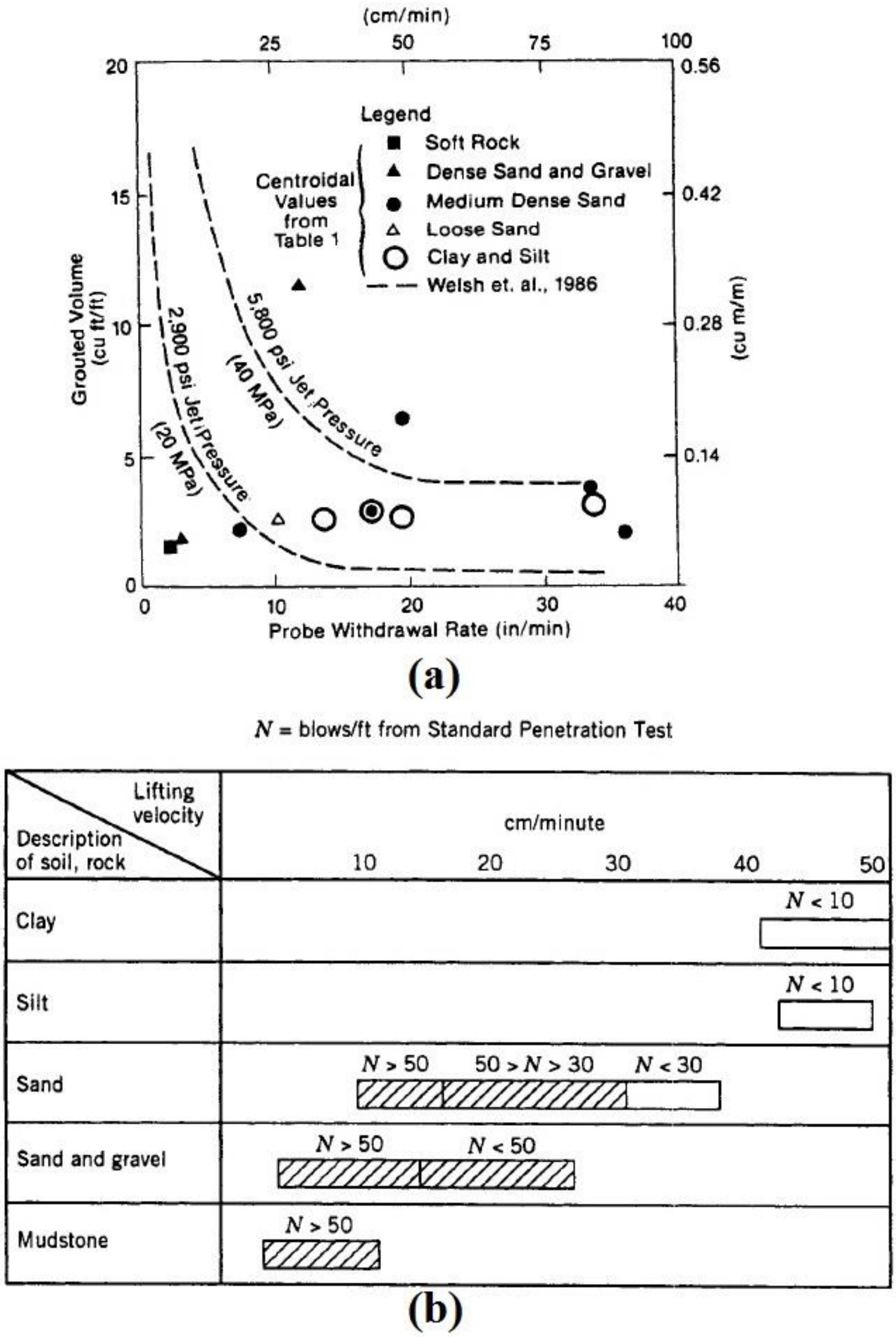

Figure 3.13 Effect of soil type on pull-out rate; (a) withdrawal rate-grout volume relation (b) stiffness-soil type-pull-out rate relation

In design of jet grout column (Wang, Shen, Ho & Kim, 2013), diameter can be computed based on either theoretical approaches or empirical relations in accordance with determined parameters (Table 3.4). However, findings should be controlled with trial jet grout columns in the site and therefore, these equations should also be calibrated.

Table 3.4 Widely accepted methods for estimation of jet grout column diameter

Methods	Equations	References
Empirical Approach	$D_0 = kp_g^{k1}Q_g^{k2}N^{k3}V_m^{k4}$	Shibazaki (2003)
	$D_0 = n_1\left(\frac{p_gQ_g}{v_s}\right)^{n2}$	Mihalis et al. (2004)
Theoretical Approach	$D_0 = 2\int_0^{t_0} V_c t dt$	Modoni et al. (2006)
	$D_0 = 12.5d_0\sqrt{\frac{p_g - p_0}{q_{bu}}} + D_r$	Ho (2007)

In empirical approach, column diameter computation is made based on grout pressure (p_g), flow rate (Q_g), N is number of passes of jet and horizontal tangential velocity of nozzle (V_m), pull-out rate (v_s) by neglecting which type of method is used including nozzle diameter and auxiliary fluid pressure. On the contrary to empirical approach, penetration rate of fluid jet in soil (V_c), duration of action of the jet in soil (t), grout pressure (p_g), pressure at nozzle outlet (p_0), nozzle diameter (d_0), ultimate soil bearing resistance (q_{bu}) and diameter of monitor (D_r) are variables in theoretical approach. Hence, Welsh, Rubright & Coomber (1986) have summarized relationship between type of soil and soilcrete characteristics:

- Grout, water and air pressures and pull-out or withdrawal rate are most influencing parameters with respect to volume of grout injected to soil.
- Volume of grout decreases as clay content increases. Therefore, in case of encountering such a problem, either withdrawal rate should be decreased or grout pressure should be increased.
- By using typical grout or water pressures, produced column diameter may not exceed 1.5 m in stiff to hard clays.
- If coefficient of uniformity (D_{60}/D_{10}) is greater than 8, effect of grain size distribution on jet grout column diameter starts to decrease.

- Up to 3 m diameter can be obtained if coefficient of uniformity is less than 8.
- If gravel or larger particle amount is greater than 50 percent, pressure should be lowered in order to obtain uniform column.

As a concluding remark, there have been significant debate on the design of nozzle in order to achieve more efficiency with respect to eroding of soil. However, suggestion of Kauschinger & Welsh (1989) that diameter of nozzle is 2 mm and optimum w/c is unity has been widely used (Lunardi, 1997).

3.5 Mechanical Properties of Jet Grout Columns

Jet grouting can be applied regardless of grain size, permeability, density and soil type by calibrating operating parameters. There exists only few case such as very stiff cohesive soil and very large particle size where jet grouting cannot provides intended properties. While smoother outer surface can be obtained with this method in fine grained soil, it enables irregular shaped soilcrete column to occur. Therefore, desired diameter should be controlled in the site. Although soilcrete diameter is an important parameter, apart from it, mechanical properties of soilcrete column are also crucial for whatever purpose jet grouting is used. Mechanical properties of jet grout column consist of unconfined compression strength, shear strength, tensile strength and modulus of elasticity.

3.5.1 Unconfined Compressive Strength (UCS)

Stiffness of soilcrete column is generally expressed in terms of unconfined compressive strength (Moseley & Kirsch, 2004). Compressive shear strength of jet grout column is directly influenced by water/cement ratio and gradation of soil. While maximum strength can be attained for sandy or gravelly soil on the order of 40-50 MPa, it decreases significantly in case of fine grained soil. Besides, as water/cement ratio decreases, strength of jet grout column rises up. Therefore, according to (Kauschinger, Hankour and Perry, 1992), low strength values in the construction of jet grout column in fine grained soils can be forced to increase by using lower values of w/c (Figure 3.14).

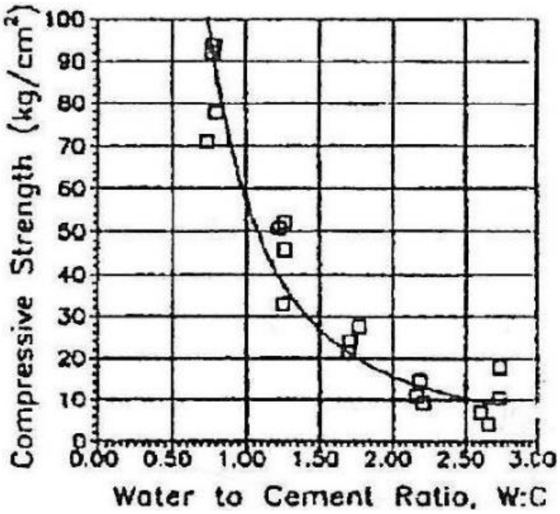

Figure 3.14 UCS with repect to w/c for clayey soil

Kauschinger, Hankour & Perry (1992) proposed an exponential function in order to relate w/c with respect to UCS:

$$wcr = \frac{\sqrt{f_c}}{7.4} \tag{3.4}$$

Where wcr is water cement ratio and f_c is unconfined compressive strength in kg/cm^2. Furthermore, Stoel (2001) was able to compute compressive strength in terms of w/c by modifying Equation (3.4) for Amsterdam sand and clay layers:

$$f_c = 7 + 8.1(wcr)^2\ (MPa)\ for\ sandy\ soil \tag{3.5}$$

$$f_c = 2 + 3.6(wcr)^2\ (MPa)\ for\ clayey\ soil \tag{3.6}$$

Where wcr is water cement ratio and f_c is compressive strength in MPa. Apart from these empirical relations, several researchers have tried to determine boundaries of UCS in accordance with all types of soil (Table 3.5).

Table 3.5 UCS with respect soil type

Soil Type	Unconfined Compressive Strength of Jet Grout Column (MPa)						
	Miki (1985)	Bell (1993)	Fang et al. (1994)	Lunardi (1997)	Stoel (2001)	Shibazaki (2003)	Okmen (2003)
Gravel		5~30		12~20	10~40		
Sand	5~10	5~25	5~21	12~20	10~40	30	5~3
Silt		4~18		4~14	5~15		
Clay	<5	0.5~8	2~10	2~6	3~7	10	1~5

The Japan Jet Grouting Association (1986) determined standard safe values for UCS values in jet grouting design water cement ratio of which is unity (Table 3.6).

Table 3.6 Standard strength values in jet grouting design

Soil Type	Unconfined Compressive Strength (MPa)	Cohesion (MPa)	Bond Strength (MPa)	Bending Tensile Strength (MPa)
Cohesive	1	0.3	0.1	0.2
Granular	3	0.5	0.17	0.33

3.5.2 Shear Strength

Shear strength of soilcrete column can be determined by triaxial tests. Also, shear strength is a function of cohesion intercept (c), drained angle of friction (φ) and effective normal stress according to Mohr-Coulomb failure criteria. Thus, Nishimatsu (1972) was able to obtain cohesion parameter of soilcrete with the following equation:

$$c = \frac{q_u q_t}{2[q_t(q_u - 3q_t)]^{0.5}} \tag{3.7}$$

Where q_u is unconfined compressive strength and q_t is tensile strength. Moreover, angle of friction of jet grout column can be obtained:

$$tg\varphi = \frac{q_u^2 - 4c^2}{4q_u c} \tag{3.8}$$

Where q_u is unconfined compressive strength and c is cohesion intercept. However, in Equation (3.8), unrealistically high values of angle of friction may be computed if UCS value is very low.

3.5.3 Tensile Strength

With the help of Brazilian Split Test (BST), tensile strength of soilcrete column can be found. However, BST slightly overestimates actual strength of jet grout column on the order of 10% according to Neville (1997). Based on findings of Neville, Stoel was able to express tensile strength (f_{ct}) based on unconfined compressive strength:

$$f_{ct} = 0.3(f_c)^{3/5}\ (MPa)\ for\ jet\ grouting\ in\ sandy\ soil \tag{3.9}$$

$$f_{ct} = 0.4(f_c)^{3/10}\ (MPa)\ for\ jet\ grouting\ in\ clayey\ soil \tag{3.10}$$

Also, tensile strength is in the range of 8% to 14% of unconfined compressive strength of soilcrete column (Bruce & Bruce, 2003).

3.5.4 Modulus of Elasticity

Elastic modulus can also be obtained via UCS. Trevi (1994) represented that elastic modulus becomes larger as UCS increases (Figure 3.15).

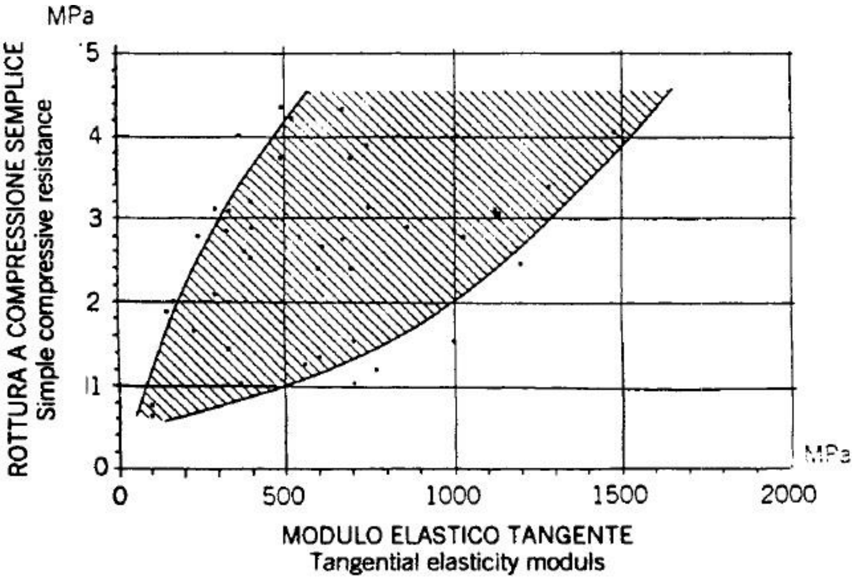

Figure 3.15 Modulus of elasticity-unconfined compressive strength relationship

Moreover, the Japan Jet Grouting Association (1986) suggested the secant modulus of elasticity modulus is in the range of $100q_u$ to $300q_u$. Stoel (2001) developed an empirical formula in prediction of elastic modulus based on UCS:

$$E_{cm} = 800(f_c)^{1/2} \ (MPa) \ for \ jet \ grouting \ in \ sandy \ soil \tag{3.11}$$

$$E_{cm} = 500(f_c)^{2/3} \ (MPa) \ for \ jet \ grouting \ in \ clayey \ soil \tag{3.12}$$

The term 'deformability' which is the ratio of secant modulus of elasticity to strength (E/R) is a highly variable term based on soil type. While this term is around 300 for cohesive soil, it rises to even higher than 900 for non-cohesive soil (Lunardi, 1997). Moreover, Durgunoglu et al. (2004) presented possible soilcrete column deformability ratios for each type of soil (Table 3.7).

Table 3.7 Deformability ratios for different soil types

Soil Type	**Unconfined Compressive Strength (MPa)**	**Deformability Ratio**
Gravel	12~18	900
Sand	7~14	600
Silt	3~7	200
Clay	2~5	150

3.6 Past Studies and Case Analyses on Effectiveness of Jet Grout Column as a Mitigation Method

Although jet grouting is simple method in application due to automatically performed steps that are drilling and grouting, it has become widely preferred method after 1999 Kocaeli Earthquake (Unutmaz, 2012). Its effectiveness against liquefaction have been verified both case analyses and numerical methods. Also, how much improvement is obtained via jet grout columns were tried to express by few study.

3.6.1 Case Histories

In 1999, Kocaeli Earthquake having magnitude of 7.4 struck northwestern Turkey. Peak ground acceleration (PGA) was in the range of 0.1g to 0.42g at the sites where they were located from 0 to 35 km from the fault rupture (Durgunoglu, Emrem, Karadayılar, Mitchell, Martin & Olgun, 2001). In this earthquake, significant damage varying from structural to foundation-related were detected. Besides, it was observed that loose to medium sand layer had been liquefied in İzmit City. Moreover, liquefaction related settlements including differential type leading to tilting of structure and sand boiling were explored in this city (Figure 3.16).

Figure 3.16 Liquefaction related damage in İzmit City after 1999 Kocaeli Earthquake; (a) tilted structure (b) sand boiling

However, there was no trace of liquefaction related damage at the site, namely; Carrefour Shopping Center and İpekkagit Tissue Factory where soil had been improved by means of jet grout columns (Figure 3.17).

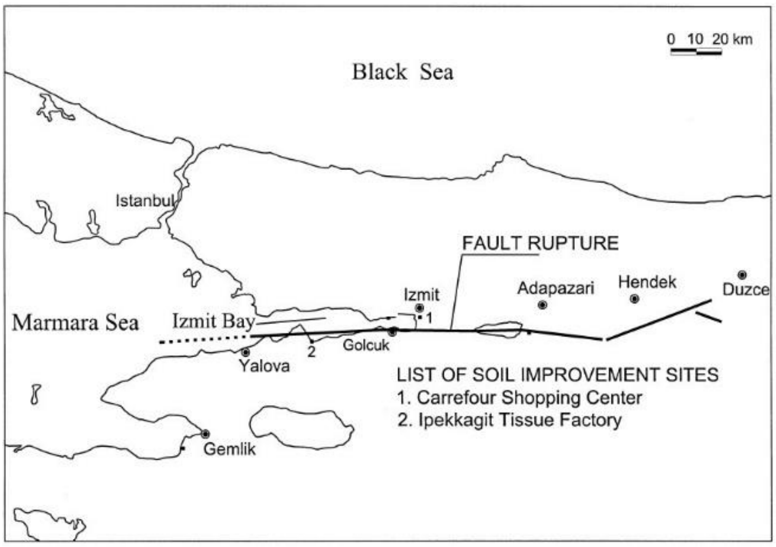

Figure 3.17 Sites treated by means of jet grouting

3.6.1.1 Carrefoursa Shopping Center

Durgunoglu et al. (2001) tried to investigate effectiveness of jet grout columns as liquefaction mitigation according to case study based on 1999 Kocaeli Earthquake. In this case, jet grout columns were able to prevent liquefaction-related settlement of Carrefoursa Shopping Center. This complex consists of shopping center and two-storey parking garage (Figure 3.18 (a)). Foundation of lot C was designed as shallow foundation. Foundation of section A and parking structure were designed for spread footings connected with tie beams while section B were of mat foundation. Entire structure were placed on jet grout columns. Also, parking garage was preloaded with 3 m thick sandy fill and wick drains were placed so as to accelerate anticipated consolidation of clayey layer due to preloading (Figure 3.18 (a)).

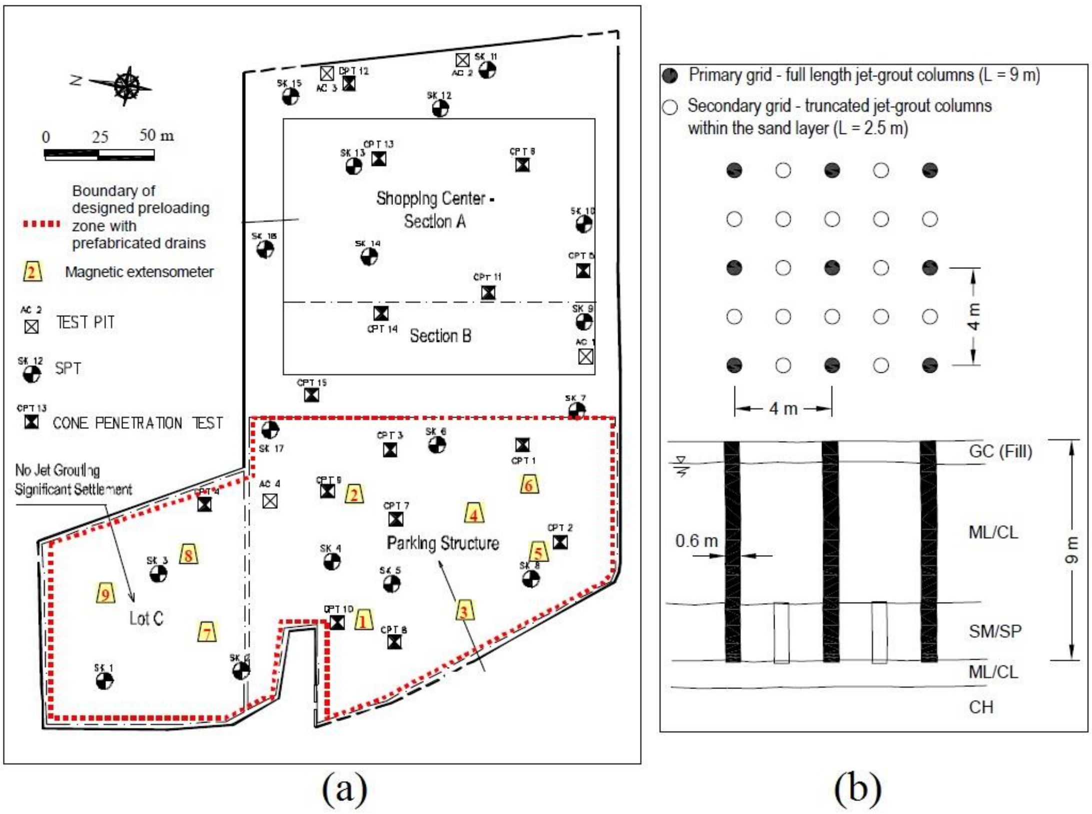

Figure 3.18 General information about structure; (a) layout of the structure (b) jet grout disposition

In determination of liquefaction initiation prior to the earthquake, updated simplified method (Idriss, 1998) was used with design PGA of 0.5g although PGA was recorded as 0.2g at this structure during the earthquake. Therefore, it was indicated that 3 m sand layer (SP-SM) was under high potential of liquefaction. In other words, the soil layer having friction ratio (R_f) lower than 1% and tip resistance (Q_c) lower than 15 MPa was considered as liquefiable (Figure 3.19).

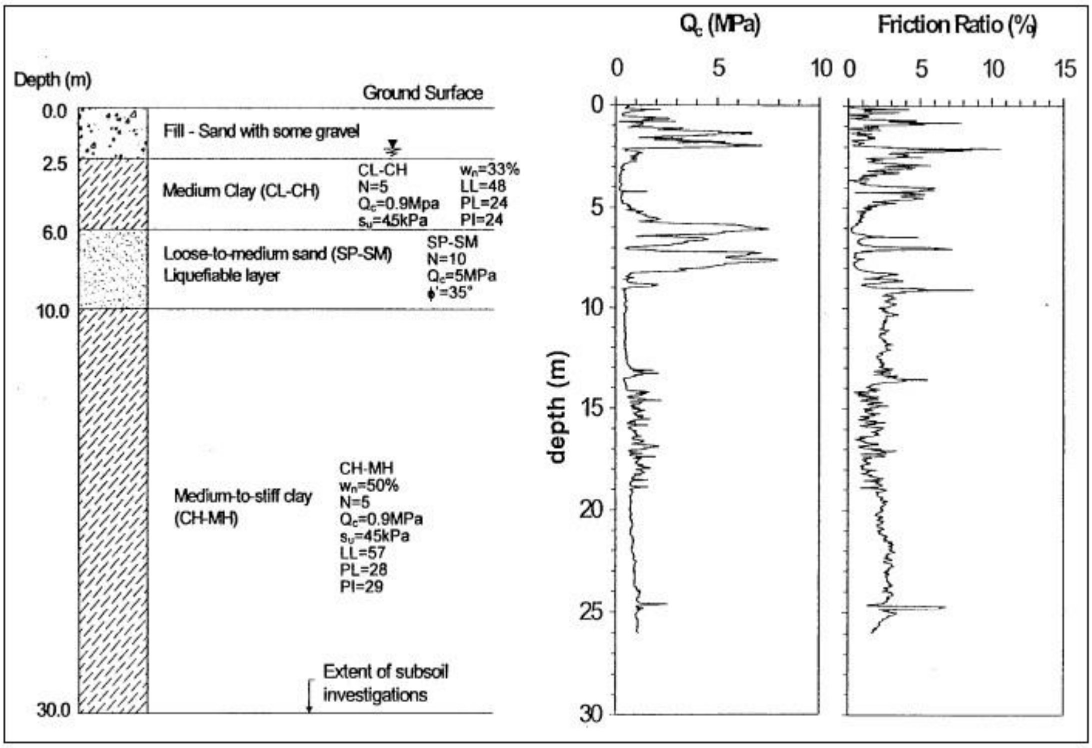

Figure 3.19 Idealized soil profile and corresponding CPT values

Although jet grout columns having diameter of 60 cm were designed to mitigate liquefaction, they were also used for extra bearing support. In this project, two groups of jet grout columns were planned to be used, namely; primary and secondary columns (Figure 3.18 (b)). For entire structure, spacing between adjacent primary jet grout columns were 4 m and secondary jet grout columns were of 2 m spacing. That is, area replacement ratio (a_r) is approximately 7% at sandy soil layer. Moreover, jet grouting parameters and UCS is indicated in Table (3.8).

Table 3.8 Jet grouting parameters

Jet Grout System	Number of Nozzles	Nozzle Size (mm)	Pull-out Rate (cm/min)	Angular Velocity (rpm)	Grout Pressure (Bar)	W/C	28 days UCS (MPa)
F1	2	2	50	20	450	1/1	4.8

Prior to earthquake, soil improvement was completed except lot C. Also, shopping center construction was finished. After earthquake, liquefaction induced settlements in lot C was verified by magnetic extensometers while there was no structural damage and settlement at shopping center (Figure 3.20). In this figure, anchor 2 represents settlements at 3.5 m depth and anchor 3 indicates settlement at 11 m depth.

Approximately, liquefaction induced settlement of liquefied sandy layer was obtained between 4.0 cm and 4.5 cm corresponding to 3.3% volumetric strain. This average settlement of 4.2 cm was compared with empirical approaches of Tokimatsu & Seed (1987) resulting in 4.6 cm and Ishihara (1993) ending up 4.8 cm for this case. To conclude, liquefaction-based settlements occurred at untreated lot C while no damage and settlement were observed at treated parts. However, the mechanism behind how these columns mitigated liquefaction has not been identified.

Although liquefaction occurred at this site, no sand boiling was observed. The reason for that is both stratified soil profile and presence of cohesive layers at the top the profile. Also, sand boiling occurs where excess pore water pressure becomes extremely high values as compared to effective overburden stress.

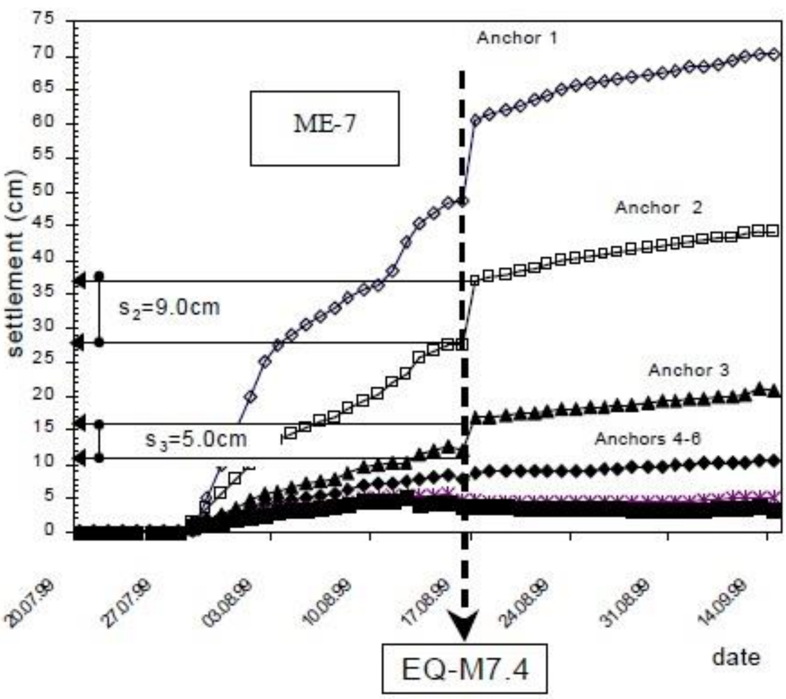

Figure 3.20 Settlement at lot C after earthquake

3.6.1.2 İpekkağıt Tissue Factory

Durgunoglu et al. (2004) studied overall performance of jet grout columns that prevent occurrence of liquefaction at İpekkağıt Tissue Factory during 1999 Kocaeli Earthquake. This complex structure is located 4 km south of main fault rupture (Figure 3.17). This complex contains machine buildings, water tanks, storage buildings and multi-purpose buildings (Figure 3.21 (a)). Prior to earthquake, Paper Machine Building (PM3) was not completed although construction of water tanks had been finished. Also, site consists of stratified soil layers where ground water level is 2 m below the ground surface (Figure 3.21 (b)).

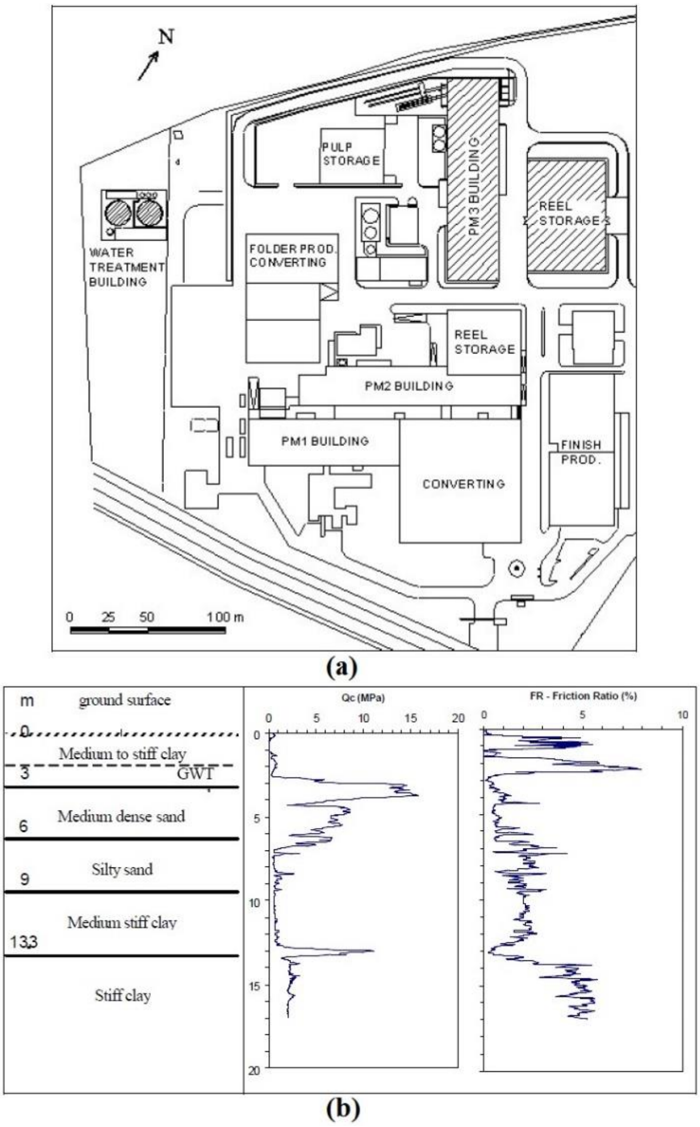

Figure 3.21 General information; (a) layout of factory (b) idealized soil profile with CPT values

Jet grouting was applied to beneath of PM3 building, water tanks and reel storage buildings. These columns having diameter of 60 cm with varying spacing were designed only for static loads (Figure 3.22). Length of jet grout columns are 12 m except outer two rows being 8 m long. In this project, ratio of shear moduli of jet grout to soil is in the order of 30 and 28 days UCS of soilcrete columns are 3.0 MPa.

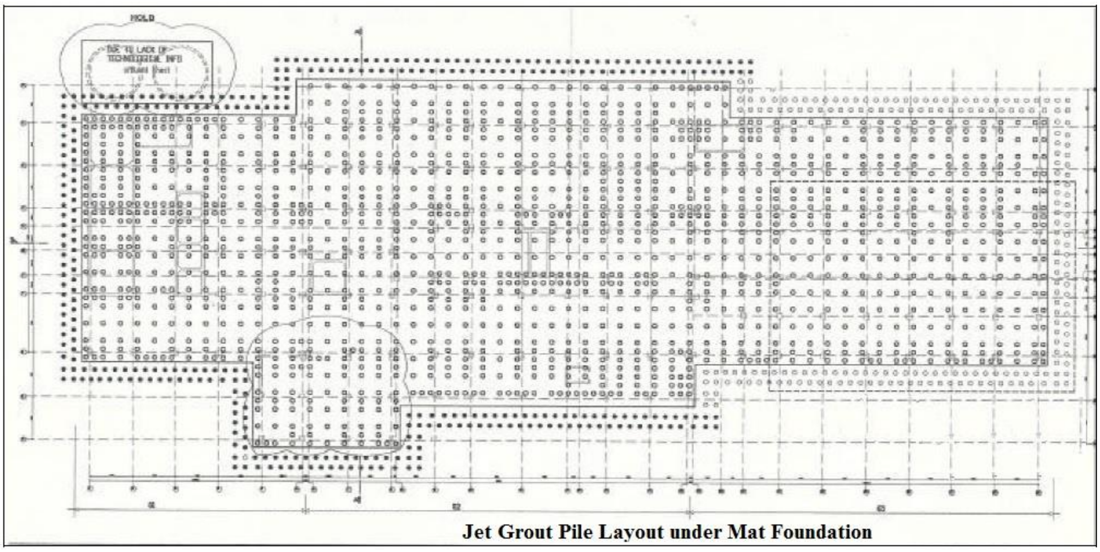

Figure 3.22 Jet grout column disposition for PM3 building

Although jet grout columns were designed to carry heavy structure, it was computed that improvement provided by jet grout columns was enough to mitigate liquefaction (Ozsoy, 2002). That is, according to jet grout column disposition, area replacement ratio was in the range of 0.07 to 0.10. Therefore, corresponding cyclic shear stress reduction factor (K_G) were 0.33 and 0.27, respectively (Ozsoy & Durgunoglu, 2003). As a result, predicted seismically induced shear stresses acting on soil should have reduced to 30% of its theoretical value. Apart from it, outer two rows of jet grout columns around perimeter of the building were closely spaced in order to prevent lateral spreading in case of liquefaction.

After earthquake, no damage was observed at the factory plant except PM2 building where soil improvement had not been performed. In that building, liquefaction related settlement observed.

3.6.2 Total Stress-Based Numerical Analyses

There exit several studies based on total stress-based numerical analyses investigating effectiveness of jet grouting against liquefaction. As mentioned earlier, in total stress analysis, 'simplified method' is adopted in the evaluation of initiation of liquefaction. In this method, effectiveness of columns are assessed based on shear stress change in soil after installation of columns.

3.6.2.1 Liquefaction Mitigation Using Jet Grout Columns-1999 Kocaeli Earthquake Case History and Numerical Modelling

In 1999 Kocaeli Earthquake, liquefaction related damages were observed. However, at Carrefour Shopping Center, liquefaction were satisfactorily mitigated by jet grout columns. But, mechanism of the way how liquefaction was mitigated has not been understood well. To better understand of role of columns on liquefaction mitigation, Martin & Olgun (2007) studied mentioned case via non-linear dynamic 3-D finite element modelling of improved site was performed using DYNAFLOW.

During earthquake, sandy and silty layer between 6 and 10 m depths liquefied at untreated areas (Figure 3.23 (a)). In Martin et al. (2004) study, liquefaction analysis based on updated simplified procedure in which PGA is taken as 0.24g indicated that factor safety against liquefaction is 0.7 for corresponding layer at untreated lot C (Figure 3.23 (b)). Besides, CH layer considered as non-liquefiable according to conventional methods, factor of safety for corresponding layer is obtained as 0.85 up to 20 m depth according to 'clay-like' soil approach of Boulanger and Idriss (2006). In that approach, it is likely to reflect the effect of surcharge of 3 m fill as preloading with the help of K_{α}. Also, it is stated that 3 m fill causes same effect with 5 or 6 story apartment buildings with respect to liquefaction-related settlement.

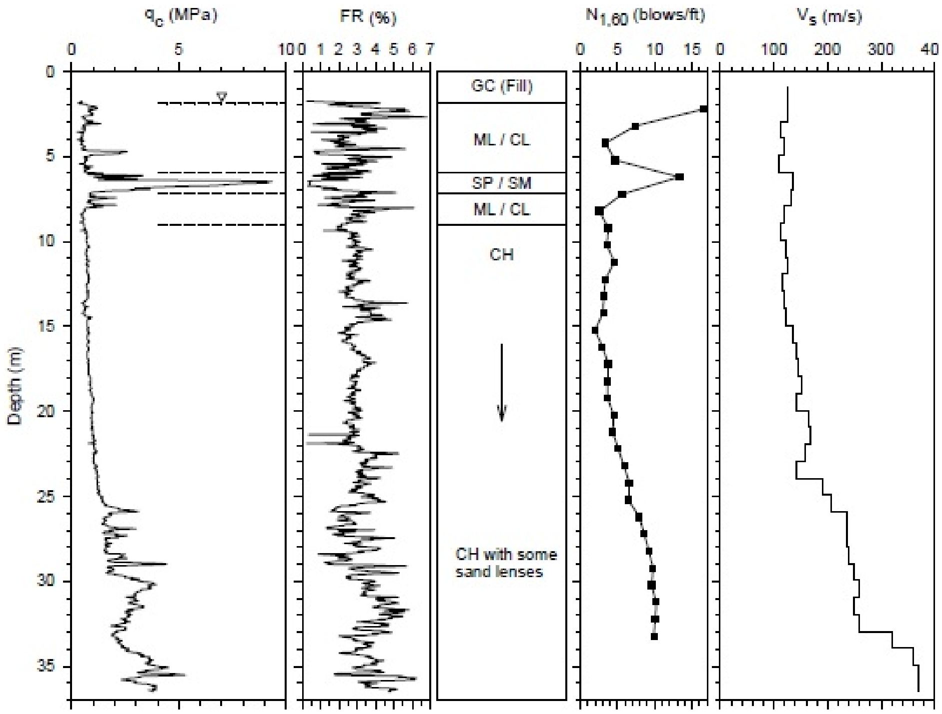

(a)

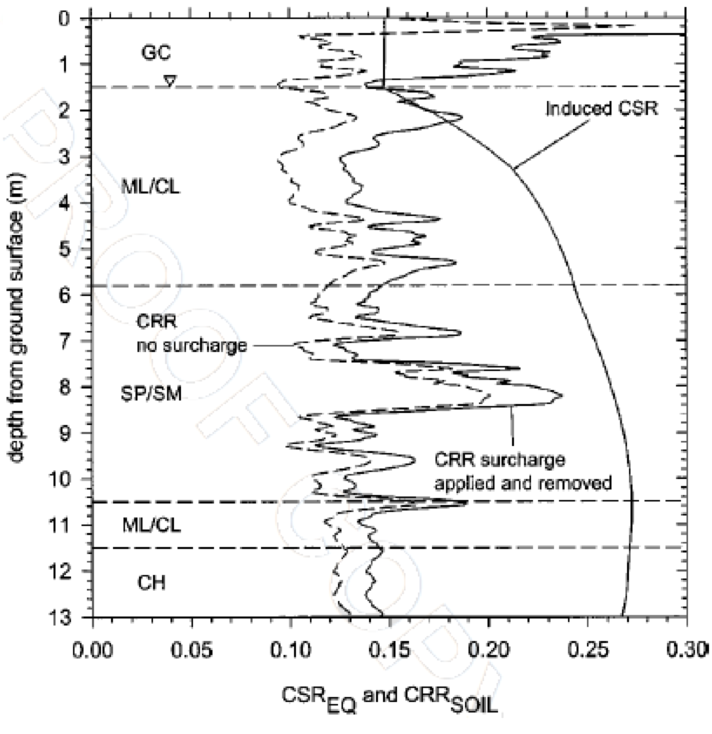

(b)

Figure 3.23 (a) Site investigation results (b) factor of safety against liquefaction for all layers

In dynamic modelling, only 4 m x 4 m grid which contains one primary jet grout column (9 m-long) and 8 secondary soilcrete columns (2.5-long) is modelled instead of entire area (Figure 3.24). However, boundary conditions are adjusted as if this small grid repeats itself infinitely. Besides, depth of the model is 15 m and total stress based analyses are performed. As dynamic motion, data of 1999 Kocaeli Earthquake are used and its horizontal components are acted in two directions simultaneously. Moreover, another model representing free field condition in which there is no jet grout column is modelled and used.

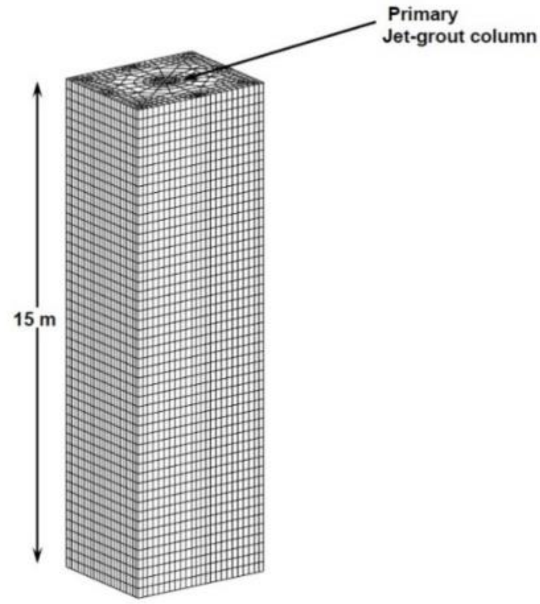

Figure 3.24 Three dimensional model of 4 m x 4 m grid

Analyses show that induced shear stresses for both improved zone that is between jet grout columns and untreated case are very close to each other while shear stresses occur in soilcrete column relatively higher than them (Figure 3.25). Likewise, shear strains for treated and untreated cases are obtained as very similar to each other and higher than those induced in jet grout column. Therefore, jet grout columns are not able to fully mitigate liquefaction according to obtained results. The reason for this undesired outcome might be attributed to structural behavior of jet grout columns. That is, jet grout columns which are 50-100 times stiffer than soil with respect to shear modulus represent flexural deformations rather than shear deformations. Therefore, induced shear stresses in treated soil are not canalized to jet grout columns. Also, shear strains in treated zone is not reduced by jet grout columns.

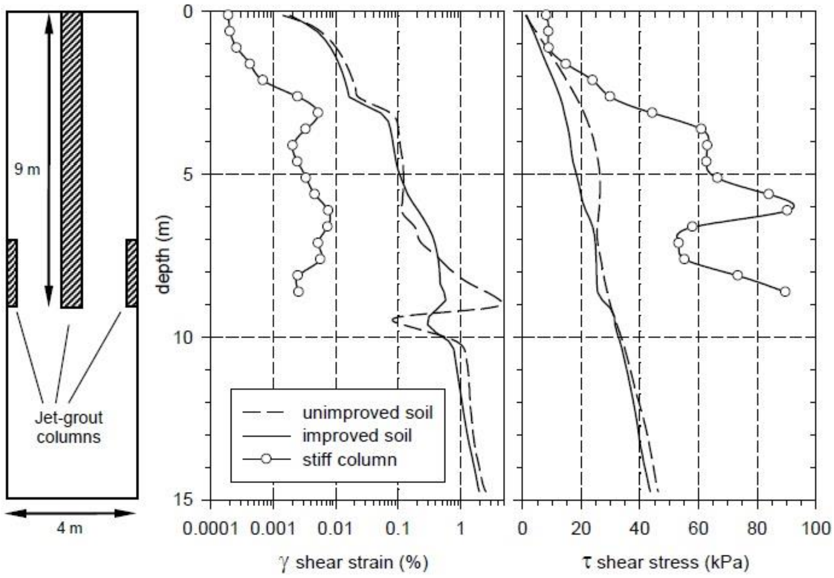

Figure 3.25 Shear strains and shear stresses for unimproved soil, improved soil and jet grout column

To conclude, jet grout columns having area replacement ratio of 7% picks up small portion of shear stresses although 80% reduction of shear stresses in treated soil has been predicted according to method of composite shear behavior suggested by Baez & Martin (1994). Although desired results are not obtained in numerical analyses, jet grout columns were able to mitigate liquefaction at Carrefour Shopping Center. The authors suggest that jet grout columns provide vertical support and prevent liquefaction induced settlements rather than reducing of seismically induced shear stresses in the soil.

3.6.2.2 Seismic Behavior of Columnar Reinforced Ground

In the study performed by Olgun & Martin (2008), potential mechanisms of shear stress reduction by means of high modulus columns are investigated. Also, composite shear behavior assumption that relies on strain compatibility between high modulus column and soil is examined. In this approach which assumes only pure shear behavior of stiff columns along with soil, it is accepted that high modulus column carries greater shear stresses as proportional to moduli ratio of itself to soil (Baez & Martin, 1994). Actually, according to Goughnour & Pestana (1998), reason of stress reduction in improved soil is due to pure shear deformation of stiff columns like shear beams as opposed to classical flexural beam theory (Figure 3.26).

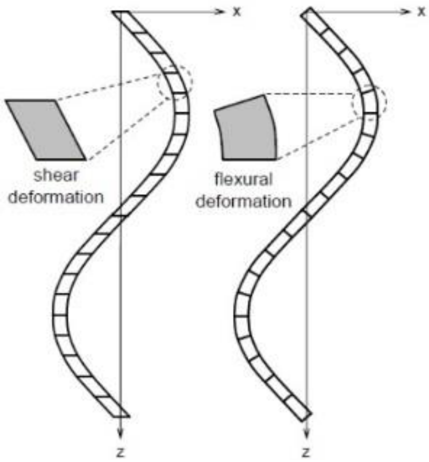

Figure 3.26 Pure shear and flexural deformations

In order to clarify mentioned approach, two layered profile containing stiff columns are modelled as linear elastic in DYNAFLOW. The upper 6 m thick soft layer has 150 m/s shear wave velocity while the lower 6 m thick stiff layer is of 250 m/s. Besides, 6 m long stiff columns having diameter of 90 cm are placed at spacing of 180 cm (Figure 3.27). The corresponding area replacement ratio for this spacing is 20%.

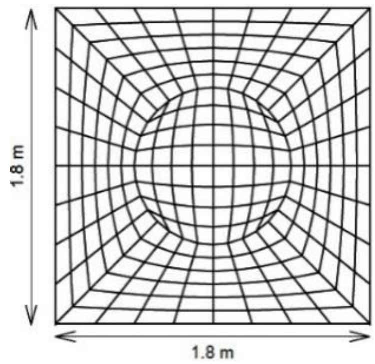

Figure 3.27 Finite element mesh of 1.8 m x 1.8 m grid

Besides effects of modulus difference between stiff column and soil and spacing are parametrically studied. 1999 Kocaeli Earthquake acceleration data is used as dynamic motion input.

According to analysis results, stiff column undergoes both pure shear and flexural deformations. However, contribution of shear deformations on total deformations increases with depth (Figure 3.28 (a)). Therefore, due to flexural deformation of soilcrete, strain compatibility between column and soil is wiggled and as a result, shear stress transfer from improved zone to column is restricted (Figure 3.28 (b)). Also, stiff column has very low strain values as compared to improved soil which is an indication of strain incompatibility. Hence, composite shear behavior overestimates amount of shear stress reduction in improved soil as stiffness difference between soil and soilcrete column increases. Nonetheless, stiff columns are still effective against liquefaction although contribution of them has been thought as much greater.

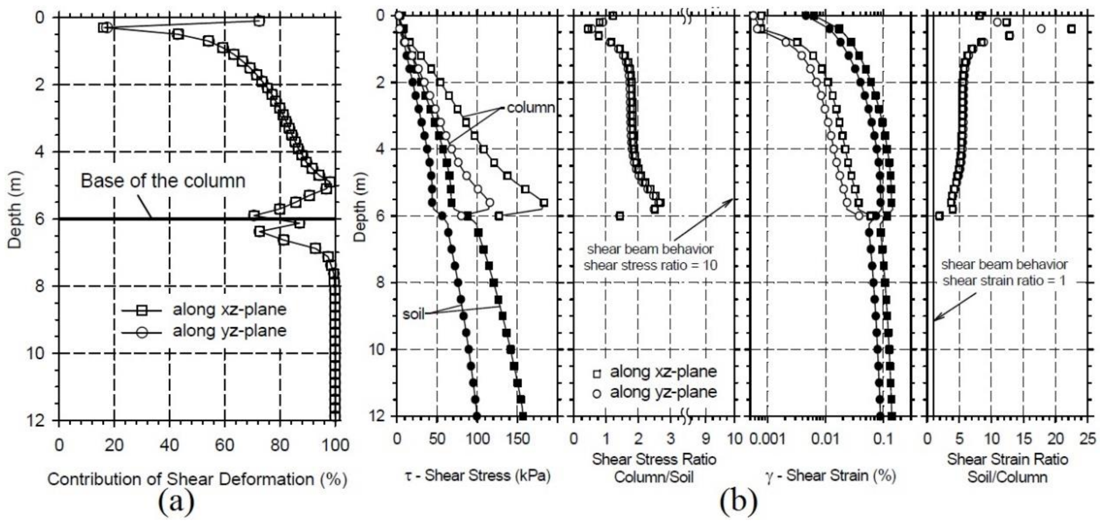

Figure 3.28 Analysis results for stiffness ratio of stiff column to soil 10 and spacing 2B; (a) contribution of shear strain to total strain (b) comparison of shear stresses and strains between improved soil and stiff column

3.6.2.3 Messina Suspension Bridge

In Messina suspension bridge project connecting Sicily to Italy, an excess amount of jet grout columns were designed to inhibit seismic liquefaction in coarse grained foundation soils and in this study, their effectiveness is verified by numerical analyses (Callisto, Rampello & Viggiani, 2013). This mentioned bridge has central span of 3300 m and 381 m height twin towers (Figure 3.29 (a)). Besides, each tower has 20 m thick two cylindrical foundations having diameter of 55 m. Besides, these two foundations are connected to each other with stiff box beam. As a final design, 23 m long jet grout columns with 1.0 area replacement ratio below foundation and 33 m long jet grout columns arranged in hexagonal array having replacement ratio of 0.42 near to towers is designed against liquefaction (Figure 3.29 (b) & (c)).

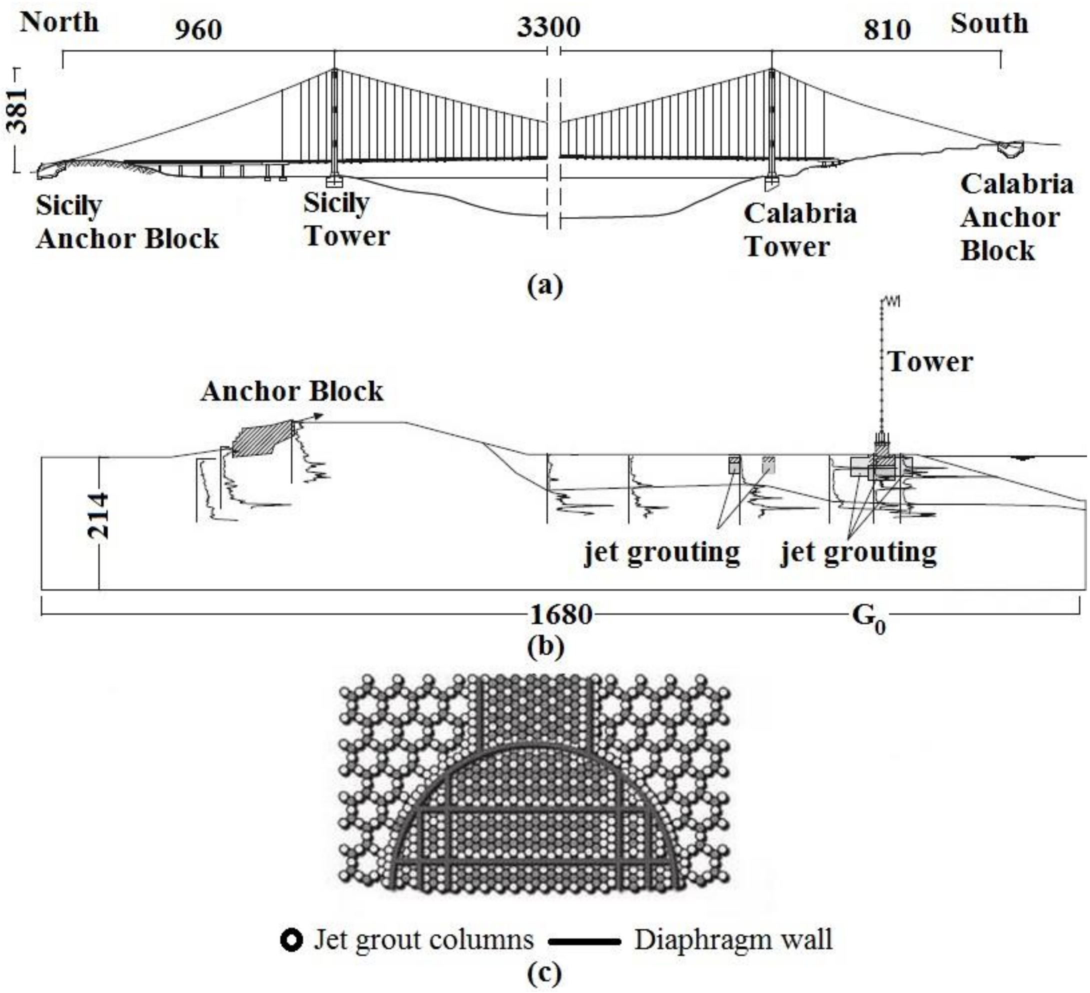

Figure 3.29 General information about structural and geotechnical design; (a) layout of entire bridge (b) layout of tower and jet grout columns on Sicily Shore (c) jet grout columns in hexagonal array near to tower

Roughly, up to 200 m depth, soil profile is idealized as two layers, namely; coastal deposits and messina gravels (Figure 3.29 (b)). Corresponding relative density of these layers is in the range of 40% and 60% in upper 50 m. Also, peak friction angle is accepted in between 42^0 and 44^0. Moreover, $(N_1)_{78}$ values are lower than 25 along 50 m depth. Based on mentioned soil properties, seismically induced shear stresses are obtained along with depth (Figure 3.30 (a)). Furthermore, liquefaction analyses are performed for free field condition by applying simplified method and therefore, high potential risk of liquefaction is determined for upper 20 m (Figure 3.30 (b)).

Furthermore, due to the fact that slight risk of liquefaction exits up to 60 m depth, length of jet grout columns is extended to this depth. In that analyses, 1999 Kocaeli Earthquake (M_w=7.4) and 2010 Christchurch Earthquake (M_w=7.1) are used as dynamic motion.

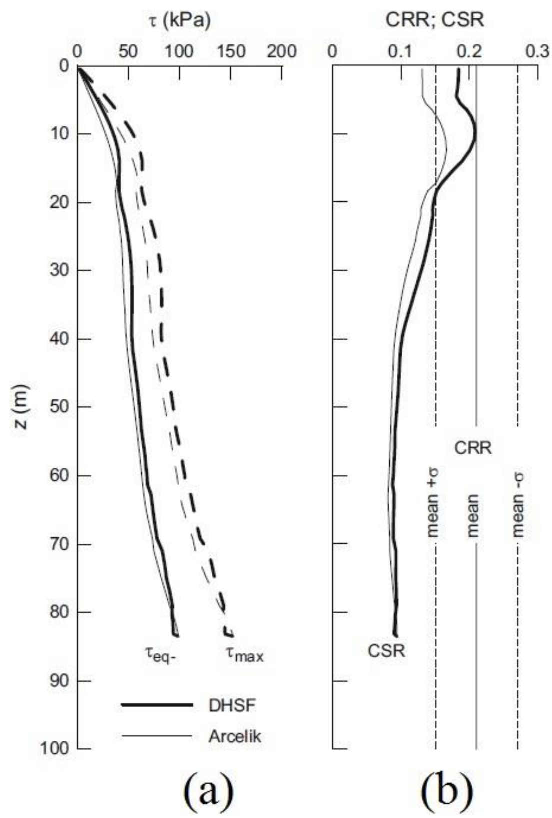

Figure 3.30 Result of liquefaction analyses; (a) equivalent and maximum values of shear stresses (b) CRR and CSR values

According to liquefaction analyses, jet grout columns are used for both beneath of foundation and around of perimeter of foundation. Prior to analyze entire structure as three dimensional, modelling is simplified to plane-strain conditions for the simplicity (Figure 3.31).

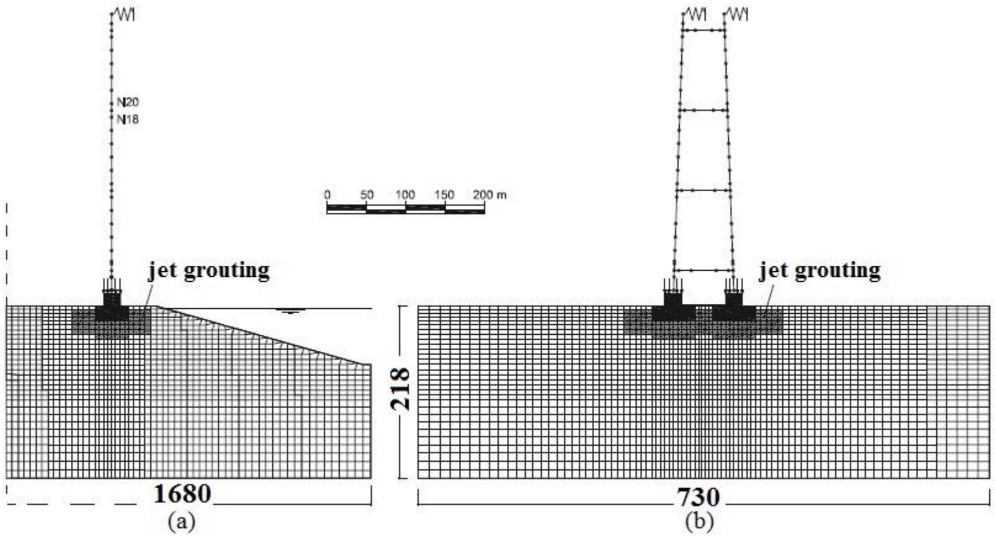

Figure 3.31 Simplified model based on plane strain conditions; (a) longitudinal section (b) transverse section

Non-linear two dimensional analyses are performed in FLAC while three dimensional analyses are done in ADINA. For both type of analyses, hysteretic damping is used based on laboratory data. Also, improved soil properties are used because of high stiffness of jet grout columns that shear wave velocity of it is greater than 350 m/s (Table 3.9).

Table 3.9 Improved soil properties

Location	**γ (kN/m^3)**	**c' (kPa)**	**Φ' (^{0})**	**ν**	**G_0 (MPa)**
Below the Foundation	22	1560	35	0.2	1250
Next to Foundation	22	655	35	0.2	525

Results obtained from both two and three dimensional models indicate that liquefaction risk is eliminated under towers by making factor of safety against liquefaction greater than 1.2 (Figure 3.32).

Figure 3.32 Zones CRR/CSR ratio lower than 1.2

3.6.2.4 Jet Grouting Columns for Building Uplift and Liquefaction Mitigation

In 2010, Christchurch Earthquake struck and triggered liquefaction in New Zealand (Figure 3.33). In that earthquake, the Christchurch Art Gallery was significantly affected and exposed to foundation related problem. That is, after earthquake, it was observed that this building had settled 15 cm. Therefore, in order to both raise building to its own level and mitigate liquefaction by improving soil, jet grout columns were designed. In this study, effectiveness of jet grout columns are proved (Cristovao et al., 2014).


(a) (b)

Figure 3.33 Liquefaction effects; (a) sinked car (b) sand boiling

Soil profile of Christchurch Gallery consists of mainly sand with gravels and silty sand. Also, geotechnical parameters are determined by CPT tests (Table 3.10).

Table 3.10 Geotechnical properties

Geotechnical Unit	Depth (m)	q_t (MPa)	γ (kN/m^3)	c' (kPa)	φ' (^{0})	E (MPa)	V_s (m/s)
Sand with Gravel	2.5-11.0	18.0	19.0	-	34	51.0	244.0
Silt	11.5-13.7	2.0	17.5	10.0	24	4.0	136.0
Silty Sand	15.0-15.8	20.0	19.0	-	34	50.0	240.0
Silt	16.5-17.2	3.0	17.5	10.0	24	5.0	147.0
Silty Sand	17.8-18.4	15.5	18.5	-	33	41.0	220.0
Silt	18.6-19.2	3.0	17.5	10.0	24	5.0	152.0
Silty sand	20.1-21.6	9.0	18.5	-	30	20.0	218.0
Sand	21.9-22.6	5.0	18.0	-	28	10.5	195.0
Clay	22.6-23.2	2.0	17.5	20.0	15	6.0	143.0
Sandy Silt	23.4-24.0	5.0	18.0	-	28	10.5	200.0

Jet grout columns are used in this project to make soil stiffer and raise the building. Therefore, 4.5 m long jet grout columns having diameter of 3.0 m are designed as a triangular pattern by transferring structure load to deeper. Also, around perimeter of structure, jet grout columns are of 4 m diameter. All jet grout columns are placed at 7.5 m spacing.

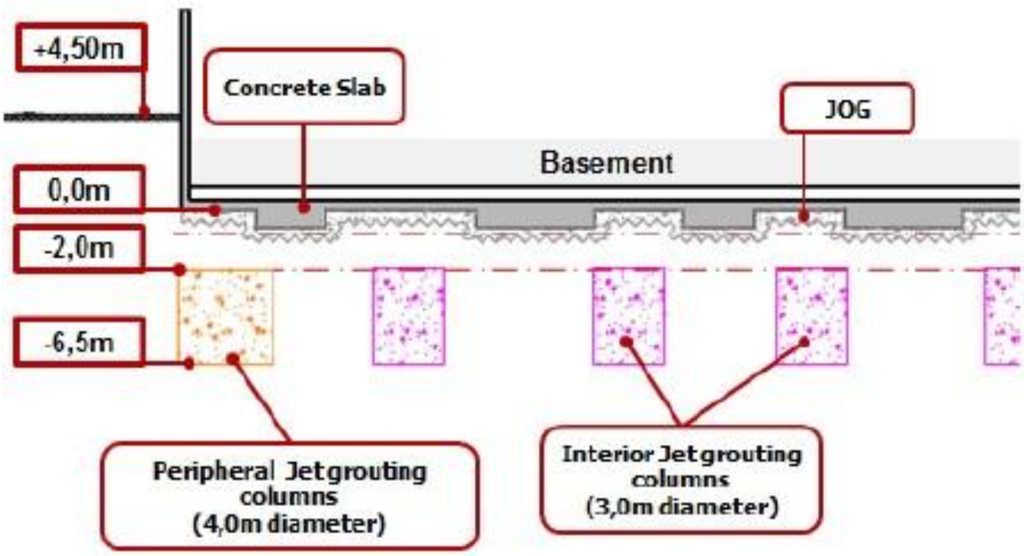

Figure 3.34 Jet grout columns cross section

Firstly, dynamic analyses are performed in PLAXIS 2D. Only one row of columns positioned beneath basement slab are modelled. Column properties are obtained by correlations (Table 3.11). By using Christchurch Earthquake data, PGA is obtained as 0.17g. Factor of safety against shear failure of column is obtained as 1.54.

Table 3.11 Jet grout column properties

UCS (MPa)	k (m/s)	E_c (GPa)	φ' (^{0})	c' (kPa)	v
2.2	1.0e-08	1.0	38	180	0.30

Secondly, in this project, liquefaction risk is computed and jet gout columns are used as a mitigation method. Before performing analysis, how much improvement is obtained is computed according to formulation of Durgunoglu (2004). Based on shear moduli ratio of jet grout column to soil which is in order of 10, CSR reduction factor is obtained as 0.36 provided that area replacement ratio is 0.196. Although safety margin against liquefaction increases according to analysis results performed in CLiq software, it is not as much as the expected (Figure 3.35). Therefore, mentioned method overestimates the change in shear stress in improved soil zone.

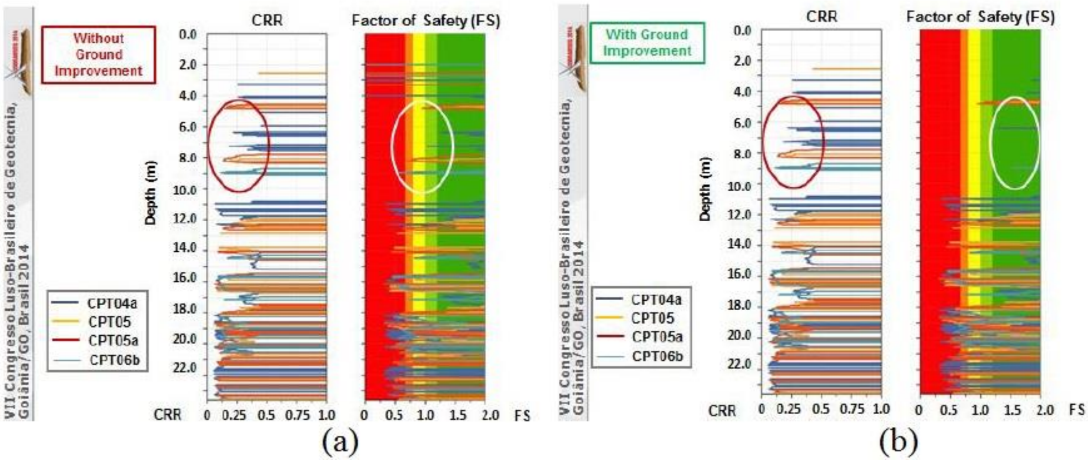

Figure 3.35 Factor of safety against liquefaction; (a) free field (b) improved site

3.6.3 Effective Stress-Based Numerical Analyses

Although total stress-based numerical analyses are popular in the assessment of effectiveness of jet grout columns, there exists certain limitation of mentioned method. In that method, presence of excess pore pressure which is driving factor in reduction in shear strength does not taken into account. However, excess pore pressure is directly used in effective stress-based numerical analysis. In this type of analyses, effectiveness of columns are assessed based on change in r_u values before and after applications of columns.

3.6.3.1 3-D Numerical Modelling of Liquefaction Induced Settlements and its Mitigation

In this study (Almani et al., 2013), effectiveness of jet grout columns on liquefaction mitigation including soil-structure interaction of square footing at shallow depth is investigated. Therefore, 3-D model is created in FLAC3D (Figure 3.36 (a)). Rectangular meshing, dimensions of 0.5 m x 0.5 m x 1.0 m, is chosen after performing analyses on mesh effect. Besides, optimum dimensions are found as 30 m x 30 m x 20 m. Also, Finn model is used so as to model liquefaction phenomenon.

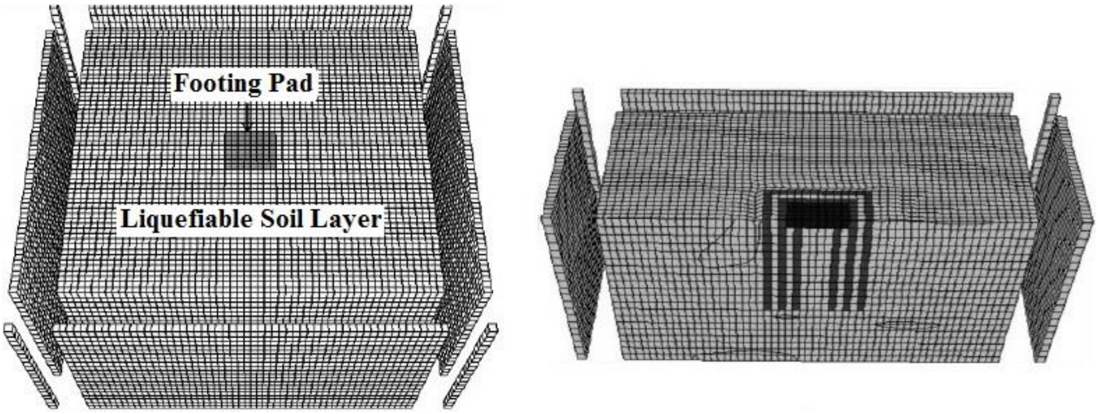

Figure 3.36 Factor of safety against liquefaction; (a) free field (b) with ground improvement

Two layered soil profile is used in this model. Corresponding soil properties are calibrated according to constant volume cyclic shear tests (Table 3.12).

Table 3.12 Soil properties

	D_R (%)	γ (kN/m³)	e	k (m/s)	φ' (⁰)	Pore Press. Cons. 1	Pore Press. Cons. 2	G_{max} (MPa)	H (m)
Medium Dense Layer	40	18.8	0.88	2e-7	32	1.2	0.33	43.2	10
Dense Layer	80	19.6	0.72	1e-7	48	0.43	3.75	93.7	10

Jet grout columns are modelled by using rectangular columns having equivalent cross sectional area of circular column. Therefore, jet grout column having diameter of 60 cm are able to be modelled with 0.5 m x 0.5 m dimension. Besides, 11 m long jet grout columns are used that end of columns bypasses liquefiable soil. As a jet grout column pattern, continuously overlapping column rows by forming lattice around footing are used (Figure 3.36 (b)). Jet grout properties are selected according to common engineering practice (Table 3.13). Furthermore, footing block is modelled as fully rigid shell having dimension of 4 m x 4 m x 1 m.

Table 3.13 Jet grout column properties

γ (kN/m³)	G_{max} (MPa)	K_{max} (MPa)	UCS (MPa)	φ' (⁰)	c' (kPa)	w/c
19	2000	2600	4.8	0	2400	1/1

In analyses, instead of real earthquake data, sinusoidal wave having horizontal velocity amplitude of 0.2 m/s is used as dynamic motion. Prior to the case containing jet grout columns, free field with footing block embedded to soil is analysed. According to analyses, footing block settles 70 mm due to effect of liquefaction. Besides, at 4 m depth under centre of the footing, maximum value of total pore water pressure value increases from 43 kPa to 138 kPa. In improved soil case, two lattices of jet grout columns are placed around of perimeter of footing at a 0.5 m spacing. In this case, settlement of footing decreases from 70 mm to 40 mm with the help of jet grout columns. Also, maximum value of total pore water pressure yields to 100 kPa. Therefore, 25% reduction in total pore water pressure is obtained (Figure 3.37).

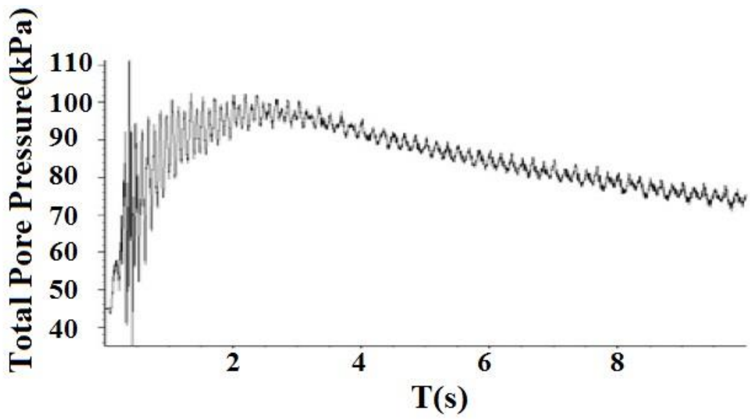

Figure 3.37 Total pore water pressure in improved soil

3.6.4 Approaches on the Prediction of Effectiveness of Jet Grout Columns

Although jet grout columns have been widely used in the prevention of liquefaction, how much safety margin is provided by jet grout column have not been exactly formulated. Therefore, with this scope, two approaches have been proposed to foresee contribution of jet grout columns to liquefaction mitigation.

3.6.4.1 Unit Cell Approach

In this approach, it is accepted that jet grout columns can reduce seismically induced shear stresses in the soil as compared to free field condition (Ozsoy & Durgunoglu, 2003). How much jet grout columns reduce shear stresses depend on both stiffness difference between soil and itself and areal coverage of jet grout columns (Figure 3.38). Mentioned coverage called as ‘area replacement ratio’ (a_r) can be expressed as the ratio of jet grout column area (A_{jg}) to unit cell area (A). Also, the area ratio (a_s) covered by soil (A_s) in unit cell is obtained by following equations:

$$A = (s_v)(s_h) \tag{3.13}$$

$$a_r = \frac{A_{jg}}{A} \tag{3.14}$$

$$a_r = \frac{A_s}{A} \tag{3.15}$$

Where s_v and s_h are vertical and horizontal spacing between jet grout columns, respectively.

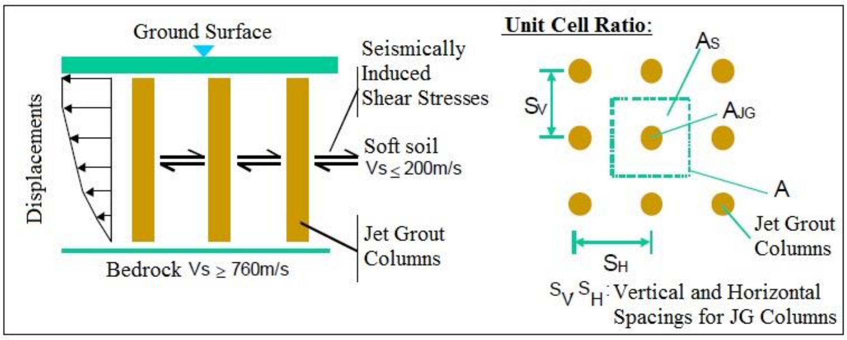

Figure 3.38 Share of seismically induced shear stresses between soil and jet grout columns

Due to strain compatibility, both soil and jet grout columns undergo same deflections and therefore, sum of induced shear stresses in both jet grout columns and soil gives total shear stress in unit cell:

$$\tau = \tau_s a_s + \tau_{jg} a_r \tag{3.16}$$

Where τ is shear stresses in unit cell, τ_s is portion of shear stresses acting on soil and τ_{jg} is shear stresses carried by jet grout columns. Also, these terms can be expressed in terms of each other by using a ratio term ($n = \tau_{jg}/\tau_s$) for the simplicity:

$$\tau_s = \frac{\tau}{(1+(n-1)a_r)} \Rightarrow \frac{\tau_s}{\tau} = \frac{1}{(1+(n-1)a_r)} \tag{3.17}$$

$$\tau_{jg} = \frac{n\tau}{(1+(n-1)a_r)} \Rightarrow \frac{\tau_{jg}}{\tau} = \frac{n}{(1+(n-1)a_r)} \tag{3.18}$$

Based on previously discussed relations, CSR is reduced by a reduction factor proportional to shared shear stresses among soil and jet grout columns. This reduction factor (K_g) can be obtained by following equation:

$$K_g = \frac{\tau_s}{\tau} = \frac{1}{(1+(G_r-1)a_r)} = \frac{1}{G_r}\frac{1}{\left(a_r + \frac{1}{G_r}(1-a_r)\right)} \tag{3.19}$$

Where G_r is the ratio of shear modulus of jet grout column to soil shear modulus. Also, CSR for improved soil can be obtained:

$$CSR_{improved\ soil} = (CSR)K_g \tag{3.20}$$

CSR reduction factor with respect to area replacement ratio and shear moduli ratio of jet grout column to soil is indicated (Figure 3.39). However, several studies criticized that this method overestimates amount of improvement by jet grout columns (Olgun & Martin, 2008; Cristoavo et al., 2014).

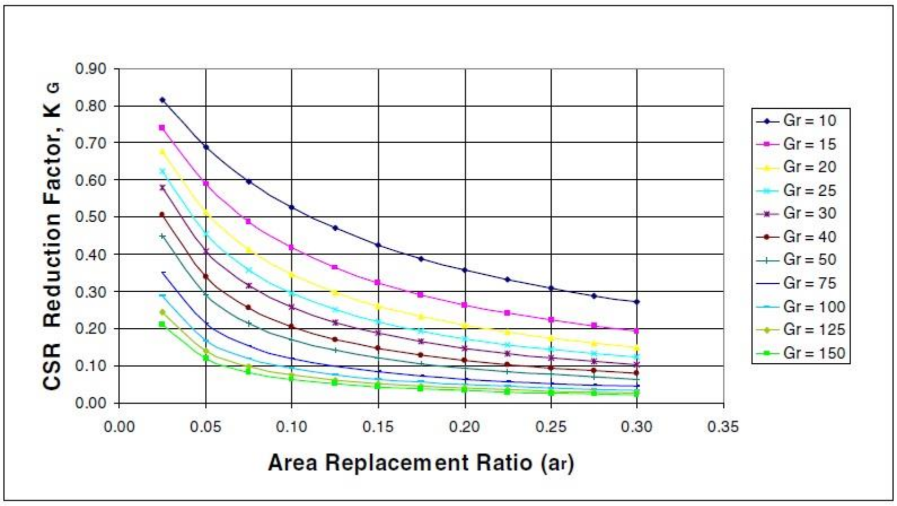

Figure 3.39 Reduction factor

3.6.3.2 Probabilistic Approach

In this approach, effect of jet grout columns on liquefaction resistance of soil is tried to predict based on assessment of liquefaction potential based on total stress approach (Unutmaz, 2012). Therefore, CSR values for both free field and improved soil are computed separately. Likewise, CRR values for mentioned cases are obtained. Then, how much improvement is obtained via jet grout columns are expressed in terms of a term ‘improvement ratio ‘(I_R) is defined:

$$I_R = \frac{CRR_{improved\ soil}/CSR_{improved\ soil}}{CRR_{free\ field}/CSR_{free\ field}} \tag{3.21}$$

While seismically induced shear stress values are obtained from numerical analyses and they are used in the simplified method to obtain CSR, corresponding CRR values are obtained following equation suggested by Cetin et al. (2004):

$$CRR(z) = \exp\left(-\frac{\begin{array}{c} N_{1,60}(1 + 0.004FC) - 29.53\,ln(M_w) \\ -3.7\,ln\left(\frac{\sigma_v'(z)}{P_a}\right) + 0.05FC + 16.85 + 2.7\varphi^{-1}(P_L) \end{array}}{13.32} \right) \tag{3.22}$$

Where $N_{1,60}$ is overburden and energy corrected SPT blow count, FC is fines content, M_w is magnitude of earthquake, $\sigma'_v(z)$ is effective vertical stress at depth z, P_a is atmospheric pressure and φ^{-1} is inverse of standard cumulative normal distribution.

To find out relation between pre-improvement CSR and post-improvement CSR, maximum likelihood procedure is utilized. Also, multidimensional regression analyses are performed so as to capture effects of jet grout columns by means of certain parameters with respect to liquefaction resistance. Actually, these parameter are categorized into three groups, namely; jet grout column properties (i.e., diameter, length, spacing, strength, number of columns), earthquake properties (i.e., magnitude, peak ground acceleration) and soil properties (i.e., stiffness, depth). With the help of mentioned regression analyses, parameters having high influence on liquefaction resistance are determined (Figure 3.40). Most effective parameters are soil stiffness, acceleration at depth of consideration, area replacement ratio, depth of interest (z) and jet grout stiffness. Although magnitude of earthquake seems effective in regression analyses, it is not included in the formulation of I_R in the final probabilistic analyses.

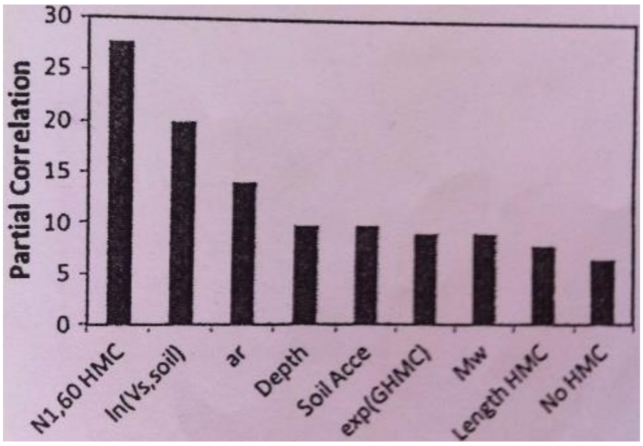

Figure 3.40 Parameters significantly influencing liquefaction resistance

Then, I_R is formulated based on probabilistic method by taking non-linearity of soil into account with both exponential function including natural logarithm:

$$I_R = \exp(V_s^{-0.267} - 0.0485\ln(z) + 1.306a_r + G_{HMC}^{0.293} - 4.179) \qquad (3.23)$$

Where V_s is stiffness of soil with respect shear wave velocity, z is depth of consideration, a_r is area replacement ratio and G_{HMC} is shear modulus of high stiff column.

Proposed relation is validated by centrifuge tests and good agreement is obtained between test results and computed values. Besides, it is computed that convergence of this equation increases with rising of soil stiffness according to this equation. Furthermore, effectiveness of jet grout columns by means of improvement ratio increase with high stiffness of soil. In other words, jet grout columns provide better improvement ratio for relatively stiff soil.

CHAPTER FOUR
INVESTIGATION OF CONTRIBUTION OF JET GROUT COLUMNS ON LIQUEFACTION MITIGATION BY EFFECTIVE STRESS-BASED NUMERICAL ANALYSES

4.1 Introduction

For the aim of assessing contribution of jet grout columns on liquefaction mitigation, series of both 1-D and 3-D numerical simulations were performed. In this study, different than previous studies mostly based on total stress based (Martin & Olgun, 2007; Callisto, Rampello & Viggiani, 2013; Cristovao et al., 2014), effectiveness of jet grout columns are investigated with respect to effective stress. Although total stress based method are simple and practical from duration of analysis point of view, it does not take pore pressure into account. As mentioned earlier, onset of liquefaction is attained when excess pore pressure equal to initial vertical effective stress (Idriss & Lee, 1966). In other words, pore pressure ratio that is ratio of dynamically induced excess pore water pressure (u_e) to initial vertical effective stress (σ'_v) should be 100% as a prerequisite of initiation of liquefaction. As effective stress converges to zero due to high positive pore pressure, significant shear strength loss occurs according to Mohr-Coulomb law.

In this study, in the light of given information, influence of soilcrete columns on liquefaction were assessed according to change of r_u values before and after soilcrete column application. Furthermore, effectiveness of jet grout columns were studied parametrically involving different strong motions, varying column stiffness with diverse area replacement ratio and depth of consideration. Hence, in this chapter, details of numerical simulations for the free field case in which soil can liquefy and for the improved site by soilcrete columns case are presented. Moreover, with respect to r_u values, comparison of free field case and improved site by jet grout columns are given.

4.2 Numerical Analyses Procedure and Definition of the Problem

The basis of this study is to investigate effectiveness of jet grout columns as a countermeasure against liquefaction by means of 3-D non-linear dynamic numerical analyses. Thus, based on mentioned aim, four sets of numerical analyses were performed, namely; static analyses of free field, dynamic free field analyses, static analyses of improved soil and dynamic improved soil analyses (Figure 4.1). Furthermore, for validation of 3-D dynamic free field analyses, additional 1-D site response analysis was performed (Figure 4.1).

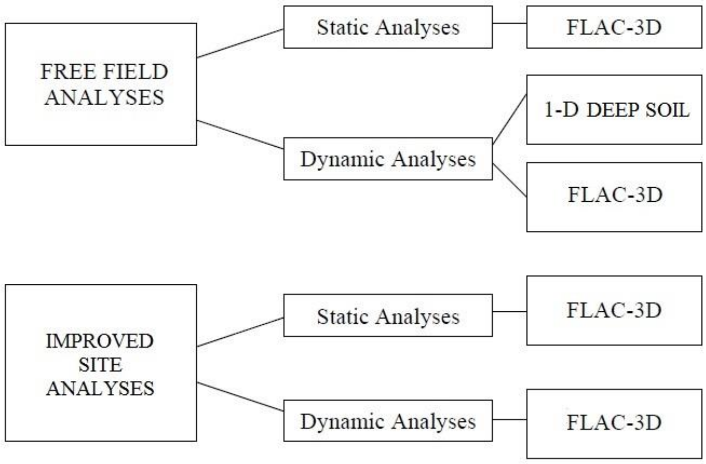

Figure 4.1 Performed numerical analyses for this study

Firstly, by performing static analyses, geostatic conditions were obtained for possibly liquefiable homogenous soil profile at free field condition. Then, whether soil has liquefied or not was also investigated according to r_u values under dynamic loading that forms dynamic site response analyses part of free field analyses. Also, for the sake of validation of FLAC3D, 1-D site response analysis was performed by using DEEPSOIL and results for corresponding software were compared.

In the second part of numerical analyses, jet grout columns have been activated and static analyses were performed. Then, by performing dynamic analyses, effectiveness of jet grout columns were assessed with respect to final r_u values. Mentioned type of analyses were repeated for each different spacing between adjacent columns of 3B, 4B, 5B and 6B in square grid pattern (Figure 4.3 (c)). Presented jet grout column spacings correspond to area replacement ratio that are 0.087, 0.049, 0.031 and 0.022. Also, varying stiffness of jet grout columns, namely; relatively stiff, stiff and very stiff with respect to soil and diverse dynamic motions were taken into account.

As mentioned earlier, in this study, assessment of liquefaction initiation of soil and effectiveness of jet grout columns against liquefaction are evaluated with respect to r_u values. Mathematical expression of r_u may be given by the following equation (Idriss & Boulanger, 2006):

$$r_u = \frac{u_{excess}}{\sigma'_{3c}} \ (for\ triaxial\ test) \ r_u = \frac{u_{excess}}{\sigma'_{vc}} \ (for\ free\ field) \tag{4.1}$$

Where u_{excess} is the excess pore pressure and σ'_{3c} is effective confining stress, σ'_{vc} is effective consolidation stress.

In this study, all 3-D numerical analyses were performed by using FLAC3D (version 4.0 upgrade level 89; 4.00.89) while 1-D site response analysis was carried out with DEEPSOIL (version 6.0) software. FLAC3D is a commercial software to solve engineering problems in 3-D by means of explicit finite-difference algorithm. In this program, for each time step, full equation of motion is solved without storing any matrices.

4.3 Soil Profile and Corresponding Properties

On November 24, 1987, Superstition Hills Earthquake (M_w=6.6) struck the Wildlife Liquefaction Array (WLA) and it caused severe liquefaction. In this earthquake, PGA was recorded as 2.02 m/s^2. Basically, general soil profile consists of three distinct layers; namely, silt, sand and silty clay from top to bottom. Actually, at the WLA, problematic layers which can liquefy are top two sandy layers and these layers take place between 2.5 and 6.8 m depth. Hence, idealized soil profile which was determined by Bennet, McLaughlin & Youd (1982) in which liquefaction took place was constructed (Figure 4.2). However, for the ease of dynamic analysis, only single layer having depth of 15 m was modelled in FLAC3D. That is, soil layer liquefied in Superstition Earthquake is modelled as if thickness of itself is 15 m.

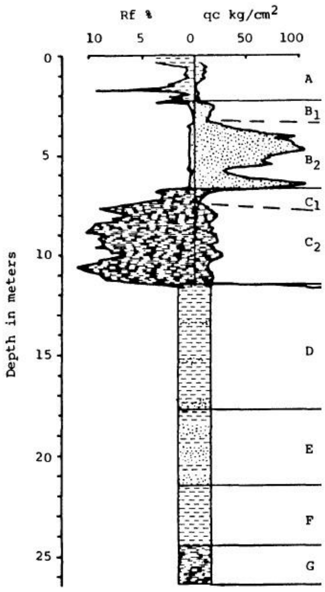

Layer	CPT Q_c/R_f	SPT N	Grain Size Characteristics sd/st/cl	Grain Size Characteristics Cu/d_{50}	Water Properties $w_n/w_l/PI$	Description
A	6/3.02	2.3	10/71/19	12/0.027	34/30/7	silt with sand and clay, LI=1.6
B1	21/0.99	3	37/55/8	11/0.055	-	sandy silt, mod sorted
B2	57/1.24	8.4	73/25/2	3/0.089	-	silty sand to sand well sorted
C1	14/4.52	10.3	4/69/27	-/0.013	30/36/16	clayey silt, LI=0.6
C2	20/7.53	18.5	2/31/67	-/0.002	26/64/32	silty clay, LI=-0.2
D	-	18	10/74/16	17+/0.03	28/28/4	silty with clayey and sandy beds moderately to poorly sorted
E	-	-	38/41/21	19+/0.051	26/-/-	silty sand alternates with clayey silt, well to very poorly sorted
F	-	-	19/60/21	17+/0.031	29/33/12	clayey silt, very poorly sorted
G	-	-	5/51/44	-/0.011	30/51/27	silty clay and clayey silt

Figure 4.2 Idealized soil profile at WLA

Besides, this layer was modelled as homogeneous and having same properties regardless of the depth. Also, the corresponding properties for 15 m thick layer were selected such that it represents index and physical properties of liquefying layer which is in between 2.5 and 6.8 m depth. That is, selected values are the arithmetic mean of values belonging to 2.5-3.5 m and 3.5-6.8 m intervals (Table 4.1). Groundwater table is at the ground surface.

Table 4.1 Index and physical properties of liquefied layer used in this study

Depth (m)	**e (%)**	**Porosity**	γ_{dry} **(kN/m³)**	γ_{wet} **(kN/m³)**	D_r **(%)**
15	60.53	0.38	16.19	19.92	35.69

Furthermore, drained mechanical properties of corresponding layer were selected according to Holzer and Youd (2007) suggested (Table 4.2).

Table 4.2 Drained mechanical properties

$(N_1)_{60}$	V_s (m/s)	c' (kPa)	φ' (^{0})	E (MPa)	G (MPa)	K (MPa)	Dilation Angle (^{0})	Tension Limit (kPa)
5.66	152.35	0	31.98	131.8	47.1	219.7	0	0

Hence, soil profile down to a depth of 15 m is shown in Figure 4.3. As mentioned earlier, soil profile consists of single layer. For both free field and improved site analyses, same properties are used.

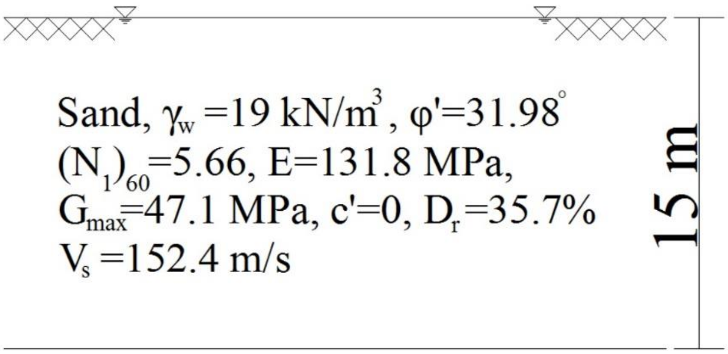

Figure 4.3: Idealized soil profile

4.4 Simulation of the Problem in Numerical Models

In this study, both 1-D and 3-D numerical models were constructed for different purposes. 1-D numerical model created in DEEPSOIL was utilized for site response analysis to investigate liquefaction phenomenon. Likewise, same problem was also modelled in FLAC3D. Furthermore, in FLAC3D, improved site by jet grout columns were modelled to find out effectiveness of them against liquefaction.

4.4.1 1-D Numerical Model in DEEPSOIL

For site response analysis to investigate liquefaction behavior, entire soil profile was divided into 15 sub-layer having equal thickness of 1 m. Although vertical (z-direction) meshing size in corresponding model for FLAC3D was equal to 0.5 m, 1 m thickness was used as optimum value according to guideline of DEEPSOIL manual (Hashash et al., 2015). In fact, it is highly recommended that layer thickness should be adjusted to convey a wave having 30 Hz frequency for time domain analysis. For this study, corresponding value for each layer is 38 Hz. Also, natural frequency of entire profile is 2.54 Hz (Figure 4.4).

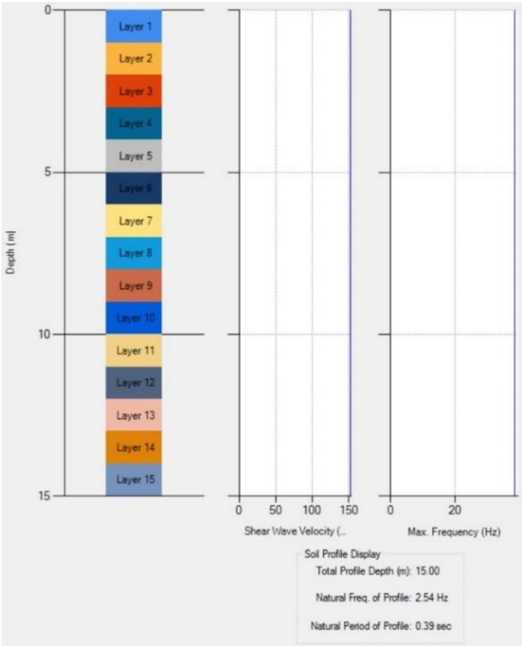

Figure 4.4 1-D numerical model in DEEPSOIL

4.4.2 3-D Numerical Models in FLAC3D

In order to both compare results for free field analyses with DEEPSOIL and to assess contribution of jet grout columns on liquefaction mitigation, 3-D numerical models were created in FLAC3D. These created models for free field analyses were also used in treated site by soilcrete columns analyses. In other words, same meshing criterion was adopted for free field and improved site cases. The reason for that will be explained in a detailed manner in forthcoming sections.

For the simulation of the problem, optimum model dimension which does not cause any distortion for each area replacement ratio is 30 m x 30 m x 15 m in x, y and z direction, respectively (Figure 4.5). Roller boundaries are utilized in static analyses while they are replaced with dashpots in dynamic analyses. Soil is modelled as Mohr-Coulomb material coupled with dynamic pore pressure generating Finn model while jet grout columns are presented by Mohr-Coulomb material type.

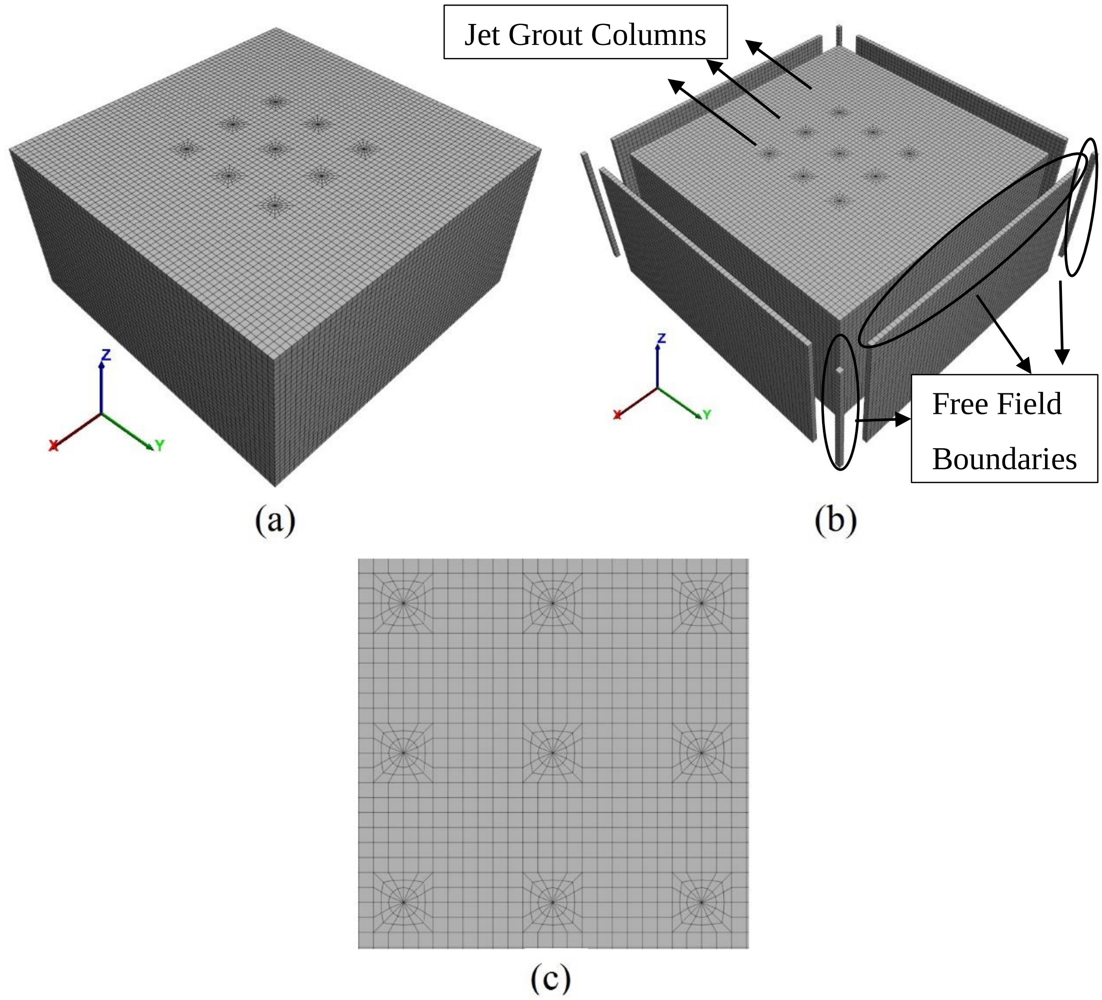

Figure 4.5 Representative numerical models; (a) for free field analyses (b) for improved site by jet grout columns having area replacement ratio equal to 0.087 corresponding to 3B spacing in x and y directions between adjacent columns (c) top view of jet grout columns

Spatial element sizes for each direction are 0.5 m except location of jet grout columns (Figure 4.5 (c)). At the locations of jet grout columns, gradually decreasing sizes rather than sudden change towards to center of jet grout column are adopted. Moreover, length and diameter of jet grout columns were selected as 12 m and 1 m, respectively.

Furthermore, layouts for corresponding spacing and area replacement ratio are given in Figure (4.6).

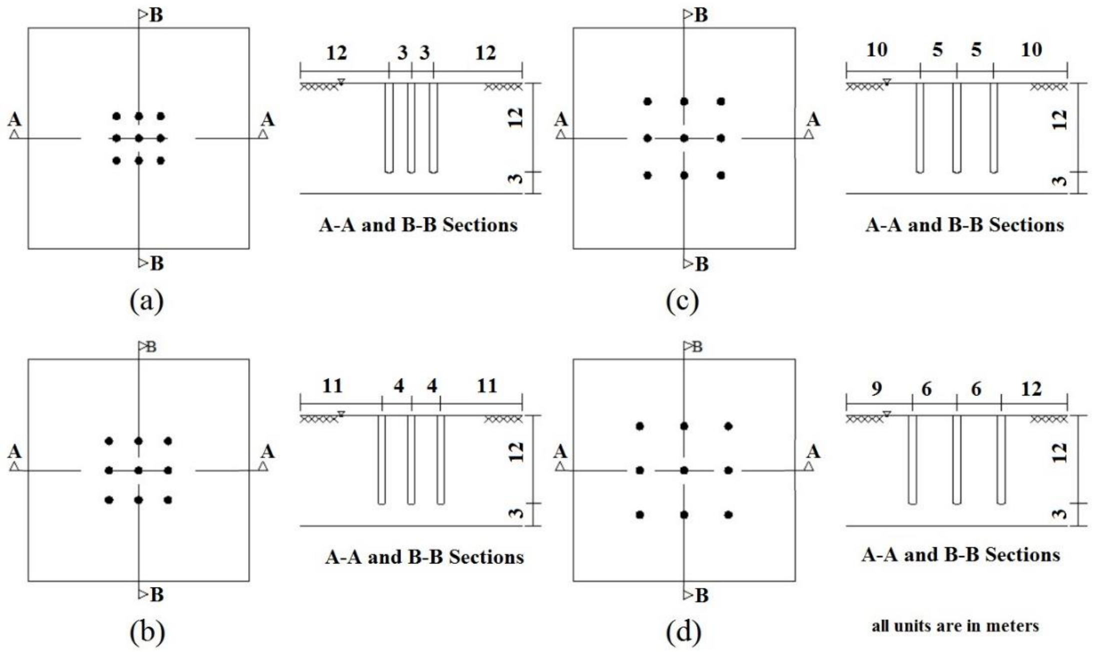

Figure 4.6 Layouts corresponding to each spacing; (a) 3B spacing in x and y directions between columns (a_r=0.087) (b) 4B spacing (a_r=0.049) (c) 5B spacing (a_r=0.031) (d) 6B spacing (a_r=0.022)

While 116640 zones and 122047 nodes are utilized in static analyses, these values increase to 123960 and 137671, respectively, at dynamic analysis stage due to presence of free field boundaries. Furthermore, from accuracy point of view, aspect ratio for each model of spacing, ratio of mesh sizes of zone adjacent edges, is forced to close as possible as to unity (Table 4.3). In this table, aspect ratio values for each zone are indicated. For example, for static analysis stage, there are 8640 zones having aspect ratio in the range of 0.3 to 0.4. Hence, overall aspect ratio is in between 0.9 and 1.0.

Table 4.3 Aspect ratio for 3B, 4B, 5B and 6B model spacing

	Number of Zones	
Aspect Ratio Range	**Static Analysis Stage**	**Dynamic Analysis Stage**
0.3-0.4	8640	8640
0.4-0.5	0	0
0.5-0.6	2160	2160
0.6-0.7	2160	2160
0.7-0.8	0	0
0.8-0.9	0	0
0.9-1.0	103680	111000

4.5 Input Dynamic Motions

Main purpose of this study is to obtain a liquefiable soil layer having very high r_u values under dynamic loading and mitigate liquefaction by means of jet grout columns. Therefore, according to this aim, dynamic motions were selected such that dynamic action can cause detrimental effects on soil from liquefaction point of view. In other words, dynamic motions which liquefy soil as much as possible were selected.

Due to imperfection of plastic Finn model which enables excess pore pressure to occur, it is not possible to use real earthquake data unless stiffness is necessarily increased that prevents occurrence of excess pore pressure. That is, soil modulus degradation cause yielding of soil before liquefaction takes place. To overcome this difficulty, simple sinusoidal wave form is adopted. By doing this, frequency content of 1987 Superstition Hills Earthquake caused severe liquefaction as mentioned earlier is obtained by using discrete fourier transformation method (Figure 4.7 (b)). Mentioned transformation is done by writing simple Matlab code which is given in Appendix A. According to frequency content of the earthquake, it is obtained that effective frequency range is in the range of 0.05 Hz to 20 Hz. Then, for our numerical model, most proper frequency is determined as 10 Hz. The details for that will be given in the following sections. Also, Holzer and Youd (2007) stated that surface waves like Love wave having frequency greater than 5 Hz cause unexpected effect on liquefaction in WLA.

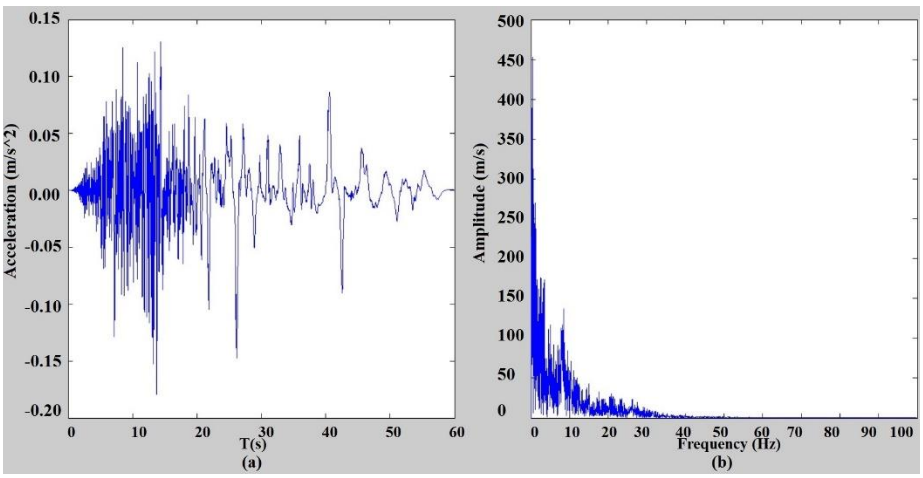

Figure 4.7 1987 Superstition Hills Earthquake; (a) time history record (b) frequency domain

After trials for different frequencies and amplitudes, most proper frequency for this study is selected as 10 Hz. Also, because of the fact that suddenly applied loading causes dominancy of inertial effects which disturbs response of the system in an undesired manner, wave function describes ramping loading in terms of acceleration are obtained:

$$a(t) = \frac{A}{2} sin(2\pi f t) \left(1 - \cos\left(\frac{\pi}{3} t\right)\right) \tag{4.2}$$

Where a(t) is time dependent acceleration, A is amplitude, f is frequency and t is real time. In this study, four wave types having peak amplitudes of 0.05g, 0.06g, 0.07g and 0.08g are adopted (Figure 4.8).

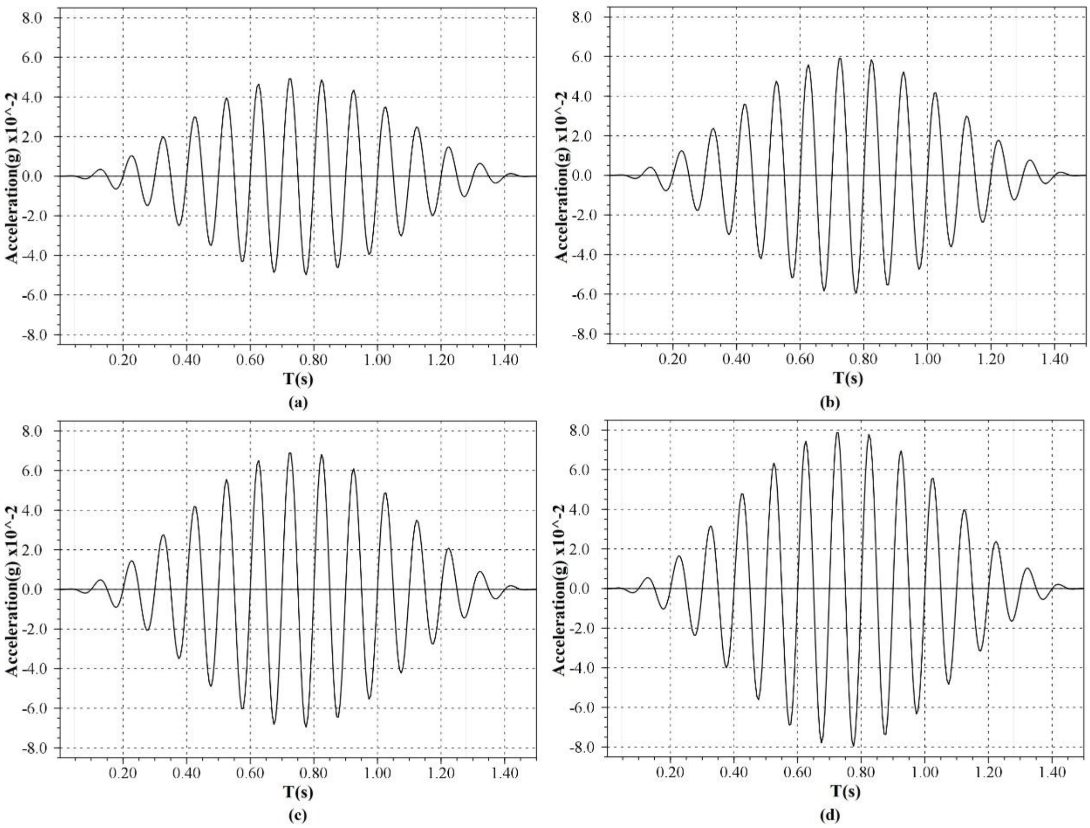

Figure 4.8 Dynamic input motions involving different peak acceleration values; (a) 0.05g (b) 0.06 g (c) 0.07g (d) 0.08g

The reason why such peak acceleration values are selected is that both 0.05g and 0.08g values are extreme values for numerical model in terms of r_u. That is, below

0.05g, liquefaction does not occur due to insignificant r_u values while yielding of soil takes place before occurrence of liquefaction in case of peak acceleration values greater than 0.08g.

4.6 Free Field Dynamic Analyses

Before determining the most proper conditions for numerical modelling of the problem with respect to liquefaction, 3-D site response analyses were performed. According to site response analyses, optimum model dimensions, most suitable meshing type that conveys wave without causing any distortions and dynamic input motions for 3-D numerical model were determined. Then, based on optimum numerical model parameters, free field analyses were performed. Besides, results for both 1-D and 3-D analyses were compared to each other whether additional calibration is necessary.

4.6.1 3-D Site Response Analyses in FLAC3D

As mentioned earlier, FLAC3D performs dynamic analysis by solving full equations of motion, using lumped grid point masses derived from real density of surrounding zones rather than fictitious masses (FLAC3D User's Manual, 2008). However, it requires compatible mesh form which makes FLAC3D mesh-oriented. Therefore, for the sake of accuracy and convergence of the numerical model, proper constitutive soil model with related boundary, correct mesh form which does not distort wave while transmitting it and, effective model dimensions should be chosen with respect to dynamic input motion.

In the optimization procedure of the above mentioned interrelated model parameters, certain outputs such as unbalanced force, plasticity state of soil, symmetric stresses, deformations and r_u values in both static and dynamic analyses were controlled. In fact, optimization was done primarily according to robustness of r_u values for symmetrical places. In other words, similar r_u values rather than fluctuating in symmetrical places were crucial concern in optimization. Locations of utilized r_u

values in each model are given in Figure (4.9). Besides, at a given place, r_u values at the depths of 2 m, 4 m, 6 m, 8 m, 10 m and 12 m are utilized throughout this study. Although 2B spacing is out of purpose in this study, it is used in the determination of final wave type. Besides, in the comparison of results obtained for each model, points having same ID number are compared to each other so as to both generalize the obtained results and get rid of negative effects of finer mesh zone close to jet grout columns. Detailed explanation is given in following sections.

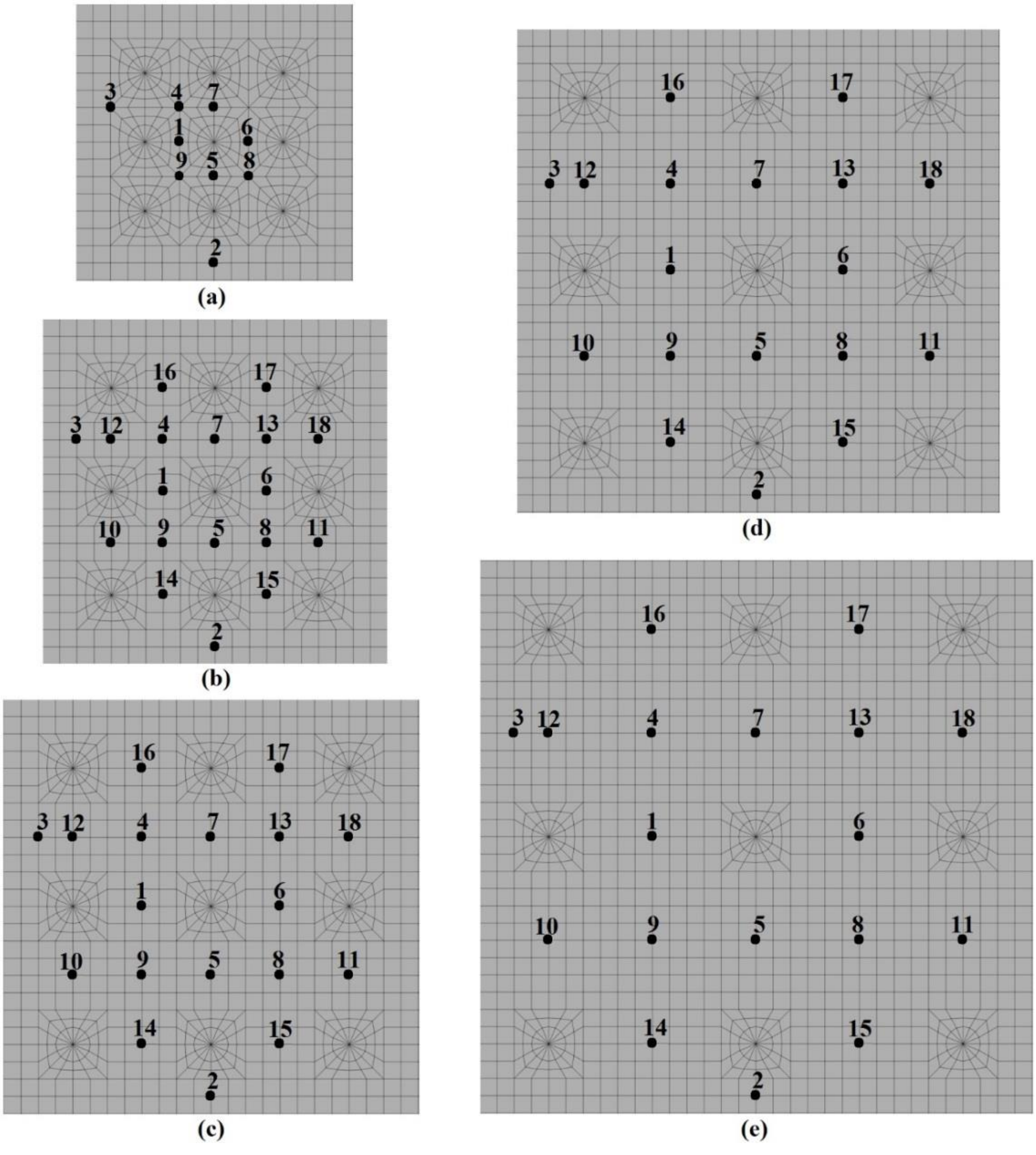

Figure 4.9 Location of data points for each model; (a) 2B spacing (b) 3B spacing (c) 4B spacing (d) 5B spacing (e) 6B spacing

4.6.1.1 Constitutive Soil Model and Boundary Conditions

In this study, Mohr-Coulomb plasticity model is adopted for soil. In this model, in case of presence of shear loading, material yields depending on only magnitude of major and minor principal stresses. Also, numerical model is coupled with dynamic pore pressure generating Finn model (Martin et al., 1975).

In order to perform effective stress-based liquefaction analysis, presence of excess pore water pressure is a necessity under dynamic loading. Martin et al (1975) and Finn (1982) express development of excess pore pressure in undrained sands by means of plastic volumetric strains generated by slips at grain contacts. As pore pressures build up, effective stress decreases that causes sand to rebound elastically. They expressed the irrecoverable volumetric strain in an incremental manner as follows:

$$\Delta\varepsilon_v = C_1(\gamma - C_2\varepsilon_v) + \left(\frac{c_3\varepsilon_v^2}{\gamma + C_4\varepsilon_v}\right) \tag{4.3}$$

Where $\Delta\varepsilon_v$ is incremental volumetric strain, ε_v is cumulative volumetric strain, γ is corresponding shear strain amplitude and C1, C_2, C_3 and C_4 are constants. Then, increase of pore pressure is given in the following equation:

$$\Delta u = E_r\Delta\varepsilon_v \tag{4.4}$$

Where Δu is amount of increase in pore pressure, E_r is rebound modulus of soil skeleton and $\Delta\varepsilon_v$ is incremental volumetric strain. Rebound modulus (E_r) can be computed for an effective stress level (σ'_v) with respect to initial vertical effective stress as follows:

$$E_r = \frac{(\sigma'_v)^{1-m}}{mk_2(\sigma'_{v0})^{n-m}} \tag{4.5}$$

In which m, n and k_2 are experimental constants for a sandy soil. Algorithm of Finn model is given in Figure (4.10).

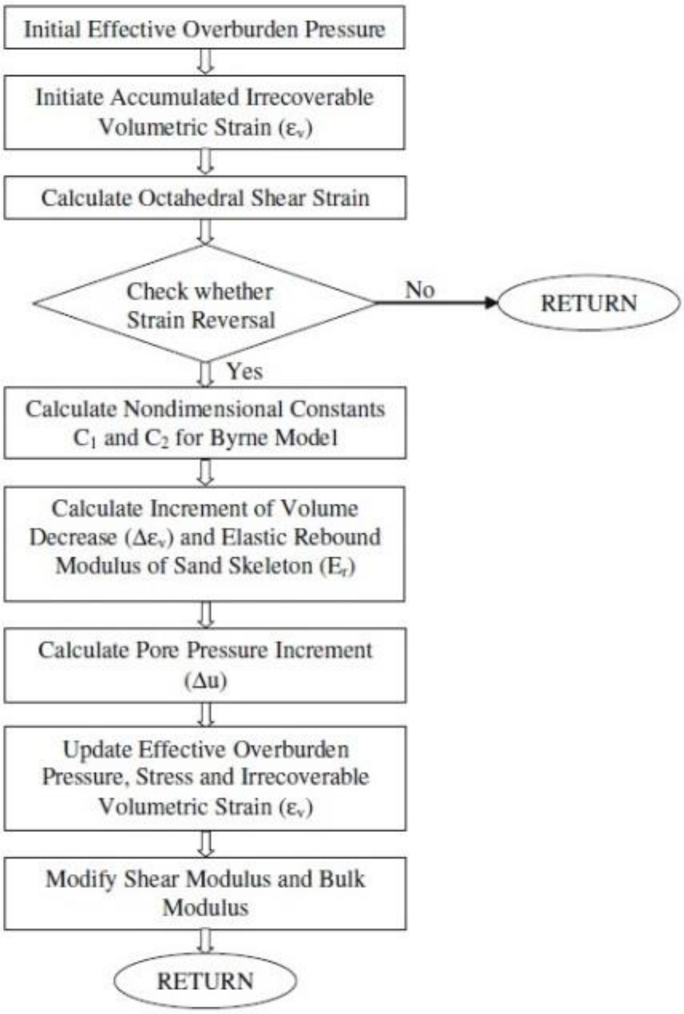

Figure 4.10 Finn model algorithm

In order to take non-linear effects into account, strain-dependent modulus and damping functions are employed. Therefore, upper range modulus reduction curve for sandy soil (Seed & Idriss, 1970) is used (Figure 4.11). By doing this, softening behavior causing liquefaction is represented. Besides, corresponding hysteric damping function which fulfills the two Masing criteria is used. Moreover, to compensate imperfection of employed modulus degradation curve at low level strains, additional Rayleigh damping is used (FLAC3D User's Manual, 2008). Corresponding damping ratio is 0.2% and its center frequency is equal to 10 Hz. By doing this, released energy is able to be removed at low strain levels.

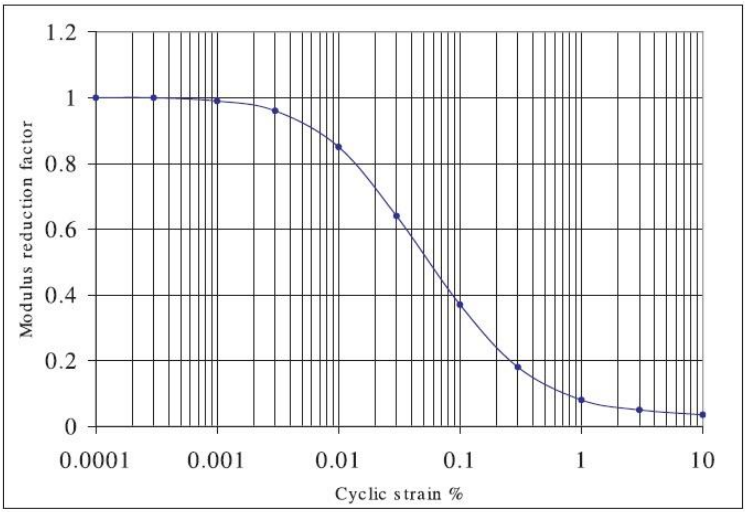

Figure 4.11 Modulus degradation curve for sandy soil

Moreover, to represent in-situ conditions, small strain modulus, known as maximum shear modulus (G_{max}), is employed based on shear wave velocity. Corresponding numerical value was given in Section 4.3. Hence, G_{max} was obtained from the following equation:

$$G_{max} = \rho(V_s)^2 \tag{4.6}$$

To obtain geostatic condition in numerical model, static analysis is performed. While doing this, it is crucial to convert Finn model to Mohr-Coulomb in this stage. That is, water bulk modulus is assumed as zero, but, it is reset to its own real value as 2 GPa in dynamic analysis. Also, minimum number of steps between reversals is set to very large value in static analysis and it is changed from 1000000 to 50 in dynamic analysis stage. Furthermore, to prevent deviation in total stresses for all nodes at a given depth in the model, iterations are performed elastically. Otherwise, it is not possible to obtain similar geostatic stresses at a given depth. Moreover, due to absence of cohesion and tension limit, at some places at shallow depths on the order of 0.5 m, state of soil changes from elastic to plastic at the end of static analysis. Therefore, plastic state is removed before dynamic analysis stage. Corresponding FLAC3D code is given in Appendix B. Geostatic vertical total stresses are given in Figure (4.12). Although conversion between Finn model and Mohr-Coulomb model is done, negligible differences can occur due to mesh effect (Figure 4.12 (b)).

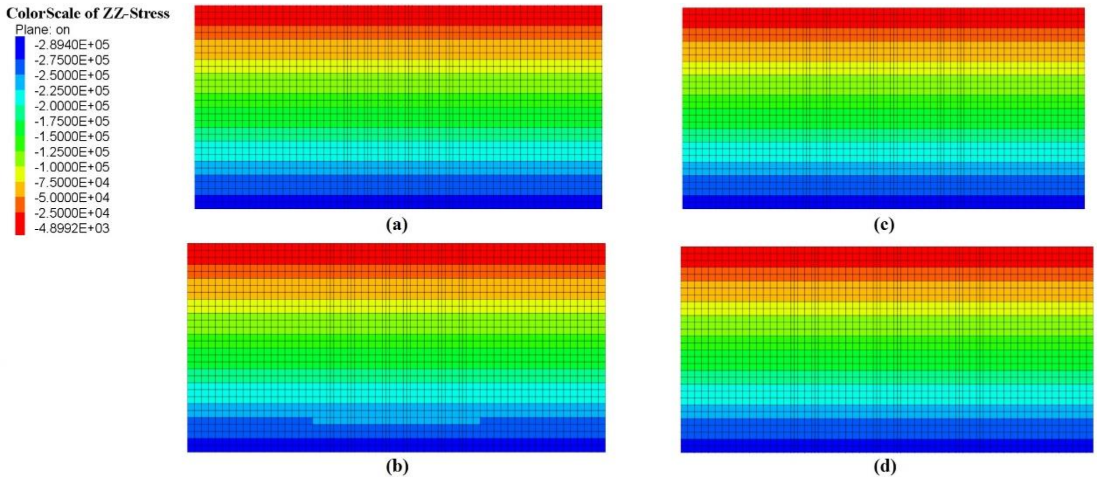

Figure 4.12 Geostatic vertical total stress for each model; (a) 3B spacing (b) 4B spacing (c) 5B spacing (d) 6B spacing

As mentioned previously, roller supports are utilized as boundary conditions in static analyses (Figure 4.13 (a)). However, in dynamic analysis stage, they are removed to prevent propagating wave reflection that reduces energy radiation at the boundaries of model. Actually, there exit two ways of simulation of in-situ conditions with respect to prevention of wave reflection and damping, namely; very large model that material damping absorbs most of energy in the waves reflected at farther boundaries and removal of roller boundaries by applying free field boundaries. Due to the fact that first option results in large computational burden, second option that adopts viscous dashpots at the boundaries which allows passing of waves through itself by simulating infinitely large model is used (Figure 4.13 (b) & (c)). Moreover, at the base of the model, quiet boundaries are also used to absorb reflecting waves.

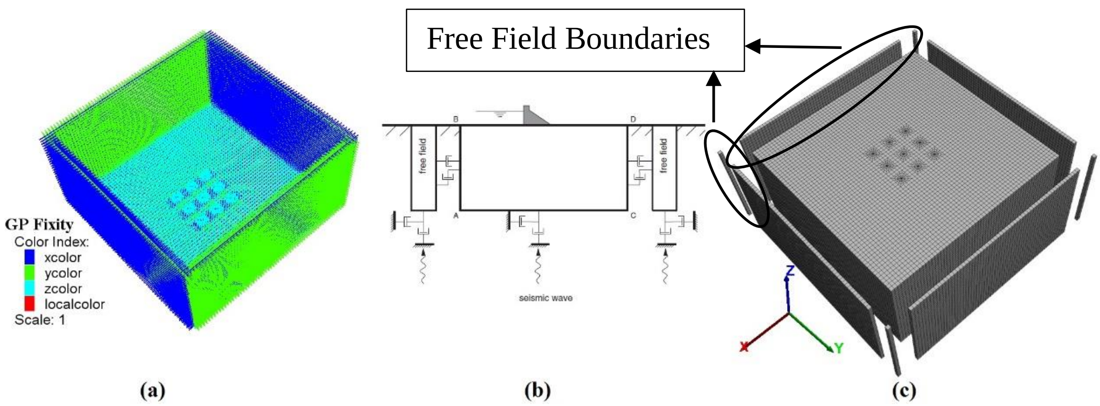

Figure 4.13 Boundary conditions; (a) roller supports (b) representation of viscous dashpots (c) free field boundaries

4.6.1.2 Determination of Proper Mesh Form

In dynamic analysis, proper energy transmission is directly related with maximum size of mesh discrete elements to obtain accurate modelling of the deformability of continuum with respect to wavelengths (Carlo, 2013). For accurate representation of wave transmission Kuhlemeyer and Lysmer (1973) stated that maximum spatial element size (Δl) should be smaller than one-tenth of the wavelength (λ) of corresponding frequency:

$$\Delta l = \frac{\lambda}{10} \tag{4.7}$$

Also, maximum frequency (f_{max}) with respect to given spatial size is obtained based on the smallest of compressional wave (V_p) and distortional shear wave (V_s) speeds:

$$f_{max} = \min\left(\frac{V_p}{10\Delta l}, \frac{V_s}{10\Delta l}\right) = \min\left(\frac{\sqrt{\frac{K+4G/3}{\rho}}}{10\Delta l}, \frac{\sqrt{\frac{G}{\rho}}}{10\Delta l}\right) \tag{4.8}$$

Where, K is bulk modulus, G is shear modulus and ρ is mass density. Therefore, in this study, it is computed that maximum frequency that can be transmitted without dispersion for mesh size of 0.5 m is 30 Hz according to Equation (4.9).

$$f_{max} = \min\left(\frac{\sqrt{\frac{10^6(21.97+4(4.71)/3}{1992.78/9.81}}}{10(0.5)}, \frac{\sqrt{\frac{10^6(4.71)}{1992.78/9.81}}}{10(0.5)}\right) = \min(75{,}30) \tag{4.9}$$

Furthermore, in finite difference method, time step (Δt) and discrete element size (Δx) should be interrelated and they should satisfy Courant-Friederichs-Levy stability condition (Carlo, 2013):

$$\frac{V_s \Delta t}{\Delta x} = C, C \leq 1 \tag{4.10}$$

In this study, C is obtained as 2.17e-03 for dynamic time step of 2.8485e-05, 0.5 m discrete element size and shear wave velocity of 152 m/s. Therefore, error magnitude is limited by providing stable algorithm.

In this study, due to presence of jet grout columns, it is not possible to use same mesh size in the entire model. That is, cubic spatial elements are used away from location of jet grout columns while type of mesh element for columns is chosen as wedge shaped as a necessity. Also, various mesh forms at different locations in a model such as soil-bridge-earthquake interaction model (Carlo, 2007) and model for effectiveness of high modulus columns against liquefaction (Unutmaz, 2012) were adopted. That is, away from interested region, large mesh size are used (Figure 4.14).

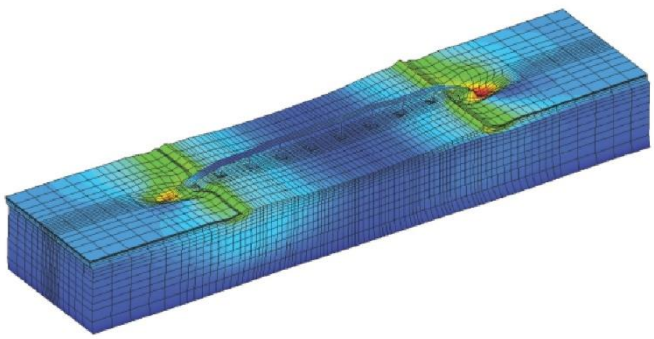

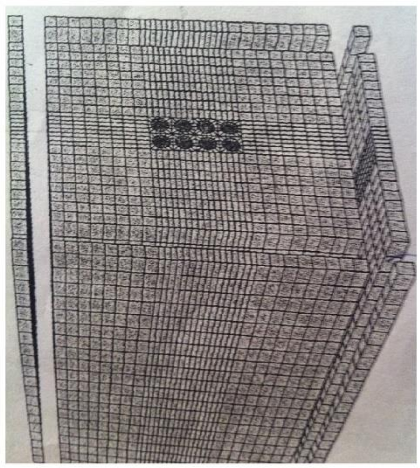

(a) **(b)**

Figure 4.14 Various mesh size at different locations

In this study, six models were constructed to investigate effect of wedge shaped mesh at the locations of columns and influence of various type of mesh forms (Figure 4.15 & Figure 4.16). All models were compared based on r_u values acquired at certain elevations in the model. In the assessment of alternatives, dynamic loading was selected as expressed in Equation (4.2). Besides, this loading is graphed in Figure (4.8 (c)).

In the first alternative model (Figure 4.15 (a) & Figure 4.16 (a)), cubic mesh elements (0.5 m x 0.5 m x 0.5 m), are adopted while same mesh form except spatial size equal to 1 m are used in the second model (Figure 4.15 (b) & Figure 4.16 (b)). In the remaining four alternatives, column mesh forms for 3B spacing are used although real jet grout columns does not take place in site response analyses, yet. That is, column mesh are used although there exists not jet grout columns in the site response analyses. The reason for that is to comprehend influence of wedge shaped mesh on r_u values. Also, in the third and fourth models (Figure 4.15 (c) & Figure 4.16 (c); (Figure 4.15 (d) & Figure 4.16 (d))), various mesh forms including rectangular and cubic forms at various locations are used. The difference between these two alternatives is the thickness of mesh element in z (vertical) direction. In alternative 3, mentioned thickness is equal to 0.5 m, but, it is 1.0 m for alternative 4. In these two model, used sizes are 1.0 m x 1.0 m 0.5 m, 0.5 m x 1.0 m x 0.5 m, 1.0 m x 0.5 m x 0.5 m for the third alternative and same sizes for alternative 4 except z (vertical) size equal to 1.0 m. Besides, in last two alternatives, uniform mesh elements except jet grout column mesh form are used (Figure 4.15 (e) & Figure 4.16 (e); (Figure 4.15 (f) & Figure 4.16 (f)). Corresponding spatial element sizes are 0.5 m x 0.5 m x 0.5 m and 0.5 x 0.5 m x 1.0 m in x, y and directions, respectively.

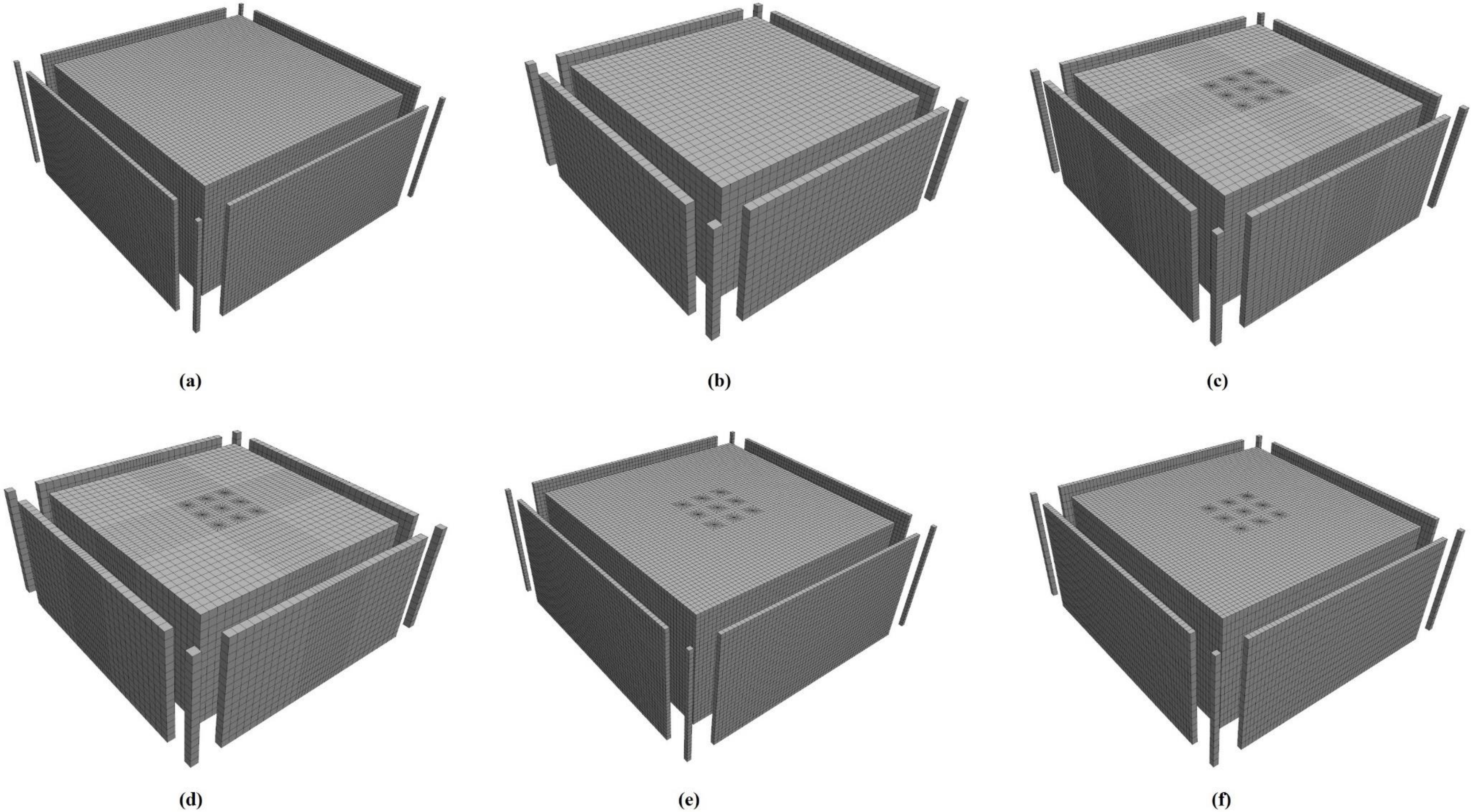

Figure 4.15 Six alternative models; (a) alternative 1 (b) alternative 2 (c) alternative 3 (d) alternative 4 (e) alternative 5 (f) alternative 6

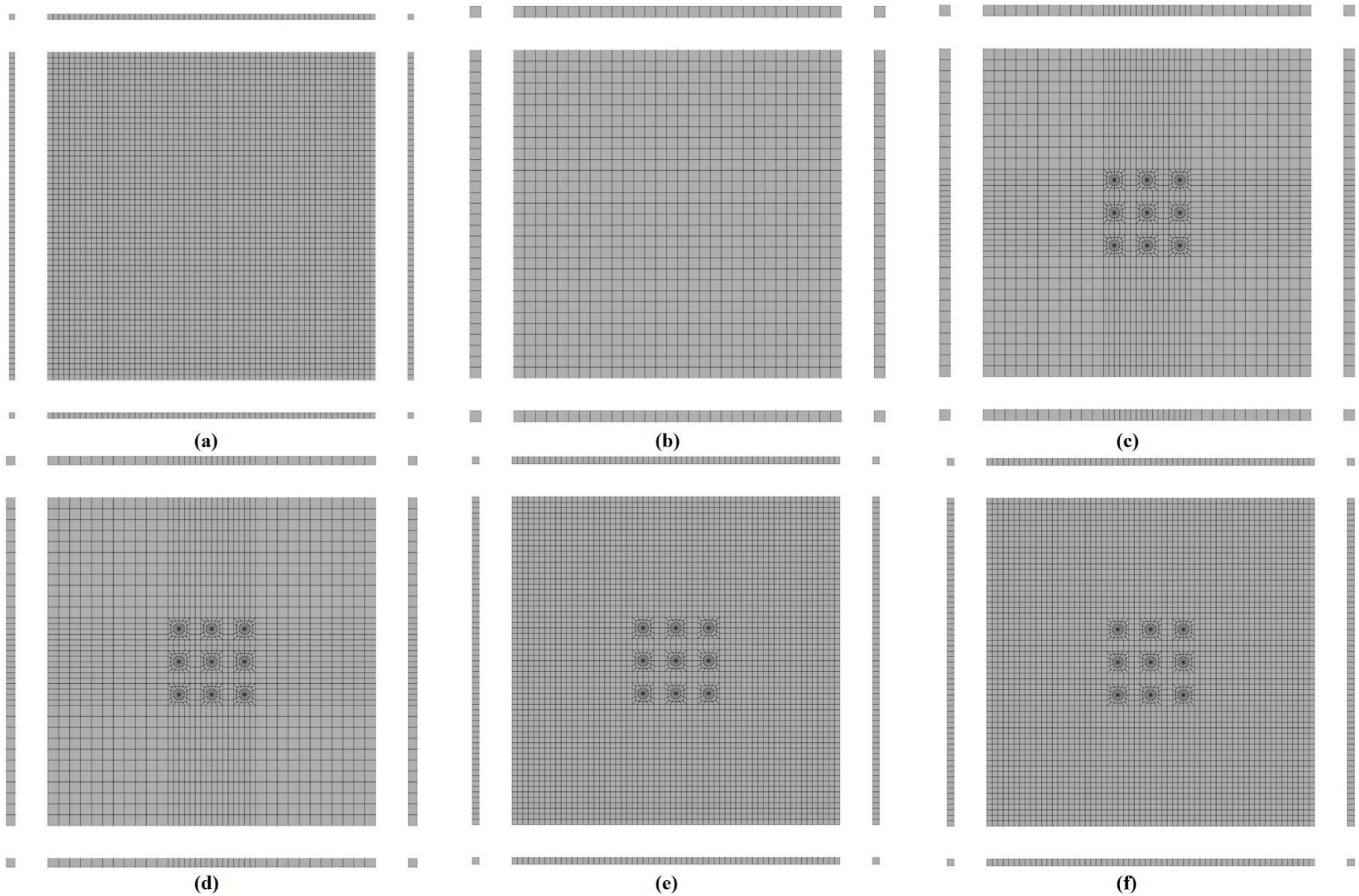

Figure 4.16 Top view of six alternative models; (a) alternative 1 (b) alternative 2 (c) alternative 3 (d) alternative 4 (e) alternative 5 (f) alternative 6

In the comparison of alternatives, r_u values at the same locations for corresponding models were taken into account. Besides, these selected points have ID numbers in the range of 1 to 6 (Figure 4.9 (b)). Although r_u values continuously change during dynamic analysis, representative value of it was accepted as the final value at the end of the analysis. Furthermore, in case of large oscillation, mean value of larger and lower values was used. Hence, r_u values are computed throughout this study according to the following equation which was defined in FLAC3D as a Fish Function:

$$r_u = \frac{u_t - u_s}{\sigma'_{v0}} \tag{4.11}$$

Where u_t is total pore pressure including dynamically induced excess pore pressure, u_s is the pore pressure at the static condition and σ'_{v0} is initial vertical effective stress. Although there has been an ongoing debate on whether major principal stress or average value of major, intermediate and minor principle stresses should be used at the denominator in Equation (4.11), in this study, major principle stress value (i.e. vertical effective stress) was used.

In the light of given information and mathematical expression, r_u values corresponding to the ID of 4 for each model are given in the Figure (4.17). Also, in this figure, r_u values for 6 different depths belonging to ID 4 is shown. Mentioned depths are 2 m, 4 m, 6 m, 8 m, 10 m and 12 m below soil surface. Corresponding sub-IDs for the depths from 2 m to 12 m, are p_r_a4, p_r_d4, p_r_g4, p_r_j4, p_r_m4 and p_r_p4, respectively. Although r_u values seem to stabilize towards to the end of analysis, exactly the same r_u values may not be obtained if same analysis is repeated under same conditions. That is, based on gained experience from this study, final r_u values occurred in an analysis may deviate on the order of ±0.05. In other words, obtained r_u equal to 0.90 for a performed analysis may attain values in the range of 0.85 to 0.95 if analysis is repeated.

Actually, in last four alternatives, jet grout column mesh form having spacing 3B is adopted. Therefore, finer but not uniform mesh as wedge shape takes place in these models. As a result, at first glance, according to Figure 4.17, it is noticeable that r_u

record history is more refined for alternative 1 and 2. In fact, the reason is that presence of fine mesh in last four alternatives reduces dynamic time step by causing much more r_u record for time interval. Besides, second important difference between alternatives, large mesh size is likely to cause relatively higher r_u values as compared to same model having smaller mesh size.

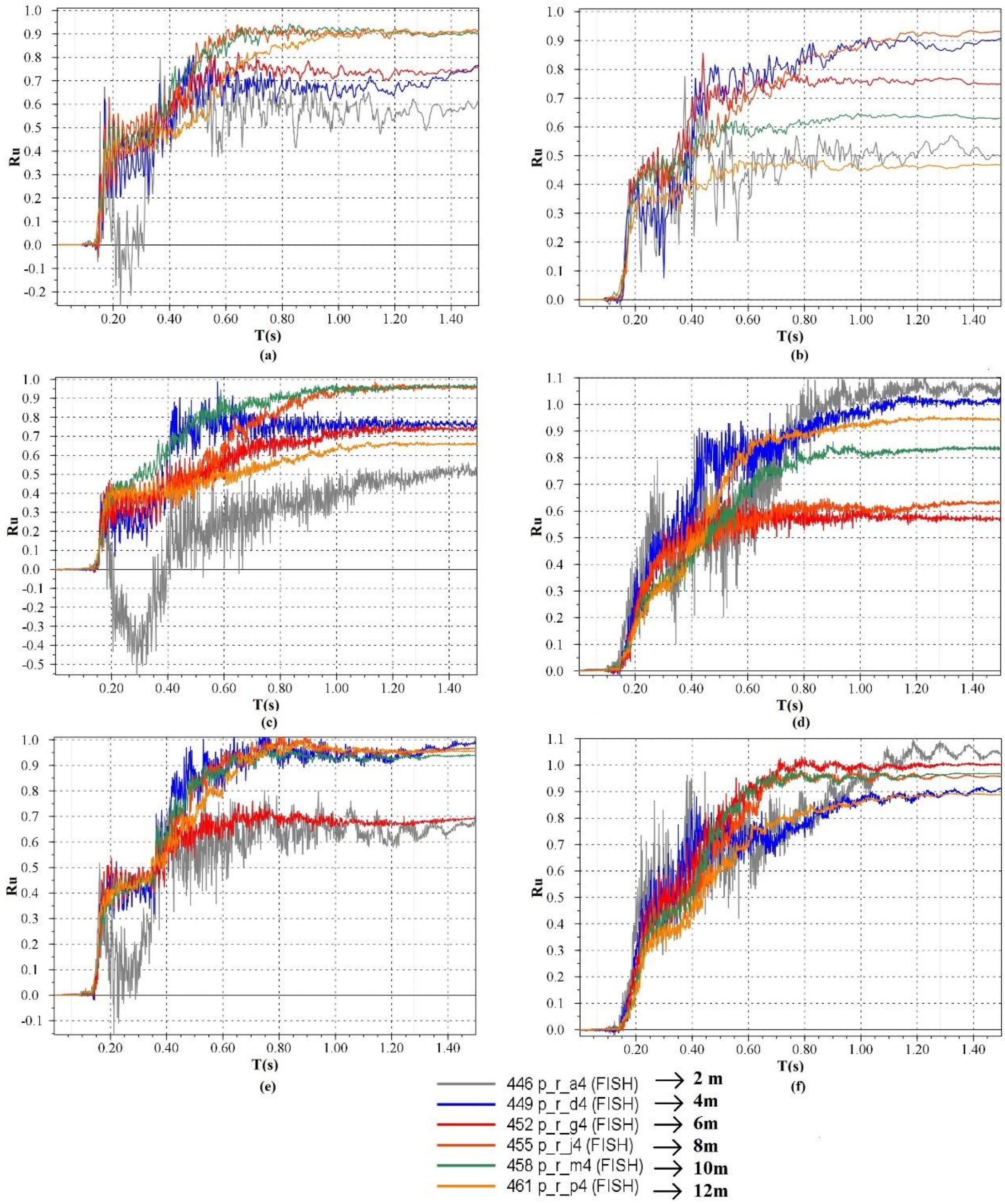

Figure 4.17 Values of r_u for ID 4 for each model; (a) alternative 1 (b) alternative 2 (c) alternative 3 (d) alternative 4 (e) alternative 5 (f) alternative 6

Contrary to mentioned major differences, there exist similarities between alternatives. First, r_u values are able to converge to a stable value in general. Second, due to low vertical stress at the depth of 2 m, trend of r_u values are different than those at deeper locations. That is, r_u value might be greater than even 1.0 at the end of analysis while it decreases to below zero at the beginning of the analysis. The reason for that decrease in r_u values at the beginning of the analysis might be due to dilation.

Based on results obtained from 6 different locations in each alternative, alternative 5 used throughout entire study is compatible with alternative 1 based on r_u (Table 4.4). In this table, shaded columns are results presented in Figure (4.17). Besides, the term 'ave' is average of r_u values for 6 different locations at a given depth.

Table 4.4 Values of r_u for each alternative with respect to 6 various locations

	ALTERNATIVE 1							**ALTERNATIVE 2**						
ID / z(m)	**1**	**2**	**3**	**4**	**5**	**6**	**Ave**	**1**	**2**	**3**	**4**	**5**	**6**	**Ave**
2	0.58	0.58	0.48	0.60	0.63	0.78	0.61	0.60	0.93	0.70	0.50	0.60	0.90	0.70
4	1.00	0.70	0.83	0.75	0.88	0.83	0.83	1.00	0.88	0.60	0.90	1.00	0.50	0.81
6	0.73	0.65	0.75	0.75	0.68	0.60	0.69	0.75	0.65	0.83	0.75	0.68	0.53	0.70
8	0.85	0.98	0.73	0.90	0.73	0.95	0.85	0.90	0.70	0.80	0.93	0.93	0.98	0.87
10	0.78	0.90	0.95	0.90	0.55	0.80	0.81	0.85	0.80	0.73	0.63	1.05	0.80	0.81
12	0.85	0.60	0.75	0.90	0.88	0.90	0.81	0.98	0.93	0.88	0.45	0.98	0.83	0.84
	ALTERNATIVE 3							**ALTERNATIVE 4**						
ID / z(m)	**1**	**2**	**3**	**4**	**5**	**6**	**Ave**	**1**	**2**	**3**	**4**	**5**	**6**	**Ave**
2	0.75	0.65	0.60	0.50	0.65	0.88	0.67	0.60	0.78	0.65	1.00	0.70	1.10	0.80
4	0.85	0.75	0.88	0.78	0.70	1.00	0.83	0.80	0.85	0.80	1.00	1.00	0.85	0.88
6	0.95	0.60	0.75	0.75	0.53	0.60	0.70	0.83	0.83	0.75	0.58	0.68	0.55	0.70
8	1.00	0.85	0.90	0.95	0.68	0.85	0.87	0.73	0.60	0.70	0.63	0.50	0.63	0.63
10	0.88	0.90	1.00	0.95	0.88	0.63	0.87	0.98	0.75	0.75	0.83	0.93	0.70	0.82
12	0.60	0.60	0.85	0.65	0.45	0.95	0.68	0.95	0.68	0.95	0.95	1.00	0.95	0.91
	ALTERNATIVE 5							**ALTERNATIVE 6**						
ID / z(m)	**1**	**2**	**3**	**4**	**5**	**6**	**Ave**	**1**	**2**	**3**	**4**	**5**	**6**	**Ave**
2	0.93	0.48	0.33	0.68	0.78	0.88	0.68	1.10	0.70	0.98	1.05	1.10	1.10	1.00
4	1.00	0.83	0.70	0.98	0.93	0.93	0.89	1.00	1.00	0.80	0.90	0.88	1.10	0.95
6	0.78	0.70	0.70	0.70	0.73	0.60	0.70	1.00	0.90	0.93	1.00	0.85	0.95	0.94
8	0.95	0.80	0.80	0.95	0.55	0.98	0.84	0.98	0.83	0.95	0.95	0.95	1.00	0.94
10	0.95	0.93	0.90	0.93	0.65	0.95	0.88	0.95	0.73	0.95	0.95	0.95	1.00	0.92
12	0.98	0.88	0.95	0.95	1.00	1.00	0.96	0.95	1.10	0.53	0.88	0.93	0.90	0.88

With the help of these analyses, negative effect of jet grout column mesh on final pore pressure values at the end of analysis are identified (Figure 4.18). Although total pore pressure values inside jet grout column mesh deviates significantly from the values where uniform mesh such as cubic and rectangular is used, beyond the transition zone between fine mesh and uniform mesh, pore pressure values converge to the compatible values what it should take. Therefore, only mid-points between adjacent columns which are indicated in Figure (4.9) are used in the assessment of both free field analyses and pure jet grout column contribution on liquefaction mitigation. Besides, according to this figure, best matching with alternative 1 is attained by alternatives 5 although it cannot be entirely comprehensible just investigating 6 locations. Thus, at later stages, additional 12 different locations are utilized in free field analyses.

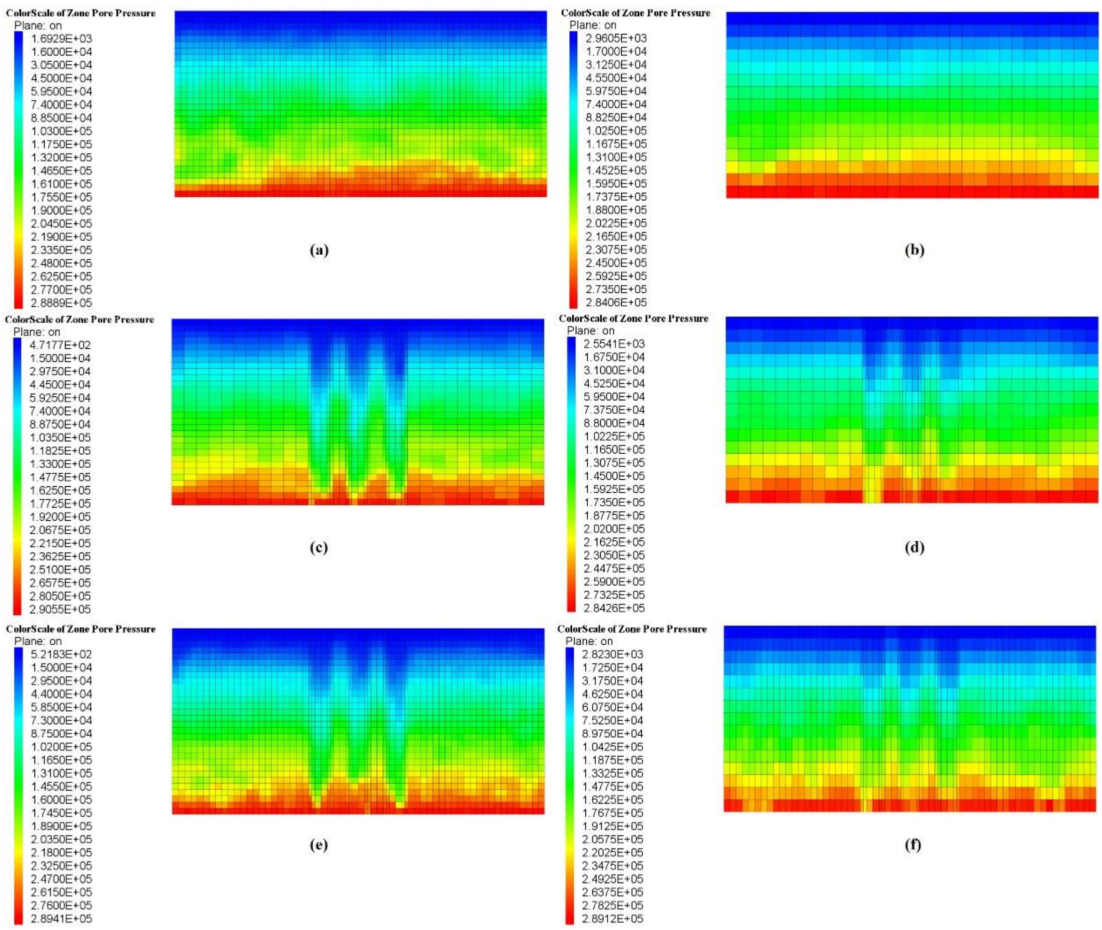

Figure 4.18 Total pore pressure values (in Pascal); (a) alternative 1 (b) alternative 2 (c) alternative 3 (d) alternative 4 (e)alternative 5 (f) alternative 6

To sum up, r_u values do not take constant values throughout the model at a given depth even if the single mesh form is adopted. However, several alternatives except alternative 4 and 6 result in good agreement with alternative 1 in accordance with r_u. This agreement is also shown in Figure (4.19) with regard to average r_u values for mentioned 6 locations. Therefore, to control such variations in r_u values for entire model, several models are constructed and compared to each other. Hence, alternative 5 is found as the most suitable model for later stages.

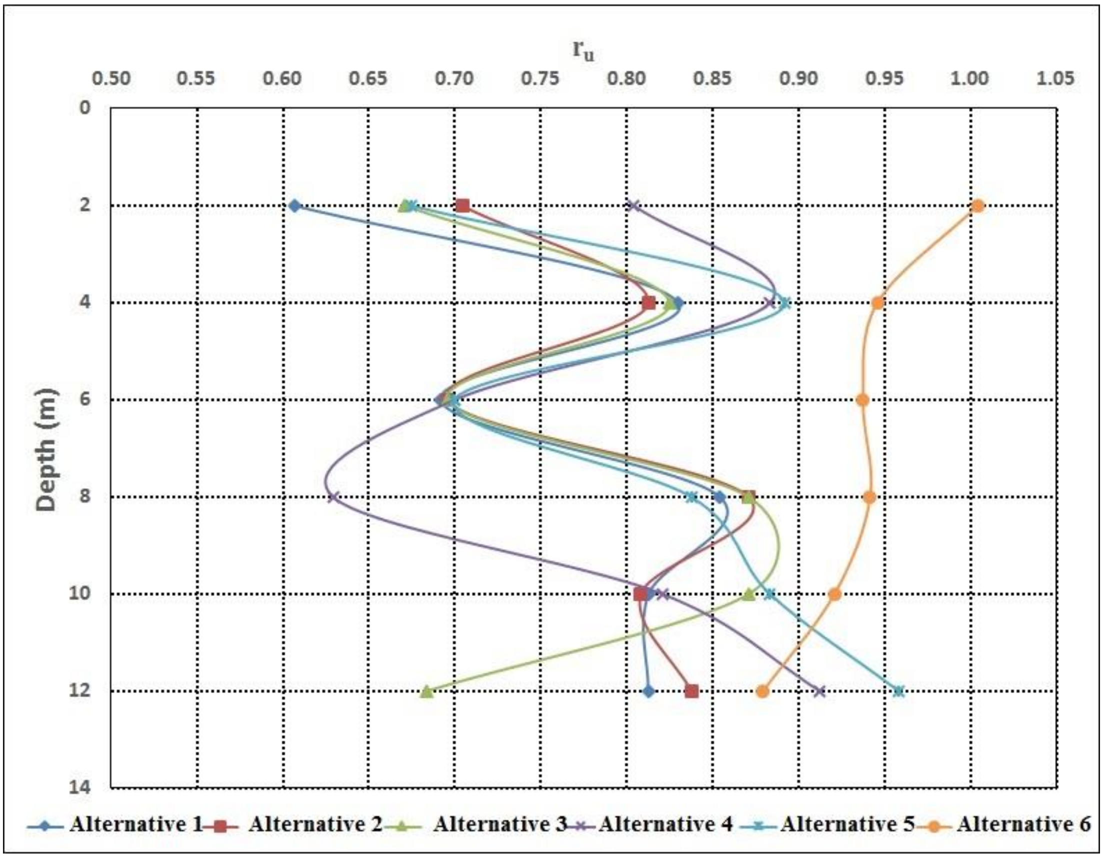

Figure 4.19 Average r_u values for each alternative

4.6.1.3 Optimum Model Dimensions

Canadian Foundation Engineering Manual (1978) suggests that 8B spacing is enough to handle pile-soil-pile interaction under static lateral loading. That is, beyond 8B spacing, effect of pile-soil-pile interaction becomes negligible in terms of p-y curve. However, such generalization has not been made for sandy soil under cyclic loading (Reese & Van Impe, 2011).

Optimum model dimensions used in this study are 30 m x 30 m x 15 m in x, y and z directions, respectively. Optimization was performed primarily for a model in which spacing between jet grout columns is equal to 6B. Also, as presented in Figure (4.6 (d)), spacing between boundary and outer jet grout column center is equal to 9 m corresponding to 9B. The reason why such a model was selected and tested is that this model is critical in terms of being close to boundary. Mentioned model was compared with larger model having same jet grout column disposition (Figure 4.20). Large model has dimensions of 60 m x 60 m x 15 m in x, y and z directions, respectively. Comparison between models was made for r_u values at the locations IDs of which are 1, 2, 3, 4, 5 and 6 (Figure 4.6 (d)). Besides, selected dynamic motion has peak acceleration value of 0.07g as shown in the Figure (4.8 (c)).

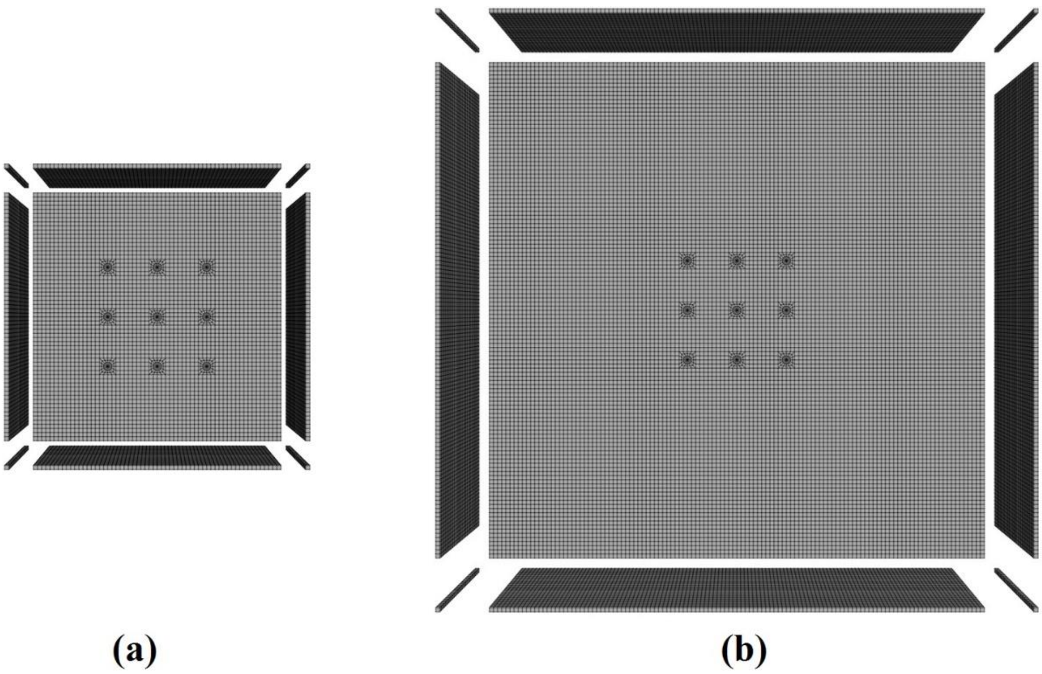

Figure 4.20 Various Model Dimensions; (a) optimum model (b) large model

Based on total pore pressure values, there exists no significant difference between these two models (Figure 4.21). Also, negative effect of jet grout column mesh disappears rapidly compared to same model with 3B spacing in transition zone.

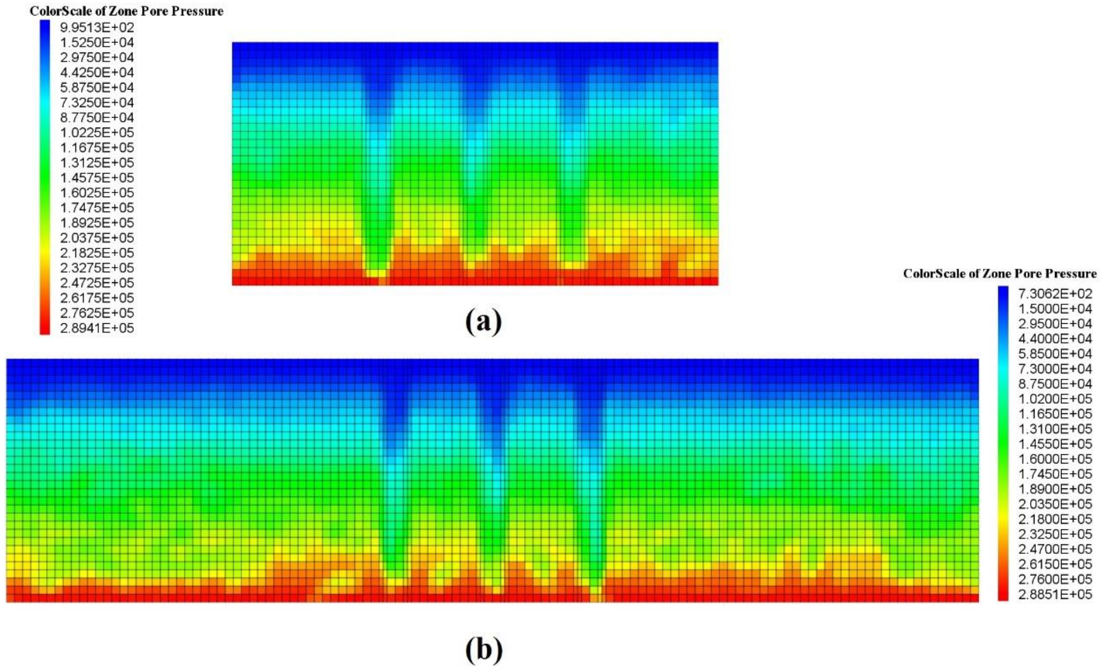

Figure 4.21 Total pore pressure values at the end of dynamic analysis; (a) optimum model (b) large model

Obtained r_u values for both model are quite similar to each other (Figure 4.22). Also, in this figure, r_u values for 6 different depths belonging to ID 2, 3 and 5 are shown. Mentioned depths are 2 m, 4 m, 6 m, 8 m, 10 m and 12 m. Corresponding sub-IDs with respect to main IDs and depth of consideration from 2 m to 12 m, are c2, f2, i2, l2, o2 and s2 (for ID 2); p_r_a6, p_r_d6, p_r_g6, p_r_j6, p_r_m6 and p_r_p6 (for ID 3); p_r_a2, p_r_d2, p_r_g4, p_r_j2, p_r_m2 and p_r_p2 (for ID 5).

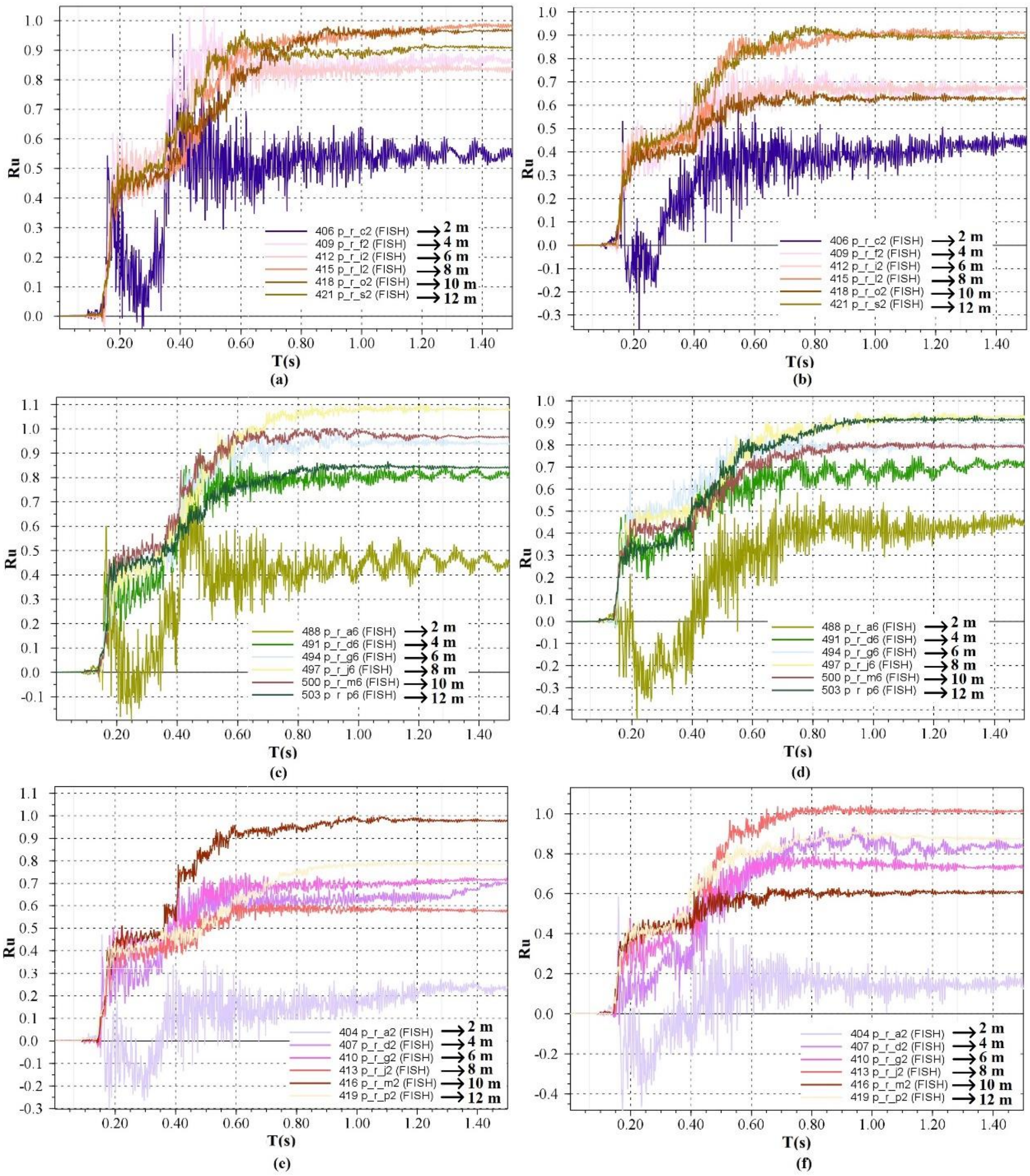

Figure 4.22 Values of r_u for IDs 2, 3 and 5 for each model; (a) optimum model (b) large model

Furthermore, average r_u values corresponding to each depth verify that both models are compatible to each other (Table 4.5). Shaded columns represent numerical results for ID 2, 3 and 5. Although obtained results are valid for site response and free field analyses, model dimension efficiency is also controlled in the improved site analyses.

Table 4.5 Values of r_u for each alternative with respect to 6 various locations

	OPTIMUM MODEL							LARGE MODEL						
ID / z(m)	**1**	**2**	**3**	**4**	**5**	**6**	**Ave**	**1**	**2**	**3**	**4**	**5**	**6**	**Ave**
2	0.45	0.55	0.45	0.55	0.38	0.40	0.46	0.75	0.45	0.45	0.43	0.18	0.53	0.46
4	0.95	0.85	0.80	0.90	0.70	0.90	0.85	0.73	0.68	0.70	0.78	0.85	0.90	0.77
6	0.78	0.83	0.93	0.73	0.73	0.70	0.78	0.60	0.68	0.80	0.55	0.75	0.68	0.68
8	0.98	0.98	1.08	0.93	0.58	0.95	0.91	0.85	0.90	0.93	1.00	1.00	0.88	0.93
10	1.00	0.95	0.98	1.03	0.98	0.80	0.95	0.78	0.63	0.80	0.83	0.60	0.93	0.76
12	0.60	0.90	0.85	0.70	0.78	0.60	0.74	0.95	0.90	0.90	0.80	0.88	0.60	0.84

4.6.1.4 Determination of Dynamic Loading

In this study, simple sinusoidal wave forms are adopted to simulate dynamic action due to limitation of plastic Finn model. Although several attempts were made to use real earthquake data, due to excessive modulus degradation, it was noticed that yielding of soil takes place before liquefaction occurs (Figure 4.23).

In Figure (4.23), modulus degradation of soil for various depths is given. Also, this strain dependent degradation data corresponds to the center of the model composed of uniform mesh elements of 0.5 m x 0.5 m x 0.5 m in x, y and z directions. According to this figure, decrease rate of modulus is such rapid that modulus becomes almost zero despite the fact that only 20 seconds of the total earthquake time are applied to the model. Besides, magnitude of earthquake is equal to 6.6 which is classified as moderate. Unless maximum shear modulus is increased resulting in prevention of occurrence of meaningful r_u values, real earthquake motion causes yielding of soil rather than liquefaction. Furthermore, real earthquake motion does not result in stable r_u values. Therefore, to handle mentioned drawbacks, simple wave forms were used. Until final selection of dynamic input motions, there exist three stages. In all stages, mesh form is adopted as indicated in Figure (4.20 (a)) and (4.15 (e)).

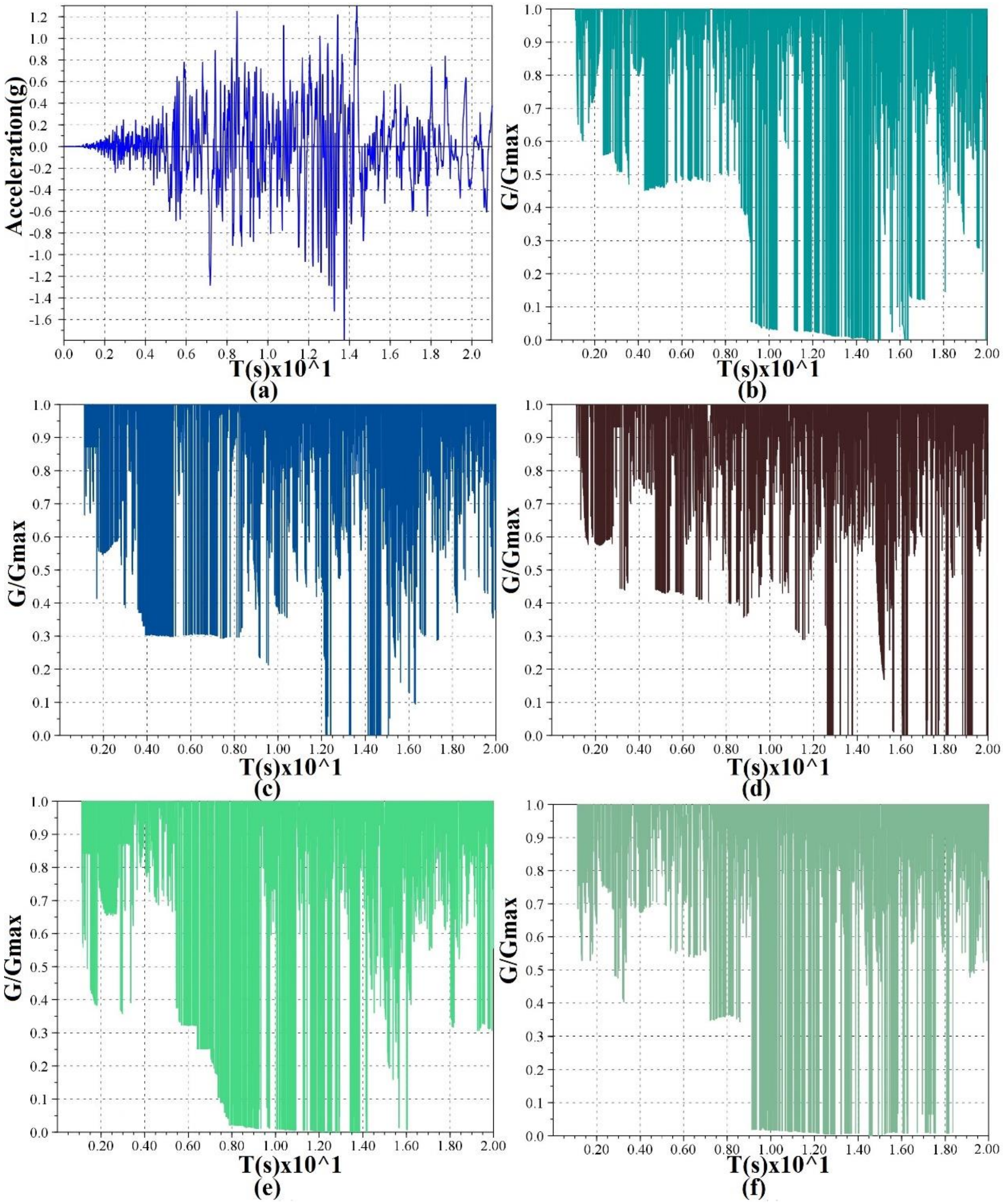

Figure 4.23 1987 Superstition Earthquake data and modulus degradation of soil; (a) acceleration record for first 20 seconds (b) depth of 2 m (c) 4 m (d) 6 m (e) 8 m (f) 10 m

In the first stage, only 3 Hz with amplitude of 0.05g and 15 Hz with amplitude of 0.15g were used to identify the effect of frequency (Figure 4.24). The reason why different amplitude values were used is because of the experience gained from past trials that higher frequency requires larger amplitude to attain logical r_u values. Values of r_u were obtained for the ID numbers of 1, 2, 3 and 4 for spacing of 2B, 3B, 4B, 5B and 6B.

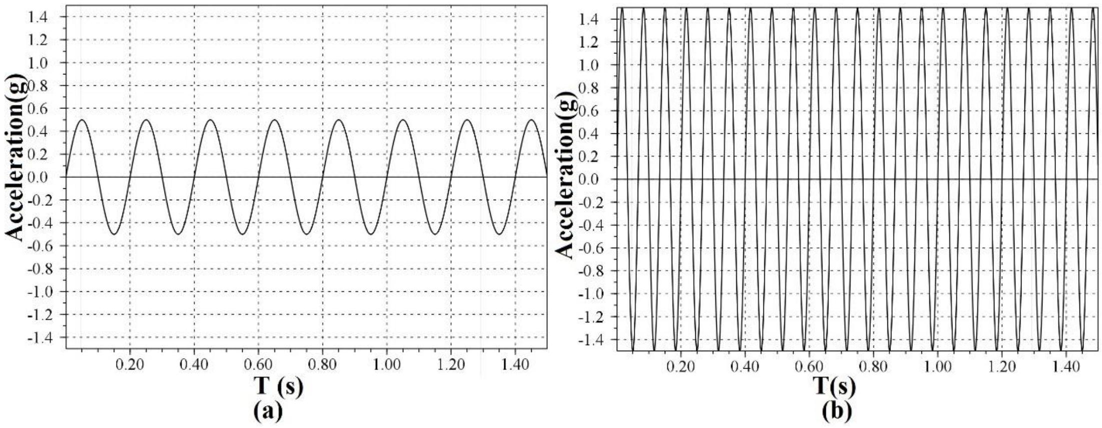

Figure 4.24 Simple wave forms; (a) 5 Hz (b) 15 Hz

For simplicity, arithmetic average of 4 different locations is represented in Figure (4.25). According to this figure, high frequency is able to result in similar trend with respect to r_u values. Besides, very low r_u values take place at shallow depths in case of presence of low frequency. Also, lower r_u values occur in the model of 2B spacing.

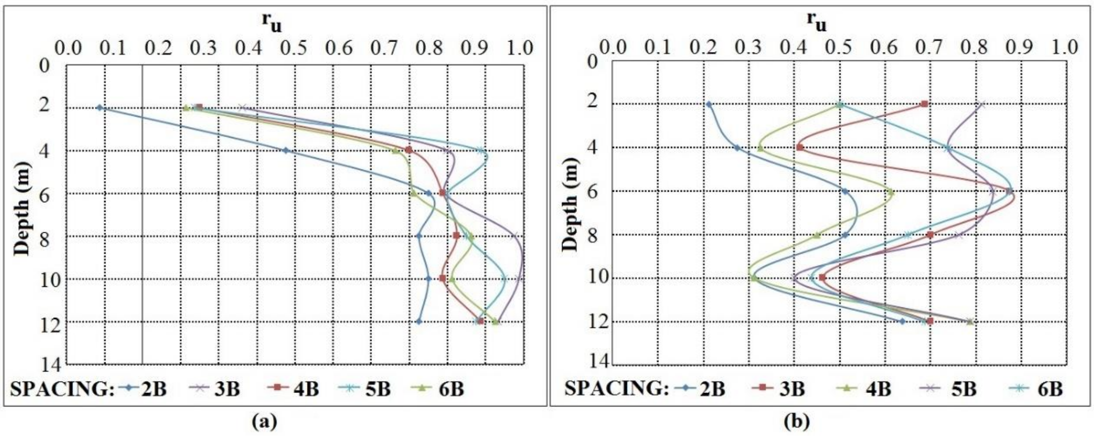

Figure 4.25 Average r_u values for each spacing under two different wave type; (a) 5 Hz and (b) 15 Hz

In the second stage, model with 4B spacing (Figure 4.9 (c)) was chosen as pivot model and effect of various wave types on r_u values were investigated for that model. For this purpose, many trials were done but only essential wave types are presented. These wave types consist of constant frequency and amplitude, constant frequency and varying amplitude and combination of different frequencies (Figure 4.26). Assessment was made based on r_u values occurred in the locations whose ID numbers are in the range of 1 to 9.

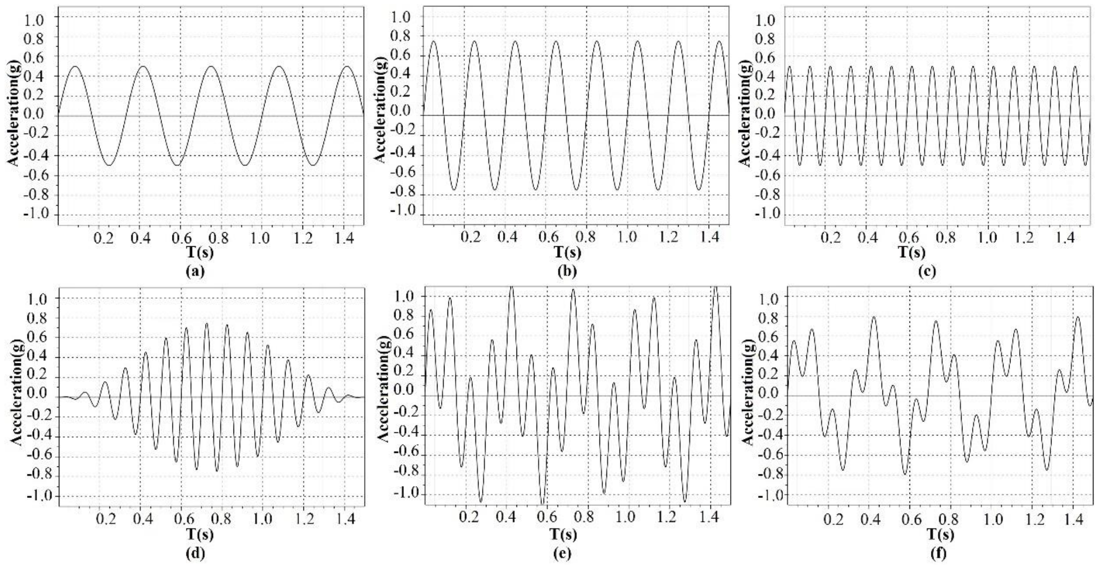

Figure 4.26 Various wave types and corresponding frequency and amplitude; (a) 3 Hz 0.05g (b) 5 Hz 0.075g (c) 10 Hz 0.05g (d) 10 Hz 0.075g(peak) (e) combination of 3 Hz 0.05g and 10 Hz 0.0625g (f) combination of 3 Hz 0.05g and 10 Hz 0.03g

Average r_u values for these 9 locations are given in the Figure (4.27). In this figure, same notation for each wave type represented in Figure (4.26) is also used. Although average r_u values corresponding to a given depth conceal fluctuations in the values, it is a good approach in the assessment of r_u values with respect to depth. That is, in the selection of dynamic motion, the criterion is to obtain a wave form causing high r_u values regardless of the depth effect. According to this figure, almost all wave types except C and E are able to induce r_u values significantly. Also, it was found that constant frequency with varying amplitude which is represented as D in Figure (4.27) provides better and higher r_u values throughout the depth. Besides, it is the only wave leading to similar results for each spacing of jet grout column mesh. In the final stage, effect of amplitude for such wave form is studied.

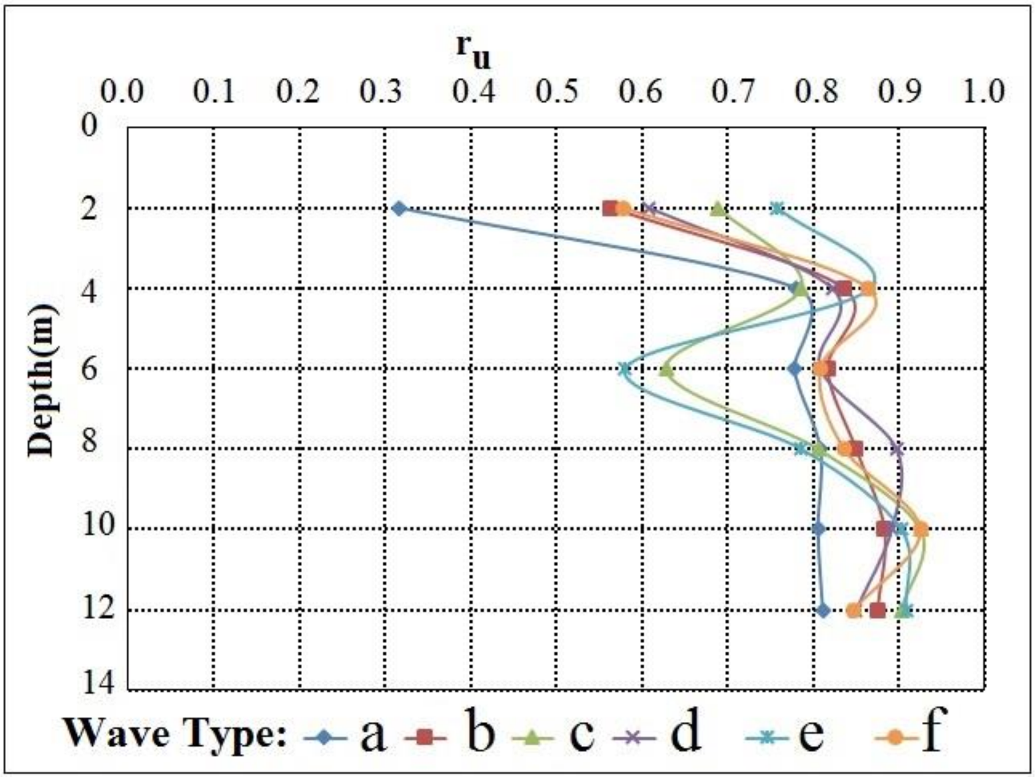

Figure 4.27 Average r_u values for 9 locations with respect to several wave forms

After selection of proper wave type which consists of constant frequency with time dependent amplitude, effect of varying amplitude on r_u values were also investigated as final stage. Although only model for 4B spacing was used in the second stage, all models for each spacing were utilized in this stage. Mentioned effect of peak acceleration was evaluated in accordance to r_u values obtained from 9 different locations (Figure 4.9). Also, peak acceleration-r_u relationship was obtained based on overall r_u values for the depths of 4 m, 6 m, 8 m, 10 m and 12 m (Figure 4.28). The reason why 2 m depth was not used is due to the fact that r_u values obtained for this depth are not compatible with values for other depths. According to this figure, obtained r_u values for 2B spacing is so low that difference between this model and others cannot be ignored. In fact, such low values for 2B spacing is totally due to negative effect of fine mesh in jet grout column locations. Therefore, model of 2B spacing is not used in the remaining parts of the study. Besides, peak acceleration lower than 0.05g was not included in remaining parts of this study because it does not cause high r_u values.

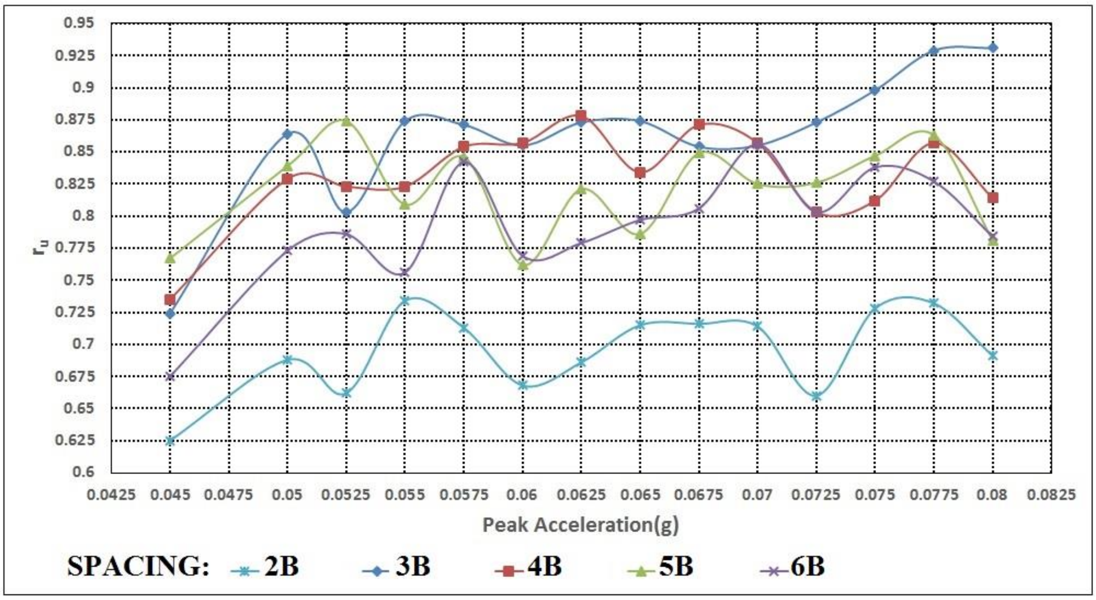

Figure 4.28 Peak acceleration-r_u relationship for each model

Moreover, upper limit for peak acceleration value was determined as 0.08g. Beyond this upper limit, r_u values start to become instable values as indicated in Figure (4.29).

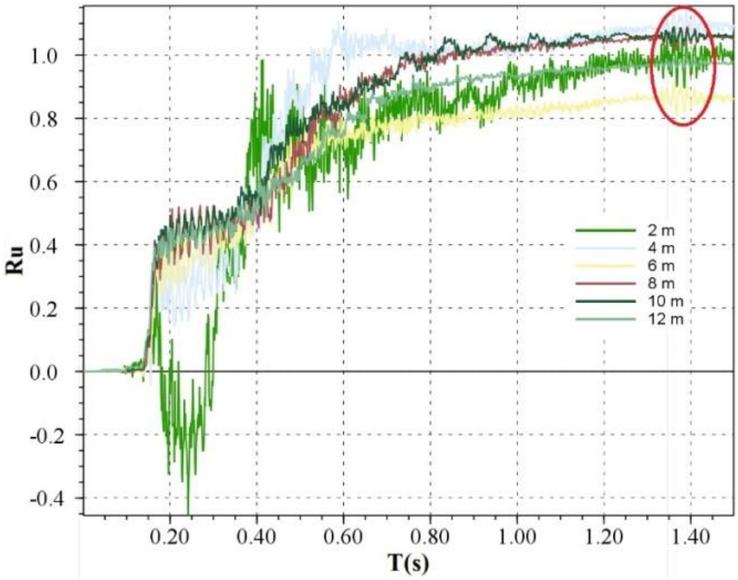

Figure 4.29 Values of r_u for ID 5

To conclude, to investigate liquefaction phenomenon in the free field conditions, dynamic motion input is selected as a wave form having constant frequency but varying amplitudes. Four peak acceleration values used for free field analyses are 0.05g, 0.06g, 0.07g and 0.08g.

4.6.2 Evaluation of Liquefaction in Free Field Conditions

From theoretical point of view, onset of liquefaction is attained when r_u is equal to 1.0. However, Seed (1986) stated that r_u values greater than 0.60 is a clear evidence of high potential of liquefaction. Besides, according to Marcuson (1990) and Idriss & Boulanger (2008), factor of safety against liquefaction for sandy soil converges to 1.0 when r_u is greater than 0.65 (Figure 4.30). Furthermore, Moradi, Khatibi and Sutubadi (2011) mentioned that liquefaction evidence starts to occur when r_u exceeds 0.90 in FLAC. Therefore, in the light of given information, it is accepted in this study that soil liquefies when stable r_u value or value at the end of the dynamic analysis is equal or greater than 0.90.

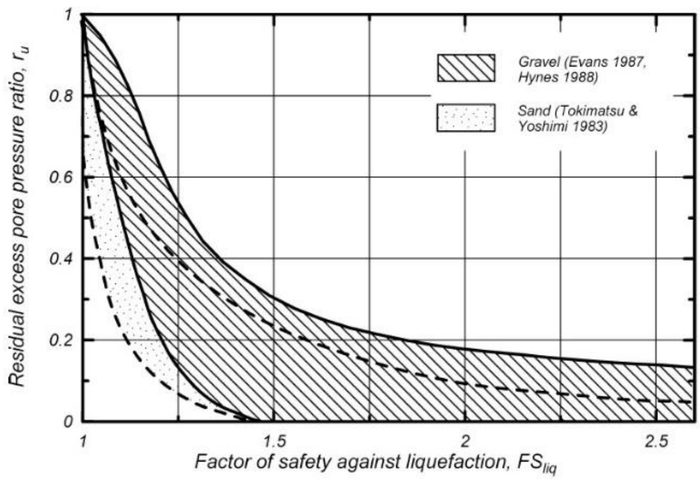

Figure 4.30 Factor of safety against liquefaction with respect to r_u values

As mentioned earlier, free field analyses were performed in both 1-D and 3-D numerical models. Corresponding results are presented in the following sections. Also, a comparison between numerical models and the simplified method will be done to evaluate simplified method's functionality on the prediction of liquefaction.

4.6.2.1 3-D Free Field Analyses

In 3-D free field analyses, r_u values corresponding to 18 different locations with 6 different depths for each model with respect to various spacing and each dynamic motion were obtained. However, for the sake of conciseness, only r_u values for only

4B spacing model under dynamic action whose peak acceleration value is equal to 0.07g are presented in this section. Remaining results for other models and for each dynamic loading will be given in the section of improved site analyses and appendices.

According to r_u values for 18 locations, liquefaction occurs at various depths of 4 m, 6 m, 8 m, 10 m and 12 m (Table 4.6). In this table, shaded cells indicate location of liquefaction ($r_u \geq 0.9$). Furthermore, depth of 14 m is not included in the analyses due to being close to source of dynamic loading. That is, almost every point at the depth of 14 m, r_u values are greater than 0.90 where r_u values are not effected by wave characteristics.

Table 4.6 Values of r_u for 18 locations

	MODEL FOR 4B-SPACING								
ID / z(m)	**1**	**2**	**3**	**4**	**5**	**6**	**7**	**8**	**9**
2	0.80	0.20	0.55	0.60	0.65	0.88	0.60	0.48	0.60
4	0.80	0.80	0.83	0.80	0.73	0.78	0.73	0.80	0.90
6	0.90	0.60	0.93	0.83	0.90	0.88	0.95	1.00	0.83
8	0.80	0.98	0.73	1.01	1.05	0.95	0.90	0.95	0.78
10	0.90	0.93	0.88	0.88	0.75	0.80	0.93	0.70	0.90
12	0.95	0.85	1.03	0.93	0.98	0.90	0.98	1.00	0.93
ID / z(m)	**10**	**11**	**12**	**13**	**14**	**15**	**16**	**17**	**18**
2	0.63	0.50	0.50	0.65	0.50	0.78	0.78	0.73	0.65
4	0.95	0.85	0.85	0.65	0.80	0.78	0.80	0.85	0.65
6	0.80	0.83	0.80	0.90	0.88	0.90	0.85	0.70	0.90
8	0.93	0.80	0.78	0.65	0.93	1.00	0.95	0.75	0.65
10	0.90	0.83	0.90	0.93	0.90	1.00	0.95	1.03	0.93
12	0.95	0.73	0.80	0.88	0.95	1.05	0.90	0.88	0.88

As mentioned before, length of jet grout column is equal to 12 m. Also, in the selection of wave type, the prime concern has been to obtain large volume of liquefaction. However, it is not always possible to obtain liquefaction throughout the depth of model. Besides, it should be reminded that numerical analysis may result in ±5% variation in r_u values for repetitive analyses. Therefore, in this study, number of locations used in this study for liquefaction is regarded as satisfactory for parametric study. Nonetheless, due to the fact that almost all r_u values for each location are greater than 0.65 which is an evidence of high potential of liquefaction, liquefaction mitigation is also needed for these locations. Development of r_u values for locations of ID 1, 7, 8, 9, 10 and 15 are shown in Figure (4.31). According to this figure, all r_u values stabilize at the end of analysis. In this study, mid-point values of oscillations are used. However, upper values of it could have been used due to stable oscillation. Rather than maximum values in r_u oscillation, arithmetic mean was used. Furthermore, at several locations, maximum values are attained before maximum acceleration takes place.

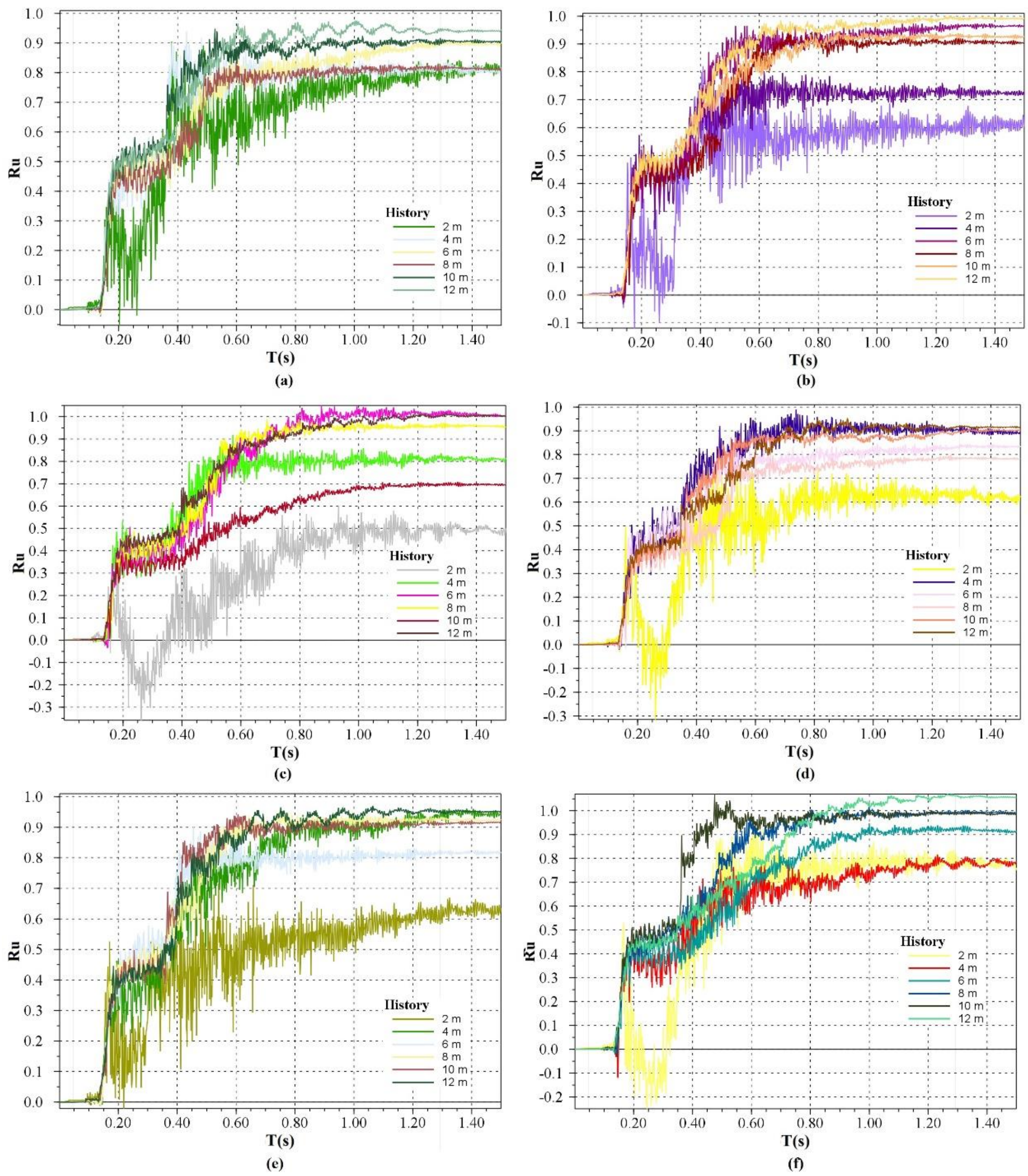

Figure 4.31 Values of r_u for different locations; (a) ID 1 (b) ID 7 (c) ID 8 (d) ID 9 (e) ID 10 (f) ID 15

4.6.2.2 1-D Free Field Analysis

Liquefaction evaluation of the free field was also performed in 1-D model. In this model, like FLAC, nonlinear backbone formulation (Modified Kodner Zelesko) was adopted. Also, same dynamic motion was used to compare 1-D and 3-D results (Figure 4.32). Used dynamic input motion have a peak acceleration of 0.07g.

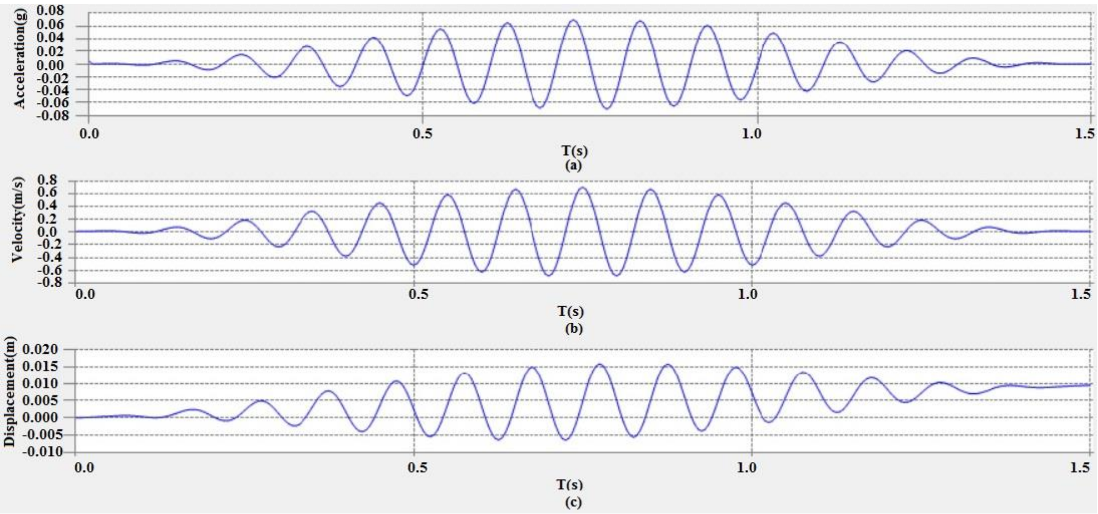

Figure 4.32 Dynamic input motion; (a) acceleration (b) velocity (c) displacement

According to obtained r_u values, below 6 m, liquefaction was identified (Figure 4.33). Also, at 6 m depth, high r_u values were obtained.

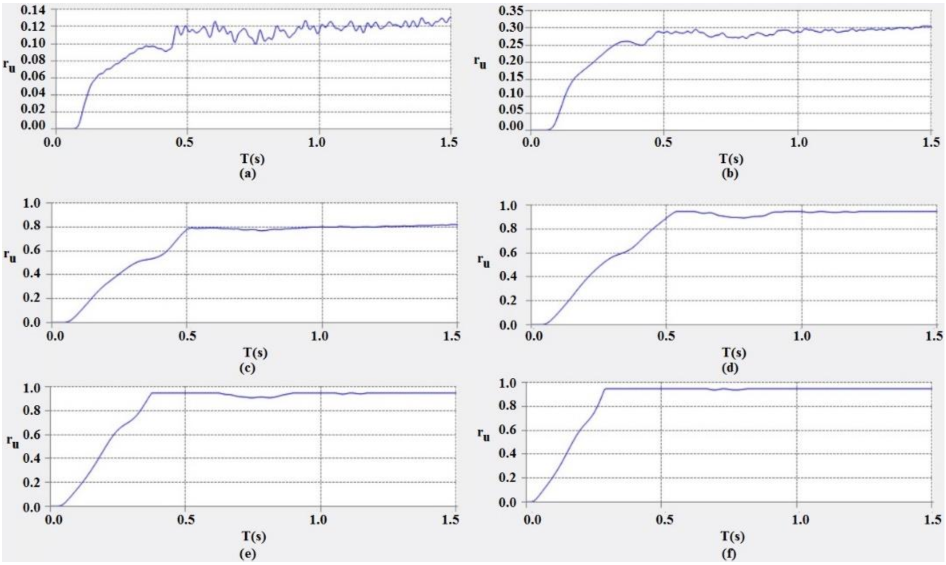

Figure 4.33 Values of r_u with respect to depth; (a) 2 m (b) 4 m (c) 6 m (d) 8 m (e) 10 m (f) 12 m

Obtained r_u values by 1-D and 3-D analyses are quite compatible with each other. However, at shallow depths, 1-D model result in more conservative values as compared to 3-D. On the contrary, shallow depths are not the main concerns in this study. Furthermore, stable r_u values occur like 3-D analysis prior to peak acceleration.

Moreover, order of strain level for liquefied soil is similar with 3-D analysis (Figure 4.34). Corresponding depth for mentioned figure is equal to 8 m.

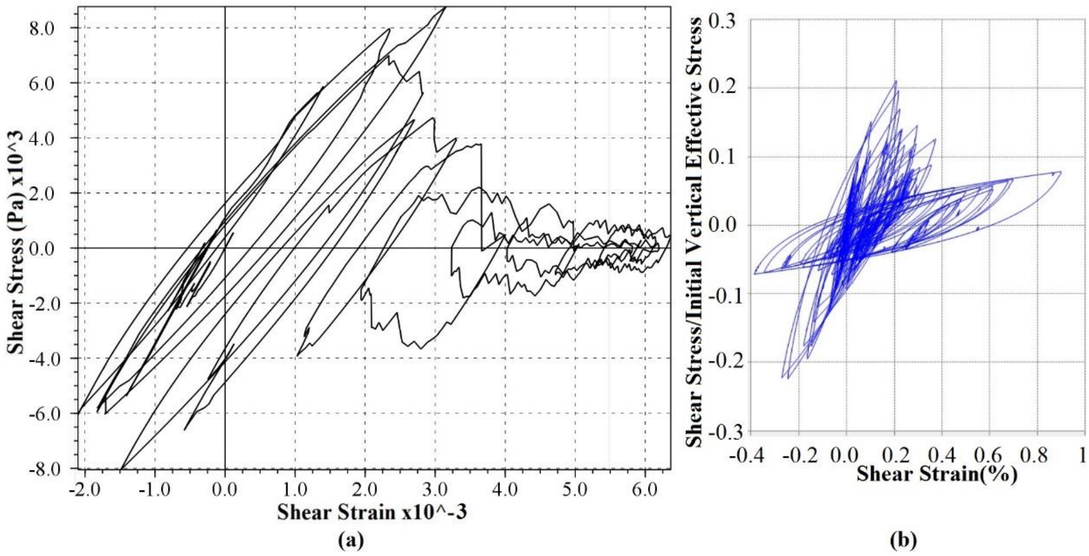

Figure 4.34 Shear stress-shear strain relationship; (a) 3-D analysis for ID 5 at depth of 8 m (b) 1-D analysis

4.6.2.3 Comparison of Numerical Analyses and Simplified Method

In order to test functionality of simplified method on the prediction of liquefaction, factor of safety calculation was made. PGA is obtained in the range of 0.42g to 0.46g in FLAC while corresponding value for 1-D analysis is 0.55g. Roughly, 0.45g was accepted as PGA. Magnitude scaling factor is taken as 1.48. However, it could have been taken as 1.8. Besides, $(N_1)_{60}$ is assumed as 5.66 throughout depth. Then, CSR and CRR values were obtained by using Equation (2.4) and (2.10), respectively (Table 4.7). Hence, according to obtained results, there exists high potential of liquefaction in 12 m. However, numerical analyses are more reliable because excess pore pressure values are directly used in the evaluation of liquefaction.

Table 4.7 Results obtained from simplified method

z (m)	σ_v (kPa)	σ_v' (kPa)	r_d	K_σ	CSR_{FF}	CRR_{FF}	FS_{FF}
2	39.846	20.226	0.987	1.100	0.569	0.125	0.221
4	79.691	40.451	0.974	1.100	0.561	0.125	0.224
6	119.537	60.677	0.960	1.100	0.553	0.125	0.227
8	159.382	80.902	0.942	1.064	0.543	0.121	0.224
10	199.228	101.128	0.912	0.997	0.526	0.114	0.216
12	239.074	121.354	0.867	0.942	0.500	0.107	0.215

4.7 Dynamic Analyses of Improved Site by Jet Grout Columns

Essential objective of this study is to investigate effectiveness of jet grout columns on liquefaction mitigation. Firstly, in the free field analyses, liquefaction state has been provided for a large volume in the model. Besides, it has been verified by r_u values. At this stage of the study, mitigation role of jet grout columns in liquefiable soil model will be examined.

As a parametric study, several factors are taken into account, namely; depth of consideration, peak acceleration value, spacing and stiffness of jet grout column. In the selection range of column stiffness, UCS range suggested by Stoel (2001) for sandy soil was used to determine mechanical parameters of jet grout column (Table 4.8). Elastic modulus was obtained using Equation (3.11) while shear strength parameters, c and φ, were computed according to Equation (3.7) and (3.8), respectively. Unit weight of jet grout columns was taken equal to soil saturated unit weight for the simplicity.

As indicated in the below table, 3 different stiffness values, namely; lower, mean and upper, were used in dynamic analyses. Much lower stiffness could have been used because it would represent stone column properties rather than jet grout column. Besides, very high stiffness values were not adopted due to the fact that there would be very high stiffness difference between soil and column which is not desired.

Table 4.8 Mechanical properties of jet grout columns

	JET GROUT MECHANICAL PROPERTIES		
	Lower Stiffness	**Mean Stiffness**	**Upper Stiffness**
E (MPa)	3099.1	4000.1	5059.8
G (MPa)	1291.3	1666.7	2108.2
K (MPa)	1721.7	2222.3	2811.0
c (MPa)	2.9	4.1	5.9
φ (^{0})	48.2	53.3	57.2
v	0.2	0.2	0.2
UCS (MPa)	10.0	25.0	40.0
G_r	27.4	35.4	44.8

Jet grout columns were modelled as Mohr-Coulomb plasticity model rather than elastic model because jet grout columns consist of cement-water mixture blended with soil (FLAC3D Manual, 2008). Therefore, they cannot represent fully elastic behavior. Also, excess pore pressure cannot occur in this type constitutive model. That is, no excess pore pressure occurs in the soilcrete columns under dynamic loading, therefore, Finn model has also not been considered.

In modelling, interface elements were used so as to represent stiffness transition between the soil and the jet grout column (Figure 4.35). Actually, in order to represent that stiffness transition, there exist several components of interface elements; namely, slider and springs representing normal stiffness and shear stiffness (Figure 4.35 (a)). Furthermore, interface elements can have cohesion, dilation and friction angles. Interface elements were utilized for each jet grout column (Figure 4.35 (b)). Moreover, for each jet grout column, interface elements were used along column perimeter and beneath of column. Also, interface elements consist of triangular elements which are linked at their vertices by nodes (Figure 4.35 (c)). In Finn model, effective stress calculation are performed during dynamic analysis, therefore, it was allowed in numerical model to calculate effective stress at the interface in order not to deviate evolution of r_u.

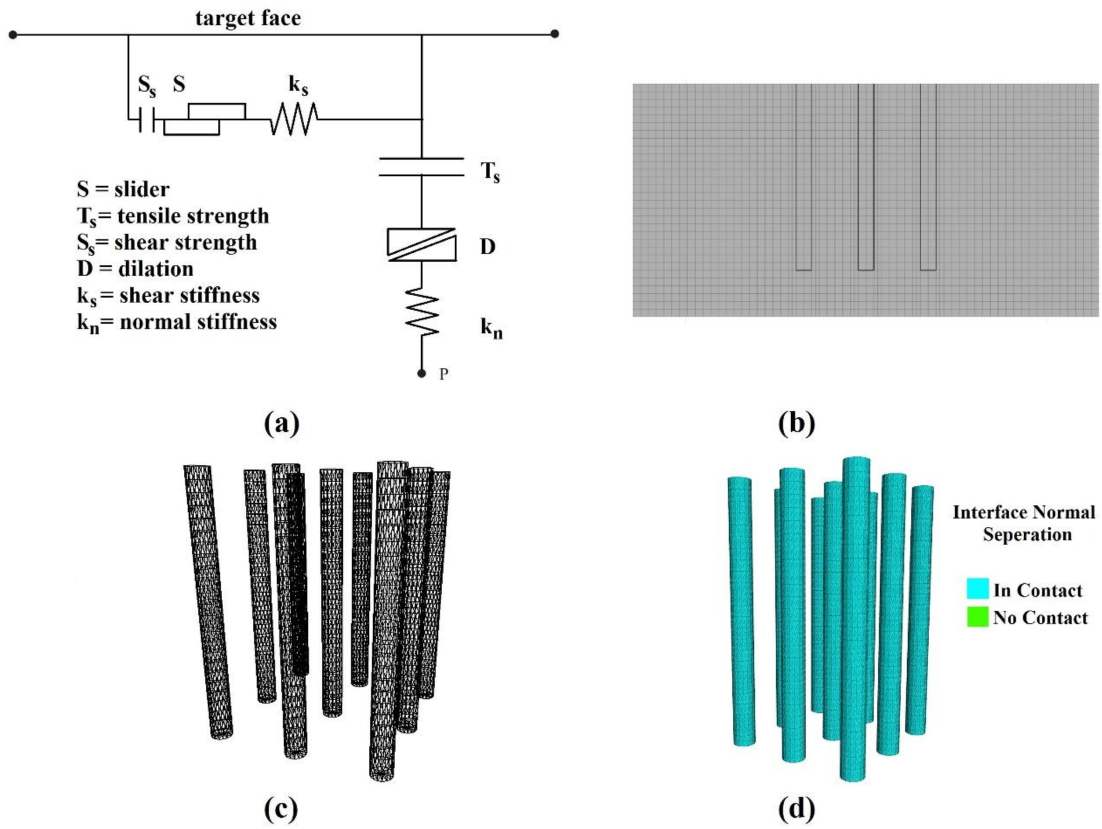

Figure 4.35 Interface; (a) constitutive model (b) interface view in the section (c) 3-D view of interface elements (d) 3-D view of interfaces and corresponding interaction situation between soil and itself

Interface properties for each jet grout stiffness level are given in the Table (4.9). According to this table, both normal stiffness (k_n) and shear stiffness (k_s) values are same for each jet grout column stiffness level. The reason for that is due to the fact that soil behavior rather than jet grout columns governs numerical model behavior and thus, interfaces properties were adjusted according to soil properties in this study.

Table 4.9 Corresponding interface properties

	INTERFACE INDEX PROPERTIES		
	Lower Stiffness	**Medium Stiffness**	**Upper Stiffness**
c (MPa)	0.0	0.0	0.0
$\varphi(^0)$	21.3	21.3	21.3
k_n (MPa/m)	11300.0	11300.0	11296.3
k_s (MPa/m)	11300.0	11300.0	11296.3

The parameters of c and φ for interface were taken 67% of corresponding value for soil. The reason is that overall behavior of model is highly affected by the soil behavior rather than jet grout columns. Besides, normal stiffness (k_n) and shear stiffness (k_s) was computed according to the following formula:

$$k_n, k_s = \max\left(\frac{\left(K + \frac{4G}{3}\right)}{\Delta z_{min}}\right) \tag{4.12}$$

Where Δz is the smallest width of an adjoining zone in the normal direction.

Furthermore, to attain uniform stress distribution at a given depth at the end of static analysis, effective stress calculation on the interface is temporarily blocked due to presence of Finn model (FLAC3D Manual, 2008). Otherwise, enormous deviation occurs in the evolution of static stresses. Prior to dynamic analysis, effective stress calculation on the interface is reactivated. Also, static analyses were performed in two stages. In the first stage, elastic analysis was performed by assuming that jet grout columns have same mechanical properties with soil. Then, their actual properties were assigned to jet grout columns and another elastic analysis was performed. After that, in case of presence of locations at shallow depths where soil gets into plastic state, their plastic state is removed. Furthermore, after static analysis, it was controlled that interfaces are fully in contact with soil (Figure 4.35 (d)). Corresponding FLAC3D code is given in Appendix C. Although negligible fluctuations occur at several points inside jet grout columns, such deviation does not take place in the soil (Figure 4.36).

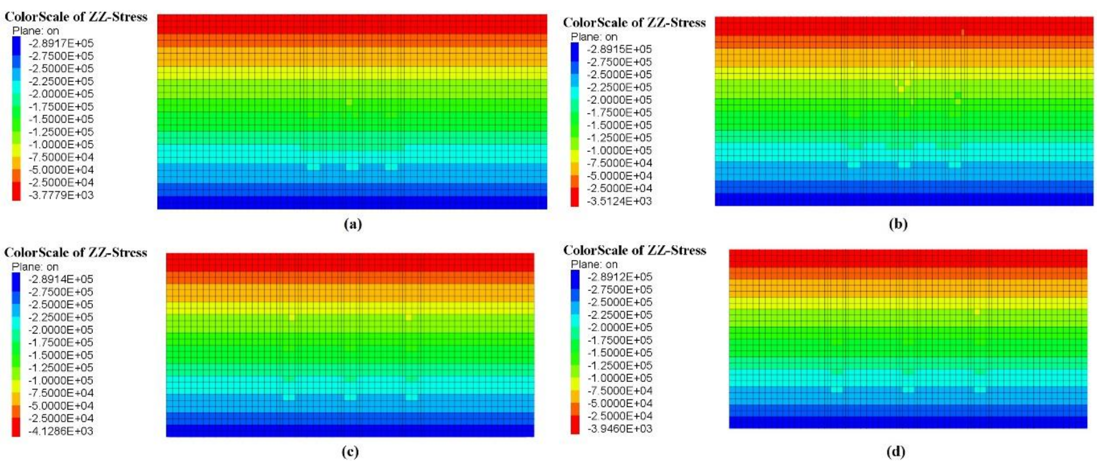

Figure 4.36 Vertical stresses after static analysis; (a) 3B spacing (b) 4B spacing (c) 5B spacing (d) 6B spacing

In dynamic analysis, energy absorption mechanism of jet grout columns was attributed to Rayleigh damping mechanism. In fact, Rayleigh damping consists of two components, namely; mass and stiffness. As frequency of dynamic motion increases, contribution of mass component tends to decrease. Unlike mass component, stiffness component becomes predominant over mass component with increasing of frequency (Figure 4.37). Hence, in this work, by neglecting stiffness component, only mass component was utilized. Used damping parameters are 5% for damping ratio and 10 Hz for center frequency. Actually, Coulier, François, Degrande & Lombaert (2013) stated that mass component of Rayleigh damping for jet grout columns can be taken as 5%.

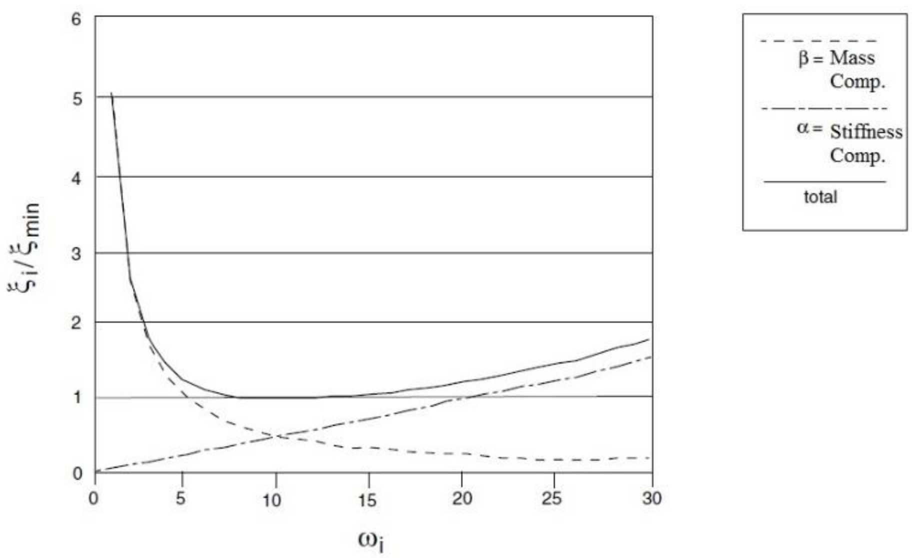

Figure 4.37 Contribution of Rayleigh Damping components

After dynamic analyses, it was found that jet grout columns are able to reduce r_u values. This positive effect is presented here for 4B spacing containing jet grout columns having low stiffness under the dynamic motion whose peak acceleration 0.07g in the Table (4.10). In this table, shaded cells indicate liquefaction locations. In Table (4.6), it was shown that 44 points out of 108 liquefy. Also, these 44 points are mainly distributed between 4 m and 12 m depths. However, after improvement, number of liquefied locations drops to 6 by neglecting the points located at the 2 m depth. Besides, in most of the locations, r_u values are reduced to be below even 0.65. Hence, onset of liquefaction is prevented by keeping r_u below 0.90.

Table 4.10 Values of r_u for improved site

	MODEL FOR 4B-SPACING								
ID / z(m)	**1**	**2**	**3**	**4**	**5**	**6**	**7**	**8**	**9**
2	0.50	0.43	0.98	0.00	0.00	0.00	0.40	0.00	1.05
4	0.45	0.93	0.83	0.33	0.30	0.28	0.80	0.35	0.50
6	0.40	0.35	0.48	0.50	0.28	0.45	0.28	0.38	0.55
8	0.70	0.40	0.50	0.65	0.38	0.53	0.48	0.48	0.65
10	0.40	0.45	0.40	0.63	0.40	0.65	0.43	0.45	0.35
12	0.65	0.85	0.60	0.95	0.60	0.88	0.88	0.70	0.50
ID / z(m)	**10**	**11**	**12**	**13**	**14**	**15**	**16**	**17**	**18**
2	0.35	0.75	0.25	0.30	0.80	0.48	0.48	0.10	0.30
4	0.80	0.48	0.85	0.35	0.40	0.70	0.73	0.35	0.35
6	0.45	0.40	0.33	0.28	0.50	0.48	0.55	0.35	0.28
8	0.63	0.43	0.38	0.35	0.55	0.63	0.55	0.53	0.35
10	0.43	0.50	0.40	0.53	0.83	0.45	0.50	0.55	0.53
12	0.60	0.83	0.90	0.58	0.80	0.90	0.90	1.00	0.58

In order to compare r_u values for improved site with free field, evolution of r_u is also given for ID points of 1, 7, 8, 9, 10 and 15 (Figure 4.38). According to this figure, like free field case, r_u values converge to stable values before dynamic analysis finishes. However, unlike free field case, stable r_u values occur after peak acceleration which is a clear evidence of the effect of jet grout columns. In other words, stable r_u evolution is retarded by soilcrete columns Another difference between improved and unimproved sites is that small oscillations in r_u starts at the beginning of the analysis. Besides, almost all r_u values for each depth except 2 m are reduced with the help of jet grout columns.

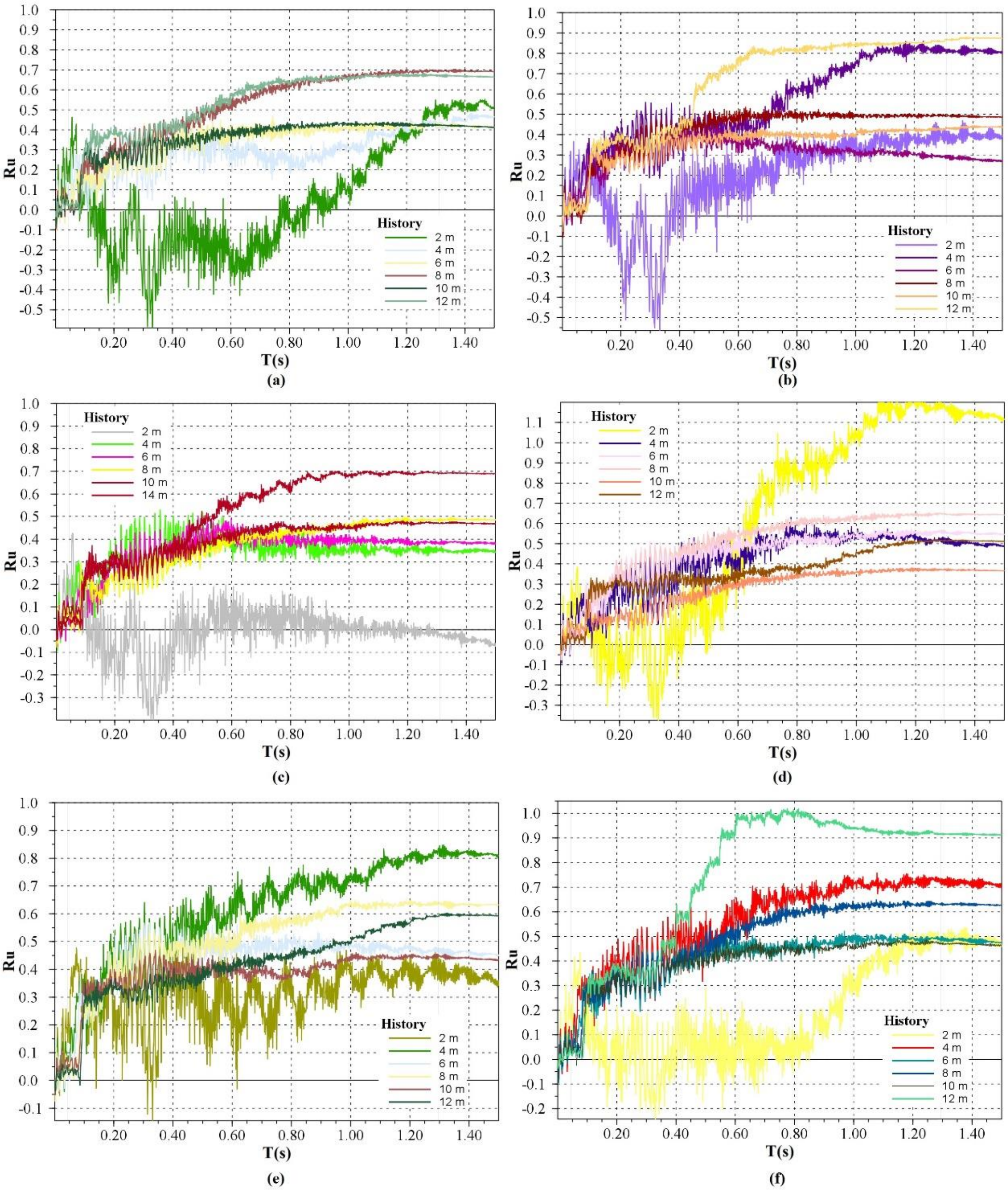

Figure 4.38 Values of r_u for different locations; (a) ID 1 (b) ID 7 (c) ID 8 (d) ID 9 (e) ID 10 (f) ID 15

Apart from r_u evolution figure, total pore pressure values of 2 m, 4 m and 6 m depths are also given for free field and improved site analyses (Figure 4.39). According to this figure, jet grout column limit development of excess pore pressure inside the region that are surrounded with soilcrete columns. Also, overall performance of jet grout columns seems to increase for deeper zone. More detailed information will be given for that in the following section. Besides, values in Figure (4.39) indicate that model dimensions are large enough to represent free field conditions away from columns. It should be reminded that dynamic action acts in the x direction and thus, there is a tendency of similar excess pore pressure values to occur normal to loading direction. Also, inside soilcrete columns modelled with Mohr-Coulomb material, pore pressure at the static condition occurs throughout the dynamic analysis. That is, excess pore pressure development is avoided.

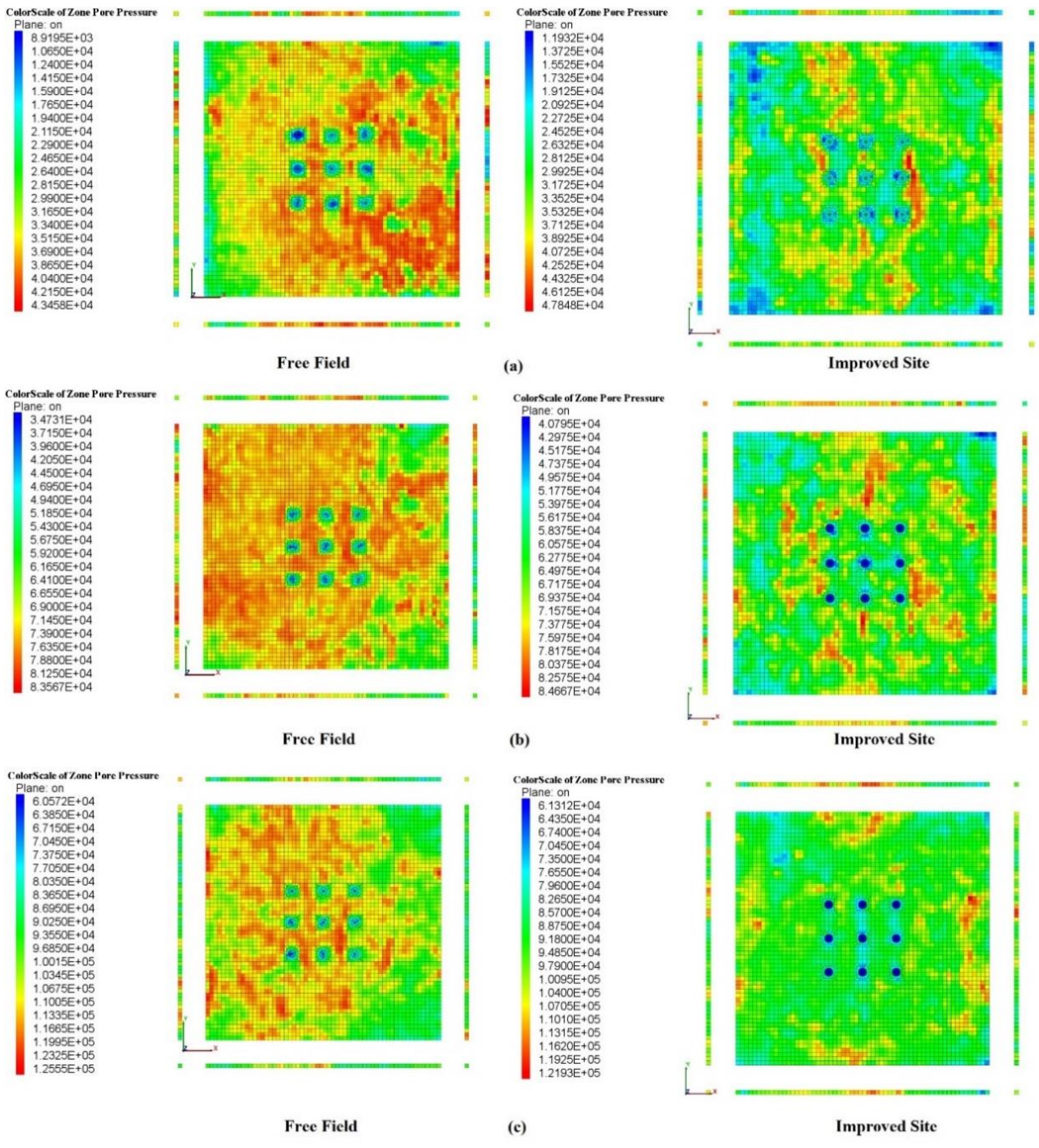

Figure 4.39 Total pore pressure values in Pa; (a) for 2 m depth (b) for 4 m depth (c) for 6 m depth

Same figure is also given for corresponding depths of 8 m, 10 m and 12 m (Figure 4.40). Except 12 m depth which is the bottom level of jet grout columns take place, pore pressure values cannot build up as much as in the free field.

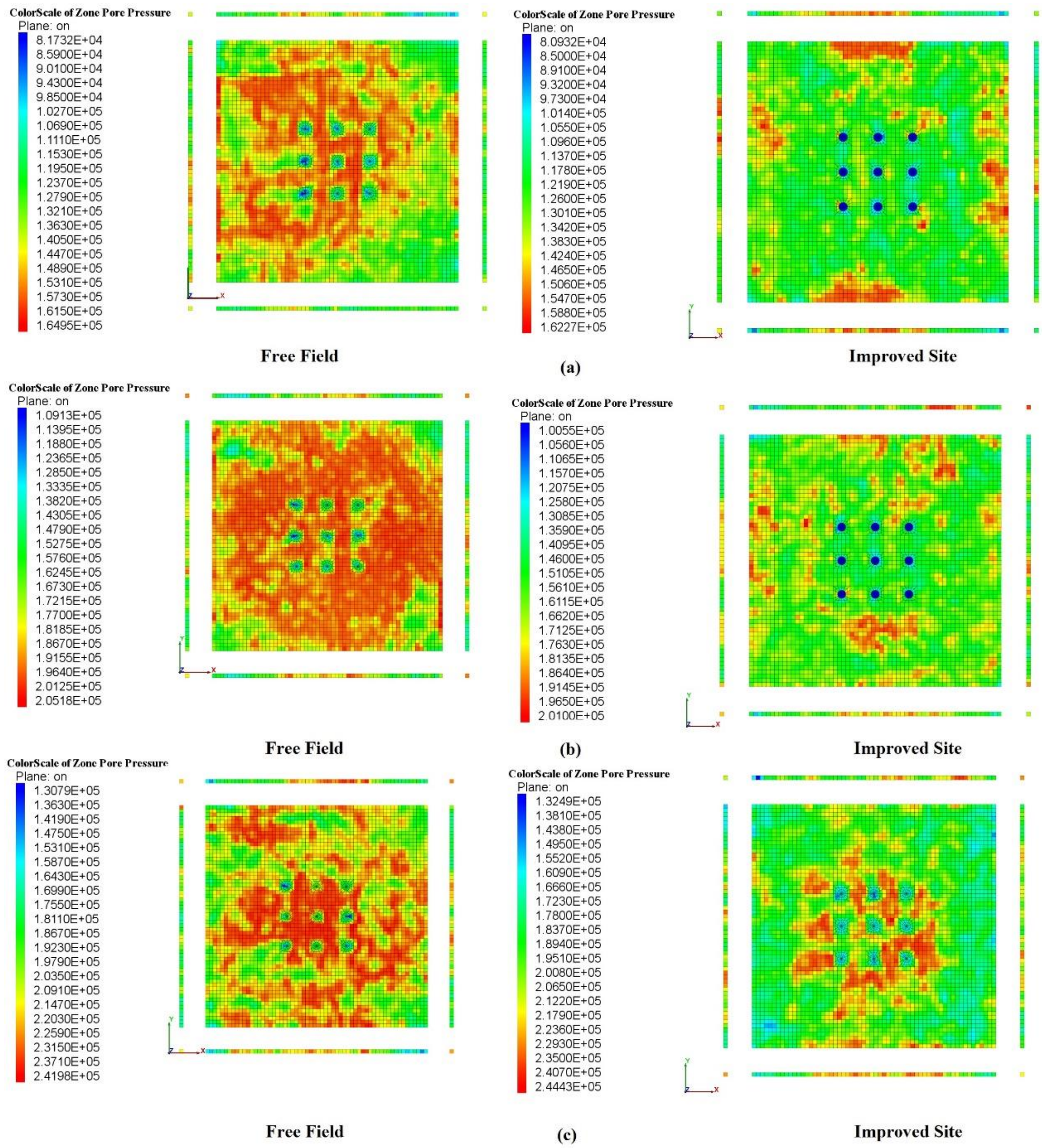

Figure 4.40 Total pore pressure values in Pa; (a) for 8 m depth (b) for 10 m depth (c) for 12 m depth

It has been found that presence of jet grout columns decrease induced shear strains in the soil. Therefore, limitation of development of excess pore pressure might be attributed to this decrease. However, mechanism of how jet grout columns mitigate liquefaction does not form primary concern in this study. Nonetheless, to illustrate mentioned behavior, shear stress and strain curve of ID 5 at depth of 8 m in xz plane that has liquefied in the free field analysis is also given in Figure (4.41).

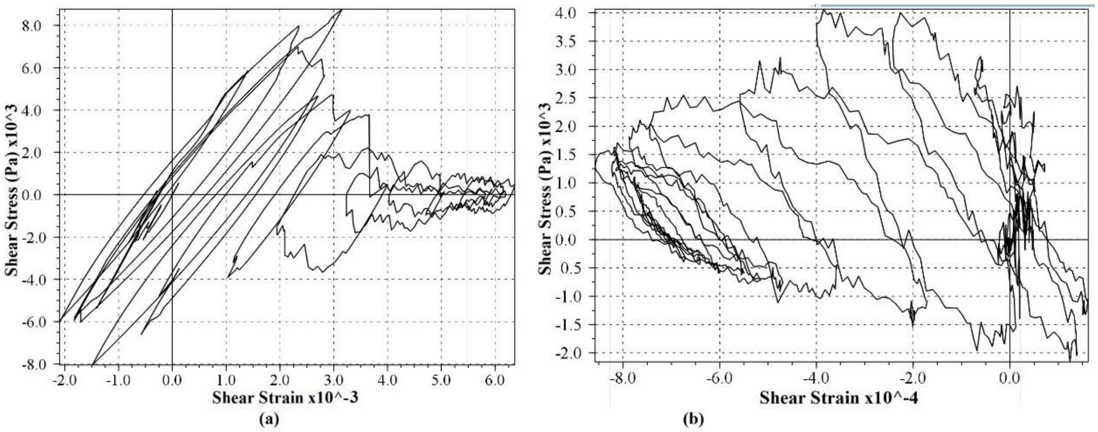

Figure 4.41 Hysteresis loops; (a) free field (b) improved site

Dynamically induced shear strain limit of jet grout columns was checked. Cheuk, Lai and Cheung (n.d.) presented that jet grout columns show brittle behavior and therefore, maximum shear strain design limit is taken as 0.5%. In this study, jet grout column were controlled with respect to strain values. However, obtained results were much lower than the prescribed limit. Therefore, detailed information is not given. Nonetheless, strain values in xz plane is given for the center jet grout column (Figure 4.42).

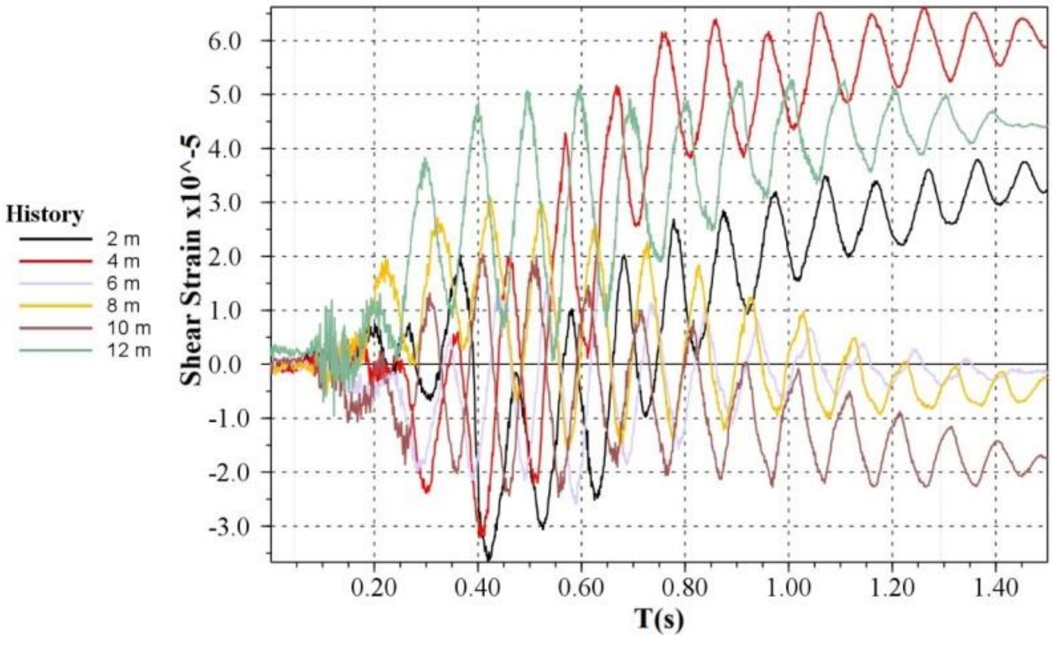

Figure 4.42 Shear strain history for the center jet grout column throughout depth

4.8 Comparison of Free Field and Improved Site Analyses with respect to r_u Values

In dynamic analyses, in the assessment of jet grout column effectiveness, to better identify effect of spacing, data points were divided into three groups, namely; intermediate points between an outer and center jet grout column (Group 1; G1), points between three outer columns and center column (Group 2; G2) and finally, points between outer two columns (Group 3; G3) (Figure 4.43).

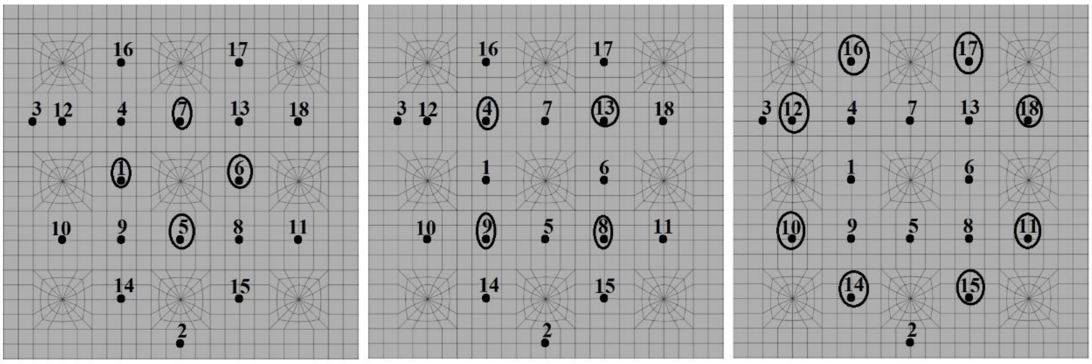

Figure 4.43 Representative group layout; (a) group 1 (b) group 2 (c) group 3

For each model, same ID numbers given as before were used to describe these groups (Table 4.11). It should be reminded that these locations describe relative positions rather than coordination.

Table 4.11 Three groups and corresponding ID locations

	GROUP 1	GROUP 2	GROUP 3
ID	1, 5, 6, 7	4, 8, 9, 13	10, 11, 12, 14, 15, 16, 17, 18

Results of r_u obtained from both dynamic free field (FF) and dynamic improved site for three different cases based on different jet grout column stiffness, namely; high stiffness (HS), mean stiffness (MS) and low stiffness (LS) analyses are given in Table (4.12) and Table (4.13). In this table, each group are divided into 3 sub-groups; top (2 m & 4 m), mid-column (6 m & 8 m) and bottom (10 m & 12 m). Besides, average values for each sub-group are also given in tables for the sake of simplicity. All r_u values corresponding to each location and each depth are given in Appendix D.

Table 4.12 Values of r_u for peak accelerations of dynamic motions; 0.08g and 0.07g, respectively

		PEAK ACCELERATION of 0.08g															
		3B Spacing				4B Spacing				5B Spacing				6B Spacing			
Group	**Depth Interval**	**FF**	**HS**	**MS**	**LS**	**FF**	**HS**	**MS**	**LS**	**FF**	**HS**	**MS**	**LS**	**FF**	**HS**	**MS**	**LS**
G1	**Top**	0.92	0.68	0.64	0.42	0.61	0.43	0.38	0.24	0.58	0.37	0.37	0.41	0.57	0.33	0.46	0.31
	Mid-Column	0.92	0.69	0.73	0.49	0.80	0.49	0.45	0.47	0.72	0.44	0.44	0.29	0.74	0.43	0.38	0.33
	Bottom	0.96	0.83	0.82	0.67	0.93	0.62	0.64	0.61	0.83	0.61	0.63	0.64	0.86	0.73	0.65	0.61
	Average	0.94	0.76	0.75	0.56	0.82	0.54	0.53	0.48	0.74	0.51	0.52	0.50	0.76	0.56	0.54	0.47
G2	**Top**	0.95	0.71	0.70	0.46	0.59	0.56	0.65	0.40	0.49	0.47	0.32	0.39	0.64	0.29	0.49	0.48
	Mid-Column	1.00	0.78	0.89	0.59	0.77	0.58	0.55	0.57	0.76	0.44	0.46	0.44	0.77	0.50	0.40	0.39
	Bottom	0.96	0.91	0.93	0.65	0.90	0.62	0.67	0.71	0.84	0.71	0.69	0.59	0.83	0.69	0.60	0.51
	Average	0.97	0.83	0.86	0.59	0.79	0.60	0.64	0.60	0.73	0.58	0.54	0.50	0.77	0.54	0.52	0.47
G3	**Top**	0.90	0.63	0.70	0.45	0.65	0.58	0.49	0.62	0.59	0.47	0.49	0.37	0.62	0.70	0.59	0.47
	Mid-Column	0.97	0.70	0.73	0.51	0.77	0.56	0.51	0.46	0.75	0.45	0.43	0.39	0.74	0.40	0.43	0.43
	Bottom	0.96	0.75	0.79	0.70	0.91	0.65	0.64	0.72	0.85	0.65	0.66	0.58	0.82	0.62	0.66	0.68
	Average	0.95	0.71	0.75	0.59	0.81	0.61	0.57	0.63	0.76	0.56	0.56	0.48	0.75	0.59	0.59	0.57
Overall Average		0.95	0.76	0.79	0.58	0.81	0.58	0.58	0.57	0.74	0.55	0.54	0.49	0.76	0.56	0.55	0.50

		PEAK ACCELERATION of 0.07g															
		3B Spacing				4B Spacing				5B Spacing				6B Spacing			
Group	**Depth Interval**	**FF**	**HS**	**MS**	**LS**	**FF**	**HS**	**MS**	**LS**	**FF**	**HS**	**MS**	**LS**	**FF**	**HS**	**MS**	**LS**
G1	**Top**	0.87	0.63	0.47	0.43	0.74	0.40	0.42	0.34	0.67	0.42	0.31	0.32	0.64	0.31	0.50	0.33
	Mid-Column	0.73	0.63	0.67	0.49	0.92	0.49	0.47	0.43	0.82	0.44	0.44	0.32	0.81	0.38	0.34	0.32
	Bottom	0.89	0.74	0.75	0.65	0.90	0.59	0.65	0.59	0.92	0.68	0.63	0.66	0.83	0.64	0.65	0.68
	Average	0.85	0.69	0.66	0.56	0.87	0.52	0.55	0.49	0.83	0.56	0.50	0.49	0.78	0.49	0.54	0.50
G2	**Top**	0.76	0.68	0.50	0.47	0.68	0.64	0.41	0.37	0.66	0.44	0.34	0.42	0.76	0.36	0.22	0.31
	Mid-Column	0.82	0.65	0.80	0.61	0.87	0.56	0.53	0.48	0.80	0.47	0.50	0.44	0.85	0.49	0.44	0.38
	Bottom	0.94	0.71	0.66	0.73	0.89	0.67	0.74	0.58	0.82	0.75	0.62	0.54	0.85	0.80	0.68	0.65
	Average	0.87	0.69	0.66	0.64	0.83	0.64	0.61	0.50	0.78	0.60	0.52	0.49	0.83	0.61	0.51	0.50
G3	**Top**	0.72	0.56	0.59	0.54	0.72	0.57	0.53	0.51	0.71	0.55	0.60	0.52	0.63	0.52	0.67	0.48
	Mid Column	0.78	0.60	0.67	0.52	0.84	0.54	0.51	0.46	0.83	0.51	0.48	0.44	0.78	0.43	0.39	0.44
	Bottom	0.91	0.77	0.68	0.71	0.91	0.60	0.63	0.67	0.83	0.65	0.61	0.64	0.85	0.61	0.60	0.66
	Average	0.83	0.68	0.66	0.62	0.85	0.58	0.58	0.58	0.80	0.59	0.58	0.56	0.78	0.54	0.57	0.56
Overall Average		0.85	0.68	0.66	0.60	0.85	0.58	0.58	0.52	0.80	0.58	0.53	0.51	0.79	0.55	0.54	0.52

Table 4.13 Values of ru for peak accelerations of dynamic motions; 0.06g and 0.05g, respectively

PEAK ACCELERATION of 0.06g

		3B Spacing				4B Spacing				5B Spacing				6B Spacing			
Group	**Depth Interval**	**FF**	**HS**	**MS**	**LS**	**FF**	**HS**	**MS**	**LS**	**FF**	**HS**	**MS**	**LS**	**FF**	**HS**	**MS**	**LS**
G1	**Top**	0.84	0.59	0.48	0.46	0.68	0.28	0.48	0.21	0.69	0.47	0.38	0.33	0.58	0.45	0.37	0.25
	Mid-Column	0.81	0.60	0.63	0.46	0.83	0.50	0.46	0.39	0.75	0.49	0.43	0.37	0.68	0.38	0.36	0.37
	Bottom	0.94	0.80	0.79	0.61	0.84	0.51	0.64	0.57	0.87	0.57	0.66	0.65	0.81	0.67	0.64	0.66
	Average	0.88	0.70	0.67	0.54	0.80	0.45	0.56	0.44	0.80	0.53	0.53	0.50	0.72	0.54	0.50	0.49
G2	**Top**	0.69	0.62	0.57	0.43	0.74	0.51	0.43	0.50	0.73	0.30	0.32	0.26	0.53	0.29	0.29	0.37
	Mid-Column	0.88	0.68	0.72	0.53	0.79	0.55	0.53	0.48	0.76	0.51	0.48	0.43	0.73	0.45	0.42	0.39
	Bottom	0.83	0.76	0.86	0.56	0.88	0.60	0.83	0.57	0.78	0.69	0.70	0.59	0.82	0.63	0.61	0.65
	Average	0.81	0.71	0.75	0.52	0.82	0.57	0.66	0.53	0.76	0.55	0.55	0.47	0.73	0.50	0.48	0.52
G3	**Top**	0.75	0.53	0.62	0.54	0.66	0.68	0.62	0.49	0.67	0.56	0.46	0.41	0.66	0.78	0.64	0.55
	Mid-Column	0.77	0.67	0.61	0.49	0.81	0.48	0.49	0.40	0.82	0.50	0.41	0.41	0.81	0.44	0.42	0.45
	Bottom	0.89	0.75	0.69	0.65	0.83	0.59	0.68	0.58	0.84	0.61	0.59	0.69	0.78	0.61	0.56	0.63
	Average	0.83	0.68	0.65	0.58	0.78	0.59	0.62	0.51	0.79	0.57	0.51	0.55	0.76	0.61	0.55	0.57
Overall Average		0.84	0.69	0.69	0.55	0.80	0.53	0.61	0.49	0.78	0.55	0.53	0.51	0.73	0.55	0.51	0.52

PEAK ACCELERATION of 0.05g

		3B Spacing				4B Spacing				5B Spacing				6B Spacing			
Group	**Depth Interval**	**FF**	**HS**	**MS**	**LS**	**FF**	**HS**	**MS**	**LS**	**FF**	**HS**	**MS**	**LS**	**FF**	**HS**	**MS**	**LS**
G1	**Top**	0.88	0.66	0.48	0.44	0.65	0.38	0.43	0.33	0.68	0.53	0.27	0.23	0.58	0.33	0.31	0.39
	Mid-Column	0.85	0.55	0.68	0.46	0.80	0.48	0.51	0.46	0.77	0.48	0.43	0.35	0.82	0.38	0.40	0.42
	Bottom	0.89	0.73	0.75	0.56	0.91	0.69	0.61	0.56	0.97	0.61	0.52	0.60	0.81	0.61	0.61	0.63
	Average	0.88	0.67	0.67	0.51	0.82	0.56	0.54	0.48	0.85	0.56	0.44	0.45	0.76	0.48	0.48	0.52
G2	**Top**	0.78	0.58	0.50	0.52	0.62	0.60	0.44	0.44	0.74	0.35	0.34	0.23	0.65	0.27	0.33	0.37
	Mid-Column	0.90	0.66	0.77	0.54	0.76	0.51	0.57	0.53	0.83	0.48	0.48	0.47	0.80	0.45	0.41	0.42
	Bottom	0.91	0.74	0.78	0.53	0.94	0.60	0.71	0.59	0.96	0.72	0.69	0.55	0.79	0.49	0.65	0.72
	Average	0.88	0.68	0.71	0.53	0.82	0.58	0.61	0.54	0.87	0.57	0.55	0.45	0.76	0.43	0.51	0.56
G3	**Top**	0.80	0.59	0.60	0.54	0.65	0.67	0.56	0.58	0.77	0.55	0.49	0.48	0.71	0.56	0.73	0.58
	Mid-Column	0.84	0.60	0.68	0.49	0.78	0.46	0.52	0.45	0.85	0.51	0.46	0.41	0.78	0.38	0.43	0.45
	Bottom	0.88	0.68	0.70	0.70	0.88	0.58	0.63	0.75	0.78	0.63	0.58	0.56	0.80	0.57	0.50	0.62
	Average	0.85	0.64	0.67	0.61	0.80	0.57	0.59	0.63	0.80	0.58	0.53	0.50	0.77	0.52	0.54	0.57
Overall Average		0.87	0.66	0.68	0.55	0.81	0.57	0.58	0.55	0.84	0.57	0.50	0.47	0.76	0.48	0.51	0.55

Although it is accepted in this study that onset of liquefaction occurs when r_u values are equal or greater than 0.90, neglecting values between 0.65 and 0.90 does not eliminate high potential of liquefaction according to the mentioned studies. Also, the term ‘liquefaction mitigation’ refers to obtain safe r_u values that there exists no potential of liquefaction. Therefore, r_u values between 0.65 and 0.90 should not be accepted as safe values. Also, in current engineering practise like liquefaction assessment for Messina suspension bridge (Callisto, Rampello & Viggiani, 2013), r_u values below than 0.65 was accepted as safe values. Also, apart from this criterion, duration of r_u in case of being greater than 0.65 is another factor in terms of safety concern, however, in this study, it is not a criterion taken into account. Hence, as indicated in the tables given before, problematic locations having r_u values greater than 0.65 form almost entire depth of model that are shown in shaded cells. As a result, whether jet grout columns mitigate liquefaction or not are assessed here according to r_u value of 0.65.

According to the tabulated tables, it is clear that jet grout columns influence r_u values for all used stiffness levels. Besides, in most cases, this influence causes reduction in r_u. However, degree of influence on decrease in r_u values is function of stiffness level of column, spacing, depth of consideration and peak acceleration value. Minimum and maximum decrease in overall r_u values are 0.15 and 0.37, respectively.

Among 3 different stiffness levels, only jet grout columns having low stiffness are able to fully mitigate liquefaction potential based on overall average r_u values. That is, much reduction in r_u values is obtained by columns having low stiffness. The reason for why better results are obtained for column having low stiffness might be due to compatible behavior of it with soil under dynamic loading. On the other hand, there exists no significant difference between mean stiffness and high stiffness. In fact, shear modulus ratio for these 2 stiffness levels are 35 and 45, respectively. Therefore, beyond a ratio of 35, effectiveness of soilcrete columns based on r_u may not increase anymore.

Although 3B spacing is popular in engineering practise, its effectiveness on reduction in r_u may not support this popularity in application. In other words, with 3B spacing, it is not possible to diminish all r_u values below 0.65 despite of fact that there exist a decrease of it. Also, even soilcrete columns having low stiffness may not provide safe r_u values throughout the depth. Nonetheless, as spacing between columns becomes wider, effectiveness of jet grout columns increase by keeping overall average r_u values lower than 0.65. However, beyond 5B spacing, effectiveness of soilcrete columns do not increase anymore except columns having high stiffness. Therefore, the relationship between efficiency of columns and spacing might be attributed to pile-soil-pile interaction. For example, in 3B spacing, high interaction may cause limited reduction in r_u values. Also, effect of different level of stiffness is almost eliminated in 6B spacing. Hence, 5B spacing provide slightly better results in terms of r_u.

The lowest r_u values are generally attained at top section of the layer except 6B spacing. Also, second lowest values are obtained at the mid-column while unsafe values among depth sub-groups occur at the bottom portion of the jet grout column. There might be two reasons for higher r_u values at the bottom section. The first is due to lack of improvement. In other words, length of jet grout column is not enough to mitigate liquefaction for corresponding depth. Second possible explanation of it might be ineffectiveness of columns at greater depths. Mentioned comments are valid for each spacing except 6B. Lowest values are likely to occur at the mid-column for corresponding spacing.

According to free field r_u values, these values do not increase as proportional to peak acceleration value of dynamic input motion. In other words, increase in peak acceleration of dynamic motion may not result in higher values as compared to values occurred in a dynamic motion having lower peak acceleration. Moreover, there exists no direct effect of peak acceleration value on effectiveness of jet grout columns with respect to r_u. Jet grout columns are able to decrease overall r_u values in the order of 0.20-0.25 for each dynamic action.

Highest reduction in r_u are obtained in Group 1 region. In other words, more conservative r_u values may be obtained with that group. Also, less conservative values are attained with Group 3 and finally, Group 2 results in least conservative values. This situation might be attributed to distance between jet grout columns and points in a given group. Mentioned distance is greater for Group 2 as compared to Group 1. Therefore, distance has important role on the r_u reduction. However, mentioned sorting changes for 6B spacing. In that spacing, most conservative values may be obtained by Group 2 while least conservative values are attained by Group 3.

Furthermore, to compute how much r_u reduction is obtained by means of jet grout columns, a term 'r_u improvement ratio' (I_r) is defined:

$$I_r = \frac{r_{u,free\ field} - r_{u,improved\ site}}{r_{u,free\ field}} \tag{4.13}$$

By using overall average r_u values mentioned in Table (4.13), r_u improvement ratio for each stiffness level and peak acceleration values of each dynamic motion corresponding to all groups are computed in Table (4.14).

In this table, most reduction in r_u values is represented by darker cells while second most reduction is indicated by lighter shaded cells. According to the table, most reduction in r_u is generally obtained by columns having low stiffness. Besides, for 3B spacing, r_u improvement ratio differences between low stiffness level and other levels are higher than other spacing. Therefore, using stiff columns for close spacing may not be beneficial. Also, reduction percentage by mean stiffness and high stiffness levels with respect to low stiffness level are influenced slightly more by spacing and slightly less by peak acceleration of dynamic motion.

Although Table (4.14) provides overall effect of columns on r_u values for locations uniformly distributed between columns, it may not show that liquefaction potential are totally eliminated. Therefore, assessment of effectiveness of columns should be made based on improved site r_u values rather than r_u improvement ratio.

Table 4.14 Values of r_u improvement ratio

	r_u IMPROVEMENT RATIO (%)											
	3B			4B			5B			6B		
Peak Acceleration	**HS**	**MS**	**LS**	**HS**	**MS**	**LS**	**HS**	**MS**	**LS**	**HS**	**MS**	**LS**
0.08g	19.7	17.1	39.1	27.8	28.3	29.3	26.3	27.5	33.8	26.0	27.8	34.0
0.07g	19.4	22.4	28.7	32.0	32.1	38.3	27.4	33.6	36.2	30.8	32.6	34.5
0.06g	17.4	17.4	34.9	33.4	23.9	38.5	30.1	32.1	35.4	25.0	30.5	28.9
0.05g	23.7	21.5	36.9	29.6	28.7	32.2	32.2	39.9	44.4	37.5	32.9	28.1

CHAPTER FIVE
CONCLUSION AND RECOMMENDATIONS

Liquefaction is loss of self-stability due to significant drop of shear strength and stiffness by means of presence of excess pore pressure under undrained conditions (Terzaghi, Peck & Mesri, 1996). Especially for saturated granular soils, liquefaction is an important phenomenon due to its possible hazardous effects. In the evaluation of liquefaction potential of soil, ‘simplified procedure’ of Seed and Idriss (1971) has become a consensus for evaluation of liquefaction initiation risk of a soil deposit. However, this method does not take excess pore water pressure into account. Apart from total stress method called as ‘simplified method’, effective stress method based on r_u values which adopts primary mechanism of liquefaction by excess pore pressure exists in the assessment of triggering of liquefaction. In this approach, onset of liquefaction is accepted when r_u becomes 1.0 (Seed & Lee, 1966).

In the past, several liquefaction related damages including collapse of dams and slopes, bearing capacity failure of foundations and lateral spreading occurred. Besides, foundation deformations based on liquefaction continue to be a major reason of damage (Dobry, 1996). Therefore, so as to eliminate liquefaction potential, several mitigation methods have evolved. Among various countermeasures against liquefaction, jet grout columns have become widely used method by offering certain advantages (Unutmaz, 2012).

Although jet grout columns satisfactorily mitigated liquefaction in 1999 Kocaeli Earthquake, effectiveness of soilcrete columns have not been verified clearly. Besides, there exits few numerical studies to indicate influence of columns on remediation of liquefaction. Most of the numerical studies adopt total stress approach (Ozsoy & Durgunoglu, 2003; Olgun & Martin, 2008; Unutmaz, 2012; Cristovao et al., 2014) while effective stress method have not been effectively utilized in the studies (Almani et al., 2013).

This study aimed to investigate contribution of jet grout columns on liquefaction mitigation based on effective stress approach by means of numerical analyses adopting finite difference method. Therefore, 3-D model was constructed in FLAC3D and soil model was coupled with dynamically excess pore pressure generating Finn Model.

Firstly, it was indicated in 1-D and 3-D free field analyses that soil properties adopted from WLA cause significant liquefaction. In these analyses, instead of real earthquake data, simple wave form having constant frequency but time dependent linearly varying amplitude was used due to limitation of Finn model in this prespect. In fact, in the assessment of liquefaction state of soil, r_u values were used. Onset of liquefaction initiation was accepted that r_u values are equal or greater than 0.90. The reason was due to the fact that factor of safety values corresponding to mentioned r_u values are very close to 1.0 according to the figure for sandy soils given by Marcuson et al. (1990).

Secondly, effect of jet grout columns on liquefaction mitigation was studied parametrically. Jet grout columns having diameter of 1 m and length of 12 m were modelled with Mohr-Coulomb plasticity model. Uniform jet grout disposition was also used. In parametric study point of view, spacing between soilcrete columns, different stiffness levels of columns, various peak acceleration of dynamic motion and depth of considerations formed used parameters in this study. Spacing parameters were 3B, 4B, 5B and 6B while stiffness parameters were low, mean and high levels based on shear modulus ratio between soil and column. These stiffness levels were determined based on ratio of shear moduli of soilcrete column to soil. Corresponding values were 27.4, 35.4 and 44.8 for low stiffness level, mean stiffness level and high stiffness level, respectively. Also, used peak acceleration values were 0.05g, 0.06g, 0.07g and 0.08g. Furthermore, r_u values were obtained for predetermined 16 locations at 2 m, 4 m, 6 m, 8 m, 10 m and 12 m depths in order to find out depth effect.

Hence, it was indicated that jet grout columns are effective against liquefaction by keeping r_u values below 0.90. Although r_u values of 0.90 and greater than it are critical in the initiation of liquefaction, values between 0.65 and 0.90 are also critical which indicates high potential of liquefaction (Idriss & Boulanger, 2008). Therefore, apart from prevention of onset of liquefaction, fully elimination of liquefaction potential was also considered in the overall assessment of contribution of jet grout columns. Hence, conclusions of this study are listed as:

- Jet grout columns affect r_u values predominantly by decreasing it.
- Only soilcrete columns having low stiffness are able to fully eliminate liquefaction potential based on overall average r_u values for all situations. However, even low stiffness level may not eliminate liquefaction potential throughout the depth at a given point.
- For each stiffness level, up to 5B, contribution of columns on the reduction in r_u generally increases. However, beyond 5B, contribution of columns on the reduction of it does not increase anymore except high stiffness level. 5B spacing ends up slightly more conservative r_u values. Effect of stiffness on overall average r_u values mostly eliminates in 6B spacing.
- Effectiveness of high and mean stiffness levels are limited in 3B spacing. Nonetheless, low stiffness level provides far better reduction in r_u values than other levels.
- The lowest r_u values are generally attained at top section of the layer except 6B spacing. Also, second lowest values are obtained at the mid-column and finally, unsafe values among depth sub-groups occur at the bottom of the jet grout column.
- Increasing peak acceleration value of dynamic motion does not necessarily rises up free field r_u values. Besides, peak acceleration does not have significant effect on r_u values for improved site case.
- Reduction percentage of r_u values by mean stiffness and high stiffness levels with respect to low stiffness level are influenced slightly more by spacing and slightly less by peak acceleration of dynamic motion.
- The lowest and the highest decrease in overall r_u values are 0.15 and 0.37, respectively.

Although this study have identified several aspects of contribution of jet grout columns on liquefaction potential, it requires more comprehensive parametric studies including different soil stiffness, varying column length, alternating patterns having same area replacement ratio, different loading frequency and use of equivalent stress cycles of real earthquake. Apart from mentioned parameters, effect of interface stiffness can be studied. Moreover, different damping ratio magnitude and possible effects of Rayleigh components for jet grout columns could be investigated. Furthermore, relation of natural frequency of soil and liquefaction behavior could be investigated if there exists. Also, formulation of effect of parameters in the reduction of r_u could be beneficial for engineering practise.

REFERENCES

Adalier K., Elgamalb A., Menesesb, J., & Baez J. I. (2003). Stone columns as liquefaction countermeasure in non-plastic silty soils. *Soil Dynamics and Earthquake Engineering*, *23*, 571-584.

Almani, Z. A., Memon A. A., Habib A. F., Lal, K., & Shah S. F. (2013). 3D numerical modelling of liquefaction-induced settlements and its mitigation. *Sindh University Research Journal*, *45* (2), 301-304.

Almani, Z. A., Memon, N. A., & Memon, A. A. (2012). Stiff columns as liquefaction mitigation measure for retrofit of existing buildings. *Mehran University Research Journal of Engineering & Technology*, *31* (4), 659-668.

Ambraseys, N. N. (1988). Engineering seismology. *Earthquake Engineering and Structural Dynamics*, *17*, 1-105.

Andrews D. C., & Martin G. R. (2000). Criteria for liquefaction of silty sands. *Proceedings of the 12th World Conference on Earthquake Engineering*, Auckland, New Zealand.

ASCE Committee on Placement and Improvement of Soils (1987). *Soil improvement-a ten year update. In Proceedings of Symposium at ASCE Convention*, April 28, Atlantic City, N. J., J. P. Welsh (Ed.), Special Pub. 12.

Baez, J. I., & Martin, G. R. (1994). Advances in the design of vibro systems for the improvement of liquefaction resistance. *The 2nd Seismic Short Course on Evaluation and Mitigation of Earthquake Induced Liquefaction Hazards*, Division of Engineering, San Francisco State University and Department of Civil Engineering University of Southern California, 1-16.

Bell, A. L. (1993). Jet grouting. In ground improvement, *Blackie Academic and Professional*, 149-172.

Bennett, M. J., McLaughlin, P. V., Sarmiento, J. S., & Youd, T. L. (1984). Geotechnical investigation of liquefaction sites Imperial Valley- California. *United States Department of the Interior Geological Survey*, 84-252.

Bishop, A. W. (1973). The stability of tips and spoil heaps. *Quarterly Journal of Engineering Geology*, *6*, 335-376.

Boulanger, R. W., & Idriss, I. M. (2004). State normalization of penetration resistances and the effect of overburden stress on liquefaction resistance. *In Proceedings, 11th International Conference on Soil Dynamics and Earthquake Engineering, and 3rd International Conference on Earthquake Geotechnical Engineering*, *2*(1), 484-491.

Boulanger, R. W., & Idriss, I. M. (2006). Liquefaction susceptibility criteria for silts and clays. *Journal of Geotechnical and Geoenvironmental Engineering*, *132*(11), 1413-1426.

Boulanger, R. W. (2003). Relating K_{α} to relative state parameter index. *Journal of Geotechnical and Geoenvironmental Engineering*, *129*(8), 770-773.

Bray, J. D., Sancio, R. B., Durgunoglu, H. T., Onalp, A., Seed, R. B., Stewart, J. P., et al. (2001). Ground failure in Adapazari, Turkey. *Proceedings of Earthquake Geotechnical Engineering Satellite Conference of the XVth International Conference on Soil Mechanics & Geotechnical Engineering*, Istanbul, Turkey.

Bruce, D. A. (1988). Developments in geotechnical construction processes for urban engineering. *Civil Engineering Practice*, *3*(1), 49-97.

Bruce, D. A. (2002). *Anchors, micropiles, rock grouting and deep mixing: A decade of progress in the United States (online pdf)*. Available:

http://www.geosystemsbruce.com/v20/biblio/z167_2002_anchorsGroutingDMM_decade.pdf [Accessed: May 24, 2015].

Bruce, D. A. & Bruce, M. E. C. (2003). The practitioner's guide to deep mixing. *Proceedings of Rapid Excavation and Tunneling Conference (RETC)*, 474-488.

Burke, G. K. (2004). Jet grouting systems: Advantages and disadvantages. *American Society of Civil Engineers*, *124*(1), 875-886.

Callisto, L., Rampello, S., & Viggiani, G. (2013). Soil–structure interaction for the seismic design of the Messina Strait Bridge. *Soil Dynamics and Earthquake Engineering*, 103-115.

Canadian foundation engineering manual. (1978). Montreal: Canadian Geotechnical Society.

Carlo, G. L. (2007). Advanced numerical modelling of soil-structure interaction: peculiarities, examples and case studies, *24th ALERT Workshop and School*.

Casagrande, A. (1936). Characteristics of cohesionless soils affecting the stability of slopes and earth fills. *Journal of Boston Society of Civil Engineers, 23*(1), 13-32.

Casagrande, A. (1965). The role of the calculated risk in earthwork and foundation engineering. The Terzaghi lecture. *Journal of Soil Mechanics and Foundation Division*, *94*(4), 1-40.

Castro, G. (1969). Liquefaction of sands. *Harvard Soil Mechanics Series 87*, Harvard University, Cambridge, Massachusetts.

Cetin, K. O., Seed, R. B., Der Kiureghian, A., Tokimatsu, K., Harder, L. F. Jr, Kayen, R. E., et al. (2004). SPT-based probabilistic and deterministic assessment of seismic soil liquefaction potential. *Journal of Geotechnical and Geoenvironmental Engineering*, *130*(12), 1314-1340.

Chen, W., & Scawthorn, C. (2003). Geotechnical and foundation aspects. *Earthquake engineering handbook*. Boca Raton, Florida: CRC Press.

Cheuk, J. C. Y., Lai, A. W. L., & Cheung, C. K. W., (n.d.). *The use of jet grouting to enhance stability of bermed excavation (online pdf)*. Retrieved June 11, 2015, from http://www.geotech-fr.org/sites/default/files/congres/cimsg/1255.pdf

Coulier, P., François, S., Degrande, G., & Lombaert, G. (2013). A numerical study of subgrade stiffening as a mitigation measure for railway induced vibrations through 2.5D and 3D FE-BE models. *In proceedings, 4th ECCOMAS Thematic Conference on Computational Methods in Structural Dynamics and Earthquake Engineering*.

Cristovao, A., Nogueira, A., Hutchinson, R., Brito, D., Tomasio, R., & Pinto, R. (2014). Jet grouting columns operating as reaction platform for building uplift and soil induced liquefaction mitigation. *In Proceedings, 17th Congresso Brasileiro de Mecanica dos Solos e Engenharia Geotecnia*.

Croce, P., & Flora, A. (2000). Analysis of single-fluid jet grouting. *Géotechnique, 50*(6), 739-748.

Dobry, R. (1996). Geotechnical engineering performance quantification of foundations. *Performance Based Seismic Design of Buildings: An Action Plan for Future Studies, 5*, 54-62.

Durgunoglu, H. T., Emrem, C., Chinchelli, M., Hurley, T., Ikiz, S., & Catalbas, F. (2004). Soil improvement with jet-grout columns: a case study from the 1999 Kocaeli Earthquake. *Proceedings: 5th International Conference on Case Histories in Geotechnical Engineering*, 1-5.

Durgunoglu, H. T., Emrem, C., Karadayilar, T., Mitchell, J. K, Martin, J. R., & Olgun, C. G. (2001). Case history for ground improvement against liquefaction Carrefoursa shopping center-Izmit, Turkey. *Proceedings of Satellite Conference Lessons Learned From Recent Strong Earthquakes*, 299-304.

Fang, Y. S., Liao J. J., & Lin, T. K. (1994). Mechanical properties of jet grouted soilcrete. *Quarterly Journal of Engineering Geology*, *27*, 257-265.

Finn, W. D. L. (1982). *Soil mechanics transient and cyclic loads*. NewYork: John Wiley & Sons Ltd.

Finn, W. D. L. (1981). Liquefaction potential: development since 1976. *Proceedings International Conference on Recent Advances in Geotechnical. Earthquake Engineering and Soil Dynamics*, Rolla, Missouri, 655-681.

FLAC3D (2008). *User's Manual-Fast Lagrangian Analysis of Continua in 3 Dimensions*. Itasca Consulting Group, Minnesota.

Goughnour, R. R., & Pestana, J. M. (1998). Mechanical behavior of stone columns under seismic loading. *In Proceedings, 2nd International Conference on Ground Improvement Techniques*, 157-162.

Guatteri, G., Kauschinger, J. L., Dona, A. C., & Perry, E. C. (1988). Advances in the construction and design of jet grouting methods in South America. *In Proceedings 2nd International Conference on Case Histories in Geotechnical Engineering*, *5*(32).

Haldar, A., & Tang, W. H. (1981). Statistical study of uniform cycles in earthquakes. *Journal of the Geotechnical Engineering Division*, *107*(GT5), 577-589.

Hashash, Y. M. A., Musgrove, M. I., Harmon, J. A., Groholski, D. R., Phillips, C. A., & Park, D. (2015). DEEPSOIL 6.0, User Manual. 116.

Hausler, E. A., & Sitar, N. (2001). Performance of soil improvement techniques in earthquakes. *Fourth International Conference on Recent Advances in Geotechnical Earthquake Engineering and Soil Dynamics*. California, USA, 10-15.

Hayden, R. F, & Baez, J. I. (1994). State of practice for liquefaction mitigation in North America. *In Proceedings of the 4th U.S.-Japan Workshop on Soil Liquefaction, Remedial Treatment of Potentially Liquefiable Soils*, 4-6.

Ho, C. E. (2007). Fluid-soil interaction model for jet grouting. *American Society of Civil Engineers*, *168*(1), 1-10.

Holzer, T., & Youd, T. (2007). Liquefaction, ground oscillation, and soil deformation at the wildlife array, California. *Bulletin of the Seismological Society of America*, 961-976.

Idriss, I. M. (1998). An update of simplified liquefaction evaluation procedure. *2nd Japan-Turkey Workshop on Earthquake Engineering*.

Idriss, I. M. (1999). An update to the Seed-Idriss simplified procedure for evaluating liquefaction potential. *In Proceedings, TRB Workshop on New Approaches to Liquefaction*, Publication No. FHWA-RD-99-165, Federal Highway Administration.

Idriss, I., & Boulanger, R. (2008). *Soil liquefaction during earthquakes*. Oakland, Calif., California: Earthquake Engineering Research Institute.

Ishihara, K. (1985). Stability of natural deposits during earthquakes. *Proceedings on llth International Conference on Soil Mechanics and Foundation Engineering*, San Francisco, *1*, 321-376.

Ishihara, K. (1993). Liquefaction and flow failure during earthquakes. *Geotechnique, 43*(3), 351-415.

Ishihara, K. (2003). *Soil behaviour in earthquake geotechnics*. Oxford: Clarendon Press.

James R. M., Olgun C. G., Mitchell J. K., & Durgunoğlu H. T. (2004). High-modulus columns for liquefaction mitigation. *Journal of the Soil Mechanics and Foundation Division*, *130* (6), 561-571.

Japan Jet Grouting Association (1986). *JSG method, technical information.* Tokyo, Japan.

Kauschinger, J. L., & Welsh, J. P. (1989). Jet grouting for urban construction. *In Proceedings 1989 Geotechnical Lecture Series, Boston Society of Civil Engineering: Design Construction and Performance of Earth Support Systems*, Cambridge, Massachusett, 60.

Kauschinger, J. L., Hankour, R, & Perry, E. B. (1992). Methods to estimate composition of jet grout bodies. *In Proceedings Conference on Grouting, Soil Improvement and Geosynthetics*, *2*(1), 194-205.

Kawasumi, H. (1968). *General report on the Niigata Earthquake of 1964.* Tokyo: Electrical Engineering College Press, 550.

Keepa, C., Saul, G., Murashev, A., & McMillan J. (2014). South Brighton Bridge: lateral spread mitigation using jet grout lattice structures. *2014 New Zealand Society of Earthquake Engineering Conference*, Auckland, New Zealand.

Kishida, T. (2008). *Seismic site effects for the Sacramento-San Joaquin Delta*. (Ph.D. dissertation), University of California, Davis.

Koppejan, A. W., Van Wamelen, B. M., & Weinber, L. J. H. (1948). Coastal landslides in the Dutch province of Zealand. *Proceedings of the 2nd International Conference on Soil Mechanics and Foundation Engineering*, Rotterdam, Holland, 89-96.

Kramer, S. (1996). *Geotechnical earthquake engineering*. Upper Saddle River, New Jersey: Prentice Hall.

Liao, S. S. C., Veneziano, D., & Whitman, R.V. (1988). Regression models for evaluating liquefaction probability. *Journal of Geotechnical Engineering Division*, *114*(4), 389–411.

Liao, S. S. C., & Whitmann, R.V. (1986). Overburden correction factors for SPT in sand. *Journal of Geotechnical Engineering, 112*(3), 373 – 377.

Littlejohn, G. S. (1982). Design of cement based grouts. *In Proceedings of the Conference on Grouting in Geotechnical Engineering*, New Orleans, 35-47.

Liu, L., & Dobry, R. (1997). Seismic response of shallow foundation on liquefying sand. *Journal of Geotechnical & Geoenvironmental Engineering*, *123*(6), 557-567.

Lunardi, P. (1997). Ground improvement by means of jet grouting. *In Proceedings of the International Conference on Engineering*, *1*(2), 65-85.

Marcuson, W. F., Hynes, M. E., & Franklin, A. G., (1990). Evaluation and use of residual strength in seismic safety analysis of embankments, *Earthquake Spectra, 6*(3), 529–72.

Marcuson, W. F., Ballard, R. F., & Ledbetter, R. H. (1978). Liquefaction failure of tailings dams resulting from the Near Izu Oshima earthquake. *In Proceedings, 6th Panamerican Conference on Soil Mechanics and Foundation Engineering*, *2*, 69–80.

Martin, G. R., & Lew, M. (1999). *Recommended procedures for implementation of DMG special publication 117, Guidelines for analyzing and mitigating liquefaction hazards in California*. Los Angeles Southern California Earthquake Center, University of Southern California.

Martin, G. R., Finn, W. D. L., & Bolton, H. B. (1975). Fundamentals of liquefaction under cyclic loading, *Journal of the Soil Mechanics and Foundation Division*, *101*, 422-438.

Martin, I., & Olgun, C. (2007). Liquefaction mitigation using jet-grout columns-1999 Kocaeli Earthquake case history and numerical modelling. *The 4th International Conference on Earthquake Geotechnical Engineering*, Thessaloniki, Greece.

Martin, J. R., Olgun, C. G., Mitchell, J. K., & Durgunoglu, H. T. (2004). High-modulus columns for liquefaction mitigation. *Journal of Geotechnical & Geoenvironmental Engineering*, *130*(6), 561-571.

Melegari, C., & Garassino, A. L. (1997). Seminar on jet grouting. *CI-Premier Pte. Ltd.*, Singapore.

Mihalis, I. K., Tsiambaos, G., & Anagnostopoulos, A. (2004). Jet grouting applications in soft rocks: The Athens Metro case. *In Proceedings Institute of Civil Engineering and Geotechnical Engineering*, *157*(4), 219–228.

Miki, G., & Nakanishi, W. (1984). Technical progress of the jet grouting method and its newest type. *In Proceedings International Conference In Situ Soil and Rock Reinforcement*, 195-200.

Miki, G. (1985). Soil improvement by jet grouting. *Third International Geotechnical Seminar on Soil Improvement Methods*, 45-52.

Mitchell, J. K. (2008). Mitigation of liquefaction potential of silty sands, *From Research to Practice in Geotechnical Engineering*, Geotechnical Special Publication 180, 433-451.

Mitchell, J. K., Cooke, H. C., & Schaeffer, J. A. (1998). Design considerations in ground improvement for seismic risk mitigation. *In Proceedings of the Conference on Geotechnical Earthquake Engineering and Soil Dynamics III*, *75*(1), 580-613.

Modoni, G., Croce, P., & Mongiovi, L. (2006). Theoretical modelling of jet grouting. *Géotechnique*, *56*(5), 335-347.

Mogami, H., & Kubo, T. (1953). The behavior of soil during vibration. *Proceedings of the 3rd International Conference on Soil Mechanics and Foundation Engineering*, 152-153.

Moradi G., Khatibi B. R., & Sutubadi, M. H. (2011). Determination of liquefaction potential of soil using $(N_1)_{60}$ by numerical modelling method. *Electronic Journal of Geotechnical Engineering*, 16.

Moseley, M. P., & Kirsch, K. (2004). *Ground improvement*. London: Spon Press, Taylor & Francis Group.

Nakanishi, W. (1974). Method for forming an underground wall comprising a plurality of columns in the earth and soil formation. *U.S. Patent 3*, *800,* 544.

National Center for Earthquake Engineering Research (NCEER) (1997). *Proceedings of the NCEER Workshop on Evaluation of Liquefaction Resistance of Soils*, Edited by Youd, T. L., Idriss, I. M., Technical Report No. NCEER-97-0022.

Neville, A. M. (1997). *Properties of concrete*, Essex Addison Wesley Longman Ltd. Publ., 306.

Nicholson, A. J. (1963). Discussion, *ICE Conference on Grouting and Drilling Muds in Engineering Practice. Buttenvorths*, London, 108-109.

Nishimatsu, Y. (1972). The mechanics of rock cutting. *International Journal of Rock Mechanics and Mining Science*, *9*, 261- 270.

Okmen, O. (2003). *A study on strength and deformation behavior of soilcrete in jet grout applications*. M. Sc. Thesis. The Middle East Technical University, Ankara.

Olgun, C., & Martin, I. (2008). Numerical modelling of the seismic response of columnar reinforced ground. *The 14th World Conference on Earthquake Engineering*, Beijing, China.

Ozsoy, B., & Durgunoglu, H. T. (2003). The Mitigation of liquefaction by means of high modulus soilcrete columns. *5th National Earthquake Engineering Conference*, 26-30.

Ozsoy, B. (2002). *The Mitigation of liquefaction by means of soil improvement techniques*. PhD. Thesis, Bogazici University, Istanbul.

Parry-Davies, R., Bruin, R. M. H, Wardle, G., & Nixon, M. G. (1992). Stabilization of pier foundation using jet grouting techniques. *In Proceedings Conference on Grouting, Soil Improvement and Geosynthetics*, *1*(1), 156-168.

Reese, L., & Impe, W. (2010). *Single piles and pile groups under lateral loading*, (2nd Edition). Hoboken: CRC Press.

Robertson, P. K., & Wride, C. E. (1997). Cyclic liquefaction potential and its evaluation based on the SPT and CPT. *Workshop on Evaluation of Liquefaction Resistance*, NCEER-97-0022, Buffalo, NY, 41-87.

Robertson, P.K., & Catherine E. F. (1997). Liquefaction of sands and its evaluation. *1st International Symposium on Earthquake Geotechnical Engineering*, Tokyo, 1253-1287.

Schaeffer, V. R. (1997). Ground improvement, ground reinforcement, ground-treatment-developments 1987-1997. *American Society for Civil Engineers*, *69*, 618.

Seed, H. (1986). *Design problems in soil liquefaction*. Berkeley, Calif., California: Earthquake Engineering Research Center, College of Engineering, University of California.

Seed, H. B., & Idriss, I. M. (1971). Simplified procedure for evaluating soil liquefaction potential. *Journal of the Soil Mechanics and Foundation Division*, *97*(SM9), 1249 – 1273.

Seed, H. B., & Idriss, I. M. (1982). Ground motions and soil liquefaction during earthquakes. *Earthquake Engineering Research Institute Monograph Series*.

Seed, H. B. (1983). Earthquake-resistant design of earth dams. *In Proceedings, Symposium of Seismic Design of Earth Dams and Caverns*, 41–64.

Seed, H. B., Arango, I., & Chan, C. K. (1976). Evaluation of soil liquefaction effects on level ground during earthquakes. Liquefaction Problems in Geotechnical Engineering, *ASCE Annual Convention and Exposition*, Philadelphia, PA, 1-109.

Seed, H. B., Idriss, I. M., Makdisi, F., & Banerjee, N. (1975). Representation of irregular stress time histories by equivalent uniform stress series in liquefaction analyses. *EERC 75-29, Earthquake Engineering Research Center*, University of California, Berkeley.

Seed, H. B., Tokimatsu, K., Harder, L. F., & Chung, R. M. (1985). The influence of SPT procedures in soil liquefaction resistance evaluations. *Journal of Geotechnical Engineering*, *111*(12), 1425–1445.

Seed, H. B., & Lee, K. L. (1966). Liquefaction of saturated sands during cyclic loading. *Journal of the Soil Mechanics and Foundations Division*, *92* (SM6), 105-134.

Seed, R. B., Cetin, K. O., Moss, R. E. S., Kammerer, A. M., Wu, J., Pestana, J. M., et al. (2003). Recent advances in soil liquefaction engineering: a unified and consistent framework. *26th Annual ASCE Los Angeles Geotechnical Spring Seminar*.

Shibazaki, M. (1996). State of the art grouting in Japan. *In Proceedings, 2nd International Conference on Ground Improvement Geosystems*, 857–862.

Shibazaki, M. (2003). State of practice of jet grouting. *International Conference on Grouting and Ground Treatment*, New Orleans.

Spagnoli, G. (2008). Theoretical evaluations of liquefaction mitigation through jet grouting. *Geotechnical News*, 41-46. Retrieved May 13, 2015.

Stoel, A. E. C. (2001). *Grouting for pile foundation improvement*. Ph. D. Thesis. Delf University of Technology, Amsterdam, Holland.

Terzaghi, K., & Peck, R. B. (1948). *Soil mechanics in engineering practice* (2nd Edition). John Wiley and Sons, Inc.

Terzaghi, K., Peck, R., & Mesri, G. (1996). *Soil mechanics in engineering practice* (3rd Edition). New York: Wiley.

Tokimatsu, K., & Seed, H. B. (1987). Evaulation of settlements in sands due to earthquake shaking. *Journal of Geotechnical Engineering*, *113* (GT8), 861-78.

Toprak, S., Holzer, T. L., Bennett, M. J., & Tinsley, J. C. (1999). CPT- and SPT-based probabilistic assessment of liquefaction potential. *Proceedings of Seventh U.S.-Japan*.

Tornaghi, R., & Perelli, C. A. (1985). Soil improvement by jet grouting for the solution of tunnnelling problems. *In Proceedings 4th International Symposium on Mine Tunnelling,* 265-276.

Trevi, K. (1994). Columnar treatment, *Illustrative Report*, Cesena.

Tsuchida, H. (1970). Prediction and countermeasure against the liquefaction in sand deposits. *Abstract of the Seminar in the port and Harbor Research Institute*, 3.1-3.33.

Unutmaz, B. (2008). *Assessment of soil-structure-earthquake interaction induced soil liquefaction triggering*. PhD dissertation, Middle East Technical University, Ankara.

Unutmaz, B. (2012). Numerical assessment of high-modulus columns on liquefaction triggering potential. *International Journal for Numerical and Analytical Methods in Geomechanics*, 1312-1325.

Vaid, Y. P., & Sivathayalan, S. (1997). Static and cyclic liquefaction potential of Fraser Delta sand in simple shear and triaxial test. *Canadian Geotechnical Journal*, *33*(2), 281–289.

Wang, Z. F., Shen, S. L., Ho, C. E., & Kim, Y. H. (2013). Jet grouting practise: an overview. *Geotechnical Engineering of the SEAGS & AGSSEA*, *44*(4), 88-96.

Welsh, J. P., Rubright, R. M., & Coomber, D. B. (1986). Jet grouting for support of structures. *In Proceeding Conference on Grouting for the Support of Structure*, 1-

16. *Workshop on Earthquake Resistant Design of Lifeline Facilities and Countermeasures against Liquefaction*.

Xanthakos, P., & Abramson, L. (1994). *Ground control and improvement*. New York: John Wiley.

Yahiro, T., & Yoshida, H. (1973). Induction grouting method utilizing high speed water jet. *In Proceedings 8th International Conference on Soil Mechanics and Foundation Engineering*.

Youd, T. L. (1984). Recurrence of liquefaction at the same site. *Proceedings, 8th World Conference on Earthquake Engineering*, *3*, 231-238.

Youd, T. L. (1991). Mapping of earthquake-induced liquefaction for seismic zonation. *Proceedings, 4th International Conference on Seismic Zonation*, Earthquake Engineering Research Institute, Stanford University, 111-147.

Youd, T. L., & Noble, S. K. (1998). Liquefaction criteria based on probabilistic analyses. *In NCEER Workshop on Evaluation of Liquefaction Resistance of Soils*, National Center for Earthquake Engineering Research Technical Report NCEER-97-0022, 201–216.

Youd, T. L., Idriss, I. M., Andrus, R. D., Arango, I., Castro, G., Christian, J. T., et al. (1997). *Summary Paper, Proceedings, NCEER Workshop on Evaluation of Liquefaction Resistance of Soils*, *97*(0022).

APPENDICES

APPENDIX A:
MATLAB Code of Discrete Fourier Transformation

```
%%%%%%%%%%UNDAMPED LINEAR ELASTIC SITE RESPONSE ANALYSIS%%%%%%%%%%
clear all
clc
              %%%%%%%%%%FLOWCHART%%%%%%%%%%
%MOTION_INPUT===>DFT===>SOIL_PROP_INPUT===>TRANSFER_FUNC===>GROUND_MOTION(I
DFT)
%
%
%%%%%%%MOTION_INPUT%%%%%%%
fileID = fopen('Superstition_Hills_Earthquake_90.txt','r');
formatSpec = '%f %f';
sizeA = [2 Inf];
A = fscanf(fileID,formatSpec,sizeA);
fclose(fileID);
f(:,1)=A(2,:).*9.81;  %GIVEN ACCELERATION VECTOR
a=-1;
img=sqrt(a);
N=length(A);
fs=1/(A(1,2)-A(1,1));
ts=1/fs;
%
%
%%%%%%%DISCRETE FOURIER TRANSFORMATION%%%%%%%
%%%%%%%%%%FOURIER MATRIX%%%%%%%%%%
Constant=exp(-2*pi*img/N);
fourier_matrix=zeros(length(A),length(A));
for k=0:N-1
   for n=0:N-1
      fourier_matrix(k+1,n+1)=Constant^(n*k);
   end
end
%%%%%%%%%%DESIRED COEFFICIENT VECTOR%%%%%%%%%%
f_cap=fourier_matrix*f;
f_cap_amp=abs(f_cap);
%%%%%%%%%%TEST FUNCTION%%%%%%%%%%
ww=zeros(N,N);
Constant_Conjugate=exp(2*pi*img/N);
for k=0:N-1
   for n=0:N-1
   ww(k+1,n+1)=Constant_Conjugate^(n*k);
   end
end
test_func=ww*f_cap/N;
%
%
%%%%%%%SOIL_PROPERTY_INPUT%%%%%%%
H=input('Enter layer thickness (m): ');
VS=input('Enter shear wave velocity (m/s): ');
while VS/(4*H)<25||VS/(4*H)>50
H=input('Enter layer thickness (m): ');
VS=input('Enter shear wave velocity (m/s): ');
end
%
%
%%%%%%%TRANSFER_FUNCTION%%%%%%%
a1=1/(N*ts);
a2=a1*(N-1);
a3=0:a1:a2;
transfer_func=1./(cos(2*pi*a3*H/VS));
%
%
%%%%%%%GROUND_MOTION(IDFT)%%%%%%%
www=zeros(N,N);
Constant_Conjugate=exp(2*pi*img/N);
```

```
for k=0:N-1
    for n=0:N-1
    www(k+1,n+1)=Constant_Conjugate^(n*k);
    end
end
t=eye(N,N);
for x=1:N
    t(x,x)=f_cap(x,1);
end
ground_motion_dummy=t*transfer_func';
ground_motion=www*ground_motion_dummy/N;
%
%
%%%%%%%%%%%PLOTS%%%%%%%%%%%
figure(1);
plot(A(1,:),A(2,:));
title('Time Domain Bedrock Motion');
xlabel(('Time (s)')); ylabel('Acceleration (m/s^2)');
figure(2);
plot(a3,f_cap_amp);
title('Frequency Domain Bedrock Motion');
xlabel(('Frequency (Hz)')); ylabel('Amplitude (m/s)');
figure(3);
plot(A(1,:),ground_motion);
title('Ground Motion');
xlabel(('Time (s)')); ylabel('Acceleration (m/s^2)');
```

APPENDIX B:

FLAC3D Code for 3B Spacing for Free Field Analyses

```
new
title "Free_Field_SL_EP2_30W_15D_SSSS3BM_v1"
config fluid dyn
set fluid off dyn off
;
; %%%%%%%SOIL BODY GEOMETRY%%%%%%%
gen zone radcyl p0(0,0,0) p1(1,0,0) p2(0,0,-9) p3(0,1,0)...
p4(1,0,-9) p5(0,1,-9) p6(1,1,0) p7(1,1,-9) p8(0.5,0,0)...
p9(0,0.5,0) p10(0.5,0,-9) p11(0,0.5,-9)...
size 1 18 4 2 ratio 1 1 1 1 fill
;
gen zone radcyl p0(0,0,-9) p1(1,0,-9) p2(0,0,-15) p3(0,1,-9)...
p4(1,0,-15) p5(0,1,-15) p6(1,1,-9) p7(1,1,-15) p8(0.5,0,-9)...
p9(0,0.5,-9) p10(0.5,0,-15) p11(0,0.5,-15)...
size 1 12 4 2 ratio 1 1 1 1 fill
;
gen zone reflect norm 1,0,0
gen zone reflect norm 0,1,0
;
gen zone copy 3 0 0 range x -1.5 1.5 y -1.5 1.5 z 0.0 -15.0
gen zone copy 6 0 0 range x -1.5 1.5 y -1.5 1.5 z 0.0 -15.0
gen zone copy 0 3 0 range x -1.5 7.5 y -1.5 1.5 z 0.0 -15.0
gen zone copy 0 6 0 range x -1.5 7.5 y -1.5 1.5 z 0.0 -15.0
;
gen zone brick p0(1,-1,0) p1(2,-1,0) p2(1,-1,-15) p3(1,1,0)...
p4(2,-1,-15) p5(1,1,-15) p6(2,1,0) p7(2,1,-15)...
size 2 30 4 ratio 1 1 1
;
gen zone copy 0 3 0 range x 1.0 2.0 y -1.0 1.0 z 0.0 -15.0
gen zone copy 0 6 0 range x 1.0 2.0 y -1.0 1.0 z 0.0 -15.0
gen zone copy 3 0 0 range x 1.0 2.0 y -1.0 7.0 z 0.0 -15.0
;
gen zone brick p0(-1,2,0) p1(-1,1,0) p2(-1,2,-15) p3(7,2,0)...
p4(-1,1,-15) p5(7,2,-15) p6(7,1,0) p7(7,1,-15)...
size 2 30 16 ratio 1 1 1
;
gen zone copy 0 3 0 range x -1.0 7.0 y 1.0 2.0 z 0.0 -15.0
;
gen zone brick p0(-1.0,-1.0,0) p1(-1.0,-12.0,0) p2(-1.0,-1.0,-15) p3(7.0,-1.0,0)...
p4(-1.0,-12,-15) p5(7.0,-1.0,-15) p6(7.0,-12,0) p7(7.0,-12,-15)...
size 22 30 16 ratio 1.0 1.0 1.0
;
group zone dummy range y -1.0 -12.0
gen zone reflect origin 0,3,0 norm 0,1,0 range group dummy
;
gen zone brick p0(-1.0,-1.0,0) p1(-1.0,7.0,0) p2(-1.0,-1.0,-15) p3(-12.0,-1.0,0)...
p4(-1.0,7.0,-15) p5(-12,-1.0,-15) p6(-12,7.0,0) p7(-12.0,7.0,-15)...
size 16 30 22 ratio 1.0 1.0 1.0
group zone dummy_2 range x -1.0 -12.0
gen zone reflect origin 3,3,0 norm 1,0,0 range group dummy_2
;
gen zone brick p0(7.0,-1.0,0) p1(7.0,-12,0) p2(7.0,-1.0,-15) p3(18,-1.0,0)...
p4(7.0,-12,-15) p5(18,-1.0,-15) p6(18,-12,0) p7(18,-12,-15)...
size 22 30 22 ratio 1.0 1.0 1.0
;
group zone dummy_3 range x 7.0 18.0 y -1.0 -12.0 z 0.0 -15.0
;
gen zone reflect origin 3,3,0 norm 1,0,0 range group dummy_3
gen zone reflect origin 3,3,0 norm 0,1,0 range group dummy_3
;
attach face
group zone soil_body
;
; %%%%%%%SOIL BODY PROPERTIES%%%%%%%
```

```
model mech finn range group soil_body
prop dens 1619.5 &
bulk 21.97e7 &
shear 4.71e7 &
fric 31.98 &
tens 0. &
dil 0. &
coh 0. &
ff_latency 1000000 &
range group soil_body
model fluid fl_iso range group soil_body
prop porosity 0.38 range group soil_body
ini fmod = 0. fden 1000. range group soil_body ; CHECK fmod later reset to 2e9 IN DYNAMIC ANALYSIS!!!!
;
; %%%%%%%BOUNDARY CONDITIONS%%%%%%%
ini xdisp 0 ydisp 0 zdisp 0
ini xvel=0 yvel=0 zvel=0
fix x y z range z -15.1 -14.9
fix x y range y -12.1 -11.9
fix x y range y 17.9 18.1
fix x y range x -12.1 -11.9
fix x y range x 17.9 18.1
;
; %%%%%%%INITIAL CONDITIONS%%%%%%%
ini pp 0 grad 0 0 -9.81e3
;ini syy 0 grad 0 0 5.25e2
;ini sxx 0 grad 0 0 5.25e2
set grav 0 0 -9.81
;
hist add unbal
plot hist 1
save Geo_Free_Field_S_S_S_S_3B_M_v1
solve elastic
ini state 0
prop ff_lat 50 range group soil_body
save post_Geo_Free_Field_S_S_S_S_3B_M_v1
;
new
title "Free_Field_SL_EP2_30W_15D_SSSS3BM_Dyn_v1"
restore post_Geo_Free_Field_S_S_S_S_3B_M_v1
hist reset
set dyn on
conf zextra 45
;
; %%%%%%%DYNAMIC FLUID PROPERTIES%%%%%%%
ini fmod = 2e9 fden 1000 ftens 0. range group soil_body
;
; %%%%%%% DYNAMIC INITIAL CONDITIONS%%%%%%%
ini xvel 0.0 yvel 0.0 zvel 0.0
ini xdisp 0.0 ydisp 0.0 zdisp 0.0
ini sxz 0.0 sxy 0.0 syz 0.0
;
; %%%%%%% DYNAMIC BOUNDARY CONDITIONS%%%%%%%
free x y z
apply ff
apply dquiet nquiet squiet range z -15.1 -14.9
;
; %%%%%%%DYNAMIC MOTION%%%%%%%
def listGp
    global gpBaseHead = null
    local p_gp = gp_head
    loop while p_gp # null
        if gp_zpos(p_gp)<-14.9 ;0.1 ;CHANGED
        local newPnt = get_mem(2)
```

```
            mem(newPnt) = gpBaseHead
            mem(newPnt+1) = p_gp
            gpBaseHead = newPnt
        end_if
        p_gp = gp_next(p_gp)
        endloop
end
@listGp
;
define sine_wave
        whilestepping
        global vv = 0.5*(1.0-cos(2*pi*dytime/1.5))*ampl*sin(2.0*pi*dytime*freq)
        local tmpPnt = gpBaseHead
        loop while tmpPnt # null
            p_gp = mem(tmpPnt+1)
            gp_xacc(p_gp) = vv
            tmpPnt = mem(tmpPnt)
        endloop
end
;
; %%%%%%%BYRNE FORMULA%%%%%%%
define _setCoeff_Byrne(n1_60)
        global ff_c1_ = 8.7*exp(-1.25*ln(n1_60))
        global ff_c2_ = 0.4 / ff_c1_
        global ff_c3_ = 0.00
        command
            prop ff_c1 = @ff_c1_
            prop ff_c2 = @ff_c2_
            prop ff_c3 = @ff_c3_
        end_command
end
;
; %%%%%ZONE LOCATIONS%%%%%
def func_a
        global p_z_a=z_near(3,3,-2)
        global p_z_b=z_near(1.5,3,-2)
        global p_z_c=z_near(4.5,3,-2)
        global p_z_d=z_near(3,3,-4)
        global p_z_e=z_near(1.5,3,-4)
        global p_z_f=z_near(4.5,3,-4)
        global p_z_g=z_near(3,3,-6)
        global p_z_h=z_near(1.5,3,-6)
        global p_z_i=z_near(4.5,3,-6)
        global p_z_j=z_near(3,3,-8)
        global p_z_k=z_near(1.5,3,-8)
        global p_z_l=z_near(4.5,3,-8)
        global p_z_m=z_near(3,3,-10)
        global p_z_n=z_near(1.5,3,-10)
        global p_z_o=z_near(4.5,3,-10)
        global p_z_p=z_near(3,3,-12)
        global p_z_r=z_near(1.5,3,-12)
        global p_z_s=z_near(4.5,3,-12)
        global p_z_t=z_near(3,3,-14)
        global p_z_u=z_near(1.5,3,-14)
        global p_z_v=z_near(4.5,3,-14)
        global p_z_a1=z_near(-6.75,3,-2)
        global p_z_b1=z_near(-1.5,3,-2)
        global p_z_c1=z_near(7.5,3,-2)
        global p_z_d1=z_near(-6.75,3,-4)
        global p_z_e1=z_near(-1.5,3,-4)
        global p_z_f1=z_near(7.5,3,-4)
        global p_z_g1=z_near(-6.75,3,-6)
        global p_z_h1=z_near(-1.5,3,-6)
        global p_z_i1=z_near(7.5,3,-6)
```

```
global p_z_j1=z_near(-6.75,3,-8)
global p_z_k1=z_near(-1.5,3,-8)
global p_z_l1=z_near(7.5,3,-8)
global p_z_m1=z_near(-6.75,3,-10)
global p_z_n1=z_near(-1.5,3,-10)
global p_z_o1=z_near(7.5,3,-10)
global p_z_p1=z_near(-6.75,3,-12)
global p_z_r1=z_near(-1.5,3,-12)
global p_z_s1=z_near(7.5,3,-12)
global p_z_t1=z_near(-6.75,3,-14)
global p_z_u1=z_near(-1.5,3,-14)
global p_z_v1=z_near(7.5,3,-14)
global p_z_a2=z_near(3,1.5,-2)
global p_z_b2=z_near(3,4.5,-2)
global p_z_c2=z_near(3,-1.5,-2)
global p_z_d2=z_near(3,1.5,-4)
global p_z_e2=z_near(3,4.5,-4)
global p_z_f2=z_near(3,-1.5,-4)
global p_z_g2=z_near(3,1.5,-6)
global p_z_h2=z_near(3,4.5,-6)
global p_z_i2=z_near(3,-1.5,-6)
global p_z_j2=z_near(3,1.5,-8)
global p_z_k2=z_near(3,4.5,-8)
global p_z_l2=z_near(3,-1.5,-8)
global p_z_m2=z_near(3,1.5,-10)
global p_z_n2=z_near(3,4.5,-10)
global p_z_o2=z_near(3,-1.5,-10)
global p_z_p2=z_near(3,1.5,-12)
global p_z_r2=z_near(3,4.5,-12)
global p_z_s2=z_near(3,-1.5,-12)
global p_z_t2=z_near(3,1.5,-14)
global p_z_u2=z_near(3,4.5,-14)
global p_z_v2=z_near(3,-1.5,-14)
global p_z_a3=z_near(3,-6.75,-2)
global p_z_b3=z_near(3,7.5,-2)
global p_z_c3=z_near(3,12.75,-2)
global p_z_d3=z_near(3,-6.75,-4)
global p_z_e3=z_near(3,7.5,-4)
global p_z_f3=z_near(3,12.75,-4)
global p_z_g3=z_near(3,-6.75,-6)
global p_z_h3=z_near(3,7.5,-6)
global p_z_i3=z_near(3,12.75,-6)
global p_z_j3=z_near(3,-6.75,-8)
global p_z_k3=z_near(3,7.5,-8)
global p_z_l3=z_near(3,12.75,-8)
global p_z_m3=z_near(3,-6.75,-10)
global p_z_n3=z_near(3,7.5,-10)
global p_z_o3=z_near(3,12.75,-10)
global p_z_p3=z_near(3,-6.75,-12)
global p_z_r3=z_near(3,7.5,-12)
global p_z_s3=z_near(3,12.75,-12)
global p_z_t3=z_near(3,-6.75,-14)
global p_z_u3=z_near(3,7.5,-14)
global p_z_v3=z_near(3,12.75,-14)
global p_z_a4=z_near(1.5,4.5,-2)
global p_z_b4=z_near(4.5,1.5,-2)
global p_z_c4=z_near(12.75,3,-2)
global p_z_d4=z_near(1.5,4.5,-4)
global p_z_e4=z_near(4.5,1.5,-4)
global p_z_f4=z_near(12.75,3,-4)
global p_z_g4=z_near(1.5,4.5,-6)
global p_z_h4=z_near(4.5,1.5,-6)
global p_z_i4=z_near(12.75,3,-6)
global p_z_j4=z_near(1.5,4.5,-8)
```

```
      global p_z_k4=z_near(4.5,1.5,-8)
      global p_z_l4=z_near(12.75,3,-8)
      global p_z_m4=z_near(1.5,4.5,-10)
      global p_z_n4=z_near(4.5,1.5,-10)
      global p_z_o4=z_near(12.75,3,-10)
      global p_z_p4=z_near(1.5,4.5,-12)
      global p_z_r4=z_near(4.5,1.5,-12)
      global p_z_s4=z_near(12.75,3,-12)
      global p_z_t4=z_near(1.5,4.5,-14)
      global p_z_u4=z_near(4.5,1.5,-14)
      global p_z_v4=z_near(12.75,3,-14)
end
@func_a
;
; %%%%%%%MODULUS DEGRADATION%%%%%%%
def mod_deg
      whilestepping
            m_d_a=z_hyst(p_z_a,'modfac')
            m_d_b=z_hyst(p_z_b,'modfac')
            …….
            …….
            …….
            m_d_u4=z_hyst(p_z_u4,'modfac')
            m_d_v4=z_hyst(p_z_v4,'modfac')
end
;
; %%%%%%%SHEAR STRAIN CHECK%%%%%%%
def shear_xz_check
      whilestepping
            array arr1(6) arr2(6) arr3(6) arr4(6) arr5(6) arr6(6) arr7(6) arr8(6) arr9(6) arr10(6) arr11(6) arr12(6)
            array arr13(6) arr14(6) arr15(6) arr16(6) arr17(6) arr18(6) arr19(6) arr20(6) arr21(6)
            dum1=z_fsi(p_z_a,arr1)
            z_extra(p_z_a,1)=arr1(6)
            s_s_a=2.0*arr1(6)
            dum2=z_fsi(p_z_b,arr2)
            z_extra(p_z_b,2)=arr2(6)
            s_s_b=2.0*arr2(6)
            …..
            …..
            …..
            dum20=z_fsi(p_z_u,arr20)
            z_extra(p_z_u,20)=arr20(6)
            s_s_u=2.0*arr20(6)
            dum21=z_fsi(p_z_v,arr21)
            z_extra(p_z_v,21)=arr21(6)
            s_s_v=2.0*arr21(6)
end


; %%%%%%%GRIDPOINT LOCATIONS%%%%%%%
def loc_of_gp_a
      global p_gp_a=gp_near(3,3,-2)
      global p_gp_b=gp_near(1.5,3,-2)
      global p_gp_c=gp_near(4.5,3,-2)
      global p_gp_d=gp_near(3,3,-4)
      global p_gp_e=gp_near(1.5,3,-4)
      global p_gp_f=gp_near(4.5,3,-4)
      global p_gp_g=gp_near(3,3,-6)
      global p_gp_h=gp_near(1.5,3,-6)
      global p_gp_i=gp_near(4.5,3,-6)
      global p_gp_j=gp_near(3,3,-8)
      global p_gp_k=gp_near(1.5,3,-8)
      global p_gp_l=gp_near(4.5,3,-8)
      global p_gp_m=gp_near(3,3,-10)
```

```
global p_gp_n=gp_near(1.5,3,-10)
global p_gp_o=gp_near(4.5,3,-10)
global p_gp_p=gp_near(3,3,-12)
global p_gp_r=gp_near(1.5,3,-12)
global p_gp_s=gp_near(4.5,3,-12)
global p_gp_t=gp_near(3,3,-14)
global p_gp_u=gp_near(1.5,3,-14)
global p_gp_v=gp_near(4.5,3,-14)
global p_gp_y=gp_near(3,3,-14.5)
global p_gp_w=gp_near(1.5,3,-14.5)
global p_gp_z=gp_near(4.5,3,-14.5)
global p_gp_a1=gp_near(-6.75,3,-2)
global p_gp_b1=gp_near(-1.5,3,-2)
global p_gp_c1=gp_near(7.5,3,-2)
global p_gp_d1=gp_near(-6.75,3,-4)
global p_gp_e1=gp_near(-1.5,3,-4)
global p_gp_f1=gp_near(7.5,3,-4)
global p_gp_g1=gp_near(-6.75,3,-6)
global p_gp_h1=gp_near(-1.5,3,-6)
global p_gp_i1=gp_near(7.5,3,-6)
global p_gp_j1=gp_near(-6.75,3,-8)
global p_gp_k1=gp_near(-1.5,3,-8)
global p_gp_l1=gp_near(7.5,3,-8)
global p_gp_m1=gp_near(-6.75,3,-10)
global p_gp_n1=gp_near(-1.5,3,-10)
global p_gp_o1=gp_near(7.5,3,-10)
global p_gp_p1=gp_near(-6.75,3,-12)
global p_gp_r1=gp_near(-1.5,3,-12)
global p_gp_s1=gp_near(7.5,3,-12)
global p_gp_t1=gp_near(-6.75,3,-14)
global p_gp_u1=gp_near(-1.5,3,-14)
global p_gp_v1=gp_near(7.5,3,-14)
global p_gp_y1=gp_near(-6.75,3,-14.5)
global p_gp_w1=gp_near(-1.5,3,-14.5)
global p_gp_z1=gp_near(7.5,3,-14.5)
global p_gp_a2=gp_near(3,1.5,-2)
global p_gp_b2=gp_near(3,4.5,-2)
global p_gp_c2=gp_near(3,-1.5,-2)
global p_gp_d2=gp_near(3,1.5,-4)
global p_gp_e2=gp_near(3,4.5,-4)
global p_gp_f2=gp_near(3,-1.5,-4)
global p_gp_g2=gp_near(3,1.5,-6)
global p_gp_h2=gp_near(3,4.5,-6)
global p_gp_i2=gp_near(3,-1.5,-6)
global p_gp_j2=gp_near(3,1.5,-8)
global p_gp_k2=gp_near(3,4.5,-8)
global p_gp_l2=gp_near(3,-1.5,-8)
global p_gp_m2=gp_near(3,1.5,-10)
global p_gp_n2=gp_near(3,4.5,-10)
global p_gp_o2=gp_near(3,-1.5,-10)
global p_gp_p2=gp_near(3,1.5,-12)
global p_gp_r2=gp_near(3,4.5,-12)
global p_gp_s2=gp_near(3,-1.5,-12)
global p_gp_t2=gp_near(3,1.5,-14)
global p_gp_u2=gp_near(3,4.5,-14)
global p_gp_v2=gp_near(3,-1.5,-14)
global p_gp_y2=gp_near(3,1.5,-14.5)
global p_gp_w2=gp_near(3,4.5,-14.5)
global p_gp_z2=gp_near(3,-1.5,-14.5)
global p_gp_a3=gp_near(3,-6.75,-2)
global p_gp_b3=gp_near(3,7.5,-2)
global p_gp_c3=gp_near(3,12.75,-2)
global p_gp_d3=gp_near(3,-6.75,-4)
global p_gp_e3=gp_near(3,7.5,-4)
```

```
global p_gp_f3=gp_near(3,12.75,-4)
global p_gp_g3=gp_near(3,-6.75,-6)
global p_gp_h3=gp_near(3,7.5,-6)
global p_gp_i3=gp_near(3,12.75,-6)
global p_gp_j3=gp_near(3,-6.75,-8)
global p_gp_k3=gp_near(3,7.5,-8)
global p_gp_l3=gp_near(3,12.75,-8)
global p_gp_m3=gp_near(3,-6.75,-10)
global p_gp_n3=gp_near(3,7.5,-10)
global p_gp_o3=gp_near(3,12.75,-10)
global p_gp_p3=gp_near(3,-6.75,-12)
global p_gp_r3=gp_near(3,7.5,-12)
global p_gp_s3=gp_near(3,12.75,-12)
global p_gp_t3=gp_near(3,-6.75,-14)
global p_gp_u3=gp_near(3,7.5,-14)
global p_gp_v3=gp_near(3,12.75,-14)
global p_gp_y3=gp_near(3,-6.75,-14.5)
global p_gp_w3=gp_near(3,7.5,-14.5)
global p_gp_z3=gp_near(3,12.75,-14.5)
global p_gp_a4=gp_near(1.5,4.5,-2)
global p_gp_b4=gp_near(4.5,1.5,-2)
global p_gp_c4=gp_near(12.75,3,-2)
global p_gp_d4=gp_near(1.5,4.5,-4)
global p_gp_e4=gp_near(4.5,1.5,-4)
global p_gp_f4=gp_near(12.75,3,-4)
global p_gp_g4=gp_near(1.5,4.5,-6)
global p_gp_h4=gp_near(4.5,1.5,-6)
global p_gp_i4=gp_near(12.75,3,-6)
global p_gp_j4=gp_near(1.5,4.5,-8)
global p_gp_k4=gp_near(4.5,1.5,-8)
global p_gp_l4=gp_near(12.75,3,-8)
global p_gp_m4=gp_near(1.5,4.5,-10)
global p_gp_n4=gp_near(4.5,1.5,-10)
global p_gp_o4=gp_near(12.75,3,-10)
global p_gp_p4=gp_near(1.5,4.5,-12)
global p_gp_r4=gp_near(4.5,1.5,-12)
global p_gp_s4=gp_near(12.75,3,-12)
global p_gp_t4=gp_near(1.5,4.5,-14)
global p_gp_u4=gp_near(4.5,1.5,-14)
global p_gp_v4=gp_near(12.75,3,-14)
global p_gp_y4=gp_near(1.5,4.5,-14.5)
global p_gp_w4=gp_near(4.5,1.5,-14.5)
global p_gp_z4=gp_near(12.75,3,-14.5)
global p_gp_a5=gp_near(0,7.5,-2)
global p_gp_b5=gp_near(1.5,6,-2)
global p_gp_c5=gp_near(4.5,6,-2)
global p_gp_d5=gp_near(0,7.5,-4)
global p_gp_e5=gp_near(1.5,6,-4)
global p_gp_f5=gp_near(4.5,6,-4)
global p_gp_g5=gp_near(0,7.5,-6)
global p_gp_h5=gp_near(1.5,6,-6)
global p_gp_i5=gp_near(4.5,6,-6)
global p_gp_j5=gp_near(0,7.5,-8)
global p_gp_k5=gp_near(1.5,6,-8)
global p_gp_l5=gp_near(4.5,6,-8)
global p_gp_m5=gp_near(0,7.5,-10)
global p_gp_n5=gp_near(1.5,6,-10)
global p_gp_o5=gp_near(4.5,6,-10)
global p_gp_p5=gp_near(0,7.5,-12)
global p_gp_r5=gp_near(1.5,6,-12)
global p_gp_s5=gp_near(4.5,6,-12)
global p_gp_t5=gp_near(0,7.5,-14)
global p_gp_u5=gp_near(1.5,6,-14)
global p_gp_v5=gp_near(4.5,6,-14)
```

```
global p_gp_a6=gp_near(-1,4.5,-2)
global p_gp_b6=gp_near(0,4.5,-2)
global p_gp_c6=gp_near(6,4.5,-2)
global p_gp_d6=gp_near(-1,4.5,-4)
global p_gp_e6=gp_near(0,4.5,-4)
global p_gp_f6=gp_near(6,4.5,-4)
global p_gp_g6=gp_near(-1,4.5,-6)
global p_gp_h6=gp_near(0,4.5,-6)
global p_gp_i6=gp_near(6,4.5,-6)
global p_gp_j6=gp_near(-1,4.5,-8)
global p_gp_k6=gp_near(0,4.5,-8)
global p_gp_l6=gp_near(6,4.5,-8)
global p_gp_m6=gp_near(-1,4.5,-10)
global p_gp_n6=gp_near(0,4.5,-10)
global p_gp_o6=gp_near(6,4.5,-10)
global p_gp_p6=gp_near(-1,4.5,-12)
global p_gp_r6=gp_near(0,4.5,-12)
global p_gp_s6=gp_near(6,4.5,-12)
global p_gp_t6=gp_near(-1,4.5,-14)
global p_gp_u6=gp_near(0,4.5,-14)
global p_gp_v6=gp_near(6,4.5,-14)
global p_gp_a7=gp_near(1,3,-2)
global p_gp_b7=gp_near(2,3,-2)
global p_gp_c7=gp_near(2.25,3,-2)
global p_gp_d7=gp_near(1,3,-4)
global p_gp_e7=gp_near(2,3,-4)
global p_gp_f7=gp_near(2.25,3,-4)
global p_gp_g7=gp_near(1,3,-6)
global p_gp_h7=gp_near(2,3,-6)
global p_gp_i7=gp_near(2.25,3,-6)
global p_gp_j7=gp_near(1,3,-8)
global p_gp_k7=gp_near(2,3,-8)
global p_gp_l7=gp_near(2.25,3,-8)
global p_gp_m7=gp_near(1,3,-10)
global p_gp_n7=gp_near(2,3,-10)
global p_gp_o7=gp_near(2.25,3,-10)
global p_gp_p7=gp_near(1,3,-12)
global p_gp_r7=gp_near(2,3,-12)
global p_gp_s7=gp_near(2.25,3,-12)
global p_gp_t7=gp_near(1,3,-14)
global p_gp_u7=gp_near(2,3,-14)
global p_gp_v7=gp_near(2.25,3,-14)
global p_gp_a8=gp_near(2.5,3,-2)
global p_gp_b8=gp_near(1.5,1.5,-2)
global p_gp_c8=gp_near(-1.5,0,-2)
global p_gp_d8=gp_near(2.5,3,-4)
global p_gp_e8=gp_near(1.5,1.5,-4)
global p_gp_f8=gp_near(-1.5,0,-4)
global p_gp_g8=gp_near(2.5,3,-6)
global p_gp_h8=gp_near(1.5,1.5,-6)
global p_gp_i8=gp_near(-1.5,0,-6)
global p_gp_j8=gp_near(2.5,3,-8)
global p_gp_k8=gp_near(1.5,1.5,-8)
global p_gp_l8=gp_near(-1.5,0,-8)
global p_gp_m8=gp_near(2.5,3,-10)
global p_gp_n8=gp_near(1.5,1.5,-10)
global p_gp_o8=gp_near(-1.5,0,-10)
global p_gp_p8=gp_near(2.5,3,-12)
global p_gp_r8=gp_near(1.5,1.5,-12)
global p_gp_s8=gp_near(-1.5,0,-12)
global p_gp_t8=gp_near(2.5,3,-14)
global p_gp_u8=gp_near(1.5,1.5,-14)
global p_gp_v8=gp_near(-1.5,0,-14)
global p_gp_a9=gp_near(-5.5,11.5,-2)
```

```
global p_gp_b9=gp_near(-4.5,10.5,-2)
global p_gp_c9=gp_near(-3.5,9.5,-2)
global p_gp_d9=gp_near(-5.5,11.5,-4)
global p_gp_e9=gp_near(-4.5,10.5,-4)
global p_gp_f9=gp_near(-3.5,9.5,-4)
global p_gp_g9=gp_near(-5.5,11.5,-6)
global p_gp_h9=gp_near(-4.5,10.5,-6)
global p_gp_i9=gp_near(-3.5,9.5,-6)
global p_gp_j9=gp_near(-5.5,11.5,-8)
global p_gp_k9=gp_near(-4.5,10.5,-8)
global p_gp_l9=gp_near(-3.5,9.5,-8)
global p_gp_m9=gp_near(-5.5,11.5,-10)
global p_gp_n9=gp_near(-4.5,10.5,-10)
global p_gp_o9=gp_near(-3.5,9.5,-10)
global p_gp_p9=gp_near(-5.5,11.5,-12)
global p_gp_r9=gp_near(-4.5,10.5,-12)
global p_gp_s9=gp_near(-3.5,9.5,-12)
global p_gp_t9=gp_near(-5.5,11.5,-14)
global p_gp_u9=gp_near(-4.5,10.5,-14)
global p_gp_v9=gp_near(-3.5,9.5,-14)
global p_gp_a10=gp_near(-2.5,8.5,-2)
global p_gp_b10=gp_near(-1.5,7.5,-2)
global p_gp_c10=gp_near(-2.5,3,-2)
global p_gp_d10=gp_near(-2.5,8.5,-4)
global p_gp_e10=gp_near(-1.5,7.5,-4)
global p_gp_f10=gp_near(-2.5,3,-4)
global p_gp_g10=gp_near(-2.5,8.5,-6)
global p_gp_h10=gp_near(-1.5,7.5,-6)
global p_gp_i10=gp_near(-2.5,3,-6)
global p_gp_j10=gp_near(-2.5,8.5,-8)
global p_gp_k10=gp_near(-1.5,7.5,-8)
global p_gp_l10=gp_near(-2.5,3,-8)
global p_gp_m10=gp_near(-2.5,8.5,-10)
global p_gp_n10=gp_near(-1.5,7.5,-10)
global p_gp_o10=gp_near(-2.5,3,-10)
global p_gp_p10=gp_near(-2.5,8.5,-12)
global p_gp_r10=gp_near(-1.5,7.5,-12)
global p_gp_s10=gp_near(-2.5,3,-12)
global p_gp_t10=gp_near(-2.5,8.5,-14)
global p_gp_u10=gp_near(-1.5,7.5,-14)
global p_gp_v10=gp_near(-2.5,3,-14)
global p_gp_a11=gp_near(-3.5,3,-2)
global p_gp_b11=gp_near(-4.5,3,-2)
global p_gp_c11=gp_near(-7.5,3,-2)
global p_gp_d11=gp_near(-3.5,3,-4)
global p_gp_e11=gp_near(-4.5,3,-4)
global p_gp_f11=gp_near(-7.5,3,-4)
global p_gp_g11=gp_near(-3.5,3,-6)
global p_gp_h11=gp_near(-4.5,3,-6)
global p_gp_i11=gp_near(-7.5,3,-6)
global p_gp_j11=gp_near(-3.5,3,-8)
global p_gp_k11=gp_near(-4.5,3,-8)
global p_gp_l11=gp_near(-7.5,3,-8)
global p_gp_m11=gp_near(-3.5,3,-10)
global p_gp_n11=gp_near(-4.5,3,-10)
global p_gp_o11=gp_near(-7.5,3,-10)
global p_gp_p11=gp_near(-3.5,3,-12)
global p_gp_r11=gp_near(-4.5,3,-12)
global p_gp_s11=gp_near(-7.5,3,-12)
global p_gp_t11=gp_near(-3.5,3,-14)
global p_gp_u11=gp_near(-4.5,3,-14)
global p_gp_v11=gp_near(-7.5,3,-14)
global p_gp_a12=gp_near(1.5,0,-2)
global p_gp_b12=gp_near(4.5,0,-2)
```

```
    global p_gp_c12=gp_near(0,1.5,-2)
    global p_gp_d12=gp_near(1.5,0,-4)
    global p_gp_e12=gp_near(4.5,0,-4)
    global p_gp_f12=gp_near(0,1.5,-4)
    global p_gp_g12=gp_near(1.5,0,-6)
    global p_gp_h12=gp_near(4.5,0,-6)
    global p_gp_i12=gp_near(0,1.5,-6)
    global p_gp_j12=gp_near(1.5,0,-8)
    global p_gp_k12=gp_near(4.5,0,-8)
    global p_gp_l12=gp_near(0,1.5,-8)
    global p_gp_m12=gp_near(1.5,0,-10)
    global p_gp_n12=gp_near(4.5,0,-10)
    global p_gp_o12=gp_near(0,1.5,-10)
    global p_gp_p12=gp_near(1.5,0,-12)
    global p_gp_r12=gp_near(4.5,0,-12)
    global p_gp_s12=gp_near(0,1.5,-12)
    global p_gp_t12=gp_near(1.5,0,-14)
    global p_gp_u12=gp_near(4.5,0,-14)
    global p_gp_v12=gp_near(0,1.5,-14)
    global p_gp_a13=gp_near(6,1.5,-2)
    global p_gp_b13=gp_near(4.5,4.5,-2)
    global p_gp_c13=gp_near(-6.5,12.5,-2)
    global p_gp_d13=gp_near(6,1.5,-4)
    global p_gp_e13=gp_near(4.5,4.5,-4)
    global p_gp_f13=gp_near(-6.5,12.5,-4)
    global p_gp_g13=gp_near(6,1.5,-6)
    global p_gp_h13=gp_near(4.5,4.5,-6)
    global p_gp_i13=gp_near(-6.5,12.5,-6)
    global p_gp_j13=gp_near(6,1.5,-8)
    global p_gp_k13=gp_near(4.5,4.5,-8)
    global p_gp_l13=gp_near(-6.5,12.5,-8)
    global p_gp_m13=gp_near(6,1.5,-10)
    global p_gp_n13=gp_near(4.5,4.5,-10)
    global p_gp_o13=gp_near(-6.5,12.5,-10)
    global p_gp_p13=gp_near(6,1.5,-12)
    global p_gp_r13=gp_near(4.5,4.5,-12)
    global p_gp_s13=gp_near(-6.5,12.5,-12)
    global p_gp_t13=gp_near(6,1.5,-14)
    global p_gp_u13=gp_near(4.5,4.5,-14)
    global p_gp_v13=gp_near(-6.5,12.5,-14)
end
@loc_of_gp_a
;
; %%%%%%%PORE PRESSURE RATIO%%%%%%%
def p_r_a
    whilestepping
        p_r_a=(gp_pp(p_gp_a)-19620)/((19410.2))
        p_r_b=(gp_pp(p_gp_b)-19620)/((19410.2))
        …..
        …..
        …..
        p_r_u13=(gp_pp(p_gp_u13)-137340)/((137071.3))
        p_r_v13=(gp_pp(p_gp_v13)-137340)/((137071.3))
end
;
; %%%%%%%DYNAMIC RUNTIME SETTINGS%%%%%%%
set fluid off
ini damp hyst default -3.325 0.823
ini damp rayl 0.002 10.0 stiff
his nstep 40
;
; %%%%%%%RECORDS OF HISTORY%%%%%%%
hist add unbal
his add dytime
```

```
his add fish @vv
;
his add fish @m_d_a
his add fish @m_d_b
…..
…..
…..
his add fish @m_d_u4
his add fish @m_d_v4
;
his add fish @s_s_a
his add fish @s_s_b
…..
…..
…..
his add fish @s_s_u
his add fish @s_s_v
;
his add fish @p_r_a
his add fish @p_r_b
…..
…..
…..
his add fish @p_r_u13
his add fish @p_r_v13
;
; %%%%%%%DYNAMIC MOTION IMPUT%%%%%%%
set @ampl=0.07 @freq=10.0;
;
; %%%%%%%DYNAMIC MOTION IMPUT%%%%%%%
prop ff_switch = 1
@_setCoeff_Byrne(5.66)
;
; %%%%%%%DYNAMIC RUN%%%%%%%
save Dyn_Free_Field_S_S_S_S_3B_M_v1
solve age 1.5
save post_Dyn_Free_Field_S_S_S_S_3B_M_v1
```

APPENDIX C:

FLAC3D Code for 3B Spacing for Improved Site Analyses

```
new
title "Free_Field_SL_EP2_30W_15D_SSSS3BMJ_v1"
config fluid dyn
set fluid off dyn off
;
; %%%%%%%SOIL BODY GEOMETRY%%%%%%%
gen zone radcyl p0(0,0,0) p1(1,0,0) p2(0,0,-12) p3(0,1,0)...
p4(1,0,-12) p5(0,1,-12) p6(1,1,0) p7(1,1,-12) p8(0.5,0,0)...
p9(0,0.5,0) p10(0.5,0,-12) p11(0,0.5,-12)...
size 1 24 4 2 ratio 1 1 1 1
;
gen zone radcyl p0(0,0,-12) p1(1,0,-12) p2(0,0,-15) p3(0,1,-12)...
p4(1,0,-15) p5(0,1,-15) p6(1,1,-12) p7(1,1,-15) p8(0.5,0,-12)...
p9(0,0.5,-12) p10(0.5,0,-15) p11(0,0.5,-15)...
size 1 6 4 2 ratio 1 1 1 1 fill
;
gen zone reflect norm 1,0,0
gen zone reflect norm 0,1,0
;
gen zone copy 3 0 0 range x -1.5 1.5 y -1.5 1.5 z 0.0 -15.0
gen zone copy 6 0 0 range x -1.5 1.5 y -1.5 1.5 z 0.0 -15.0
gen zone copy 0 3 0 range x -1.5 7.5 y -1.5 1.5 z 0.0 -15.0
gen zone copy 0 6 0 range x -1.5 7.5 y -1.5 1.5 z 0.0 -15.0
;
gen zone brick p0(1,-1,0) p1(2,-1,0) p2(1,-1,-15) p3(1,1,0)...
p4(2,-1,-15) p5(1,1,-15) p6(2,1,0) p7(2,1,-15)...
size 2 30 4 ratio 1 1 1
;
gen zone copy 0 3 0 range x 1.0 2.0 y -1.0 1.0 z 0.0 -15.0
gen zone copy 0 6 0 range x 1.0 2.0 y -1.0 1.0 z 0.0 -15.0
gen zone copy 3 0 0 range x 1.0 2.0 y -1.0 7.0 z 0.0 -15.0
;
gen zone brick p0(-1,2,0) p1(-1,1,0) p2(-1,2,-15) p3(7,2,0)...
p4(-1,1,-15) p5(7,2,-15) p6(7,1,0) p7(7,1,-15)...
size 2 30 16 ratio 1 1 1
;
gen zone copy 0 3 0 range x -1.0 7.0 y 1.0 2.0 z 0.0 -15.0
;
gen zone brick p0(-1.0,-1.0,0) p1(-1.0,-12.0,0) p2(-1.0,-1.0,-15) p3(7.0,-1.0,0)...
p4(-1.0,-12,-15) p5(7.0,-1.0,-15) p6(7.0,-12,0) p7(7.0,-12,-15)...
size 22 30 16 ratio 1.0 1.0 1.0
;
group zone dummy range y -1.0 -12.0
gen zone reflect origin 0,3,0 norm 0,1,0 range group dummy
;
gen zone brick p0(-1.0,-1.0,0) p1(-1.0,7.0,0) p2(-1.0,-1.0,-15) p3(-12.0,-1.0,0)...
p4(-1.0,7.0,-15) p5(-12,-1.0,-15) p6(-12,7.0,0) p7(-12.0,7.0,-15)...
size 16 30 22 ratio 1.0 1.0 1.0
group zone dummy_2 range x -1.0 -12.0
gen zone reflect origin 3,3,0 norm 1,0,0 range group dummy_2
;
gen zone brick p0(7.0,-1.0,0) p1(7.0,-12,0) p2(7.0,-1.0,-15) p3(18,-1.0,0)...
p4(7.0,-12,-15) p5(18,-1.0,-15) p6(18,-12,0) p7(18,-12,-15)...
size 22 30 22 ratio 1.0 1.0 1.0
;
group zone dummy_3 range x 7.0 18.0 y -1.0 -12.0 z 0.0 -15.0
;
gen zone reflect origin 3,3,0 norm 1,0,0 range group dummy_3
gen zone reflect origin 3,3,0 norm 0,1,0 range group dummy_3
;
attach face
group zone soil_body
; %%%%%%%SOIL BODY PROPERTIES%%%%%%%
model mech finn range group soil_body
```

```
prop    dens        1619.5  &
        bulk        21.97e7 &
        shear       4.71e7  &
        fric        31.98   &
        tens        0.      &
        dil         0.      &
        coh         0.      &
        ff_latency  1000000 &
        range group soil_body
;
model fluid fl_iso range group soil_body
prop porosity 0.38 range group soil_body
ini fmod = 0. fden 1000. range group soil_body   ; CHECK fmod later reset to 2e9 IN DYNAMIC
ANALYSIS!!!!
;
; %%%%%%%INTERFACE DISPOSITION%%%%%%%
interface 1 face range cylinder end1 (0,0,0) end2 (0,0,-12.1) radius .51 &
cylinder end1 (0,0,0) end2 (0,0,-12.1) radius .49 not
interface 2 face range cylinder end1 (0,0,-11.9) end2 (0,0,-12.1) radius .51
interface 3 face range cylinder end1 (3,0,0) end2 (3,0,-12.1) radius .51 &
cylinder end1 (3,0,0) end2 (3,0,-12.1) radius .49 not
interface 4 face range cylinder end1 (3,0,-11.9) end2 (3,0,-12.1) radius .51
…..
…..
…..
interface 15 face range cylinder end1 (3,6,0) end2 (3,6,-12.1) radius .51 &
cylinder end1 (3,6,0) end2 (3,6,-12.1) radius .49 not
interface 16 face range cylinder end1 (3,6,-11.9) end2 (3,6,-12.1) radius .51
interface 17 face range cylinder end1 (6,6,0) end2 (6,6,-12.1) radius .51 &
cylinder end1 (6,6,0) end2 (6,6,-12.1) radius .49 not
interface 18 face range cylinder end1 (6,6,-11.9) end2 (6,6,-12.1) radius .51
;
; %%%%%%%INTERFACE PROPERTIES%%%%%%%
interface 1 prop kn 11.3e9 ks 11.3e9 fric 21.32 coh 0
interface 2 prop kn 11.3e9 ks 11.3e9 fric 21.32 coh 0
…..
…..
…..
interface 17 effective off
interface 18 effective off
;
; %%%%%%%JET GROUT DISPOSITION%%%%%%%
gen zone cylind p0(0,0,13) p1(0.5,0,13) p2(0,0,1) p3(0,0.5,13)...
p4(0.5,0,1)...
size 1 24 4 ratio 1 1 1 fill
gen zone reflect norm 1,0,0 range z 1 13
gen zone reflect norm 0,1,0 range z 1 13
gen zone copy 3 0 0 range x -0.5 0.5 y -0.5 0.5 z 1 13
gen zone copy 6 0 0 range x -0.5 0.5 y -0.5 0.5 z 1 13
gen zone copy 0 3 0 range y -0.5 0.5 z 1 13
gen zone copy 0 6 0 range y -0.5 0.5 z 1 13
group zone jet_grout_columns range z 1 13

; %%%%%%%DUMMY JET GROUT PROPERTIES %%%%%%%
model mech mohr range group jet_grout_columns
prop    dens        1619.5  &
        bulk        21.97e7 &
        shear       4.71e7  &
        fric        31.98   &
        tens        0.      &
        dil         0.      &
        coh         0.      &
        range group jet_grout_columns
;
```

```
ini zposition add -13.0 range group jet_grout_columns
;model fluid fl_iso range group jet_grout_columns
;prop porosity 0.38 range group jet_grout_columns
;ini fmod = 0. fden 1000. range group jet_grout_columns
;
; %%%%%%%BOUNDARY CONDITIONS%%%%%%%
ini xdisp 0 ydisp 0 zdisp 0
ini xvel=0 yvel=0 zvel=0
fix x y z range z -15.1 -14.9
fix x y range y -12.1 -11.9
fix x y range y 17.9 18.1
fix x y range x -12.1 -11.9
fix x y range x 17.9 18.1
;
; %%%%%%%INITIAL CONDITIONS%%%%%%%
ini pp 0 grad 0 0 -9.81e3
set grav 0 0 -9.81
;
;
hist add unbal
plot hist 1
;
save Geo_Free_Field_S_S_S_S_3B_M_J_s7c
solve elastic
save Post_Geo_Free_Field_S_S_S_S_3B_M_J_s7c
;
; %%%%%%%JET GROUT PROPERTIES%%%%%%%
model mech mohr range group jet_grout_columns
prop bulk 1.721e9 shear 1.291e9 fric 48.18 coh 2.87e6 range group jet_grout_columns
;
;
save Geo_Free_Field_S_S_S_S_3B_M_J_s8c
solve ratio 1e-06
;
ini state 0
;
prop ff_lat 50 range group soil_body
;
interface 1 effective on
interface 2 effective on
…..
…..
…..
interface 17 effective on
interface 18 effective on
;
save post_Geo_Free_Field_S_S_S_S_3B_M_J_s8c
return
```

APPENDIX D:

All r_u values for Free Field and Improved Site Analyses

Table D-1 Values of r_u for 3B spacing and dynamic motion of 0.08g peak acceleration

Dynamic Motion of 0.08g Peak Acceleration and 3B Spacing

Group 1	Free Field					High Stiffness Level					Mean Stiffness Level					Low Stiffness Level				
ID / z (m)	1	5	6	7	Ave	1	5	6	7	Ave	1	5	6	7	Ave	1	5	6	7	Ave
2	1.00	0.53	1.35	0.75	0.91	0.40	0.63	0.48	0.65	0.54	0.23	0.55	0.55	1.03	0.59	0.08	0.43	0.15	0.43	0.27
4	1.10	0.68	1.15	0.80	0.93	0.50	0.90	1.18	0.70	0.82	0.55	0.73	0.83	0.68	0.69	0.50	0.78	0.38	0.63	0.57
6	0.85	0.65	1.03	0.93	0.86	0.80	0.53	0.60	0.70	0.66	0.78	0.70	0.80	0.60	0.72	0.40	0.35	0.48	0.50	0.43
8	1.05	0.95	1.08	0.80	0.97	0.85	0.68	0.68	0.70	0.73	0.70	0.70	0.75	0.85	0.75	0.60	0.65	0.53	0.43	0.55
10	1.05	0.93	1.13	0.80	0.98	1.00	0.53	1.08	0.60	0.80	0.98	0.65	0.98	0.73	0.83	0.75	0.35	0.58	0.53	0.55
12	0.98	0.93	0.95	0.90	0.94	1.03	0.68	0.98	0.80	0.87	1.05	0.55	1.05	0.60	0.81	0.98	0.55	1.00	0.60	0.78

Group 2	Free Field					High Stiffness Level					Mean Stiffness Level					Low Stiffness Level				
ID / z(m)	4	8	9	13	Ave	4	8	9	13	Ave	4	8	9	13	Ave	4	8	9	13	Ave
2	1.15	1.35	0.55	0.95	1.00	1.03	0.60	0.63	0.65	0.73	0.85	0.55	0.45	0.45	0.58	0.10	0.80	0.33	0.30	0.38
4	0.88	0.98	0.75	0.98	0.89	0.83	0.58	0.68	0.68	0.69	0.63	0.85	0.88	0.95	0.83	0.38	0.68	0.45	0.68	0.54
6	0.98	1.13	0.75	0.88	0.93	0.75	0.83	0.70	0.70	0.74	0.68	0.75	0.78	0.75	0.74	0.48	0.58	0.50	0.58	0.53
8	1.05	1.05	1.00	1.15	1.06	0.80	0.78	0.70	0.98	0.81	0.95	1.03	1.03	1.15	1.04	0.50	0.83	0.63	0.63	0.64
10	1.00	1.03	0.95	1.00	0.99	0.88	1.15	1.05	0.70	0.94	0.90	0.60	0.88	0.78	0.79	0.53	0.33	0.50	0.48	0.46
12	0.95	1.00	0.80	0.95	0.93	1.03	0.50	1.08	0.93	0.88	1.13	1.15	1.00	1.03	1.08	0.65	0.93	0.80	1.03	0.85

Group 3	Free Field								High Stiffness Level								
ID / z(m)	10	11	12	14	15	16	17	18	Ave	10	11	12	14	15	16	17	18	Ave
2	0.85	0.68	0.63	0.58	1.00	1.15	1.05	0.63	0.82	0.53	0.50	0.60	0.80	0.58	0.70	0.45	0.30	0.56
4	0.88	1.08	0.90	0.95	0.95	1.05	1.15	0.85	0.98	0.63	0.63	0.90	0.63	0.78	0.98	0.65	0.45	0.70
6	0.65	1.00	1.00	0.88	0.98	1.00	1.08	1.05	0.95	0.85	0.65	0.78	0.75	0.80	0.95	0.50	0.65	0.74
8	0.78	0.95	0.90	1.05	1.13	1.03	1.13	0.98	0.99	0.53	0.55	0.70	0.65	0.70	0.80	0.60	0.68	0.65
10	0.90	0.98	0.95	0.95	1.10	1.03	1.03	0.70	0.95	0.50	0.48	0.75	0.70	0.95	0.80	0.88	0.65	0.71
12	0.85	1.03	0.98	1.03	0.93	0.90	1.08	0.90	0.96	0.55	0.63	0.65	0.98	0.90	1.00	1.05	0.60	0.79

Group 3	Mean Stiffness Level								Low Stiffness Level								
ID / z(m)	10	11	12	14	15	16	17	18	Ave	10	11	12	14	15	16	17	18	Ave
2	0.70	0.48	0.60	0.55	0.88	0.68	0.80	0.48	0.64	0.33	0.25	0.28	0.30	0.38	0.28	0.35	0.30	0.31
4	0.73	0.83	0.55	0.60	0.75	0.88	1.03	0.78	0.77	0.75	0.73	0.55	0.55	0.60	0.45	0.45	0.60	0.58
6	0.73	0.90	0.78	0.78	0.55	0.88	0.75	0.75	0.76	0.45	0.40	0.48	0.58	0.45	0.48	0.60	0.50	0.49
8	0.73	0.65	0.70	0.65	0.70	0.68	0.83	0.68	0.70	0.45	0.33	0.55	0.55	0.58	0.50	0.60	0.63	0.52
10	0.70	0.68	0.68	0.80	0.68	0.93	0.73	0.63	0.73	0.78	0.70	0.53	0.55	0.50	0.93	0.45	0.98	0.68
12	0.65	0.60	0.58	1.00	1.05	1.05	1.00	0.93	0.86	0.45	0.63	0.48	1.00	0.90	1.03	0.73	0.55	0.72

Table D-2 Values of r_u for 3B spacing and dynamic motion of 0.07g peak acceleration

Dynamic Motion of 0.07g Peak Acceleration and 3B Spacing

Group 1	Free Field					High Stiffness Level					Mean Stiffness Level					Low Stiffness Level				
ID / z (m)	1	5	6	7	Ave	1	5	6	7	Ave	1	5	6	7	Ave	1	5	6	7	Ave
2	0.93	0.78	0.85	0.55	0.78	0.38	0.50	0.40	0.65	0.48	0.04	0.48	0.25	0.83	0.40	0.15	0.30	0.15	0.60	0.30
4	1.00	0.93	0.93	1.03	0.97	0.58	0.78	1.03	0.70	0.77	0.40	0.55	0.70	0.50	0.54	0.45	0.80	0.45	0.50	0.55
6	0.78	0.73	0.60	0.48	0.64	0.53	0.55	0.60	0.75	0.61	0.68	0.63	0.60	0.55	0.61	0.40	0.38	0.45	0.48	0.43
8	0.93	0.55	0.98	0.78	0.81	0.80	0.60	0.55	0.70	0.66	0.70	0.70	0.70	0.80	0.73	0.58	0.60	0.55	0.48	0.55
10	0.95	0.65	0.95	0.85	0.85	0.75	0.80	0.83	0.60	0.74	0.93	0.45	0.83	0.80	0.75	0.60	0.40	0.55	0.55	0.53
12	0.98	1.00	1.00	0.78	0.94	0.93	0.75	0.75	0.55	0.74	0.85	0.53	0.95	0.68	0.75	0.93	0.58	1.00	0.58	0.77
Group 2	Free Field					High Stiffness Level					Mean Stiffness Level					Low Stiffness Level				
ID / z(m)	4	8	9	13	Ave	4	8	9	13	Ave	4	8	9	13	Ave	4	8	9	13	Ave
2	0.65	0.65	0.63	0.60	0.63	0.78	0.48	0.60	0.90	0.69	0.55	0.15	0.28	0.25	0.31	0.23	0.73	0.20	0.33	0.37
4	0.98	0.90	0.85	0.80	0.88	0.83	0.60	0.65	0.60	0.67	0.50	0.65	0.90	0.73	0.69	0.38	0.83	0.50	0.55	0.56
6	0.68	0.73	0.78	0.63	0.70	0.73	0.55	0.65	0.60	0.63	0.68	0.50	0.70	0.75	0.66	0.45	0.55	0.55	0.83	0.59
8	0.95	1.00	0.95	0.85	0.94	0.73	0.65	0.70	0.63	0.68	0.80	1.04	0.85	1.05	0.93	0.65	0.55	0.75	0.53	0.62
10	0.93	0.88	0.95	0.95	0.93	0.70	0.55	0.63	0.70	0.64	0.75	0.50	0.68	0.65	0.64	0.55	0.45	0.48	0.70	0.54
12	0.95	0.93	0.95	0.98	0.95	1.03	0.65	0.93	0.50	0.78	0.93	0.40	0.60	0.80	0.68	0.98	0.63	1.03	1.03	0.91

Group 3	Free Field									High Stiffness Level								
ID / z(m)	10	11	12	14	15	16	17	18	Ave	10	11	12	14	15	16	17	18	Ave
2	0.45	0.30	0.55	0.77	0.78	0.90	0.18	0.35	0.53	0.50	0.40	0.55	0.70	0.45	0.55	0.48	0.38	0.50
4	0.95	0.78	0.98	0.98	0.98	0.90	0.88	0.85	0.91	0.75	0.63	0.50	0.65	0.65	0.75	0.60	0.43	0.62
6	0.78	0.95	0.80	0.60	0.78	0.68	0.60	0.80	0.75	0.53	0.60	0.65	0.53	0.70	0.48	0.50	0.70	0.58
8	0.68	0.70	0.65	0.93	1.03	1.00	0.93	0.63	0.82	0.58	0.53	0.53	0.70	0.80	0.80	0.55	0.50	0.62
10	0.85	0.95	0.93	0.93	0.95	1.00	1.05	0.93	0.95	0.53	0.68	0.73	0.90	0.73	0.70	0.85	0.63	0.72
12	0.78	0.95	0.70	1.00	1.00	0.73	0.98	0.88	0.88	0.70	0.48	0.78	0.85	0.95	0.95	0.98	0.90	0.82
Group 3	Mean Stiffness Level									Low Stiffness Level								
ID / z(m)	10	11	12	14	15	16	17	18	Ave	10	11	12	14	15	16	17	18	Ave
2	0.53	0.38	0.65	0.43	0.43	0.88	0.75	0.40	0.55	0.75	0.25	0.30	0.35	0.33	0.55	0.40	0.25	0.40
4	0.53	0.50	0.58	0.45	0.65	0.73	1.10	0.53	0.63	0.75	0.88	0.55	0.83	0.63	0.75	0.48	0.63	0.68
6	0.50	0.58	0.85	0.75	0.60	0.68	0.55	0.65	0.64	0.43	0.35	0.43	0.45	0.48	0.45	0.55	0.63	0.47
8	0.55	0.55	0.53	1.00	0.63	0.80	0.78	0.73	0.69	0.60	0.38	0.65	0.63	0.65	0.60	0.50	0.63	0.58
10	0.83	0.73	0.75	0.55	0.68	0.85	0.65	0.58	0.70	0.75	0.90	0.68	0.70	0.58	0.48	0.63	0.73	0.68
12	0.48	0.48	0.50	0.68	0.90	0.68	0.73	0.78	0.65	0.43	0.63	0.43	1.00	1.00	1.00	0.83	0.60	0.74

Table D-3 Values of r_u for 3B spacing and dynamic motion of 0.06g peak acceleration

Dynamic Motion of 0.06g Peak Acceleration and 3B Spacing

Group 1	Free Field					High Stiffness Level					Mean Stiffness Level					Low Stiffness Level				
ID / z (m)	1	5	6	7	Ave	1	5	6	7	Ave	1	5	6	7	Ave	1	5	6	7	Ave
2	0.80	0.70	0.68	0.80	0.74	0.35	0.55	0.33	0.58	0.45	0.10	0.40	0.33	1.10	0.48	0.25	0.43	0.25	0.38	0.33
4	1.00	0.85	1.00	0.90	0.94	0.50	0.75	1.13	0.58	0.74	0.43	0.48	0.55	0.48	0.48	0.55	0.75	0.35	0.70	0.59
6	0.80	0.48	0.85	0.88	0.75	0.70	0.60	0.50	0.68	0.62	0.65	0.50	0.65	0.48	0.57	0.43	0.40	0.43	0.28	0.38
8	0.95	0.70	0.95	0.88	0.87	0.70	0.45	0.60	0.58	0.58	0.60	0.70	0.60	0.83	0.68	0.55	0.70	0.55	0.35	0.54
10	1.00	0.88	1.03	0.88	0.94	0.55	0.55	0.75	0.68	0.63	1.25	0.50	1.00	0.70	0.86	0.70	0.53	0.30	0.48	0.50
12	1.00	0.83	0.93	0.98	0.93	1.13	0.98	0.93	0.85	0.97	0.95	0.45	0.85	0.63	0.72	0.73	0.53	1.05	0.58	0.72

Group 2	Free Field					High Stiffness Level					Mean Stiffness Level					Low Stiffness Level				
ID / z(m)	4	8	9	13	Ave	4	8	9	13	Ave	4	8	9	13	Ave	4	8	9	13	Ave
2	0.70	0.50	0.60	0.68	0.62	0.75	0.45	0.15	0.88	0.56	0.83	0.48	0.05	0.20	0.39	0.40	0.35	0.10	0.45	0.33
4	0.75	0.68	0.83	0.83	0.77	0.68	0.73	0.45	0.88	0.68	0.45	0.90	0.88	0.80	0.76	0.50	0.53	0.58	0.55	0.54
6	0.78	0.85	0.65	0.78	0.76	0.58	0.70	0.65	0.73	0.66	0.65	0.45	0.75	0.60	0.61	0.40	0.43	0.43	0.48	0.43
8	1.00	0.90	0.95	1.10	0.99	0.68	0.68	0.70	0.75	0.70	0.83	0.80	0.83	0.85	0.83	0.85	0.55	0.55	0.58	0.63
10	0.95	0.78	0.75	0.78	0.81	0.80	0.70	0.50	0.68	0.67	1.00	0.68	0.75	0.73	0.79	0.58	0.43	0.53	0.50	0.51
12	0.78	0.83	0.83	0.93	0.84	1.00	0.83	0.95	0.65	0.86	1.10	0.63	1.00	0.98	0.93	0.60	0.70	0.40	0.78	0.62

Group 3	Free Field									High Stiffness Level								
ID / z(m)	10	11	12	14	15	16	17	18	Ave	10	11	12	14	15	16	17	18	Ave
2	0.85	0.43	0.53	0.70	0.33	0.68	0.58	0.78	0.61	0.35	0.43	0.40	0.55	0.50	0.38	0.40	0.38	0.42
4	0.78	0.95	0.95	0.88	0.98	0.88	0.88	0.93	0.90	0.65	0.60	0.48	0.58	0.63	0.80	0.70	0.63	0.63
6	0.73	0.75	0.75	0.75	0.68	0.58	0.68	0.83	0.72	0.73	0.63	0.70	0.75	0.48	0.90	0.75	0.65	0.70
8	0.85	0.70	0.68	0.85	1.03	0.88	0.90	0.73	0.83	0.55	0.58	0.70	0.63	0.88	0.70	0.50	0.60	0.64
10	0.90	0.73	1.00	1.00	0.90	0.95	0.85	0.75	0.88	0.50	0.53	0.58	0.65	0.78	1.05	0.63	0.63	0.67
12	0.95	1.03	0.95	0.68	0.90	0.98	0.90	0.85	0.90	0.80	0.63	0.78	0.85	1.00	1.00	0.98	0.63	0.83

Group 3	Mean Stiffness Level									Low Stiffness Level								
ID / z(m)	10	11	12	14	15	16	17	18	Ave	10	11	12	14	15	16	17	18	Ave
2	0.40	0.40	0.75	0.28	0.80	0.70	0.78	0.40	0.56	0.55	0.40	0.75	0.30	0.43	0.35	0.40	0.33	0.44
4	0.58	0.65	0.55	0.43	0.65	0.85	1.15	0.63	0.68	0.70	0.60	0.80	0.95	0.58	0.55	0.45	0.50	0.64
6	0.45	0.63	0.50	0.70	0.58	0.58	0.63	0.75	0.60	0.40	0.30	0.40	0.55	0.48	0.45	0.48	0.40	0.43
8	0.55	0.50	0.65	0.75	0.58	0.75	0.53	0.70	0.63	0.50	0.45	0.45	0.63	0.60	0.58	0.55	0.63	0.55
10	0.83	0.50	0.68	0.73	0.65	0.80	0.75	0.50	0.68	0.58	0.90	0.45	0.43	0.60	0.60	0.48	0.78	0.60
12	0.65	0.58	0.63	0.90	0.78	0.80	0.63	0.70	0.71	0.45	0.50	0.50	0.88	1.00	0.93	0.75	0.55	0.69

Table D-4 Values of r_u for 3B spacing and dynamic motion of 0.05g peak acceleration

Dynamic Motion of 0.05g Peak Acceleration and 3B Spacing

Group 1	Free Field					High Stiffness Level					Mean Stiffness Level					Low Stiffness Level				
ID / z (m)	1	5	6	7	Ave	1	5	6	7	Ave	1	5	6	7	Ave	1	5	6	7	Ave
2	0.95	0.70	1.05	0.75	0.86	0.40	0.50	0.53	0.73	0.54	0.28	0.45	0.30	0.85	0.47	0.38	0.40	0.28	0.53	0.39
4	1.03	0.85	0.85	0.85	0.89	0.68	0.70	1.25	0.48	0.78	0.45	0.53	0.45	0.50	0.48	0.38	0.60	0.45	0.55	0.49
6	0.95	0.85	0.98	0.78	0.89	0.58	0.53	0.53	0.58	0.55	0.63	0.68	0.68	0.48	0.61	0.35	0.40	0.50	0.35	0.40
8	1.00	0.65	0.95	0.63	0.81	0.58	0.50	0.55	0.58	0.55	0.63	0.85	0.73	0.78	0.74	0.50	0.65	0.60	0.35	0.53
10	1.03	1.03	0.90	0.95	0.98	0.50	0.65	0.83	0.58	0.64	1.10	0.55	0.78	0.65	0.77	0.43	0.48	0.35	0.50	0.44
12	0.85	0.65	0.95	0.75	0.80	1.03	0.75	0.90	0.65	0.83	0.85	0.53	0.83	0.73	0.73	0.80	0.63	0.73	0.55	0.68

Group 2	Free Field					High Stiffness Level					Mean Stiffness Level					Low Stiffness Level				
ID / z(m)	4	8	9	13	Ave	4	8	9	13	Ave	4	8	9	13	Ave	4	8	9	13	Ave
2	0.85	0.50	0.90	0.80	0.76	0.73	0.25	0.50	0.78	0.56	1.00	0.28	0.18	0.20	0.41	0.45	0.63	0.50	0.58	0.54
4	0.88	0.85	0.75	0.70	0.79	0.80	0.55	0.55	0.50	0.60	0.40	0.58	0.65	0.75	0.59	0.38	0.60	0.35	0.65	0.49
6	0.88	0.88	0.93	0.93	0.90	0.63	0.55	0.68	0.70	0.64	0.60	0.60	0.70	0.65	0.64	0.38	0.45	0.45	0.50	0.44
8	1.00	0.80	1.00	0.80	0.90	0.73	0.55	0.70	0.75	0.68	0.75	0.93	0.95	0.95	0.89	0.65	0.48	0.78	0.63	0.63
10	0.88	0.90	0.95	0.78	0.88	0.65	0.88	0.58	0.55	0.66	0.95	0.45	0.70	0.73	0.71	0.50	0.53	0.55	0.65	0.56
12	0.98	1.08	0.83	0.93	0.95	0.93	0.68	0.98	0.73	0.83	0.95	0.78	0.75	0.95	0.86	0.53	0.33	0.30	0.83	0.49

Group 3	Free Field									High Stiffness Level								
ID / z(m)	10	11	12	14	15	16	17	18	Ave	10	11	12	14	15	16	17	18	Ave
2	0.83	0.65	0.58	0.90	0.85	0.78	0.95	0.70	0.78	0.45	0.45	0.38	0.65	0.53	0.78	0.48	0.40	0.51
4	0.83	0.83	0.88	0.90	0.83	0.80	0.93	0.60	0.82	0.55	0.60	0.63	0.55	0.75	1.10	0.50	0.63	0.66
6	0.93	0.65	0.60	0.95	1.05	0.78	0.90	0.75	0.83	0.50	0.58	0.63	0.55	0.50	0.58	0.63	0.70	0.58
8	0.60	0.85	0.90	0.95	0.98	1.05	0.90	0.55	0.85	0.45	0.48	0.55	0.63	0.88	0.60	0.70	0.60	0.61
10	0.95	0.85	0.88	1.00	0.93	0.98	1.15	0.83	0.94	0.53	0.60	0.60	0.65	0.75	0.60	0.80	0.73	0.66
12	0.78	0.68	0.63	0.93	0.70	0.95	1.00	0.90	0.82	0.60	0.53	0.58	0.90	0.83	0.70	0.90	0.68	0.71

Group 3	Mean Stiffness Level									Low Stiffness Level								
ID / z(m)	10	11	12	14	15	16	17	18	Ave	10	11	12	14	15	16	17	18	Ave
2	0.53	0.40	0.38	0.38	0.85	0.45	0.60	0.48	0.51	0.70	0.25	0.55	0.40	0.43	0.43	0.30	0.15	0.40
4	0.90	0.55	0.58	0.45	0.45	0.88	1.08	0.68	0.69	0.83	0.65	0.90	0.90	0.70	0.43	0.45	0.60	0.68
6	0.48	0.70	0.48	0.75	0.75	0.55	0.75	0.75	0.65	0.28	0.33	0.23	0.45	0.48	0.40	0.38	0.35	0.36
8	0.68	0.48	0.55	0.88	0.88	0.75	0.83	0.65	0.71	0.85	0.50	0.58	0.65	0.80	0.58	0.55	0.50	0.63
10	0.95	0.70	0.55	0.80	0.80	0.70	0.60	0.58	0.71	0.90	1.10	0.58	0.45	0.50	0.65	0.50	0.90	0.70
12	0.55	0.50	0.73	0.78	0.78	0.98	0.55	0.73	0.70	0.50	0.63	0.48	0.83	0.93	0.85	0.93	0.53	0.71

Table D-5 Values of r_u for 4B spacing and dynamic motion of 0.08g peak acceleration

Dynamic Motion of 0.08g Peak Acceleration and 4B Spacing

Group 1	Free Field					High Stiffness Level					Mean Stiffness Level					Low Stiffness Level				
ID / z (m)	1	5	6	7	Ave	1	5	6	7	Ave	1	5	6	7	Ave	1	5	6	7	Ave
2	0.50	0.65	0.58	0.43	0.54	0.40	0.30	0.20	0.68	0.39	0.55	0.58	0.10	0.20	0.36	0.00	0.18	0.00	0.23	0.10
4	0.63	0.73	0.73	0.65	0.68	0.60	0.40	0.50	0.40	0.48	0.33	0.40	0.35	0.55	0.41	0.23	0.35	0.28	0.65	0.38
6	0.70	0.70	0.85	0.70	0.74	0.60	0.43	0.40	0.35	0.44	0.50	0.38	0.40	0.35	0.41	0.45	0.50	0.45	0.25	0.41
8	0.95	0.78	0.95	0.75	0.86	0.70	0.40	0.68	0.40	0.54	0.70	0.33	0.60	0.35	0.49	0.70	0.30	0.60	0.50	0.53
10	0.95	0.88	0.90	0.95	0.92	0.45	0.50	0.68	0.50	0.53	0.58	0.53	0.55	0.38	0.51	0.43	0.40	0.93	0.40	0.54
12	0.90	0.85	1.03	0.95	0.93	0.75	0.68	0.88	0.55	0.71	0.80	0.55	0.85	0.88	0.77	0.73	0.48	0.83	0.70	0.68

Group 2	Free Field					High Stiffness Level					Mean Stiffness Level					Low Stiffness Level				
ID / z(m)	4	8	9	13	Ave	4	8	9	13	Ave	4	8	9	13	Ave	4	8	9	13	Ave
2	0.55	0.63	0.40	0.40	0.49	0.00	0.05	1.00	0.33	0.34	0.85	0.60	0.65	0.33	0.61	0.00	0.48	0.45	0.38	0.33
4	0.85	0.45	0.70	0.75	0.69	0.50	1.03	0.63	0.93	0.77	0.70	0.80	0.58	0.70	0.69	0.43	0.33	0.58	0.55	0.47
6	0.70	0.45	0.90	0.70	0.69	0.55	0.48	0.53	0.40	0.49	0.60	0.45	0.50	0.40	0.49	0.75	0.58	0.63	0.35	0.58
8	0.93	0.85	0.90	0.73	0.85	0.70	0.58	0.65	0.80	0.68	0.65	0.75	0.55	0.48	0.61	0.58	0.65	0.68	0.33	0.56
10	0.88	0.95	0.90	1.03	0.94	0.50	0.45	0.48	0.45	0.47	0.53	0.55	0.48	0.55	0.53	0.68	0.65	0.35	0.70	0.59
12	0.90	0.78	0.85	0.90	0.86	1.13	0.80	0.65	0.48	0.76	0.90	0.90	0.68	0.75	0.81	1.05	0.80	0.85	0.60	0.83

Group 3	Free Field									High Stiffness Level								
ID / z(m)	10	11	12	14	15	16	17	18	Ave	10	11	12	14	15	16	17	18	Ave
2	0.58	0.73	0.35	0.80	0.70	0.45	0.60	0.40	0.58	0.53	0.45	0.45	0.13	0.38	0.55	0.68	0.33	0.43
4	0.78	0.73	0.68	0.75	0.65	0.80	0.65	0.75	0.72	0.83	0.85	0.78	0.65	0.80	0.40	0.65	0.93	0.73
6	0.83	0.55	0.75	0.93	0.78	0.73	0.70	0.70	0.74	0.43	0.63	0.33	0.48	0.55	0.53	0.43	0.40	0.47
8	0.60	0.80	0.78	0.65	1.08	0.95	0.85	0.73	0.80	0.68	0.68	0.55	0.58	0.63	0.65	0.65	0.80	0.65
10	0.88	0.85	0.85	0.98	0.85	0.93	0.90	1.03	0.91	0.65	0.45	0.50	0.45	0.48	0.58	0.68	0.45	0.53
12	0.85	1.13	0.83	0.98	0.95	0.95	0.80	0.90	0.92	0.70	0.58	0.65	0.95	1.03	1.00	0.80	0.48	0.77

Group 3	Mean Stiffness Level									Low Stiffness Level								
ID / z(m)	10	11	12	14	15	16	17	18	Ave	10	11	12	14	15	16	17	18	Ave
2	0.20	0.55	0.43	0.33	0.25	0.40	0.23	0.33	0.34	0.45	0.70	0.23	0.68	1.05	0.20	0.25	0.38	0.49
4	0.65	0.58	0.45	0.75	0.58	0.88	0.58	0.70	0.64	1.10	0.55	0.90	0.80	0.80	0.75	0.48	0.55	0.74
6	0.38	0.58	0.38	0.50	0.40	0.60	0.48	0.40	0.46	0.35	0.30	0.50	0.45	0.40	0.58	0.43	0.35	0.42
8	0.58	0.58	0.55	0.55	0.55	0.63	0.50	0.48	0.55	0.50	0.45	0.30	0.58	0.68	0.68	0.50	0.33	0.50
10	0.65	0.48	0.58	0.70	0.43	0.58	0.45	0.55	0.55	0.65	0.48	0.45	0.73	0.40	0.98	0.70	0.70	0.63
12	0.65	1.05	0.58	0.60	0.70	0.73	0.80	0.75	0.73	0.60	0.83	1.00	0.65	0.93	0.98	0.88	0.60	0.81

Table D-6 Values of r_u for 4B spacing and dynamic motion of 0.07g peak acceleration

Dynamic Motion of 0.07g Peak Acceleration and 4B Spacing

Group 1	Free Field					High Stiffness Level					Mean Stiffness Level					Low Stiffness Level				
ID / z (m)	1	5	6	7	Ave	1	5	6	7	Ave	1	5	6	7	Ave	1	5	6	7	Ave
2	0.80	0.65	0.88	0.60	0.73	0.00	0.55	0.15	0.65	0.34	0.53	0.68	0.15	0.23	0.39	0.50	0.00	0.00	0.40	0.23
4	0.80	0.73	0.78	0.73	0.76	0.20	0.55	0.68	0.45	0.47	0.60	0.35	0.40	0.40	0.44	0.45	0.30	0.28	0.80	0.46
6	0.90	0.90	0.88	0.95	0.91	0.53	0.30	0.43	0.38	0.41	0.43	0.34	0.50	0.30	0.39	0.40	0.28	0.45	0.28	0.35
8	0.80	1.05	0.95	0.90	0.93	0.65	0.65	0.65	0.38	0.58	0.65	0.48	0.75	0.35	0.56	0.70	0.38	0.53	0.48	0.52
10	0.90	0.75	0.80	0.93	0.67	0.55	0.50	0.50	0.48	0.51	0.78	0.40	0.65	0.33	0.54	0.40	0.40	0.50	0.43	0.47
12	0.95	0.98	0.90	0.98	0.95	0.73	0.50	0.85	0.60	0.67	0.68	0.55	0.80	1.00	0.76	0.65	0.60	0.88	0.88	0.75

Group 2	Free Field					High Stiffness Level					Mean Stiffness Level					Low Stiffness Level				
ID / z(m)	4	8	9	13	Ave	4	8	9	13	Ave	4	8	9	13	Ave	4	8	9	13	Ave
2	0.60	0.48	0.60	0.65	0.58	0.00	0.95	0.70	0.25	0.48	0.50	0.00	0.45	0.55	0.38	0.00	0.00	1.10	0.30	0.35
4	0.80	0.80	0.90	0.65	0.79	0.83	0.90	0.78	0.70	0.80	0.65	0.35	0.35	0.40	0.44	0.33	0.35	0.50	0.35	0.38
6	0.83	1.00	0.83	0.90	0.89	0.50	0.50	0.63	0.53	0.54	0.53	0.50	0.45	0.38	0.46	0.50	0.38	0.55	0.28	0.43
8	1.01	0.95	0.78	0.65	0.85	0.68	0.53	0.65	0.50	0.59	0.80	0.55	0.65	0.43	0.61	0.65	0.48	0.65	0.35	0.53
10	0.88	0.70	0.90	0.93	0.85	0.53	0.60	0.53	0.40	0.51	0.48	0.60	0.73	0.58	0.59	0.63	0.45	0.35	0.53	0.49
12	0.93	1.00	0.93	0.88	0.93	0.83	1.00	0.90	0.60	0.83	0.83	0.80	0.98	0.93	0.88	0.95	0.70	0.50	0.58	0.68

Group 3	Free Field								High Stiffness Level							
ID / z(m)	10	11	12	14	15	16	17	18	Ave	10	11	12	14	15	16	17	18	Ave
2	0.63	0.50	0.50	0.50	0.78	0.78	0.73	0.65	0.63	0.55	0.83	0.45	0.43	0.48	0.20	0.15	0.25	0.42
4	0.95	0.85	0.85	0.80	0.78	0.80	0.85	0.65	0.82	0.68	1.00	1.00	0.70	0.58	0.60	0.55	0.70	0.73
6	0.80	0.83	0.80	0.88	0.90	0.85	0.70	0.90	0.83	0.38	0.48	0.40	0.48	0.58	0.45	0.48	0.55	0.47
8	0.93	0.80	0.78	0.93	1.00	0.95	0.75	0.65	0.85	0.83	0.63	0.40	0.75	0.55	0.63	0.63	0.50	0.61
10	0.90	0.83	0.90	0.90	1.00	0.95	1.03	0.93	0.93	0.43	0.40	0.70	0.38	0.50	0.40	0.65	0.40	0.48
12	0.95	0.73	0.80	0.95	1.05	0.90	0.88	0.88	0.89	0.73	0.38	0.60	0.88	0.98	0.63	0.98	0.60	0.72

Group 3	Mean Stiffness Level								Low Stiffness Level								
ID / z(m)	10	11	12	14	15	16	17	18	Ave	10	11	12	14	15	16	17	18	Ave
2	0.80	0.60	0.30	0.18	0.80	0.30	0.03	0.55	0.44	0.35	0.75	0.25	0.80	0.48	0.48	0.10	0.30	0.44
4	0.45	0.48	0.55	0.70	0.90	0.80	0.63	0.40	0.61	0.80	0.48	0.85	0.40	0.70	0.73	0.35	0.35	0.58
6	0.40	0.43	0.45	0.40	0.53	0.45	0.55	0.38	0.45	0.45	0.40	0.33	0.50	0.48	0.55	0.35	0.28	0.42
8	0.58	0.43	0.48	0.70	0.70	0.65	0.65	0.43	0.58	0.63	0.43	0.38	0.55	0.63	0.55	0.53	0.35	0.50
10	0.40	0.40	0.58	0.58	0.50	0.53	0.45	0.58	0.50	0.43	0.50	0.40	0.83	0.45	0.50	0.55	0.53	0.52
12	0.73	0.63	0.60	0.65	0.75	0.95	0.80	0.93	0.75	0.60	0.83	0.90	0.80	0.90	0.90	1.00	0.58	0.81

Table D-7 Values of r_u for 4B spacing and dynamic motion of 0.06g peak acceleration

Dynamic Motion of 0.06g Peak Acceleration and 4B Spacing

Group 1	Free Field					High Stiffness Level					Mean Stiffness Level					Low Stiffness Level				
ID / z (m)	1	5	6	7	Ave	1	5	6	7	Ave	1	5	6	7	Ave	1	5	6	7	Ave
2	0.65	0.55	0.50	0.50	0.55	0.05	0.45	0.00	0.30	0.20	0.43	0.83	0.00	0.65	0.48	0.00	0.00	0.00	0.10	0.03
4	0.80	0.75	0.83	0.90	0.82	0.23	0.30	0.63	0.25	0.35	0.40	0.33	0.63	0.60	0.49	0.48	0.30	0.10	0.68	0.39
6	0.88	0.78	0.90	0.80	0.84	0.45	0.40	0.45	0.28	0.39	0.45	0.43	0.45	0.28	0.40	0.35	0.30	0.30	0.25	0.30
8	0.63	0.75	1.03	0.93	0.83	0.60	0.65	0.65	0.55	0.61	0.60	0.48	0.60	0.38	0.51	0.65	0.30	0.58	0.40	0.48
10	0.78	0.88	0.60	0.98	0.81	0.43	0.45	0.48	0.40	0.44	0.48	0.45	0.53	0.53	0.49	0.33	0.43	0.85	0.43	0.51
12	0.93	0.95	0.85	0.80	0.88	0.60	0.60	0.65	0.45	0.58	0.88	0.50	0.95	0.80	0.78	0.50	0.68	0.73	0.60	0.63

Group 2	Free Field					High Stiffness Level					Mean Stiffness Level					Low Stiffness Level				
ID / z(m)	4	8	9	13	Ave	4	8	9	13	Ave	4	8	9	13	Ave	4	8	9	13	Ave
2	0.45	0.45	0.75	0.55	0.55	0.00	0.50	0.50	0.28	0.32	0.65	0.00	0.33	0.45	0.41	0.23	0.60	1.15	0.35	0.58
4	1.03	1.00	0.85	0.88	0.94	0.30	0.85	0.70	0.98	0.71	0.53	0.48	0.38	0.63	0.50	0.25	0.30	0.70	0.40	0.41
6	0.73	0.73	0.75	0.93	0.78	0.55	0.45	0.55	0.28	0.46	0.63	0.48	0.48	0.33	0.48	0.48	0.48	0.50	0.20	0.41
8	0.80	0.80	0.95	0.65	0.80	0.55	0.60	0.65	0.78	0.64	0.63	0.55	0.68	0.45	0.58	0.55	0.60	0.60	0.43	0.54
10	0.95	0.93	0.98	0.88	0.93	0.50	0.53	0.65	0.45	0.53	0.68	0.85	0.55	0.80	0.72	0.43	0.68	0.40	0.48	0.49
12	0.98	0.98	0.70	0.68	0.83	0.90	0.83	0.45	0.53	0.68	0.95	1.00	0.95	0.85	0.94	0.80	0.70	0.45	0.60	0.64

Group 3	Free Field									High Stiffness Level								
ID / z(m)	10	11	12	14	15	16	17	18	Ave	10	11	12	14	15	16	17	18	Ave
2	0.58	0.35	0.73	0.63	0.35	0.50	0.40	0.55	0.51	0.85	0.50	1.05	0.28	0.68	0.13	0.20	0.73	0.55
4	0.80	0.68	0.80	0.80	0.85	0.90	0.78	0.88	0.81	0.88	0.90	0.80	1.00	0.40	0.70	0.88	0.98	0.82
6	0.78	0.85	0.78	0.88	0.70	0.85	0.83	0.93	0.82	0.30	0.38	0.30	0.45	0.40	0.35	0.43	0.28	0.36
8	0.70	0.75	0.90	0.98	0.95	0.75	0.78	0.65	0.81	0.78	0.30	0.48	0.55	0.65	0.65	0.65	0.78	0.60
10	0.73	0.93	0.68	0.93	0.95	0.90	0.93	0.88	0.86	0.48	0.40	0.50	0.53	0.58	0.58	0.63	0.45	0.52
12	0.65	0.95	0.98	0.75	0.88	0.65	0.90	0.68	0.80	0.85	0.75	0.65	0.63	0.83	0.40	0.65	0.53	0.66

Group 3	Mean Stiffness Level									Low Stiffness Level								
ID / z(m)	10	11	12	14	15	16	17	18	Ave	10	11	12	14	15	16	17	18	Ave
2	0.90	0.68	0.40	0.53	0.45	0.73	0.58	0.45	0.59	0.75	0.70	0.35	0.45	0.70	0.10	0.00	0.35	0.43
4	0.88	0.65	0.85	0.33	0.73	0.85	0.35	0.63	0.66	0.80	0.43	0.50	0.48	0.60	0.95	0.30	0.40	0.56
6	0.28	0.30	0.48	0.48	0.48	0.40	0.55	0.33	0.41	0.30	0.25	0.20	0.45	0.38	0.45	0.30	0.20	0.32
8	0.63	0.33	0.50	0.65	0.68	0.65	0.68	0.45	0.57	0.45	0.40	0.45	0.45	0.50	0.58	0.58	0.43	0.48
10	0.45	0.60	0.58	0.60	0.50	0.53	0.48	0.80	0.57	0.68	0.35	0.38	0.43	0.55	0.75	0.50	0.48	0.51
12	0.75	0.83	0.48	0.83	0.68	0.88	1.00	0.85	0.78	0.50	0.88	0.58	0.40	0.95	0.60	0.65	0.60	0.64

Table D-8 Values of r_u for 4B spacing and dynamic motion of 0.05g peak acceleration

Dynamic Motion of 0.05g Peak Acceleration and 4B Spacing

Group 1	Free Field					High Stiffness Level					Mean Stiffness Level					Low Stiffness Level				
ID / z (m)	1	5	6	7	Ave	1	5	6	7	Ave	1	5	6	7	Ave	1	5	6	7	Ave
2	0.63	0.40	0.28	0.50	0.45	0.00	0.35	0.10	0.85	0.33	0.48	0.50	0.15	0.40	0.47	0.00	0.00	0.80	0.10	0.23
4	0.80	0.95	0.80	0.85	0.85	0.53	0.38	0.55	0.30	0.38	0.55	0.38	0.68	0.35	0.49	0.40	0.20	0.43	0.73	0.44
6	0.73	0.75	0.75	0.73	0.74	0.48	0.40	0.50	0.35	0.43	0.48	0.40	0.48	0.30	0.41	0.53	0.45	0.38	0.30	0.41
8	0.95	0.85	0.80	0.83	0.86	0.58	0.50	0.65	0.35	0.52	0.75	0.55	0.60	0.50	0.60	0.55	0.40	0.58	0.50	0.51
10	0.95	0.90	0.93	0.95	0.93	0.60	0.53	0.70	0.53	0.59	0.65	0.43	0.45	0.48	0.50	0.58	0.43	0.45	0.50	0.49
12	1.00	0.85	0.85	0.83	0.88	0.95	0.68	0.88	0.70	0.80	0.73	0.68	0.78	0.70	0.72	0.60	0.48	0.83	0.65	0.64

Group 2	Free Field					High Stiffness Level					Mean Stiffness Level					Low Stiffness Level				
ID / z(m)	4	8	9	13	Ave	4	8	9	13	Ave	4	8	9	13	Ave	4	8	9	13	Ave
2	0.60	0.08	0.50	0.50	0.38	0.00	0.13	0.78	0.80	0.52	0.60	0.00	0.85	0.60	0.51	0.05	0.00	0.83	0.93	0.45
4	0.78	0.80	0.88	0.80	0.81	0.83	0.73	0.80	0.73	0.77	0.38	0.40	0.35	0.35	0.37	0.40	0.35	0.55	0.45	0.44
6	0.60	0.70	0.83	0.65	0.69	0.50	0.55	0.50	0.40	0.49	0.53	0.48	0.55	0.38	0.48	0.65	0.55	0.63	0.28	0.53
8	0.88	0.60	1.10	0.70	0.82	0.60	0.68	0.48	0.40	0.54	0.65	0.60	0.60	0.78	0.66	0.63	0.63	0.55	0.38	0.54
10	0.93	0.95	0.90	1.05	0.96	0.55	0.48	0.48	0.48	0.49	0.73	0.68	0.55	0.95	0.73	0.70	0.58	0.45	0.65	0.59
12	0.98	0.98	0.93	0.80	0.92	0.85	0.85	0.48	0.63	0.70	0.75	0.85	0.58	0.63	0.70	0.60	0.70	0.53	0.53	0.59

Group 3	Free Field									High Stiffness Level								
ID / z(m)	10	11	12	14	15	16	17	18	Ave	10	11	12	14	15	16	17	18	Ave
2	0.53	0.30	0.55	0.90	0.45	0.55	0.83	0.48	0.53	0.90	0.20	1.05	0.20	0.60	0.58	0.70	0.80	0.63
4	0.80	0.48	0.63	0.73	0.70	0.78	0.95	0.80	0.73	0.43	0.80	0.95	0.55	0.40	0.68	1.10	0.73	0.70
6	0.83	0.55	0.80	0.78	0.98	0.60	0.85	0.65	0.75	0.25	0.35	0.23	0.40	0.48	0.53	0.53	0.40	0.39
8	0.80	0.75	0.93	0.88	1.00	0.93	0.55	0.70	0.82	0.65	0.35	0.43	0.60	0.65	0.58	0.63	0.40	0.53
10	1.00	1.03	0.88	0.93	0.90	0.90	0.85	1.05	0.94	0.50	0.38	0.80	0.73	0.48	0.50	0.55	0.48	0.55
12	0.80	0.85	0.73	0.95	0.90	0.83	0.73	0.80	0.82	0.68	0.45	0.55	0.85	0.75	0.55	0.50	0.63	0.62

Group 3	Mean Stiffness Level									Low Stiffness Level								
ID / z(m)	10	11	12	14	15	16	17	18	Ave	10	11	12	14	15	16	17	18	Ave
2	0.85	0.58	0.63	0.25	0.30	0.10	0.85	0.60	0.52	0.23	0.65	1.15	0.18	0.33	0.55	0.13	0.93	0.52
4	0.78	0.95	0.70	0.53	0.65	0.50	0.40	0.35	0.61	1.03	0.35	1.13	0.60	0.45	0.70	0.40	0.45	0.64
6	0.33	0.25	0.35	0.50	0.50	0.50	0.58	0.38	0.42	0.35	0.28	0.45	0.50	0.35	0.45	0.45	0.28	0.39
8	0.63	0.35	0.58	0.55	0.75	0.63	0.63	0.78	0.61	0.45	0.55	0.38	0.50	0.65	0.65	0.58	0.38	0.52
10	0.55	0.35	0.55	0.50	0.38	0.45	0.45	0.95	0.52	0.50	0.68	0.55	0.75	0.68	0.48	0.75	0.65	0.63
12	0.63	0.90	0.45	0.70	0.85	1.00	0.83	0.63	0.75	0.60	1.05	0.75	1.05	1.00	0.95	1.00	0.53	0.87

Table D-9 Values of r_u for 5B spacing and dynamic motion of 0.08g peak acceleration

Dynamic Motion of 0.08g Peak Acceleration and 5B Spacing

Group 1	Free Field					High Stiffness Level					Mean Stiffness Level					Low Stiffness Level				
ID / z (m)	1	5	6	7	Ave	1	5	6	7	Ave	1	5	6	7	Ave	1	5	6	7	Ave
2	0.38	0.25	0.28	0.55	0.25	0.25	0.13	0.48	0.55	0.35	0.00	0.70	0.00	0.65	0.34	0.45	0.00	1.13	1.03	0.65
4	0.90	0.80	0.78	0.73	0.80	0.63	0.28	0.30	0.35	0.39	0.33	0.25	0.28	0.75	0.40	0.08	0.35	0.10	0.13	0.16
6	0.65	0.53	0.73	0.75	0.66	0.50	0.38	0.50	0.33	0.43	0.43	0.33	0.35	0.43	0.38	0.30	0.10	0.55	0.13	0.27
8	0.80	0.70	0.80	0.83	0.78	0.45	0.48	0.48	0.43	0.46	0.63	0.33	0.73	0.33	0.50	0.45	0.13	0.45	0.23	0.31
10	0.80	0.80	0.70	0.85	0.79	0.55	0.60	0.50	0.40	0.51	0.68	0.55	0.43	0.45	0.53	0.45	0.38	0.35	0.30	0.37
12	0.85	0.93	0.73	1.03	0.88	0.98	0.60	0.88	0.40	0.71	0.83	0.48	0.93	0.68	0.73	1.03	0.78	1.03	0.85	0.92

Group 2	Free Field					High Stiffness Level					Mean Stiffness Level					Low Stiffness Level				
ID / z(m)	4	8	9	13	Ave	4	8	9	13	Ave	4	8	9	13	Ave	4	8	9	13	Ave
2	0.08	0.25	0.23	0.28	0.21	0.00	0.25	0.78	0.50	0.38	0.30	0.03	0.00	0.10	0.11	0.00	0.13	0.28	0.93	0.33
4	0.78	0.78	0.78	0.78	0.78	0.35	0.63	0.73	0.50	0.55	0.45	0.98	0.30	0.38	0.53	0.45	0.70	0.30	0.38	0.46
6	0.70	0.55	0.68	0.60	0.63	0.58	0.53	0.53	0.45	0.52	0.33	0.53	0.40	0.58	0.46	0.43	0.25	0.58	0.30	0.39
8	0.88	0.85	0.85	0.98	0.89	0.38	0.43	0.35	0.30	0.36	0.53	0.33	0.55	0.43	0.46	0.55	0.63	0.38	0.45	0.50
10	0.65	0.65	0.75	0.95	0.75	0.53	0.63	0.65	0.68	0.62	0.60	0.48	0.65	0.50	0.56	0.35	0.50	0.38	0.43	0.41
12	0.85	1.00	0.98	0.93	0.94	0.80	0.98	0.60	0.83	0.80	0.60	0.90	0.83	0.95	0.82	1.03	1.13	0.50	0.40	0.76

Group 3	Free Field								High Stiffness Level								
ID / z(m)	10	11	12	14	15	16	17	18	Ave	10	11	12	14	15	16	17	18	Ave
2	0.30	0.30	0.25	0.25	0.50	0.65	0.63	0.25	0.36	0.18	0.58	0.25	0.20	0.75	0.70	0.10	0.23	0.37
4	0.83	0.78	0.70	0.83	0.90	0.70	0.78	0.80	0.79	0.75	0.75	0.50	0.40	0.43	0.95	0.40	0.38	0.57
6	0.80	0.68	0.80	0.83	0.65	0.65	0.50	0.73	0.70	0.38	0.33	0.30	0.60	0.60	0.45	0.48	0.45	0.45
8	0.50	0.78	0.65	0.90	0.95	0.90	0.75	0.90	0.79	0.40	0.55	0.30	0.53	0.50	0.50	0.50	0.43	0.46
10	1.00	0.75	0.98	0.93	0.93	0.85	0.83	0.80	0.88	0.53	0.48	0.35	0.33	0.43	0.65	0.63	0.65	0.50
12	1.00	0.85	0.95	0.53	0.85	0.65	1.00	0.78	0.83	0.48	0.65	0.95	0.88	0.95	0.70	0.90	0.95	0.81

Group 3	Mean Stiffness Level								Low Stiffness Level								
ID / z(m)	10	11	12	14	15	16	17	18	Ave	10	11	12	14	15	16	17	18	Ave
2	0.45	0.63	0.75	0.10	0.40	0.38	0.13	0.60	0.43	0.65	0.73	0.00	0.00	0.70	0.00	0.00	0.10	0.27
4	0.43	0.53	0.93	0.48	0.83	0.33	0.40	0.48	0.55	0.65	0.80	0.65	0.40	0.43	0.50	0.18	0.13	0.47
6	0.40	0.20	0.30	0.38	0.45	0.53	0.48	0.40	0.39	0.28	0.35	0.15	0.40	0.35	0.30	0.48	0.23	0.32
8	0.35	0.50	0.40	0.50	0.53	0.45	0.43	0.63	0.47	0.48	0.35	0.38	0.45	0.55	0.45	0.53	0.58	0.47
10	0.55	0.55	0.43	0.43	0.48	0.58	0.58	0.43	0.50	0.25	0.53	0.40	0.60	0.35	0.68	0.45	0.30	0.44
12	0.40	0.88	0.60	0.98	1.00	0.65	1.03	1.03	0.82	0.58	0.50	0.55	0.70	0.68	0.85	0.93	0.88	0.71

Table D-10 Values of r_u for 5B spacing and dynamic motion of 0.07g peak acceleration

Dynamic Motion of 0.07g Peak Acceleration and 5B Spacing

Group 1	Free Field					High Stiffness Level					Mean Stiffness Level					Low Stiffness Level				
ID / z (m)	1	5	6	7	Ave	1	5	6	7	Ave	1	5	6	7	Ave	1	5	6	7	Ave
2	0.75	0.28	0.73	0.40	0.54	0.13	0.40	0.80	0.08	0.43	0.15	0.08	0.15	0.20	0.14	0.45	0.00	0.60	0.58	0.41
4	0.95	0.60	0.90	0.75	0.80	0.80	0.25	0.53	0.40	0.49	0.25	0.58	0.30	0.80	0.48	0.15	0.35	0.13	0.33	0.24
6	0.70	0.95	0.80	0.70	0.79	0.48	0.33	0.53	0.40	0.43	0.55	0.40	0.38	0.35	0.42	0.35	0.25	0.38	0.23	0.30
8	0.85	0.68	0.93	0.93	0.84	0.38	0.50	0.50	0.40	0.44	0.50	0.38	0.55	0.40	0.46	0.50	0.25	0.50	0.13	0.34
10	0.98	0.90	0.95	0.75	0.89	0.45	0.80	0.80	0.43	0.62	0.83	0.35	0.75	0.48	0.60	0.40	0.20	0.40	0.43	0.36
12	0.85	1.00	0.95	0.98	0.94	0.95	0.58	0.93	0.53	0.74	0.90	0.50	0.65	0.58	0.66	1.05	0.90	1.00	0.90	0.96
Group 2	**Free Field**					**High Stiffness Level**					**Mean Stiffness Level**					**Low Stiffness Level**				
ID / z(m)	4	8	9	13	Ave	4	8	9	13	Ave	4	8	9	13	Ave	4	8	9	13	Ave
2	0.55	0.33	0.53	0.53	0.48	0.00	0.00	0.00	0.90	0.23	0.00	0.33	0.25	0.00	0.14	0.00	0.15	0.10	0.55	0.20
4	0.98	0.73	0.85	0.83	0.84	0.78	0.60	0.78	0.50	0.66	0.55	0.63	0.65	0.33	0.54	0.45	0.28	1.15	0.70	0.64
6	0.79	0.88	0.88	0.60	0.78	0.40	0.65	0.45	0.43	0.48	0.45	0.45	0.45	0.53	0.47	0.50	0.40	0.60	0.30	0.45
8	0.88	0.65	0.83	0.93	0.82	0.35	0.65	0.45	0.38	0.46	0.50	0.40	0.75	0.50	0.54	0.45	0.48	0.40	0.38	0.43
10	0.65	0.73	0.90	0.78	0.76	0.83	0.58	0.55	0.78	0.68	0.63	0.48	0.43	0.58	0.53	0.43	0.53	0.38	0.45	0.44
12	0.85	0.95	0.98	0.73	0.88	0.98	0.83	0.78	0.70	0.82	0.48	0.90	0.48	1.00	0.71	0.58	0.98	0.68	0.35	0.64

Group 3	Free Field									High Stiffness Level								
ID / z(m)	10	11	12	14	15	16	17	18	Ave	10	11	12	14	15	16	17	18	Ave
2	0.55	0.45	0.48	0.60	0.73	0.33	0.80	0.50	0.55	0.48	1.05	0.23	0.68	0.20	0.00	1.05	0.35	0.50
4	0.78	0.88	0.88	0.93	0.80	0.93	0.90	0.85	0.87	0.63	0.50	0.80	0.85	0.55	0.73	0.33	0.33	0.59
6	0.88	0.78	0.83	0.68	0.68	0.75	0.83	0.75	0.77	0.25	0.60	0.20	0.48	0.70	0.73	0.58	0.63	0.52
8	1.05	0.65	0.95	0.93	0.95	0.95	0.83	0.75	0.88	0.55	0.40	0.45	0.43	0.50	0.70	0.45	0.48	0.49
10	0.80	1.00	0.83	0.98	0.85	0.68	0.80	0.90	0.85	0.65	0.65	0.65	0.50	0.40	0.70	0.50	0.65	0.59
12	0.88	0.98	0.50	0.78	0.60	0.95	0.88	0.98	0.82	0.48	0.68	0.90	0.78	0.90	0.55	0.80	0.68	0.72
Group 3	**Mean Stiffness Level**									**Low Stiffness Level**								
ID / z(m)	10	11	12	14	15	16	17	18	Ave	10	11	12	14	15	16	17	18	Ave
2	1.05	0.65	0.20	1.00	0.13	0.50	0.20	0.40	0.52	1.00	0.63	0.90	0.00	0.20	0.43	0.00	0.73	0.48
4	0.43	1.10	0.40	0.60	0.55	0.68	1.08	0.63	0.68	0.83	0.43	1.00	0.35	0.33	0.75	0.35	0.43	0.56
6	0.45	0.55	0.35	0.40	0.60	0.50	0.60	0.38	0.48	0.20	0.35	0.18	0.53	0.43	0.53	0.33	0.30	0.35
8	0.65	0.38	0.30	0.55	0.45	0.55	0.58	0.43	0.48	0.48	0.40	0.65	0.68	0.53	0.43	0.50	0.50	0.52
10	0.38	0.38	0.53	0.48	0.45	0.40	0.48	0.83	0.49	0.13	0.75	0.73	0.45	0.43	0.53	0.75	0.30	0.51
12	0.65	0.70	0.63	0.98	0.68	0.55	0.90	0.75	0.73	0.70	0.90	0.68	0.85	0.68	0.70	0.88	0.75	0.77

Table D-11 Values of r_u for 5B spacing and dynamic motion of 0.06g peak acceleration

Dynamic Motion of 0.06g Peak Acceleration and 5B Spacing																				
Group 1	**Free Field**					**High Stiffness Level**					**Mean Stiffness Level**					**Low Stiffness Level**				
ID / z (m)	**1**	**5**	**6**	**7**	**Ave**	**1**	**5**	**6**	**7**	**Ave**	**1**	**5**	**6**	**7**	**Ave**	**1**	**5**	**6**	**7**	**Ave**
2	0.73	0.65	0.75	0.48	0.65	0.13	0.53	0.43	0.25	0.33	0.00	0.38	0.00	0.58	0.24	0.00	0.00	0.33	1.15	0.37
4	0.85	0.70	0.68	0.70	0.73	0.80	0.70	0.50	0.45	0.61	0.25	0.80	0.35	0.65	0.51	0.05	0.35	0.23	0.55	0.29
6	0.53	0.78	0.48	0.55	0.58	0.58	0.30	0.55	0.30	0.43	0.60	0.43	0.45	0.35	0.46	0.40	0.30	0.50	0.15	0.34
8	0.90	1.08	0.83	0.85	0.91	0.48	0.45	0.70	0.55	0.54	0.43	0.40	0.53	0.30	0.41	0.45	0.33	0.50	0.30	0.39
10	0.95	0.73	0.88	1.08	0.91	0.38	0.65	0.70	0.50	0.56	1.00	0.68	0.45	0.53	0.66	0.30	0.28	0.60	0.35	0.38
12	1.15	0.83	0.88	0.48	0.83	0.80	0.50	0.65	0.40	0.59	0.58	0.80	0.58	0.70	0.66	0.88	1.00	1.03	0.78	0.92
Group 2	**Free Field**					**High Stiffness Level**					**Mean Stiffness Level**					**Low Stiffness Level**				
ID / z(m)	**4**	**8**	**9**	**13**	**Ave**	**4**	**8**	**9**	**13**	**Ave**	**4**	**8**	**9**	**13**	**Ave**	**4**	**8**	**9**	**13**	**Ave**
2	0.53	0.88	0.85	0.65	0.73	0.03	0.00	0.00	0.55	0.14	0.35	0.35	0.00	0.00	0.18	0.00	0.00	0.00	0.00	0.00
4	0.90	0.55	0.73	0.78	0.74	0.43	0.50	0.38	0.55	0.46	0.45	0.45	0.75	0.20	0.46	0.23	0.60	0.53	0.70	0.51
6	0.78	0.55	0.65	0.80	0.69	0.45	0.55	0.53	0.48	0.50	0.50	0.50	0.50	0.40	0.48	0.53	0.30	0.55	0.45	0.46
8	0.73	0.58	1.00	0.98	0.82	0.40	0.50	0.60	0.58	0.52	0.40	0.40	0.65	0.48	0.48	0.35	0.53	0.33	0.43	0.41
10	0.90	0.58	0.68	0.98	0.78	0.43	0.35	0.70	0.70	0.54	0.48	0.48	0.50	0.55	0.50	0.48	0.78	0.43	0.50	0.54
12	0.63	0.55	1.00	0.95	0.78	1.00	1.03	0.55	0.80	0.84	0.98	0.95	0.55	1.10	0.89	0.43	0.85	0.75	0.50	0.63

Group 3	**Free Field**									**High Stiffness Level**								
ID / z(m)	**10**	**11**	**12**	**14**	**15**	**16**	**17**	**18**	**Ave**	**10**	**11**	**12**	**14**	**15**	**16**	**17**	**18**	**Ave**
2	0.60	0.50	0.55	0.70	0.45	0.80	0.38	0.53	0.56	0.03	0.70	0.80	1.00	0.10	0.55	0.63	0.60	0.55
4	0.78	0.85	0.78	0.93	0.90	0.70	0.55	0.75	0.78	0.53	0.65	0.60	0.70	0.45	0.60	0.50	0.53	0.57
6	0.83	0.53	1.00	0.93	0.83	0.90	0.65	0.68	0.79	0.43	0.43	0.35	0.58	0.60	0.50	0.45	0.50	0.48
8	0.70	0.90	0.88	1.00	0.90	0.90	0.93	0.60	0.85	0.55	0.50	0.50	0.50	0.45	0.48	0.48	0.70	0.52
10	0.85	0.78	0.98	1.00	0.83	0.90	1.03	0.88	0.90	0.50	0.55	0.35	0.60	0.48	0.70	0.60	0.60	0.55
12	0.90	0.73	0.45	0.90	0.55	0.88	0.78	0.98	0.77	0.53	0.55	0.73	0.88	0.90	0.53	0.85	0.40	0.67
Group 3	**Mean Stiffness Level**									**Low Stiffness Level**								
ID / z(m)	**10**	**11**	**12**	**14**	**15**	**16**	**17**	**18**	**Ave**	**10**	**11**	**12**	**14**	**15**	**16**	**17**	**18**	**Ave**
2	0.68	0.25	0.85	0.10	0.08	0.45	0.20	0.65	0.41	1.13	0.20	0.05	0.00	0.00	0.00	0.15	0.60	0.27
4	0.40	0.45	0.48	0.53	0.23	0.40	0.75	0.95	0.52	0.90	0.30	0.88	0.55	0.23	0.85	0.40	0.40	0.56
6	0.30	0.25	0.28	0.43	0.55	0.50	0.43	0.33	0.38	0.05	0.28	0.23	0.45	0.63	0.38	0.40	0.33	0.34
8	0.60	0.25	0.25	0.45	0.45	0.50	0.55	0.50	0.44	0.33	0.48	0.40	0.48	0.53	0.45	0.53	0.60	0.47
10	0.95	0.40	0.55	0.70	0.65	0.38	0.48	0.68	0.60	0.50	0.40	0.35	0.55	0.48	0.50	0.85	0.75	0.55
12	0.65	0.53	0.48	0.68	0.45	0.65	0.65	0.55	0.58	0.68	0.73	0.85	0.95	0.98	0.88	0.98	0.58	0.83

Table D-12 Values of r_u for 5B spacing and dynamic motion of 0.05g peak acceleration

Dynamic Motion of 0.05g Peak Acceleration and 5B Spacing

Group 1	Free Field					High Stiffness Level					Mean Stiffness Level					Low Stiffness Level				
ID / z (m)	1	5	6	7	Ave	1	5	6	7	Ave	1	5	6	7	Ave	1	5	6	7	Ave
2	0.73	0.48	0.68	0.48	0.59	0.00	0.83	0.50	0.90	0.56	0.00	0.40	0.00	0.03	0.11	0.00	0.00	0.15	0.50	0.16
4	0.85	0.75	0.58	0.93	0.78	0.50	0.60	0.58	0.30	0.49	0.35	0.50	0.13	0.78	0.44	0.00	0.53	0.35	0.35	0.31
6	0.80	0.68	0.75	0.57	0.70	0.48	0.40	0.48	0.35	0.43	0.43	0.30	0.45	0.35	0.38	0.35	0.25	0.48	0.08	0.29
8	1.00	0.75	1.00	0.65	0.85	0.53	0.43	0.55	0.60	0.53	0.45	0.38	0.63	0.43	0.47	0.45	0.35	0.50	0.33	0.41
10	0.90	0.95	1.10	0.95	0.98	0.45	0.60	0.55	0.45	0.51	0.65	0.40	0.58	0.45	0.52	0.45	0.25	0.28	0.28	0.31
12	0.95	0.95	1.00	0.93	0.96	1.05	0.73	0.58	0.45	0.70	0.43	0.55	0.53	0.60	0.53	1.00	0.63	1.08	0.85	0.89

Group 2	Free Field					High Stiffness Level					Mean Stiffness Level					Low Stiffness Level				
ID / z(m)	4	8	9	13	Ave	4	8	9	13	Ave	4	8	9	13	Ave	4	8	9	13	Ave
2	0.75	0.28	0.65	0.80	0.62	0.00	0.00	0.00	0.35	0.09	0.00	0.45	0.05	0.35	0.21	0.00	0.00	0.55	0.00	0.14
4	0.95	0.78	0.98	0.78	0.87	0.65	0.65	0.63	0.55	0.62	0.58	0.75	0.33	0.25	0.48	0.20	0.30	0.23	0.55	0.32
6	0.75	0.65	0.98	0.75	0.78	0.38	0.55	0.50	0.50	0.48	0.50	0.40	0.45	0.53	0.47	0.55	0.50	0.53	0.50	0.52
8	0.90	0.75	1.05	0.85	0.89	0.50	0.43	0.48	0.50	0.48	0.43	0.55	0.60	0.40	0.49	0.50	0.48	0.35	0.38	0.43
10	1.03	0.98	0.95	1.05	1.00	0.55	0.43	0.78	0.80	0.64	0.65	0.50	0.63	0.60	0.59	0.50	0.40	0.38	0.48	0.44
12	0.88	0.93	1.00	0.90	0.93	0.68	0.88	0.73	0.95	0.81	0.58	0.83	0.70	1.08	0.79	0.85	0.88	0.45	0.50	0.67

Group 3	Free Field									High Stiffness Level								
ID / z(m)	10	11	12	14	15	16	17	18	Ave	10	11	12	14	15	16	17	18	Ave
2	0.78	0.63	0.73	0.90	0.73	0.75	0.93	0.65	0.76	0.78	1.00	0.35	0.00	0.05	0.03	0.68	0.50	0.42
4	0.75	0.65	0.68	0.80	0.73	0.78	0.85	1.00	0.78	0.53	1.15	0.88	0.70	0.55	0.75	0.53	0.38	0.68
6	0.90	0.75	0.93	0.88	0.88	0.73	0.90	0.53	0.81	0.40	0.45	0.28	0.53	0.58	0.68	0.55	0.38	0.48
8	0.75	0.98	0.93	0.75	0.90	0.98	0.93	0.98	0.90	0.63	0.85	0.35	0.58	0.48	0.48	0.53	0.45	0.54
10	0.63	1.03	0.65	0.83	1.03	0.90	0.95	1.00	0.88	0.38	0.50	0.58	0.45	0.33	0.95	0.45	0.55	0.52
12	0.90	0.63	0.63	0.53	0.45	0.85	0.65	0.83	0.68	0.63	0.70	0.75	0.95	0.85	0.58	0.90	0.53	0.73

Group 3	Mean Stiffness Level									Low Stiffness Level								
ID / z(m)	10	11	12	14	15	16	17	18	Ave	10	11	12	14	15	16	17	18	Ave
2	0.40	0.40	0.50	0.30	0.73	0.50	0.18	0.88	0.48	0.55	0.88	0.60	0.00	0.30	0.00	0.08	0.70	0.39
4	0.30	0.65	0.50	0.55	0.35	0.45	0.45	0.65	0.49	1.10	1.08	0.65	0.43	0.33	0.28	0.40	0.38	0.58
6	0.35	0.33	0.23	0.50	0.60	0.53	0.50	0.33	0.42	0.20	0.20	0.15	0.45	0.60	0.48	0.43	0.38	0.36
8	0.60	0.48	0.38	0.48	0.55	0.48	0.55	0.58	0.51	0.40	0.40	0.48	0.40	0.48	0.45	0.55	0.58	0.47
10	0.63	0.63	0.63	0.55	0.48	0.40	0.68	0.73	0.59	0.53	0.43	0.30	0.40	0.65	0.53	0.65	0.40	0.48
12	0.60	0.45	0.50	0.83	0.50	0.60	0.63	0.53	0.58	0.63	0.45	0.75	0.80	0.80	0.80	0.45	0.48	0.64

Table D-13 Values of r_u for 6B spacing and dynamic motion of 0.08g peak acceleration

Dynamic Motion of 0.08g Peak Acceleration and 6B Spacing

Group 1	Free Field					High Stiffness Level					Mean Stiffness Level					Low Stiffness Level				
ID / z (m)	1	5	6	7	Ave	1	5	6	7	Ave	1	5	6	7	Ave	1	5	6	7	Ave
2	0.48	0.38	0.53	0.45	0.46	0.00	1.05	0.00	0.08	0.28	1.15	0.63	0.00	0.00	0.44	0.00	0.03	0.28	0.13	0.11
4	0.75	0.53	0.93	0.55	0.69	0.25	0.48	0.35	0.45	0.38	0.25	0.68	0.50	0.45	0.47	0.23	0.65	0.55	0.63	0.51
6	0.68	0.70	0.53	0.58	0.62	0.55	0.40	0.53	0.35	0.46	0.50	0.38	0.35	0.35	0.39	0.40	0.18	0.38	0.28	0.31
8	0.68	0.95	1.00	0.83	0.86	0.50	0.43	0.35	0.35	0.41	0.33	0.38	0.30	0.48	0.37	0.40	0.30	0.43	0.30	0.36
10	0.83	0.80	0.83	0.95	0.85	0.50	0.90	0.60	0.45	0.61	0.45	0.35	0.45	0.45	0.43	0.55	0.45	0.48	0.35	0.46
12	0.85	0.83	0.83	1.00	0.88	0.70	0.90	0.98	0.78	0.84	0.55	1.00	1.00	0.95	0.88	0.73	0.75	0.70	0.85	0.76

Group 2	Free Field					High Stiffness Level					Mean Stiffness Level					Low Stiffness Level				
ID / z(m)	4	8	9	13	Ave	4	8	9	13	Ave	4	8	9	13	Ave	4	8	9	13	Ave
2	0.48	0.53	0.60	0.63	0.56	0.80	0.13	0.25	0.00	0.29	0.50	0.33	0.00	0.90	0.43	0.33	0.00	0.55	0.63	0.38
4	0.48	0.70	0.98	0.75	0.68	0.13	0.48	0.23	0.30	0.28	0.80	0.40	0.75	0.25	0.55	0.90	0.65	0.25	0.50	0.58
6	0.48	0.83	0.75	0.75	0.70	0.75	0.65	0.63	0.43	0.61	0.40	0.33	0.55	0.40	0.42	0.33	0.48	0.35	0.45	0.40
8	0.88	0.90	0.85	0.73	0.84	0.40	0.35	0.45	0.35	0.39	0.28	0.48	0.43	0.33	0.38	0.55	0.30	0.28	0.43	0.39
10	0.80	0.90	0.73	0.75	0.79	0.80	0.73	0.35	0.73	0.65	0.45	0.60	0.80	0.43	0.57	0.58	0.40	0.23	0.35	0.39
12	0.85	0.90	0.90	0.85	0.88	0.65	0.73	0.73	0.83	0.73	0.78	0.83	0.38	0.58	0.64	0.65	0.45	0.70	0.75	0.64

Group 3	Free Field									High Stiffness Level								
ID / z(m)	10	11	12	14	15	16	17	18	Ave	10	11	12	14	15	16	17	18	Ave
2	0.35	0.53	0.50	0.48	0.45	0.53	0.45	0.50	0.47	0.93	0.30	0.93	0.30	0.00	0.93	0.90	0.90	0.65
4	0.88	0.85	0.83	0.83	0.60	0.90	0.38	0.88	0.77	0.65	0.70	0.88	0.40	0.58	0.88	0.98	0.98	0.75
6	0.68	0.90	0.73	0.73	0.63	0.85	0.68	0.95	0.77	0.38	0.35	0.25	0.40	0.48	0.25	0.30	0.30	0.34
8	0.83	0.85	0.80	0.85	0.80	0.50	0.60	0.50	0.72	0.73	0.38	0.53	0.43	0.45	0.53	0.33	0.33	0.46
10	0.90	0.90	0.80	0.93	0.73	0.98	0.63	0.93	0.85	1.00	0.35	0.38	0.53	0.43	0.38	0.48	0.48	0.50
12	0.93	0.95	0.85	1.00	0.93	0.53	0.78	0.40	0.79	0.55	0.75	0.65	0.95	0.85	0.65	0.73	0.73	0.73

Group 3	Mean Stiffness Level									Low Stiffness Level								
ID / z(m)	10	11	12	14	15	16	17	18	Ave	10	11	12	14	15	16	17	18	Ave
2	0.93	0.45	0.20	0.03	0.55	0.20	0.68	0.68	0.46	0.38	1.15	0.70	0.00	0.00	0.30	0.65	0.65	0.48
4	0.93	0.65	0.50	0.73	0.83	0.50	0.80	0.80	0.72	0.45	0.23	0.20	0.40	0.80	0.55	0.78	0.25	0.46
6	0.60	0.48	0.30	0.35	0.40	0.30	0.43	0.43	0.41	0.50	0.45	0.30	0.50	0.43	0.35	0.50	0.48	0.44
8	0.83	0.43	0.38	0.43	0.40	0.38	0.40	0.40	0.45	0.30	0.55	0.55	0.50	0.35	0.28	0.55	0.30	0.42
10	0.50	0.55	0.53	0.83	0.55	0.53	0.68	0.68	0.60	0.98	0.30	0.58	0.63	0.70	0.35	0.35	0.55	0.55
12	0.48	0.88	0.75	0.85	0.70	0.75	0.68	0.68	0.72	0.60	0.78	1.03	0.93	0.90	0.60	0.90	0.75	0.81

Table D-14 Values of r_u for 6B spacing and dynamic motion of 0.07g peak acceleration

Dynamic Motion of 0.07g Peak Acceleration and 6B Spacing

Group 1	Free Field					High Stiffness Level					Mean Stiffness Level					Low Stiffness Level				
ID / z (m)	1	5	6	7	Ave	1	5	6	7	Ave	1	5	6	7	Ave	1	5	6	7	Ave
2	0.45	0.38	0.40	0.53	0.44	0.28	0.00	0.55	0.08	0.23	0.38	0.70	0.70	0.00	0.44	0.45	0.40	0.00	0.30	0.29
4	0.95	0.70	0.90	0.85	0.85	0.38	0.35	0.40	0.48	0.40	0.23	1.15	0.25	0.63	0.56	0.20	0.30	0.48	0.50	0.37
6	0.78	0.73	0.70	0.85	0.76	0.33	0.33	0.43	0.33	0.35	0.50	0.30	0.25	0.33	0.34	0.40	0.18	0.35	0.13	0.26
8	0.98	0.58	0.95	0.90	0.85	0.48	0.45	0.33	0.40	0.41	0.33	0.30	0.38	0.38	0.34	0.53	0.28	0.45	0.25	0.38
10	1.00	0.98	0.80	0.93	0.93	0.50	0.43	0.60	0.53	0.51	0.58	0.60	0.60	0.35	0.53	0.95	0.40	0.60	0.58	0.63
12	0.60	0.78	0.60	0.95	0.73	0.53	0.85	0.98	0.73	0.77	0.65	0.90	0.80	0.75	0.78	0.93	0.60	0.65	0.78	0.74

Group 2	Free Field					High Stiffness Level					Mean Stiffness Level					Low Stiffness Level				
ID / z(m)	4	8	9	13	Ave	4	8	9	13	Ave	4	8	9	13	Ave	4	8	9	13	Ave
2	0.55	0.55	0.75	0.58	0.61	0.00	0.00	0.00	0.90	0.23	0.00	0.00	0.00	0.43	0.11	0.15	0.00	0.20	0.10	0.11
4	0.90	0.98	0.83	0.95	0.91	0.50	0.35	0.33	0.80	0.49	0.33	0.25	0.50	0.23	0.33	0.20	0.95	0.25	0.60	0.50
6	0.73	0.85	0.78	0.85	0.80	0.50	0.58	0.70	0.40	0.54	0.30	0.48	0.60	0.53	0.48	0.38	0.35	0.45	0.45	0.41
8	0.93	0.90	0.90	0.90	0.91	0.45	0.28	0.45	0.60	0.44	0.40	0.50	0.35	0.35	0.40	0.38	0.43	0.23	0.35	0.34
10	1.03	0.98	0.95	0.80	0.94	0.73	0.85	0.73	0.85	0.79	0.50	0.83	0.40	0.55	0.57	0.53	0.43	0.43	0.40	0.44
12	0.70	0.83	0.65	0.90	0.77	0.58	1.10	0.70	0.90	0.82	0.58	1.13	0.45	1.00	0.79	0.75	0.68	1.05	0.95	0.86

Group 3	Free Field									High Stiffness Level								
ID / z(m)	10	11	12	14	15	16	17	18	Ave	10	11	12	14	15	16	17	18	Ave
2	0.40	0.45	0.25	0.73	0.48	0.25	0.65	0.55	0.47	0.93	0.55	0.53	0.00	0.00	0.53	0.73	0.75	0.50
4	0.93	0.85	0.70	0.78	0.85	0.60	0.85	0.75	0.78	0.55	0.83	0.43	0.28	0.35	0.43	0.70	0.70	0.53
6	0.70	0.85	0.75	0.63	0.85	0.75	0.78	0.60	0.74	0.25	0.18	0.35	0.40	0.48	0.35	0.38	0.38	0.34
8	0.80	0.83	0.70	0.68	1.00	0.70	0.90	0.95	0.82	0.65	0.38	0.50	0.38	0.45	0.53	0.63	0.63	0.52
10	0.93	0.68	0.90	0.80	0.88	0.90	1.00	0.90	0.87	0.45	0.63	0.70	0.45	0.43	0.70	0.33	0.33	0.50
12	0.73	0.98	0.68	1.00	0.98	0.68	0.90	0.75	0.83	0.60	0.75	0.68	0.80	1.03	0.68	0.65	0.65	0.73

Group 3	Mean Stiffness Level									Low Stiffness Level								
ID / z(m)	10	11	12	14	15	16	17	18	Ave	10	11	12	14	15	16	17	18	Ave
2	1.13	1.15	1.15	0.35	0.48	1.15	0.55	0.55	0.81	1.00	0.25	0.75	0.03	0.00	0.30	0.90	0.20	0.43
4	1.05	0.50	0.30	0.65	0.63	0.30	0.40	0.40	0.53	0.60	0.28	1.15	0.38	0.45	0.50	0.50	0.35	0.53
6	0.38	0.45	0.18	0.45	0.40	0.18	0.55	0.55	0.39	0.35	0.28	0.35	0.38	0.50	0.38	0.58	0.43	0.40
8	0.38	0.40	0.43	0.38	0.40	0.43	0.35	0.35	0.39	0.40	0.65	0.40	0.50	0.63	0.50	0.33	0.45	0.48
10	0.30	0.38	0.38	0.50	0.45	0.38	0.30	0.30	0.37	0.60	0.40	0.40	0.40	0.73	0.63	0.55	0.33	0.50
12	0.63	0.55	1.00	1.03	0.45	1.00	0.98	0.98	0.83	0.58	0.80	0.90	1.08	0.98	0.43	0.98	0.75	0.81

Table D-15 Values of r_u for 6B spacing and dynamic motion of 0.06g peak acceleration

Dynamic Motion of 0.06g Peak Acceleration and 6B Spacing

Group 1	Free Field					High Stiffness Level					Mean Stiffness Level					Low Stiffness Level				
ID / z (m)	1	5	6	7	Ave	1	5	6	7	Ave	1	5	6	7	Ave	1	5	6	7	Ave
2	0.60	0.35	0.55	0.23	0.43	0.05	1.15	0.60	0.13	0.48	0.00	0.33	0.43	0.00	0.19	0.00	0.00	0.43	0.00	0.11
4	0.75	0.60	0.68	0.85	0.72	0.25	0.35	0.35	0.73	0.42	0.23	0.93	0.40	0.65	0.55	0.33	0.28	0.65	0.33	0.39
6	0.50	0.80	0.80	0.55	0.66	0.43	0.25	0.43	0.25	0.34	0.35	0.30	0.43	0.30	0.34	0.50	0.28	0.50	0.13	0.35
8	0.90	0.68	0.78	0.48	0.71	0.48	0.43	0.30	0.45	0.41	0.40	0.30	0.33	0.45	0.37	0.38	0.38	0.43	0.40	0.39
10	0.98	0.75	0.88	0.83	0.86	0.50	0.45	0.55	0.38	0.47	0.53	0.33	0.50	0.45	0.45	0.65	0.80	1.03	0.30	0.69
12	0.55	0.95	0.83	0.70	0.76	0.93	0.78	1.10	0.68	0.87	0.65	0.70	1.13	0.85	0.83	0.60	0.60	0.60	0.73	0.63

Group 2	Free Field					High Stiffness Level					Mean Stiffness Level					Low Stiffness Level				
ID / z(m)	4	8	9	13	Ave	4	8	9	13	Ave	4	8	9	13	Ave	4	8	9	13	Ave
2	0.23	0.50	0.48	0.20	0.35	0.00	0.00	0.00	0.30	0.08	0.00	0.15	0.30	0.00	0.11	0.00	0.63	0.13	0.00	0.19
4	0.85	0.50	0.80	0.70	0.71	0.25	0.43	0.43	0.90	0.50	0.48	0.48	0.58	0.33	0.46	0.55	0.90	0.35	0.38	0.54
6	0.75	0.75	0.78	0.58	0.71	0.65	0.40	0.60	0.35	0.50	0.45	0.53	0.45	0.48	0.48	0.38	0.28	0.45	0.45	0.39
8	0.88	0.55	0.85	0.75	0.76	0.38	0.48	0.35	0.40	0.40	0.40	0.50	0.23	0.35	0.37	0.43	0.35	0.45	0.35	0.39
10	0.90	1.00	0.80	0.68	0.84	0.68	1.15	0.43	0.55	0.70	0.40	0.65	0.48	0.40	0.48	0.60	0.45	0.43	0.65	0.53
12	1.08	0.85	0.50	0.78	0.80	0.70	0.40	0.55	0.55	0.55	0.78	0.95	0.35	0.90	0.74	0.45	1.03	0.70	0.88	0.76

Group 3	Free Field									High Stiffness Level								
ID / z(m)	10	11	12	14	15	16	17	18	Ave	10	11	12	14	15	16	17	18	Ave
2	0.58	0.53	0.38	0.83	0.78	0.48	0.30	0.43	0.53	0.80	0.70	0.85	0.08	0.50	0.85	0.70	0.70	0.65
4	0.65	0.73	0.85	0.73	0.78	0.90	0.80	0.85	0.78	1.15	0.73	0.65	0.90	1.03	0.63	1.08	1.08	0.90
6	0.85	0.93	0.93	0.65	0.58	0.85	0.90	0.90	0.82	0.35	0.28	0.30	0.58	0.50	0.30	0.35	0.35	0.38
8	0.75	0.70	0.55	0.88	0.78	0.93	0.83	1.05	0.81	0.48	0.35	0.70	0.40	0.50	0.70	0.45	0.45	0.50
10	0.58	0.88	0.93	0.78	0.90	0.70	0.85	0.70	0.79	0.40	0.53	0.58	0.30	0.38	0.58	0.50	0.50	0.47
12	1.00	0.78	0.65	0.90	0.90	0.50	0.50	1.00	0.78	0.68	0.73	0.83	0.95	0.90	0.83	0.55	0.55	0.75

Group 3	Mean Stiffness Level									Low Stiffness Level								
ID / z(m)	10	11	12	14	15	16	17	18	Ave	10	11	12	14	15	16	17	18	Ave
2	1.15	1.03	0.75	0.00	0.20	0.75	0.28	0.28	0.55	1.13	0.70	0.75	0.00	0.38	0.35	0.60	0.03	0.49
4	0.80	0.83	0.68	0.93	0.53	0.68	0.70	0.70	0.73	0.55	0.38	0.45	0.43	0.83	0.85	1.03	0.43	0.62
6	0.45	0.50	0.48	0.40	0.38	0.48	0.43	0.43	0.44	0.45	0.18	0.33	0.50	0.50	0.45	0.50	0.35	0.41
8	0.35	0.35	0.38	0.45	0.45	0.38	0.40	0.40	0.39	0.45	0.50	0.53	0.40	0.58	0.50	0.55	0.40	0.49
10	0.28	0.35	0.40	0.45	0.53	0.40	0.53	0.53	0.43	0.53	0.65	0.30	0.58	0.38	0.38	0.45	0.50	0.47
12	0.55	0.78	0.60	0.58	0.83	0.60	0.80	0.80	0.69	0.70	0.60	0.78	1.10	0.90	0.70	1.08	0.53	0.80

Table D-16 Values of r_u for 6B spacing and dynamic motion of 0.05g peak acceleration

Dynamic Motion of 0.05g Peak Acceleration and 6B Spacing

Group 1	Free Field					High Stiffness Level					Mean Stiffness Level					Low Stiffness Level				
ID / z (m)	1	5	6	7	Ave	1	5	6	7	Ave	1	5	6	7	Ave	1	5	6	7	Ave
2	0.38	0.50	0.65	0.53	0.51	0.30	0.15	0.25	0.00	0.18	0.00	0.00	0.38	0.50	0.22	0.00	0.78	0.00	0.80	0.39
4	0.40	0.65	0.85	0.68	0.64	0.48	0.35	0.40	0.68	0.48	0.25	0.35	0.30	0.68	0.39	0.60	0.35	0.45	0.13	0.38
6	0.85	1.05	0.68	0.68	0.81	0.48	0.20	0.48	0.20	0.34	0.43	0.30	0.55	0.25	0.38	0.50	0.30	0.43	0.25	0.37
8	0.98	0.85	0.98	0.53	0.83	0.38	0.45	0.35	0.50	0.42	0.30	0.35	0.50	0.53	0.42	0.63	0.40	0.50	0.38	0.48
10	0.75	0.93	1.08	0.55	0.83	0.58	0.50	0.38	0.35	0.45	0.40	0.50	0.43	0.40	0.43	0.75	0.50	0.60	0.58	0.61
12	0.85	1.00	0.90	0.45	0.80	0.70	0.70	1.03	0.63	0.76	0.63	0.85	1.03	0.68	0.79	0.68	0.53	0.75	0.70	0.66

Group 2	Free Field					High Stiffness Level					Mean Stiffness Level					Low Stiffness Level				
ID / z(m)	4	8	9	13	Ave	4	8	9	13	Ave	4	8	9	13	Ave	4	8	9	13	Ave
2	0.58	0.60	0.45	0.43	0.51	0.00	0.30	0.30	0.00	0.15	0.00	0.43	0.33	0.00	0.19	0.00	0.53	0.60	0.60	0.43
4	0.78	0.80	0.78	0.78	0.78	0.38	0.63	0.13	0.45	0.39	0.70	0.90	0.23	0.10	0.48	0.33	0.30	0.18	0.40	0.30
6	0.90	0.60	0.78	0.80	0.77	0.40	0.50	0.68	0.43	0.50	0.40	0.48	0.55	0.40	0.46	0.40	0.50	0.45	0.45	0.45
8	1.05	0.88	0.65	0.73	0.83	0.38	0.38	0.40	0.45	0.40	0.40	0.45	0.33	0.25	0.36	0.48	0.40	0.30	0.40	0.39
10	0.88	0.75	0.98	0.88	0.87	0.35	0.68	0.60	0.60	0.56	0.78	1.00	0.40	0.55	0.68	0.83	0.70	0.55	0.55	0.66
12	0.48	0.88	0.75	0.78	0.69	0.50	0.43	0.55	0.25	0.43	0.68	0.40	0.55	0.85	0.62	0.93	0.90	0.75	0.58	0.79

Group 3	Free Field									High Stiffness Level								
ID / z(m)	10	11	12	14	15	16	17	18	Ave	10	11	12	14	15	16	17	18	Ave
2	0.73	0.48	0.48	0.68	1.00	0.60	0.35	0.45	0.59	0.63	0.63	1.15	0.00	0.00	1.15	0.13	0.13	0.48
4	0.80	0.85	0.85	0.93	0.88	0.78	0.80	0.70	0.82	1.00	0.35	0.35	0.30	0.85	0.35	1.00	1.00	0.65
6	0.43	1.00	0.83	0.85	0.78	0.40	0.78	0.73	0.72	0.33	0.35	0.20	0.45	0.43	0.20	0.40	0.40	0.34
8	0.60	1.03	0.85	0.98	0.80	0.85	0.85	0.68	0.83	0.43	0.33	0.43	0.35	0.45	0.43	0.48	0.48	0.42
10	0.98	0.93	0.78	1.08	0.78	1.05	0.95	0.83	0.92	0.50	0.65	0.43	0.43	0.40	0.43	0.43	0.43	0.46
12	0.75	0.53	0.53	0.80	0.50	0.80	0.65	0.95	0.69	0.65	0.65	0.55	0.85	0.60	0.55	0.80	0.80	0.68

Group 3	Mean Stiffness Level									Low Stiffness Level								
ID / z(m)	10	11	12	14	15	16	17	18	Ave	10	11	12	14	15	16	17	18	Ave
2	1.08	0.73	0.45	0.30	1.15	0.45	0.78	0.78	0.71	1.05	0.38	1.15	0.58	0.00	0.05	0.30	0.55	0.51
4	0.98	0.88	0.63	0.80	0.35	0.63	0.90	0.90	0.76	0.53	0.75	0.83	0.35	0.85	1.10	0.50	0.33	0.65
6	0.50	0.48	0.48	0.53	0.45	0.48	0.43	0.43	0.47	0.45	0.28	0.28	0.45	0.50	0.53	0.45	0.50	0.43
8	0.45	0.63	0.38	0.30	0.35	0.35	0.33	0.33	0.39	0.50	0.60	0.40	0.45	0.55	0.43	0.48	0.45	0.48
10	0.53	0.35	0.33	0.53	0.70	0.33	0.40	0.40	0.44	0.30	0.60	0.35	0.33	0.70	0.53	0.43	0.30	0.44
12	0.35	0.60	0.65	0.43	0.53	0.65	0.65	0.65	0.56	0.60	0.50	0.90	0.90	0.95	0.80	0.98	0.70	0.79